

Geomorphological Watershed Analysis Project
Biennial Report For The Period From 10/1/91 to 6/30/93

BY

David R. Montgomery
Thomas Dunne
William E. Dietrich



June 30, 1993

Geomorphological Watershed Analysis Project
Biennial Report for **1991-1993**

Background

The **Geomorphological Watershed Analysis** project was developed by TFW to conduct research on watershed processes **with** goal of developing tools for watershed analysis and developing understanding of watershed **processes**. This project was **conceived** as a **multi-biennium** project, with the goals originally laid out in **our** proposal [TFW-SH10-91-002] **providing** guidance for a **continuing** research program. Our project aims to provide a rigorous foundation for watershed analysis by applying **state-of-the-art** approaches to geomorphological problems within a watershed context.

Geomorphological Watershed Analysis Project

The **overall** goal of the Geomorphological Watershed Analysis project is to improve the scientific basis for predicting the response of hillslopes and channel systems in forested mountains to both long-term **average** conditions [climate, geology, topography, vegetation] and short-term perturbations [**fire**, extreme storm events, and timber harvest]. **Our** approach is oriented toward developing objective, physically-based procedures for assessing and interpreting the current condition of channels and **hillslopes**, and for predicting response to watershed **perturbations**, such as those that accompany timber harvesting. Conceptually, we view potential hillslope and channel **responses** as linked through the processes controlling sediment mobilization, routing, and storage within a watershed. While maintaining this watershed context, we have divided our project into three distinct components: shallow sediment sources, deep-seated landslides, and channel condition and response. **Project** objectives **include** development of an interactive team of researchers working on **problems** in watershed **processes** and analysis, and **specific** research goals in each of the three project components.

The format of this report reflects this organization. In the following sections, we review project goals and **summarize** progress to date. Specific research results are presented in a series of appendices consisting of published, submitted, and draft **research** papers, and **summaries** of **other technical** results from ongoing studies.

Interactive Team of Researchers

The first goal of the Geomorphological Watershed Analysis project is the creation of an interactive team of researchers studying watershed processes and developing methods of watershed analysis. **This** was accomplished through both direct hiring, student support, and collaborative projects undertaken **with** scientists not supported by TFW. Personnel directly

funded by the project include one of the **PI's [Montgomery]** and at various times five graduate **students** [Abbe, **Bauer, Buffington, Schmidt, and Stock**] working on aspects of our project. Two part-time computer programmers [Greenberg and Reissl were partially supported by TFW funding. Two additional **programmers** were employed intermittently on an hourly basis. A staff geologist [Miller] was funded for portions of the academic year **'92-'93** on the deepseated mass wasting component of the project.

Several **non-funded** collaborators worked on **tasks** directly relating to **project** goals. Dr. **Weihua Zhang**, a University of Washington postdoctoral researcher funded from federal sources, collaborated with Dr. Montgomery to **examine** the effect of digital elevation model (**DEM**) resolution on simulations of surface and hydrologic **processes** (Appendix **4**). Dr. **Efi Foufoula (Univ. of Minnesota)** collaborated with Dr. Montgomery to investigate methods to delineate the extant of channel networks from **DEM's** (Appendix **3**). Dr. Montgomery also has been **coordinating** research efforts on channel **assessment** and response with Dr. Lee MacDonald at Colorado **State** University with the goal of standardizing data collection procedures **so** as to maximize the usefulness of data collected by both groups Dr. Cathy Win of **CSIRO** (Australia) visited UW and arranged for project use of future versions of **TOPOG** currently under development.

The Geomorphological Watershed Analysis **Project** provided input to other TFW funded, or related, **projects** through consultations, collaboration, and loans of equipment. The Ambient Monitoring **Project** approached us for advice on **data** collection methodologies and analysts in October and November, 1991. Prior to the program's termination, we suggested revisions to their field methods that would have increased the utility of their **data** for use in **our** analyses and those of other resource management professionals. We also suggested revisions in their analysis procedures that they incorporated with productive results. A desired set of data for collection in any future effort was transmitted to the Ambient Monitoring Committee through Jeff Light and Kate Sullivan. We also provided input to Ed **Rashin's** project on BMP evaluation at Washington **State** Department of Ecology, **JoAnne Metzler's** peak discharge channel damage assessment methodology, and Phil Peterson's response thresholds review.

In an effort to stimulate collaboration **between** fisheries biologists and **geomorphologists** we have worked on field **measurements** with, and loaned equipment to, Phil Peterson of the TFW "Big Fish" project for his **study** on channel scour and bed modifications at **Kennedy** Creek. Further collaborative efforts with Phil Peterson and Tom **Quinn** should result in at least two **manuscripts** on linkages between channel processes and **salmonids**: one paper focusing on the effect of channel armoring by spawning activity on stream bed mobilization (Appendix **5**) and the other on the role of channel **processes** in controlling the spatial distribution and timing of **salmonid** spawning.

The Geomorphological Watershed Analysis Project also has been involved with other programs working on watershed process issues. We co-hosted a **NCASI** workshop on methods for channel **assessment** methodologies held at the Quaternary Research Center on April 5-9, 1993. **Participants** from **research** organizations, private companies, and the U.S. Forest Service attended the workshop, which produced useful discussions between **researchers** and resource professionals charged with **implementing assessment** methodologies. In addition, Dr. Montgomery served on the **Federal Ecosystem Management Assessment Team (FEMAT)** convened in Portland **after** the Forest Summit in the spring of 1993. He contributed to the development of a watershed analysis orientation to the recommendations for future management of Federal lands. Many of the goals of the federal program parallel those of TFW.

In summary, we have established an active research group **studying** watershed **processes**. This group extends well beyond the size of our TFW-funded personnel and we are involved in projects that broaden the impact of TFW support significantly beyond the scope of our original proposal.

Shallow Sediment Sources

Progress toward the objectives of the shallow sediment source **component** outlined in our proposal is **summarized** below.

- 1) *Develop a method for determining how well digital elevation data represent **actual** watershed topography to the degree necessary for locating sediment sources.*

We developed two methods for **examining** the quality of landscape representation in digital elevation models. One of these methods was presented in a draft manuscript included as Appendix 1 of our 1991-1992 **annual report** [Bauer, submitted]. This method is based on calculating the signal-to-noise ratio of a digital elevation surface, providing a method for determining the quality with which an object of a given size (a hillslope or a debris flow source area, for **example**) is represented in a DEM. The approach developed by Zhang and Montgomery [Appendix 4] **examines** the effect of DEM grid size on the distribution of the topographic parameters that **influence** both runoff generation and surface process models and on hydrologic simulations based on these models. We analyzed landscape representation for two small watersheds where high-resolution DEM data were available and found that a grid size of 10 m provided a reasonably accurate portrayal of the ground surface; standard 30 m and 90 m grid size data involved significant **compromises** in landscape representation. Both of these studies have fundamental implications for the use of **DEM's** in surface **process** models and point

to the need to use a **DEM** scale that is appropriate for **resolving** landscape features and **processes** of interest.

- 2) *Test **the use Of** a steady state shallow **subsurface runoff** model to **predict** spatial distribution **of** ground saturation in **steep**, realistically complex **terrain**.*

We published two **TFW-supported** papers on predicting the spatial pattern of runoff **production** and **erosion mechanisms** using the steady-state shallow subsurface runoff model **TOPOG** (Appendix 3). These papers discuss the partitioning of landscapes into process **regimes** on the basis of slope, contributing drainage area, and threshold process theories. We also conducted **steady-state** sprinkler **experiments** on a small catchment in Coos Bay, Oregon, from May 26 to June **14, 1992**, in part to provide a data set against which to test the predictions of steady-state shallow **subsurface runoff** models. These experiments are also **supported** by the National Science Foundation and the Weyerhaeuser Company. **Preliminary** data analyses suggest that **TOPOG** predicts the general pattern of soil saturation, but that flow characteristics of near-surface bedrock control specific patterns of soil saturation and strongly influence locations of debris-flow initiation. These results are currently **being** written **into** a draft research paper and will provide the basis for a planned field test of the model for predicting areas prone to shallow mass-wasting by conducting a field-scale experiment at our **instrumented site** in coos Bay, Oregon.

- 3) ***Develop** a method for predicting **areas** prone to shallow landsliding in **a** watershed through the use of topographic **analysis software**.*

We have developed a DEM-based method for predicting relative potential for shallow landsliding in a catchment. Our paper **describing** the model and our tests of its predictions has been accepted pending **revision** for publication in Water Resources Research (Appendix **3**). A final version of the paper will be forwarded to **TFW** when revisions are complete. We tested the model in three **catchments**: one in **Marin** County, California, one in the Oregon Coast Range near Coos Bay, and one on the Olympic Peninsula, Washington. Model results indicate that **this** method provides a viable tool for predicting spatial patterns of slopes potentially **subject** to shallow landsliding. We are exploring development of a grid-based analysis to facilitate interfacing results **with GIS** systems, such as ARC/INFO. Once we have developed the method, we intend to test it on larger watersheds in the Cascades and the Olympic Peninsula.

- 4) **Develop and test** DEM-based predictions of channels most **likely** to be affected by debris flows.

In the shallow slope instability, manuscript we outline a method for identifying channels subject to potential debris flow scour. To date, the method has been applied to three small **catchments** and the debris-flow run out algorithm has not **been** adequately tested. We anticipate expanding this aspect of our **study** in **conjunction** with further predictions of debris-flow run out paths in **other catchments** where we can test model predictions against observations. Funding restrictions prevented **further** progress on this goal, which has been deferred until the '93-'95 biennium.

In **summary**, we have met the objectives of the shallow sediment source component of our project and many of our results have been accepted for publication in the scientific literature. Further development, testing, and refinement of model predictions and investigations of the effect of DEM scale on process models are anticipated to proceed in the upcoming biennium.

Deep-Seated Mass Failures

Progress toward the objectives of the deep-seated mass failure component outlined in our proposal is **summarized** below.

- 1) Develop a *method for systematic* prediction of *potential sites of* deep-seated **mass failures in a watershed**.

Kevin Schmidt conducted extensive field-surveys of large-scale mass wasting in the **Chuckanut** formation in the northern Cascades. He compared empirical observations with predictions of a one-dimensional slope stability model and found evidence for both topographic and local **structural** and hydrologic controls on the size of stable hillslopes. A summary of his **research to date is presented** in Appendix 6.

Dan Miller, currently a Ph.D. candidate in Geological Sciences at UW, was employed intermittently as a staff geologist on the deep-seated mass wasting **component** of the project to develop DEM-based predictions of relative slope stability based on the approach developed by Kevin Schmidt. Preliminary results are promising and are **presented** in Appendix 7.

- 2) **Developing** a *method for* predicting *the alteration of stability as a result* of changes in hydrology due to **natural** weather **fluctuations** or to management.

Kevin Schmidt has incorporated **groundwater** pore pressures into his model **for** slope-height control on deep-seated mass **failures**. Further exploration of land use effects on **deep-seated failures** requires development of a model for the **effect** of timber **harvest and** road **construction** on **groundwater recharge**.

- 3) Development *of guidelines for field studies* to *refine* predictions in *areas that have* been *flagged as potentially* unstable.

Kevin Schmidt has developed a preliminary set of guidelines for field studies of **deep-seated** bedrock landslides based on simple quantitative **assessment** of outcrop-scale factors related to rock **strength**. These guidelines are presented in Appendix 8.

Assessment of Channel Condition and Response

In addition to the **objectives** listed below, we developed a **process-based** channel classification for use in watershed analysis. This classification is presented in a separate report [**TFW-SH10-93-002**] and was developed in response to a request from the SHAMW committee when presented with our initial ideas on the subject. Version 1.01 of the Watershed Analysis Manual adopted by the Forest Practice Board drew liberally from a draft manuscript of this report.

Progress toward our other objectives in the channel **assessment** project is outlined below.

- 1) Test the ability *of* digital **elevation** data to **resolve** local channel slope *with sufficient* accuracy to be **useful for** geomorphic **modelling** and **habitat classification**.

Field data collected during summer 1992 indicates that channel slopes derived from topographic maps exhibit significant **variance** from reach-level slopes measured **in the** field, but that **map-derived and field slopes** are in **general agreement**. The work on grid size effects on **DEMs** reported in Appendix 4 shows that grid size effects are much less pronounced for channels than for hillslopes. Our initial test of predicting **channel** types from DEM data is **discussed** under item 3. Our results indicate that good-quality **DEM** data is very useful for modelling channel **processes** and morphology at the channel reach level, but our data also show that DBM data **is too** coarse to allow meaningful predictions at the channel unit level. Habitat-level classification is not feasible from standard **DEM's**.

- 2) *Produce a summary of existing data on channel properties from forested mountainous watersheds that can be used to test our threshold and transport controlled characterization of channels.*

John Buffington, a TFW-supported graduate student, has collected and analyzed much of the available data pertinent to assessing our threshold channel model for predicting sediment size from channel slope and bankfull depth. Much of the available data from previous studies, however, is unsatisfactory because we either do not know exactly how it was collected, or do not approve of the methods used during data collection. John will be finishing his thesis this fall.

- 3) *Develop a method for prediction of channel attributes from a digital elevation model (DEM) and field observations that test the predictions.*

Our initial test of a DEM-based channel prediction method relying on channel slope predicted a pattern of channel types in close agreement with those surveyed in the field for the Owl Mountain quadrangle in the Hoh River basin [see TFW-SH10-93-002].

- 4) *Develop methods for predicting sediment flux through a channel network.*

The channel classification outlined in TFW-SH10-93-002 provides a coarse model for sediment routing and transport through channel networks. Development of other methods for predicting sediment flux through a channel network were severely impaired by budget cuts early in the program. These cuts eliminated a post-doctoral position that was intended to focus on this problem.

Another aspect of this project that was completed was a study of road drainage concentration as a factor in the extension of channels to road drainage locations (thus ensuring delivery of fine sediment produced on the road surface into the channel) and the association of sites of landslide initiation with road drainage concentration [Appendix 4]. Our surveys show that there is a limit to the road length that can be drained to a specific site without adverse impacts. This critical road length decreases as the slope of the ground surface onto which road drainage is concentrated increases. It also varies for channel extension and landslide initiation and will be different in different areas. The form of the observed relations, however, conform to the predictions of a simple theoretical model. This approach provides a method for assessing appropriate road drainage criteria for inclusion in BMP's.

Other work accomplished to date toward this goal has been by Tim Abbe, a graduate student. He is starting to study the interaction woody debris and sediment routing and storage in forested drainage basins. Although many workers have studied aspects of this problem, this interaction has not been studied systematically and we are developing a theoretical context within which to view this interaction. Tim began graduate studies in the fall of 1992, and this summer (1993) will be his **first** field season.

Dietrich and others (1989) proposed the dimensionless sediment transport ratio q^* as an indicator of channel sediment supply relative to transport capacity. John Buffington has developed a discussion of appropriate applications and potential problems in using this method for channel condition assessments. This discussion is presented in Appendix 9.

Another control on sediment routing through channel networks is the spatial distribution of sediment contributed across channel banks. Bill Dietrich is developing methods for predicting the flux of sediment into channels from across channel banks. This is a crucial component of any spatially distributed sediment budget.

We also have substantial data on channels from field work during summer 1992 that we need to supplement prior to final interpretation. This data provides empirical support to the theoretical basis for the channel classification and response potential scheme presented in TFW-SH10-93-002. Much of this data has been presented informally to SHAMW. Dr. Montgomery hopes to write up these studies in the upcoming year.

Goals for '93-'95 Biennium

We plan on achieving a number of goals in the '93-'95 biennium. Most of our planned activity centers around the channel component of the project, with additional activity on the shallow mass wasting component. The deep-seated mass wasting component was eliminated from the project as a result of severe budget cuts. However, we have secured one-year of funding for the deep-seated mass failure component of the project from the Washington Forest Protection Association.

We have a number of goals for the channel component of the project. First, we intend to explore further and test DEM-based channel classifications in several watersheds in the Cascades and on the Olympic peninsula. Second, we plan on continuing our investigations of the utility of our proposed channel classification as a tool for predicting potential channel response. We plan on accomplishing this through case studies of watershed response, probably using the Green River, Hoh River, and Finney Creek watersheds as examples. We also intend to collect data on the influence of large woody debris on pool frequency in different channel types to develop rational criteria for defining desired future channel conditions that reflect

differences in channel **processes** through a channel network. Finally, Tim Abbe is developing a study to **document** and model the interaction between LWD, sediment storage, and channel morphology in a channel network **context**. Field work on this component of the project is starting this summer. We anticipate that these projects will significantly advance the state of our knowledge of channel processes in forested mountain drainage basins and that this information will prove valuable for implementing watershed analyses both in the State of Washington and elsewhere.

Plans for the shallow sediment source component of the project center on further development and testing of our model for shallow mass wasting, downslope run out, and deposition. A **primary** goal is the development of an **ARC/INFO** compatible model to replace the TOPOG based model that we developed **during** the 91-93 biennium. Conversion to this format will greatly enhance **the** applicability of this model to watershed analyses. We also intend to start developing more complicated models by adding root strength and soil depth to the simulations. We **particularly** want to further develop and test our **preliminary** model for debris flow routing and deposition.

Unfortunately, we also lost funding for the development of a **GIS-based** watershed analysis model. While we have developed many of the pieces as part of this project (**DEM**-based channel classification, shallow landsliding model, and **OUT** preliminary deep-seated **landsliding** model), we currently lack the funds to develop and test an integrated model using these components. Although we have no support for the **GIS** component of our **project**, we will pursue opportunities as they arise. **In** summary, we have achieved more than the deliverables **outlined** for the '91-93 biennium and we intend to continue progress toward the long-term goals outlined in **our** original proposal.

APPENDIX 1 Abstracts published or accepted **during '91-'93** biennium

Montgomery, D. R., and **Foufoula-Georgiou, E.**, Channel **network** source representation from digital **elevation** models, **EOS**, Transactions of the **American** Geophysical Union, v. 74, no. 16, p. **152, 1993.**

Dietrich, W. E., Wilson, C. J., Montgomery, D. R., and McKean, J., Analysis of erosion thresholds and land surface **morphology** using a digital terrain model, **EOS**, Transactions of the American Geophysical Union, v. 74, no. 16, p. **194, 1993.**

Montgomery, D. R., Buffington, **J. M.,** and **Massong, T.,** Channel classification and prediction of channel response in mountain drainage basins, **EOS**, Transactions of the **American** Geophysical Union, v. 73, no. 43, p. **230-231, 1992.**

Buffington, **J. M.,** and Montgomery, D. R., Effects of hydraulic roughness and **sediment** supply on bed surface textures in gravel-bed streams, **EOS**, **Transactions** of the American Geophysical Union, v. 73, no. 43, p. **231, 1992.**

Schmidt, K. M., and Montgomery, D. R., Mountain-scale strength properties, deep-seated **landsliding**, and **limits** to local relief, **EOS**; **Transactions** of the **American** Geophysical Union, v. 73, no. 43, p. **227-228, 1992.**

Dietrich, W. E., and Montgomery, D. R., A digital terrain model for predicting debris flow source areas, **EOS**, **Transactions** of the American Geophysical Union, v. 73, no. 43, p. **227, 1992.**

APPENDIX 2 **Papers Published** during **'91-'93** Biennium

Dietrich, **W. E., Wilson, C. J., Montgomery, D. R., McKean, J.,** **Analysis** of Erosion Thresholds, Channel Networks and Landscape Morphology Using a Digital Terrain Model, **Journal** of Geology, v. 101, p. **259-278, 1993.**

Dietrich, W. E., Wilson, C. J., Montgomery, D. R., McKean, J., and Bauer, R., **Channelization** Thresholds and Land Surface Morphology, **Geology**, v. 20, p. **675-679, 1992.**

Montgomery, D. R., and Buffington, **J. M.,** Channel **Classification**, Prediction of Channel Response, and Assessment of Channel Condition, **TFW-SH10-93-002**, Washington State Timber/Fish/Wildlife Agreement, **84p.**

APPENDIX 3 Papers In Press at **Time** of Report Preparation

Montgomery, D. R., and **Dietrich, W. E.,** Landscape Dissection and **Drainage** Area/Slope Thresholds, in 'Process Models and Theoretical **Geomorphology**' edited by M. J. **Kirkby,** John Wiley & Sons.

Montgomery, D. R., and **Foufoula-Georgiou, E.,** Network Source Representation from Digital Elevation Models: Water Resources Research.

APPENDIX 4 **Papers** Submitted to **Journals** at **Time** of Report Preparation

Zhang, W., and Montgomery, D. R., Digital **elevation** model grid size, landscape representation and **hydrologic** simulations: Water Resources Research.

Montgomery, D. R., and **Dietrich**, W. E., A Physically-Based Model for the Topographic Control on Shallow Landsliding: Water Resources Research.

Montgomery, D. R., Impact of road drainage concentration on the stability of natural landscapes, submitted to water Resources **Research**.

Montgomery, D. **R.**, and Buffington, J. **M.**, A **process-based** channel classification, submitted to **Environmental Management**.

Bauer, R, Evaluating digital elevation models, submitted to Water Resources Research.

APPENDIX 5 Draft Paper

Montgomery, D. R., Peterson, N. P., Buffington, J. **M.**, **Schuett-Hames**, **D.**, and Quinn, T., Channel Bed Coarsening by **Salmonid Spawning**: Feedback Mechanism for Population Stability.

APPENDIX 6

Schmidt, K. **M.**, and Montgomery, D. R, Mountain-scale strength properties, **deep-seated landsliding**, and limits to local relief.

APPENDIX 7

Miller, D., **BigDirt**: deep-seated mass wasting project report.

APPENDIX 6

Schmidt, K. M., **Deep-seated** bedrock landslides and rock mass strength analysis.

APPENDIX 9

Buffington, J. M., **Fluvial processes** and **interpretation** of stream-bed surface textures.

Appendix 1

Channel Network Source **Representation** from Digital Elevation Models

D R Montgomery (Department of Geological Sciences, University of Washington, Seattle, WA 98195)

E **Foufoula-Georgiou** (St. Anthony Falls Hydraulic Laboratory, Department of Civil and Mineral **Engineering**, University of Minnesota, Minneapolis, MN 55414)

Methods for the identification of the size, or scale, of hillslopes and the extent of channel networks from digital elevation models (**DEM's**) are examined critically. Theoretically, a constant critical support area, the method most commonly used at present for channel network extraction from **DEM's**, is more appropriate for depicting **the hillslope/valley transition** than for identifying channel heads. Analysis of **high-resolution** DEM data **confirms that** a constant contributing **area** per unit contour length depicts the extent of divergent topography, or the hillslope scale, although there is considerable variance about the average value. In steep topography, however, a DEM resolution finer than the typical 30 m by 30 m grid size is required to accurately resolve the **hillslope/valley** transition. Analysis of high-resolution DEM data from **catchments** in which channels were mapped in the **field** [Montgomery and Dietrich, **1989**] indicates that the inflection in the drainage area-slope relation **reported** by **Tarboton et al. [1991]** to define the extent of the channel network occurs **within** the channel network and probably reflects a **transition** from steep **debris-flow**-dominated channels to lower-gradient alluvial channels. Field data [Montgomery and **Dietrich**, 1988; 1989; **1992**] indicate that for many soil-mantled landscapes, a slope-dependent critical support area defines the scale of channel initiation, and thus the extent of channel networks. Several methods for estimating this relation from DEM data **are** examined.

1. 1993 Spring Meeting
2. 007852754
- 3a. David R. Montgomery
Dept. of Geological Sci.
Univ. of Washington
Seattle, WA 98195
- 3b. (206) 685-2560
- 3c. (206) 543-3836
4. H
- 5a. HO8 **Predicting**
Process from Form
- 5b. 1824 **Geomorphology**
- 6.
7. 25%
Field data is published
8. Invoice \$60 to PO #
T267410, QRC, AK-60
University of Washington
Seattle, WA 98195
9. C.
- 10.
11. No

A Digital Terrain Model for Predicting Debris Flow Source Areas

W.E. Dietrich (Department of Geology and Geophysics, University of California, Berkeley, CA 94720)

D R Montgomery (Department of Geological Sciences and Quaternary Research Center, University of Washington, Seattle, WA 98195)

It is widely known that debris flows commonly originate in topographic hollows, but they also occur in other topographic locations. Digital terrain models provide an idea) format for examining quantitatively whether such failures occur in hydrologically similar locations. A digital terrain model for predicting topographic controls on the potential for debris flow initiation throughout a catchment is developed by **coupling near-surface throughflow** and slope **stability** models. The hydrologic model uses the program TOPOG (O'Loughlin, 1986) to determine the proportion of the soil thickness that is saturated in response to a steady-state rainfall for topographic elements defined by the intersection of contours and flow **tube** boundaries. The slope stability component uses this relative soil saturation in the infinite slope stability model to **analyze the** stability of each topographic element for the case of **cohesionless** soils. **The** coupled model allows prediction of relative debris flow initiation potential through **mapping** the steady-state rainfall **necessary** to generate slope instability for **each topographic** element in a catchment. Model sensitivity is **examined** with **respect** to the physical parameters **incorporated** in the model [soil thickness, conductivity, bulk density, and angle of **internal** friction], as well as the simulated rainfall intensity. Patterns of **predicted** debris **flow initiation** potential are consistent with **spatial patterns** of Observed debris **flow scarps** for **three** study catchments in the **western** United States where detailed digital elevation data **were** obtained [Tennessee Valley in **Marin** County, California; **Mettman** Ridge in the **Oregon Coast** Range; and Split **Creek** in the **Olympic** Peninsula, Washington]. Estimates of the steady-state rainfall **necessary** to cause debris flows in these areas constrain model simulations that identify as **unstable** the locations of approximately **90%** of the observed debris flow **scarps** in the study **catchments**. **Unfailed** locations predicted to be unstable probably **represent** likely **locations** for future instability. The model, however, does not **account** for either spatial variations in soil properties or the **influence** of bedrock flow on debris flow initiation. Such effects may **determine specific failure** locations within areas potentially subject to **failure** and may **explain** those debris flows occurring outside **zones** of predicted **instability**.

1. 1992 Fall Meeting
2. 007852754
- 3.a **William E. Dietrich**
Dept. of Geology &
Geophysics
Univ. of California
Berkeley, CA 94720
- 3.b (510) **642-2633**
- 3.c (510) 6439980
4. H
- 5.(a) H14
Hillslope Processes
- (b) 1824 Geomorphology
- 6.
7. 30%
Geology, **8/92**
8. **Invoice \$70 to attached**
PO# 203576. QRC, AK-60
Univ. of Washington, Seattle,
WA 98195
9. C
- 10.
11. No.

Effects of Hydraulic Roughness and Sediment Supply on Red Surface Textures in Gravel-bed Streams

J.M. Buffington and D.R. Montgomery (Department of Geological Sciences and Quaternary Research Center, University of Washington, Seattle, Wa. 98195)

The size of the material forming the bed of alluvial channels reflects the channel depth and slope, energy dissipation due to in-channel roughness elements, and the sediment supply of the channel. The median surface grain size of the bed material (D50) can be predicted from channel depth and slope, using a simple threshold channel competence model in which armored conditions are assumed and only grain roughness is considered. The model provides a reference point from which to examine textural response to both increased sediment supply and the introduction of other roughness elements. Stream beds respond to sediment supply changes by armoring when deprived of sediment and fining when inundated with sediment (Dietrich et al., 1989), allowing a range of grain roughness response that may accommodate changes in sediment loading without otherwise significantly altering channel morphology. However, other roughness elements must also be considered in evaluations of potential textural response to changes in sediment supply. Theoretical considerations and field measurements indicate that roughness associated with bedforms and large woody debris (LWD) results in bed surface textures that are finer than model predictions. Data from a variety of sources indicate that threshold channel predictions are inappropriate for both sand-bedded channels, in which regime bedforms are the dominant roughness element, and steeper channel morphologies, in which there may not be a simple threshold for bed mobility.

In order to partition the relative effects of different roughness elements in gravel-bed channels, for which the threshold model applies, three distinctly different channel types were identified: plane-bed, pool-riffle with minimal LWD loading, and pool-riffle with significant LWD loading. Detailed textural and topographic maps were constructed for each channel type, and LWD dimensions and orientations were mapped. Textural changes in response to roughness elements are clearly observed at local scales. When textures are spatially averaged and on a reach level, the study channels segregate by channel type into distinct zones of textural response (relative to the theoretical armored D50 limit). Surface and subsurface (bedload) grain size distributions were also measured for each texture in order to determine the relative effects of sediment loading. Preliminary results indicate that textural change due to increased sediment supply can be of comparable magnitude to those caused by in-channel roughness elements.

With this theoretical framework a comparison of surface and subsurface D50's to the theoretical armored D50 enables assessment of both channel condition and potential to convey increased sediment loads. This assumes that bed textures will fine to the subsurface (bedload) limit in order to accommodate increased sediment supplies before significant morphological change occurs. Channels in which surface textural fining has already occurred, due to the presence in-channel roughness elements, are hypothesized to be more sensitive to perturbations in sediment supply.

1. 1992 Fall Meeting
2. 011960042
- 3.a John M Buffington
Dept. of Geological Sci.
Univ. of Washington
Seattle, WA 98195
- 3.b (206) 543-1975
- 3.c (206) 543-3836
4. H
- 5.(a) H16 Biological
Influences on
Alluvial Channels
- (b) 1824 Geomorphology
6. prefer oral
7. 0 %
8. Invoice \$40 to attached
PO# 575027, QRC. AK-60
Univ. of Washington, Seattle,
WA 98195
9. c
10. Schedule after
Montgomery/Buffington
11. Yes

Mountain-Scale Strength Properties, Deep-Seated Landstiding, and Limits to **Local Relief**

K.M. Schmidt & D.R. Montgomery (Department of Geological
Sciences, AJ-20, University of Washington, Seattle, Wa.
98195)

Controls on **the size** of mountains and the stability of bedrock slopes **are** only poorly **constrained**, but., wide potentially important limits **to** the development of local **relief**. Determining the strength **properties** of a mountain is difficult, however, because such **properties** integrate both material and structural **discontinuities** and also may be **time** dependent. We hypothesize that in a threshold landscape such integrated rock strength properties **limit local** relief development and **effectively determine** the **size** of stable **hillslopes** for mountain drainage basins in a **given lithology**, climate, and tectonic regime. The **Culmann** wedge stability model predicts a limiting relation between hillslope gradient and ridge height. Assuming conditions for plane failure **in** this limit equilibrium analysis, **this** model may be used to ascertain the properties of cohesion and internal friction angle characteristic of the material as a whole, including its discontinuities. These time-integrated **properties** differ **from laboratory-derived** values in that they reflect all **the** destabilizing influences **experienced** by **the** slope and thus represent the minimum **strength** mobilized **during** its history.

Ridge gradients and heights **were measured** for slopes underlain by the strongly bedded Eocene **Chuckanut** Formation, as well as for **Quaternary glacio-fluvial** deposits forming channel **banks within** the **Nooksack River** drainage in northern Washington state. **Material** properties calculated from this procedure are lower than values typically derived from laboratory **measurements**. This suggests two alternative hypotheses. First, that **strength** properties derived from the limits **to** local relief are lower than actual values and that the landscape **may** be **dissected** further without inducing slope instability. Alternatively, these properties reflect the true strength of **the material which**, in turn, **impart** a limit to **relief development**. A **high** density of large, **deep-seated** bedrock landslides **provides evidence** for this limit being reached, at **least** locally in the study area. We suspect that these material properties essentially represent the strength of the entire formation including discontinuities, such as **weak shale beds** and clay **filled** joints.

In addition, the regional **geologic structure** strongly influences slope stability. Landslide sites situated well below the observed maximum relief for a given **hillslope** gradient are predominantly dip slope failures. Also, for a given **ridge** height, anti-dip slopes are capable of sustaining steeper gradients **than** dip slopes. Remnant glacial deposits forming benches in the valley bottoms also act as local buttresses, temporarily stabilizing portions of the mountain **front**. As these deposits erode, the local relief increases **and the slope** evolves closer to its maximum stable relief. The largest, steepest stable slopes in the study area **are** those with glacial material buttressing their toe. Similar slopes where **buttresses** have been eroded have **failed**. Defining the limit to relief development and the **local** modifiers to this limit provide a connection between the **size** of mountains, presence of deep-seated landslides, and **the depth** of incision in the **intervening** valleys.

1. 1992 Fall Meeting
2. 012034109 (AGU Number)
3. (a) **Kevin Schmidt**
Dept. of Geological Sciences
AJ-20
Univ. of Washington
Seattle, WA 98195
(b) Tel: 206-543-1996
(c) FAX: 206-543-3836
4. H
5. (a) H14 **Hillslope Processes**
(b) 1824 **Gcomorphology**
6. --
7. 0%
8. \$40; for PO# 203576
ORC AR-69
University of Washington
Seattle, Wa. 98195
9. . c
10. --
11. Yes

Channel Classification and Prediction of Channel Response in Mountain Drainage Basins

D.R. Montgomery, J.M. Buffington, and T. Massong (Department of Geological Sciences and Quaternary Research Center, University of Washington, Seattle, WA 98195)

While a great deal of the geomorphic literature pertains to low-gradient alluvial channels little is known about the morphology and dynamics of channels in mountain drainage basins. An understanding of the response of such channels to perturbation is critical for assessing potential watershed impacts from changes in either land management or natural processes. Furthermore, any effort to understand interactions of alluvial processes and biological systems requires a process-based scheme for classifying different portions of a channel network. At present, the available channel classification schemes are primarily descriptive and do not lead directly to prediction of channel response or the importance of biological processes on channel morphology. We propose a process-based channel classification that allows identification of portions of a channel network that will respond similarly to changes in discharge, sediment supply, and large woody debris loading. This classification is based on systematic variations in bed morphology that we hypothesize represent different roughness configurations and modes of energy dissipation controlled primarily by the channel slope and local sediment supply. In this scheme, channels are classified as regime, pool-riffle, plane bed, step-pool, and cascade based on the configuration of roughness elements within the channel. Field measurements from channels in several areas indicate that this suite of channel types may be distinguished on a plot of channel slope versus relative roughness. Each of these channel morphologies imposes different constraints on channel response. For example, steep channel morphologies (step-pool, cascade-pool, and cascade) have sufficient transport capacity to rapidly transmit increased sediment loads to downslope channels. Lower gradient pool-riffle channels, however, possess less transport capacity and may undergo significant morphologic change (bed fining, pool tilling, etc...) in order to accommodate increased sediment loads. Plane bed channels, on the other hand, are particularly susceptible to changes in large woody debris loading, as pool formation in such channels depends upon the presence of local flow obstructions. Valley confinement, the influence of large woody debris on pool formation and sediment storage, and the potential for debris flow impacts supplement the morphologic classification. At the most general level, this classification system allows for rapid identification of portions of the channel network with an excess of sediment supply or transport capacity. More specifically, it allows stratification of a channel network based on channel processes and response potential.

1. 1992 Fall Meeting
2. 007852754
- 3.a David R. Montgomery
Dept. of Geological Sci.
Univ. of Washington
Seattle, WA 98195
- 3.b (206) 685-2560
- 3.c (206) 543-3836
4. H
- S.(a) H16 Biological
Influences on
Alluvial Channels
- (b) 1824 Geomorphology
6. prefer oral
7. 0%
8. Invoice \$70 to attached
PO# 203576, QRC, AK-60
Univ. of Washington, Seattle,
WA 98195
9. c
10. Schedule before
Buffington/Montgomery
11. No.

Appendix 2

Erosion thresholds and land surface morphology

William E. Dietrich

Department of Geology and Geophysics, University of California, Berkeley, California 94720

Cathy J. Wilson

Australian Center for Catchment Hydrology, CSIRO, Canberra, A.C.T. 2601, Australia

David R. Montgomery

Department of Geological Sciences, University of Washington, Seattle, Washington 96195

James McKean, Romy Bauer

Department of Geology and Geophysics, University of California, Berkeley, California 94720

ABSTRACT

We propose a graphical technique to analyze the entirety of landforms in a catchment to define quantitatively the spatial variation in the dominance of different erosion processes. High-resolution digital elevation data of a 1.2 km² hilly area where the channel network had been mapped in the field were used in the digital terrain model, TOPOG, to test threshold theories for erosion. The land surface was divided into ~20 m² elements whose shapes were then classified as convergent, planar, or divergent. The entire landscape plotted on a graph of area per unit contour length against surface gradient shows each planform plotting as a separate field. A simple steady-state hydrologic model was used to predict zones of saturation and areas of high pore pressure to mimic the extreme hydrologic events responsible for erosive instability of the land surface. The field observation that saturation overland flow is rare outside convergent zones provided a significant constraint on the hydrologic parameter in the model. This model was used in threshold theories to predict areas of slope instability and areas subject to erosion by saturation overland flow, both of which can contribute to channel initiation. The proportion of convergent elements predicted to exceed the threshold varies greatly with relatively small changes in surface resistance, demonstrating a high sensitivity to land use such as cattle grazing. Overall, the landscape can be divided, using erosion threshold lines, into areas prone to channel instability due to runoff and stable areas where diffusive transport predominates.

INTRODUCTION

Although numerical models can create realistic-looking landscapes by generating ridge and valley topography (e.g., Ahnert, 1976; Kirkby, 1987; Howard, 1990; Willgoose et al., 1991), the three-dimensional form of ml landscapes and the processes shaping them are, surprisingly, not well quantified. The recent development of digital terrain models, however, permits quantitative analysis of actual landscapes and thus provides an opportunity to examine the relation between sediment transport processes and landscape form (e.g., Moore et al., 1988a, 1988b; Vertessey et al., 1990; Tarboton et al., 1991).

Herein we propose a graphical technique for characterizing real landscapes using digital elevation data to examine the application of erosion theories. We focus on a landscape where previous studies (Montgomery and Dietrich, 1988, 1989, 1992; Montgomery, 1991) have indicated that there is good evidence that threshold-based erosion models are appropriate. Field monitoring and mapping suggest that surface erosion leading to channel initiation occurs where a resistance to saturation overland flow (see Dunne, 1980), seepage erosion (see Dunne, 1990), or shallow landsliding is exceeded. These processes predominate in valleys, whereas on ridges the shallow soil is currently transported primarily by biogenic activity such as burrowing by gophers (Black and Montgomery, 1991), a process that perhaps can be treated as largely slope dependent. Although our analysis focuses on current runoff and erosion processes, our

results give insight into how erosion would vary with land use and climate change as well as what erosion lam appear appropriate for modeling long-term landscape evolution.

THRESHOLD THEORIES

We use three simple threshold equations to explore the relation between landform and current erosion. These equations predict a threshold condition for ground saturation, a threshold to landslide instability of the ground due to high pore pressures, and a threshold of erosion due to saturation overland flow. All three theories have been proposed in various forms by others. Here we write them in a form useful for analysis using a digital terrain model. Several simplifying assumptions are made to reduce the parameters to those that can be crudely estimated from field data and the proposed graphical analysis. These theories, however, are at the same general level of simplicity as those in most numerical models of landscape evolution. Specifically, we use a steady-state runoff model that assumes that runoff occurs as subsurface flow parallel to the ground surface during significant hydrologic events and that saturated conductivity and transmissivity of the soil mantle are spatially constant. (Despite large differences in soil thickness between ridges and unchanneled valleys, the saturated conductivity and, consequently, the transmissivity are dominated by highly conductive near-surface soil [Wilson, 1988; Montgomery, 1991].) We propose that steady-state runoff for an extreme event will mimic the spatial variation in surface saturation and overland flow that would occur in natural transient storm events responsible for saturation overland flow erosion and landsliding. We also assume that the vegetation and soil properties controlling surface resistance to erosion are spatially constant.

For steady-state, shallow subsurface runoff parallel to the ground surface, the ground will be saturated if the precipitation (minus evaporation and deeper drainage), q , times the area of the upslope catchment, a , equals or exceeds the maximum flux the surface layer can conduct, computed from the product of transmissivity, T , surface slope, M , and unit length of the contour across which the catchment is draining, b (O'Loughlin, 1986). Because of the steep slopes in the study area, M is calculated as the more physically correct sine of the ground-surface inclination, θ , rather than $\tan \theta$, as used by O'Loughlin (1986). The threshold of ground saturation can be expressed as:

$$\frac{a}{b} \geq \frac{T}{q} M \quad (1)$$

This simple hydrologic model has been used with good success to predict saturated zones and runoff response in the computer model TOPOG by O'Loughlin (1986) and by Moore et al. (1988a, 1988b). It is essentially the same model that underlies the widely used TOPMODEL by Beven and Kirkby (1979).

All parts of the landscape where the area per unit contour length, a/b , equals or exceeds the term on the right-hand side of equation 1 will be saturated. Note that if measured values from a landscape of a/b are

plotted against M , then equation 1 will be a straight line with a slope given by the hydrologic parameters T/q , and all points above this line will be saturated. This observation suggests that a useful analysis of digital elevation data is to divide the land surface into the small catchments for which the physical attributes a/b and M can be determined and plotted on such a graph. Other threshold criteria can be expressed as functions of these two physical characteristics.

A coupled hydrologic and slope stability model proposed by Dietrich et al. (1986) and subsequently modified and tested by Montgomery and Dietrich (1989) can be written as:

$$\frac{a}{b} \geq 2 \left(1 - \frac{\tan \theta}{\tan \phi} \right) \frac{T}{q} M. \quad (2)$$

Slope instability occurs where a/b equals or exceeds the term on the right-hand side, which varies with the ratio of ground surface, $\tan \theta$, to angle of internal friction, $\tan \phi$. Note that the hydrologic component of equation 2 is the same model as that which leads to equation 1 and that equation 2 uses a form of the infinite slope model that ignores strength contribution due to cohesion; i.e., at failure $\tan \theta = [(\rho_s - \rho_w m) / \rho_s] \phi$, where ρ_s and ρ_w are the soil and water bulk densities and m is the proportion of the soil that is saturated. Field data suggest that $(\rho_s - \rho_w) / \rho_s$ is -0.5. The hydrologic model is hydrostatic; hence, excessive pore pressures are not predicted and all slopes less than $0.5 \tan \phi$ are stable even if saturated.

Several authors have suggested that channel initiation by overland flow can be estimated by assuming that incision occurs where some critical boundary shear stress, τ_c , or some other measure of resistance is exceeded (e.g., Horton, 1945; Schaefer, 1979; Moore et al., 1988b; Vertessey et al.,

1990; Montgomery, 1991). In the steady-state model used here, saturation overland flow discharge is simply equal to $qa - Tmb$; i.e., water that cannot be carried as shallow subsurface flow must travel overland. This equation can be solved for the discharge that attains sufficient depth for a given slope to produce a boundary shear stress equal to the critical value for the surface. Letting $qa - Tmb = udb$, $\tau_c = \rho_w g d M$, $u = (2gdM)^{0.5} (f)^{-0.5}$, and $f = K\nu/ud$, the following threshold of erosion equation can be derived in the desired form:

$$\frac{a}{b} \geq \frac{\alpha}{qM^2} + \frac{T}{q} M. \quad (3)$$

Here $\alpha = 2 \times 10^{-4} \tau_c^3 K^{-1}$ and τ_c is the critical boundary shear stress, K is the roughness intercept for the inverse relation between friction factor, f , and Reynolds number (velocity, u , times depth, d , divided by the kinematic viscosity, ν that typifies laminar-like flow in grasslands (Dunne and Dietrich, 1980; Wilson, 1988; see review in Reid, 1989). Gravitational acceleration is g , and the numerical constant is for 10 °C water and has units of $(\text{cm-s})^5/\text{g}^3$.

DIGITAL TERRAIN MODEL ANALYSIS

We selected an area in the hilly grass and chaparral lands north of San Francisco where extensive mapping and hydrologic studies have been conducted (Wilson and Dietrich, 1987; Montgomery and Dietrich, 1988, 1989; Black and Montgomery, 1991; Montgomery, 1991). These studies have shown that saturation overland flow is common in the lower-gradient valleys, and most of the larger debris-flow scars originate at channel heads. Digital elevation data were obtained at a density of about every 10 m for the 1.21 km² catchment from stereo digitization of low-level black and

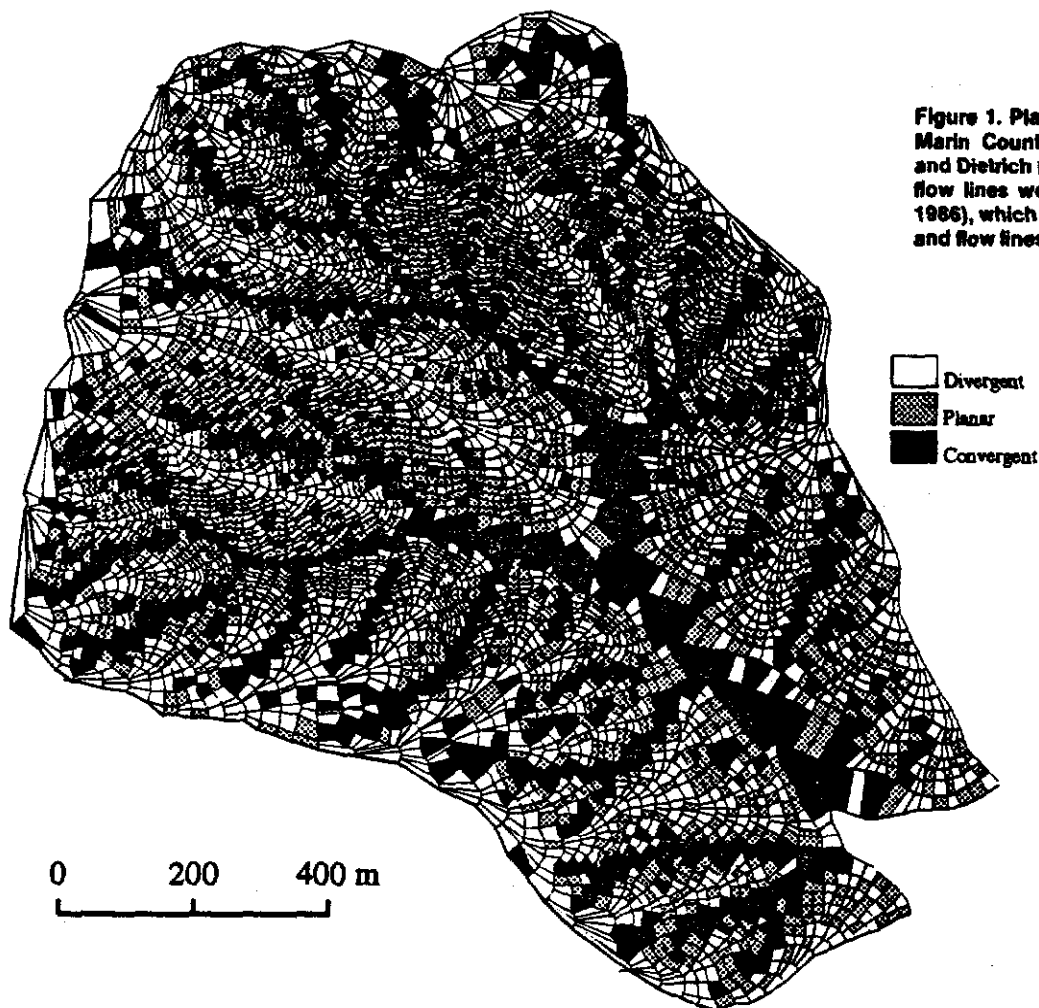


Figure 1. Planform analysis of 1.2 km² catchment in Marin County, California, studied by Montgomery and Dietrich (1989, 1992). Topographic contours and flow lines were generated by TOPOG (O'Loughlin, 1986), which in this case gives contour interval of 5 m and flow lines - 20 m apart. Element types are shown.

while aerial photographs; several mapped ground features were used to control the registration of digital coordinates. Taking advantage of the clear ground visibility, we selected data points to capture topographic change rather than to follow a regular grid. The digital elevation model component of TOPOG (O'Loughlin, 1986) was then used to construct digital surfaces. A second program in TOPOG divides the surface by drawing the equivalent of flow lines across the contours from valley bottoms to divides at a user-specified interval (see O'Loughlin, 1986, for examples). The program draws flow lines starting at low elevations and projects upslope, so contour length separating flow lines tend to narrow on topographically divergent slopes. Individual elements defined by a pair of contour lines on the upslope and downslope sides of the element and a pair of streamlines on the lateral boundaries (Fig. 1) are thus created.

For each element, the total contributing area, a , can be calculated and the ratio a/b determined from the bottom contour length of the element. The local slope between the two contour lines making up the element is also determined. Each element shape was classified as convergent, planar, or divergent, according to the difference in length of the upslope, b_1 , and downslope contour length, b_2 , of the element; i.e., whether the ratio $(b_2 - b_1)/(b_2 + b_1)$ exceeded a set percentage change. This percentage is somewhat arbitrary. We chose the smallest values estimated to be relatively free of artifacts of the model (< -0.10 is convergent, > 0.10 is divergent, other-

wise planar). These values clearly delineated the convergent valley axes in the landscape (Fig. 1). In addition, we did detailed field mapping of the current extent of the channel network to classify those elements (always convergent) that contained a channel.

Figure 2 shows the data field for each element type as a function of specific catchment (a/b) and local slope ($\tan \theta$) for a 5 m contour interval and 20 m interval between flow lines. For a given slope, the channel elements drain the largest specific catchment, whereas the divergent elements drain the smallest. There is very little overlap between divergent and convergent element data fields and essentially none between divergent and channel elements. These differences are much larger than that which might be created by the definition of element types. Comparison of the data fields for different contour intervals and flow-line spacing shows that there are some artifacts in Figure 2. The apparent log-linear data in the divergent elements are a portion of the triangular-shaped elements created at divides by diverging flow lines. They have no physical relation to each other, and although they are purely an artifact of the analysis, they still describe aspects of the divergent topography and so were retained. For planar elements, the minimum size of the elements varies with slope as controlled by the contour spacing (5 m in this use), hence a/b (minimum) = $5/\tan \theta$, and no points plot below this value in Figure 2. Reducing the contour spacing and the flow-line spacing, however, had negligible effect on the

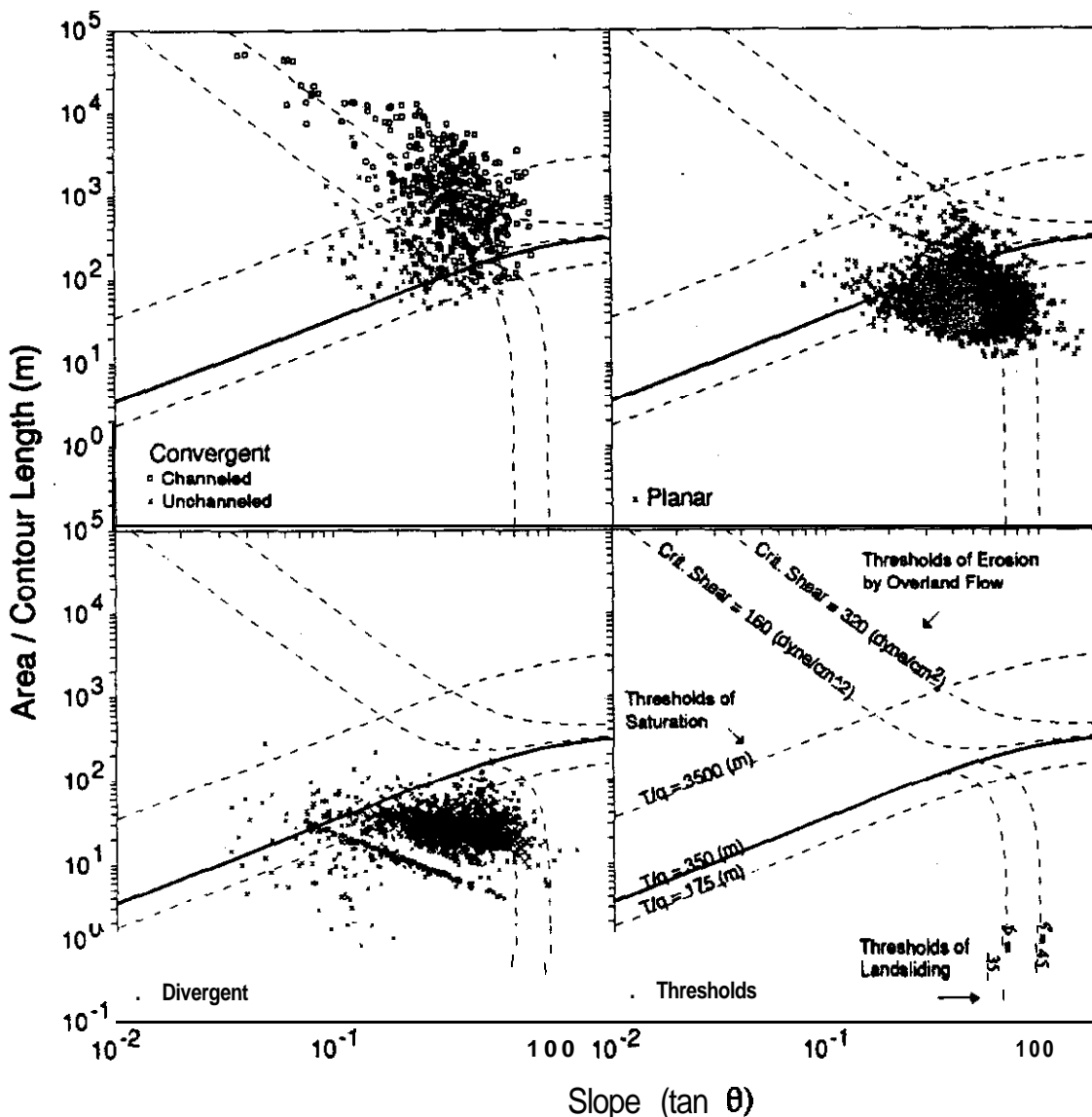


Figure 2. Plot of element topographic properties and comparison of threshold lines with data fields. Channeled elements were identified on basis of field observations. Solid line represents threshold of saturation consistent with field data.

general distribution of the data. Furthermore, we found that grid-digital terrain model developed by one of us (Bauer) also produced very similar results.

LANDFORM AND PROCESS THRESHOLDS

In order to apply the threshold equations 1-3, the parameters controlling their predictions must be estimated. This problem is more constrained than may at first be apparent. We know from field work in this area during major runoff events (Wilson and Dietrich, 1987; Montgomery, 1991) that extensive saturation overland flow does not occur on divergent and planar slopes. We have seen exceptions, but they are of local extent only. This allows us to vary the hydrologic ratio, T/q , and note where the line of saturation crosses the various topographic elements (see thresholds box and the " comparison with data in other boxes; Fig. 2). Note that T/q of 350 m dips just the top of the divergent and planar elements. Conversely, we would expect most of the channel elements to be saturated during an extreme event, and, as expected, the line with T/q of 350 m lies below most of the elements; halving this value adds few more channel elements but cuts deeply across the divergent element field. We have observed saturation overland flow extend up to nearly the divide in this area in common storms; it is therefore realistic to predict that nearly all of the convergent elements will saturate in a major storm. On the basis of previous studies (Wilson, 1988), the transmissivity is largely controlled at saturation by the high conductivity of the near-surface soils, apparently differing little between nose and hollow. We estimate this value to be $17 \text{ m}^2/\text{d}$, which indicates that for a T/q of 350 m, the q is equal to 5 cm/d of precipitation or runoff. According to the analytical procedure of Iida (1984), it would take about 9 d for a 59-m-long planar slope to reach steady state with this estimated transmissivity and rainfall; a storm of about this magnitude (45 cm) and duration occurred here in 1986 (Wilson, 1988).

With T/q defined, the only remaining parameter in equation 2 is the angle of internal friction; previous studies indicate that this value may commonly be as high as 45° (Reneau et al., 1984). This stability analysis ignores the contribution of apparent cohesion from root strength. In Figure 2, the slope stability threshold line is plotted for values of ϕ equal to 35° and 45° . The number of elements predicted to fail is greatly increased with the diminished friction angle, including many divergent elements. This is inconsistent with field observations in which shallow soil landslides are mostly in convergent zones. Decreasing T/q tends to overpredict the number of planar elements in which failure might be expected. Preliminary field mapping indicates that all but 5 of the 39 shallow landslide scars currently visible in the study area lie above the predicted threshold line for a T/q of 350 m and $\phi = 40^\circ$. Hence, the position of the slope stability curve is reasonably well defined. This curve lies on the outer edge of the data fields, suggesting that this stability criterion imposes a physical limit on hillslope morphology, as traditionally argued from simpler analyses (i.e., Strahler, 1950). The steeper channel and convergent elements lie above the threshold line of slope stability; this is consistent with field observations.

The saturation overland flow erosion threshold given in equation 3 requires estimates of K , τ_c , and q for a specified T/q and water temperature (which sets the value of ν). Measurements at times of significant overland flow at a nearby grassland site document that K is about 10000 for well-vegetated surfaces (Wilson, 1988, p. 109) and that shear stresses in excess of 200 dyne/cm² generated by this flow did not cause measurable incision into the vegetated areas. High runoff events, however, have caused scour in the unvegetated tips of the channel networks. Reid (1989), in a thorough review of critical shear stress values, showed that τ_c must exceed 1000 dyne/cm² to incise a well-vegetated mat, whereas values of 250 to 500 dyne/cm² are sufficient to incise the underlying soils. If τ_c

were 1000 dyne/cm², for a threshold line defined by equation 3 to separate channeled from unchanneled elements, q would have to be $\sim 1.5 \text{ m/d}$, clearly a " impossibility. As argued by Reid (1989), channel initiation in grasslands is likely to occur where local barren areas caused by fire, trampling, or other effects reduce the critical shear stress to the underlying valve of the soil.

Figure 2 shows the position of threshold lines for a τ_c of 160 dyne/cm² and 320 dyne/cm² for q of 5 cm/d (appropriate for $T/q = 350 \text{ m}$ and $T = 17.5 \text{ m}^2/\text{d}$). Given the observed roughness value, τ_c and q are constrained by the threshold relation required to separate channeled from unchanneled elements. The critical shear stress cannot be significantly different from 160 to 320 dyne/cm² without requiring either too great or too small a precipitation rate. Note that, as indicated in equation 3, a doubling of critical boundary shear stress is equivalent to decreasing precipitation or K by a factor of 8. Such a doubling greatly alters the location of this erosion threshold line and raises questions concerning the worth of trying to measure a parameter in the field, the value of which is so difficult to estimate but so greatly affects the pattern of channelization. This analysis also shows, however, how land use practices or climate change that only modestly alter surface resistance (τ_c) could lead to a great expansion of the channel network into previously unchanneled elements. Such an expansion due to the introduction of cattle grazing and presumed reduction in surface resistance has been proposed for this area by Montgomery and Dietrich (1989) and Montgomery (1991). The inverse dependence of the erosion threshold on precipitation is also consistent with the proposal by Reneau et al. (1986) and Montgomery (1991) that drying and warming of this area from the Pleistocene into the Holocene caused channel heads to retreat downslope.

In Figure 3, stability fields generated by the combination of equations 1 through 3 are labeled with the dominant hydrologic and erosion processes. Simple field observations constrain the threshold of saturation and

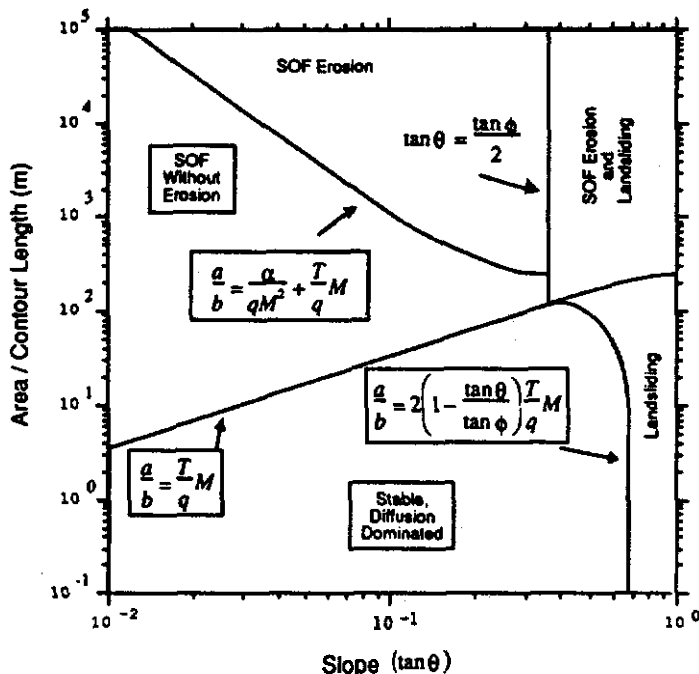


Figure 3. Definition of stability fields using threshold lines for case of $T/q = 350 \text{ m}$, $\phi = 35^\circ$, $K = 10000$, critical shear stress = 160 dyne/cm², and $q = 0.06 \text{ m/d}$. SOF is saturation overland flow and SOF erosion means erosion by " alutlo" overland flow. Shaded region is below threshold of erosion by either saturation overland flow or landsliding.

slope stability liner and lead to the interpretation that a significant proportion of the landscape, nearly all the divergent elements, most of the planar, and some of the convergent ones, are currently stable or resistant to surface erosion due to runoff. In this region below the erosion threshold lines (shaded region in Fig. 3), surface transport is currently dominated by the slop-driven (diffusive) processes of soil creep, rain splash, and biogenic disturbance. The area labeled "YOF Without Erosion" mostly includes elements lying in unchanneled valleys currently collecting colluvium (but which in the long term undergo periodic erosion, apparently driven by climatic change [Reneau et al., 1986]). Hence, this graph shows a new way to analyze the entirety of landscapes to define quantitatively the spatial variation in the dominance of different erosion processes in a catchment. An analysis of this kind should also be a useful tool in constructing sediment budgets for catchments, when the spatial distribution of dominant transport processes must be ascertained (i.e., Dietrich and Dunne, 1978; Dietrich et al., 1982; Reid, 1989).

CONCLUSIONS

The plotting of discrete elements of landscapes separated by planform on a graph of the two topographic variables that control runoff and erosion (area per unit contour width and surface gradient) provides a powerful means to evaluate hydrologic and erosional hypotheses about real landscapes. This analysis and the parallel study reported by Montgomery and Dietrich (1992) on the relation between position of the channel head and landscape scale add considerable support to the Horton hypothesis of a threshold control on surface instability leading to channel development (Horton, 1945). The simple, steady-state, hydrologic models employed here could be made more realistic by using a transient model, but this introduces more parameters, and at least for the problem of examining the relations between form and erosion thresholds, it is not clear that the transient model is essential to the outcome. The threshold theories are similar to those used to model landscape evolution; the analysis performed here suggests a procedure to evaluate transport laws used in numerical models. The plotting of threshold lines on a data field of a/b vs. M is an instructive procedure for examining the possible effects of land use and climatic change.

REFERENCES CITED

- Ahnert, F., 1976, Brief description of a comprehensive three-dimensional process-response model of landform development: *Zeitschrift für Geomorphologie*, Supplement Band 25, p. 25-49.
- Beven, K., and Kirkby, M.J., 1979, A physically based variable contributing area model of basin hydrology: *Hydrological Sciences Bulletin*, v. 24, p. 43-69.
- Black, T., and Montgomery, D.R., 1991, Sediment transport by burrowing mammals, Marin County, California: *Earth Surface Processes and Landforms*, v. 16, p. 163-172.
- Dietrich, W.E., and Dunne, T., 1978, Sediment budget for a small catchment in mountainous terrain: *Zeitschrift für Geomorphologie*, Supplement Band 29, p. 191-206.
- Dietrich, W.E., Dunne, T., Humphrey, N.F., and Reid, L.M., 1982, Construction of sediment budgets for drainage basins, in Swanson, F.J., et al., eds., *Sediment budgets and routing in forested drainage basins*: Portland, Oregon, US Department of Agriculture Forest Service General Technical Report PNW-141, Pacific Northwest Forest and Range Experiment Station, p. 5-23.
- Dietrich, W.E., Wilson, C.J., and Reneau, S.L., 1986, Hollows, colluvium, and landslides in soil-mantled landscapes, in Abrahams, A.D., ed., *Hillslope processes*: London, Allen and Unwin, p. 361-388.
- Dunne, T., 1980, Formation and controls of channel networks: *Progress in Physical Geography*, v. 4, p. 211-239.
- Dunne, T., 1990, Hydrology, mechanics and geomorphic implications of erosion by subsurface flow, in Higgins, C.G., and Coates, D.R., eds., *Groundwater geomorphology: The role of subsurface water in Earth-surface processes and landforms*: Geological Society of America Special Paper 252, p. 1-28.
- Dunne, T., and Dietrich, W.E., 1980, Experimental study of Horton overland flow on tropical hillslopes; 1. Soil conditions, infiltration and frequency of runoff. 2. Hydraulic characteristics and hillslope hydrographs: *Zeitschrift für Geomorphologie*, Supplement Band 35, p. 40-80.
- Howard, A., 1990, Prospects for simulation modelling of valley networks on Mars: *Planetary Geology and Geophysics Program Report*, NASA TM 4211, p. 348-350.
- Horton, R.E., 1945, Erosional development of streams and their drainage basin: hydrophysical approach to quantitative morphology: *Geological Society of America Bulletin*, v. 56, p. 275-370.
- Iida, T., 1984, A hydrological method of estimation of the topographic effect on the saturated throughflow: *Japanese Geomorphological Union Transactions*, v. 5, p. 1-17.
- Kirkby, M.J., 1987, Modelling some influences of soil erosion, landslides and valley gradient on drainage density and hollow development, in Ahnert, F., ed., *Geomorphological models: Catena*, Supplement 10, p. 1-11.
- Montgomery, D.R., 1991, Channel initiation and landscape evolution [Ph.D. thesis]: Berkeley, University of California, 421 p.
- Montgomery, D.R., and Dietrich, W.E., 1988, Where do channels begin?: *Nature*, v. 336, p. 232-234.
- Montgomery, D.R., and Dietrich, W.E., 1989, Source areas, drainage density and channel initiation: *Water Resources Research*, v. 25, p. 1907-1918.
- Montgomery, D.R., and Dietrich, W.E., 1992, Channel initiation and the problem of landscape scale: *Science*, v. 255, p. 826-830.
- Moore, I.D., O'Loughlin, E.M., and Burch, G.J., 1988a, A contour-based topographic model for hydrological and ecological applications: *Earth Surface Processes and Landforms*, v. 13, p. 305-320.
- Moore, I.D., Burch, G.J., and Mackenzie, D.H., 1988b, Topographic effects on the distribution of surface soil water and location of ephemeral gullies: *American Society of Agricultural Engineers Transactions*, v. 31, p. 1098-1107.
- O'Loughlin, E.M., 1986, Prediction of surface saturation zones in natural catchments by topographic analysis: *Water Resources Research*, v. 22, p. 794-804.
- Reid, L.U., 1989, Channel incision by surface runoff in grassland catchments [Ph.D. thesis]: Seattle, University of Washington, 135 p.
- Reneau, S.L., Dietrich, W.E., Wilson, C.J., and Rogers, J.D., 1984, Colluvial deposits and associated landslides in the northern S.F. Bay Area, California, USA, in *N International Symposium on Landslides*, Toronto: Downsview, Ontario, Canadian Geotechnical Society, p. 425-430.
- Reneau, S.L., Dietrich, W.E., Dorn, R.I., Berger, C.R., and Rubin, M., 1986, Geomorphic and paleoclimatic implications of latest Pleistocene radiocarbon dates from colluvium-mantled hollows, California: *Geology*, v. 14, p. 655-661.
- Schaefer, M.G., 1979, The zero order watershed [Ph.D. thesis]: Rolla, University of Missouri, 69 p.
- Strahler, A.N., 1950, Equilibrium theory of erosional slopes approached by frequency distribution analysis: *American Journal of Science*, v. 248, p. 673-696, 800-814.
- Tarboton, D.G., Bras, R.L., and Rodriguez-Iturbe, I., 1991, On the extraction of channel networks from digital elevation data: *Hydrological Processes*, v. 5, p. 81-100.
- Vertessy, R.A., Wilson, C.J., Silburn, D.M., Connolly, R.D., and Ciesiolka, C.A., 1990, Predicting erosion hazard areas using digital terrain analysis: IAHS-AISH Publication 192, p. 298-308.
- Willgoose, G.R., Bras, R.L., and Rodriguez-Iturbe, I., 1991, A coupled channel network growth and hillslope evolution model: *Water Resources Research*, v. 27, p. 1671-1702.
- Wilson, C.J., 1988, Runoff and pore pressure development in hollows [Ph.D. thesis]: Berkeley, University of California, 284 p.
- Wilson, C.J., and Dietrich, W.E., 1987, The contribution of bedrock groundwater flow to storm runoff and high pore pressure development in hollows: IAHS-AISH Publication 165, p. 49-59.

ACKNOWLEDGMENTS

Supported by National Science Foundation grant EAR-891 7467, Washington State Department of Natural Resources grant TFW-FY92-010, and the Australian Center for Catchment Hydrology (Wilson). We thank the U.S. Department of Agriculture Forest Service, Pacific Southwest Region, engineering staff for providing access to an analytical stereo plotter for generating the digital elevation data. Rob Reiss played a crucial role in running TOPOG and generating plots, and Keith Loughe and Bob Anderson provided useful reviews.

Manuscript received January 3, 1992
 Revised manuscript received April 15, 1992
 Manuscript accepted April 22, 1992

Analysis of Erosion Thresholds, Channel Networks, and Landscape Morphology Using a Digital Terrain Model¹

William E. Dietrich, Cathy J. Wilson², David R. Montgomery³, and James McKean
Department of Geology and Geophysics, University of California, Berkeley, CA 94720

ABSTRACT

To investigate the linkage between erosion process and channel network extent, we develop **two** simple erosion threshold theories driven by a steady state runoff model that are used in the digital terrain model TOPOG to predict the pattern of **channelization**. TOPOG divides the land surface into elements **defined** by topographic contours and flow lines, which can be classified as divergent, convergent and planar elements. The calibration parameter for the runoff model is determined using empirical evidence that the divergent elements which comprise **the** ridges in **our** study area do not experience saturation overland flow, where as the convergent elements in the valleys do **during** significant runoff events. A threshold theory for shallow landsliding predicts a pattern of instability consistent with the distribution of landslide scars in our 1.2 **km²** study site and confirms the interpretation, based on field observations, that indicate the steeper channel heads **to** be at least partially controlled by slope instability. **Most** sites of predicted and observed slope instability do not, however, support a channel head, hence landslide instability alone is not sufficient for **channelization**. In contrast, most elements predicted **to** be eroded by saturation overland flow **coincide** with the observed location of the channel **network**. In addition, areas of predicted downslope decrease in relative sediment transport capacity were found **to** correspond to locations where channels became discontinuous. The topographic threshold given by the saturation overland flow erosion theory varies with the third power of critical boundary shear **stress, suggesting** that critical shear **stress**, although difficult to quantify with much precision in the field, is a dominant control on the **extent** of the channel network where saturation overland flow is significant. **Current** extent of the channel network in our field site, for example, may best be explained as resulting from grazing-induced reduction in surface resistance.

Introduction

Landscape dissection is controlled by **the tendency** for runoff to **channelize** into avenues of concentrated erosion (e.g., Horton 1945; Smith and Bretherton 1972). Field studies have revealed that the **upslope extent** of the channel network may be well defined by an inverse relationship between drainage area and slope (Montgomery and Dietrich 1988, 1989, 1992). These studies have also shown that at the channel head, there is typically a process change, **upslope** of which mass wasting and diffusive processes predominate and downslope of which runoff-driven incision occurs (e.g., Dietrich and Dunne 1993). Hence, in a **given catchment**,

there appears to be a threshold of erosion resistance which sets the location of a channel head at a specific drainage area and local slope, and therefore **determines the extent of the channel network in a watershed**. This concept has been explored in a landscape evolution model by Willgoose et al. (1991).

Acquisition of high-resolution digital elevation data allows a comparison between the location of channel networks mapped in the field and networks predicted by process-based theories. Other than the comparison between predicted and observed ephemeral gullies in an agricultural field by Moore et al. (1988a), however, we know of no such studies. Numerical models can convert the elevation data into a digital surface upon which water and sediment **can** be routed. At **present**, however, digital elevation data, even at very high resolution (say 1 m grid spacing) are **too sparse** to capture the local topography around typical small channel

¹ Manuscript received October 19, 1992; accepted December 1, 1992.

² Australian Center for Catchment Hydrology, CSIRO, Canberra, ACT 2601, Australia.

³ Department of Geological Sciences, University of Washington, Seattle, WA 98195.

heads, which often are only decimeters in size at their tips. Process-based models for channel networks, then, are best thought of as attempting to **define** where in the landscape there would be a tendency for erosion to **channelize**, rather than as attempting to predict the size and downstream topographic evolution of discrete channels that collect to form the network.

In this paper we build upon a recent study (Dietrich et al. 1992) to propose two simple threshold of erosion models that, based on field observations, appear appropriate for explaining channel initiation in a small watershed where the full extent of the channel network has been mapped. We develop these theories in a form which can be easily tested using digital elevation data and a simple hydrologic routing model. Our analysis suggests that both the **upslope** extent and discontinuous nature of the channel network in our field area in **Marin** County, California, can be explained primarily by saturation overland flow erosion. Shallow **landsliding**, while active at **many** of the steeper channel heads, also occurs in areas that do not have sufficient runoff to maintain a downslope channel. Hence landsliding does not uniquely **define** channel-head locations. The mechanistic analysis proposed here, although crude, does strongly suggest how the channel network in our study area has responded to climatic change and **landuse**. It also leads to further testable hypotheses regarding erosion thresholds.

Theory

Three simple theories for predicting runoff, slope instability, and erosion by saturation **overland flow**. Although these theories were reported by Dietrich et al. (1992), their derivations were not given. These theories are developed here in a form to take advantage of two topographic attributes easily determined from digital elevation data: drainage area per unit contour length, and local ground slope.

Runoff Model. In well-vegetated semi-arid to humid landscapes where precipitation intensity does not exceed the soil **infiltration** capacity, runoff occurs by subsurface and saturation overland flow (e.g., Dunne 1978). Erosion thresholds will be crossed **during** precipitation events that elevate pore pressures associated with subsurface flow to the point of mass failure of the ground or where subsurface flow returns to the surface and combines with incoming precipitation to generate saturation overland flow of sufficient depth to cause surface incision of the ground. On exposed cuts

such as in channel heads, seepage erosion may require a critical hydraulic gradient to displace surface materials (Dunne 1990; Montgomery 1991, but this process will not be considered here.

Although erosion events are clearly driven by storms of varying intensity and duration that occur on watersheds of seasonally varying antecedent conditions, the modeling of such unsteady rainfall-runoff processes **introduces** considerable complexity and several calibration parameters for which spatial and temporal variability is difficult to **define**. Given that we can only ask whether a particular place in a landscape is likely to experience hydrologic conditions favorable for a threshold of erosion to be exceeded, rather than make specific predictions about the size and dynamics of individual channels, it seems appropriate to keep the hydrologic driving function as simple as possible, while still retaining the essential physics. Here we use a steady-state runoff model that can **be** interpreted as mimicking the topographic dependence of runoff during transient storm events. This makes evaluation of the predicted storm runoff difficult, but we suggest that the landscape topography itself places some constraint on the magnitude of the saturated flow response. We will also assume that transmissivity, saturated conductivity, and the ground resistance to **runoff** and erosion are spatially constant.

Following the formulation proposed by O'Loughlin (1986) for subsurface flow, we can write the conservation of mass for steady-state, shallow subsurface flow and saturation overland flow as follows:

$$qa - TMb = udb. \quad (1)$$

As shown in figure 1, a is the catchment draining across a contour of length, b . The total runoff per unit area, q , is equal to the precipitation, p , minus the evaporation, e , minus deep drainage, r , i.e., ($q = p - e - r$). As O'Loughlin (1986) correctly points out, even in the steady-state case, p , e , and r need not be spatially constant, although we assume so here. The shallow subsurface flow modeled here is assumed to flow parallel to the ground surface and at saturation is equal to the **transmissivity**, T , times the surface slope, M , times the contour **length**, b . Here M **equals** sine. Runoff that cannot **be** transmitted in the subsurface must travel overland, and does so with a mean velocity of u for a depth, d , **across the contour** length, b . Hence, equation (1) simply states that the difference between the total runoff and the saturated

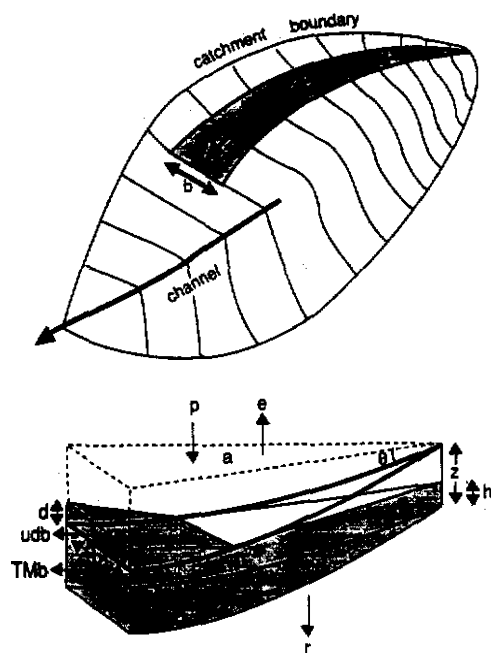


Figure 1. Plan view and cross section of area draining across the contour length, b , as defined by "flow lines" generated by the program TOPOG (O'Loughlin 19861). In the cross section, the heavy line depicts the ground surface. The stippled area is the shallow subsurface flow and saturation overland flow with discharge of Tmb and udb , respectively. Here q equals precipitation, p , minus evaporation, e , and deep drainage, r ; a is drainage area, h , z , and d [measured normal to the ground surface], are the thickness of the subsurface saturated flow, thickness of the potentially unstable mass, and thickness of the saturation overland flow, and u is the mean overland flow velocity parallel to the ground surface. T is the transmissivity and M is $\sin \theta$.

subsurface flow is the overland flow at steady-state conditions.

According to equation (1), the ground will saturate everywhere that these conditions hold:

$$\frac{a}{b} \geq \frac{T}{q} M. \quad (2)$$

Equation (2) can be rearranged to state that where the topographic ratio, $a/(bM)$, is greater than or equal to the hydrologic ratio, T/q , the ground will saturate. In essence, $a/(bM)$ is the topographic term that expresses the tendency for flow convergence (high a/b) and for the flow to travel quickly as shallow subsurface flow (large M) rather than as saturation overland flow (small M). Large areas draining to gentle slopes (i.e., where this ratio is large) are prone to saturation. The hydrologic ratio, T/q , can be thought of as the ability of the subsurface to transmit flow relative to the applied runoff.

Hence, where this ratio is small, the ground tends to saturate.

If the hydrologic parameter, T/q , is roughly spatially constant for a given storm, then a survey of the upslope extent of saturation at points throughout a watershed should find these points having the same value of $a/(bM)$ (e.g., Kirkby 1978; Beven and Kirkby 1979). Equation (2), when used in combination with knowledge of the landscape form derived from a digital elevation model, will also prove useful in establishing the value of T/q , as discussed later.

Slope Stability Threshold. Shallow landsliding occurs when pore water pressure reduces the frictional strength of the soil to the point where the shear stress due to the downslope weight of the soil exceeds the strength. We assume that the zone of shallow surface storm runoff is confined to a cohesionless (at failure) soil overlying a less conductive, but stronger bedrock. Hence, in figure 1, z defines not only the maximum thickness of shallow surface flow, but also the thickness of the shallow, potentially unstable surface layer. The ground does not have to be saturated for failure to occur; hence the local thickness of saturated flow, h , can be less than or equal to z . If $T = Kz \cos \theta$, in which K is the saturated conductivity, then for subsurface flows equal to or less than saturated, the ratio of the actual runoff to maximum subsurface flow is:

$$\frac{qa}{bTM} = \frac{K \sin \theta h \cos \theta}{K \sin \theta z \cos \theta} = \frac{h}{z} \quad (3)$$

Because our hydrologic model assumes flow parallel to the ground surface, excessive pore pressure associated with exfiltrating gradients cannot be modeled. The thickness of the saturated zone required to convey the imposed runoff varies from a small value up to z , the thickness of the conducting layer; hence h/z varies from nearly zero to 1.0.

For cohesionless material, the infinite slope stability model can be written as:

$$\rho_s z \tan \theta = (\rho_s z - \rho_w h) \tan \phi$$

and with substitution of equation (3) for h/z this becomes:

$$\frac{a}{b} \geq \frac{\rho_s}{\rho_w} \left(1 - \frac{\tan \theta}{\tan \phi} \right) \frac{T}{q} M. \quad (4)$$

This states that instability will occur when the area per unit contour length is greater than or equal to the product of four terms: the bulk density ratio

of wet soil (ρ_s) to water (ρ_w), the ratio of the tangent of the ground surface to the angle of internal friction ($\tan \phi$), the hydrologic ratio (T/q), and the ground slope ($\sin \theta$). Although it would be more realistic to include a cohesion term in equation (4), this requires additional information about soil depth, or at least the depth of rooting. Again, for simplicity, here the contribution of cohesion is neglected. Because of the condition of flow parallel to the ground surface, slopes greater than or equal to the friction angle are chronically unstable and would be in areas where bedrock is exposed. Also, for slopes with $\tan \theta \leq [(\rho_s z - \rho_w h)/(\rho_s z)] \tan \phi$, the ground is stable even if saturated.

Threshold of Erosion by Saturation Overland Flow. In general, we can write the conservation of mass equation for erosion due to sediment transport as:

$$\nabla \cdot \vec{q}_s = -\rho_s \frac{\partial z}{\partial t}$$

in which \vec{q}_s is the sediment transport vector, ρ_s is the dry bulk density of the soil surface, t is time, and z is the local elevation of the ground surface. Sediment transport by running water varies in proportion to boundary shear stress (e.g., Slattery and Bryan 1992; Dunne 1991); therefore divergence of the boundary shear stress [in excess of some critical value] will induce erosion. The threshold of erosion by overland flow, however, is not necessarily equivalent to the threshold of channel incision by that flow. This was clearly the case in rill incision on both an unvegetated surface (i.e., Slattery and Bryan 1992), and on poorly vegetated surfaces (Dunne and Aubrey 1986). Dunne (1980) has argued that one reason for this stability, at least in coarser sediments, is the diffusive behavior of rain-splash transport in shallow sheet flow, which would tend to damp the tendency for the flow to incise. Based on flume experiments in somewhat cohesive materials, there is evidence that although the lateral instability of the flow develops, it does not cut a channel (or rill) until the flow has become approximately supercritical and causes the formation of an upslope propagating knickpoint (Slattery and Bryan 1992).

Because of the high resistance to surface erosion in the well-vegetated areas where saturation overland flow occurs and the resulting significant flow depth needed to generate boundary shear stress to cause sediment transport, we will assume that once a critical boundary shear stress (τ_c) is exceeded, the flow will incise and form a channel. This is particularly true where the surface, due to

roots, stems and decayed organic matter, is considerably more resistant than the immediate subsurface. As long as the actual relationship between boundary shear stress (τ_b) and sediment transport rate is strongly non-linear, as might be expected in this case, the characterization of the surface as having a threshold boundary shear stress is reasonable. If we also assume that sediment transport, q_s , is proportional to an excess boundary shear stress, as is usually shown for sand and coarser material (e.g., Yalin 1972), then

$$q_s \propto (\tau_b - \tau_c)^n$$

and channels would be expected to form when ($\tau_b \geq \tau_c$) and tend to thin and disappear if $[\partial(\tau_b - \tau_c)^n / \partial x] < 0$. On poor- to well-vegetated surfaces, the availability of sediment for transport is limited, so the actual transport rate will be well below the transport capacity estimated from an excess boundary shear stress equation. Nonetheless, we propose that the tendency for scour or deposition will still respond to spatial change in excess of shear stress.

Boundary shear stress in nonaccelerating flows can be written as:

$$\tau_b = \rho_w g d M. \quad (5)$$

Gravitational acceleration, g , and fluid density, ρ_w , are known, and the local slope can be determined from a sufficiently high-resolution digital elevation model. The flow depth must be calculated based on runoff rate and surface roughness. Rewriting equation (1) to solve for flow depth,

$$d = \frac{1}{ub} (qa - TMb),$$

multiplying each side by $\rho_w g M$, and substituting into (5), gives

$$\tau_b = \frac{\rho_w g M}{ub} (qa - TMb). \quad (6)$$

To eliminate the velocity term in (6), we use a form of the Darcy-Weisbach equation often employed in overland flow studies (e.g., Dunne and Dietrich 1980),

$$u = \left(\frac{2gdM}{f} \right)^{0.5}. \quad (7)$$

For turbulent flow the friction factor, f , is constant but for laminar flow the friction factor varies in-

versely with Reynolds number, i.e., $f = Kv/ud$ in which ν is the kinematic viscosity and K is a constant for a given roughness condition. Using the frictional relationship given in equation (7), the boundary shear stress for turbulent flow is

$$\tau_b = \rho_w[Mg]^{2/3} \left(\frac{f}{2}\right)^{1/3} \left(q\frac{a}{b} - TM\right)^{2/3}, \quad (8)$$

whereas for **laminar** flow

$$\tau_b = \rho_w[Mg]^{2/3} \left(\frac{Kv}{2}\right)^{1/3} \left(q\frac{a}{b} - TM\right)^{1/3}. \quad (9)$$

Setting equations (8) and (9) equal to the critical shear stress and solving for the topographic condition where the critical shear stress is equaled or exceeded gives

$$\frac{a}{b} \geq \frac{1.41 \tau_c^{3/2}}{\rho_w^{3/2} g M f^2 q} + \frac{T}{q} M \quad (10)$$

for turbulent flow and

$$\frac{a}{b} \geq \frac{2 \tau_c^3}{\rho_w^3 K v g^2 M^2 q} + \frac{T}{q} M \quad (11)$$

for laminar flow.

This analysis shows that if channel initiation by saturation overland flow can be characterized as occurring once a critical boundary shear stress is exceeded, then the area per unit contour length up slope of the channel varies with critical shear stress and inversely with roughness, precipitation and, if critical shear stress is sufficiently large, inversely with ground slope. If the critical shear stress is very small, then equations (10) and (11) reduce to equation (2), that is, channel initiation is equivalent to ground saturation. Montgomery (1991) has suggested that in some instances ground saturation may be the appropriate criteria for channel head advance by seepage erosion. In this case, channel incision might result from saturation overland flow draining a large area, but once incision has occurred, seepage erosion advances the channel head **upslope** to the point where the ground does not saturate.

Field Site

To test the application of the **runoff** and erosion thresholds, we selected a field site where extensive mapping and process studies have been conducted

(**figure 2**). The general area, known as Tennessee Valley, lies north of San Francisco in **Marin** County, California, and is underlain by intensely deformed **greywacke**, **chert**, and **greenstone** (Wahrhaftig 1984). The ground is mostly soil-mantled, with the gravelly soil typically thin (<1 m) on side slopes and ridge tops and **thickening** to several meters in the colluvial fills in the valley axes. Local bedrock outcrops occur on some ridges and on steep slopes. The climate is Mediterranean with an average annual precipitation of about 760 mm (Rantz 1968). Vegetation varies with topographic position and aspect, with native and European grasses covering many of the ridgetops and gentler side slopes, and dense stands of coyote brush mixed with locally impenetrable poison oak occurring in many of the hollows and the steep side slopes in narrow canyons. The area was grazed by cattle from the early 1800s until about 1981; this grazing apparently increased the area of grass relative to brush and, when it was most heavily **grazed** in the late 19th century, the grass cover was probably greatly reduced relative to the present condition (Montgomery 1991).

The channel network mapped in the field [Montgomery and Dietrich 1989] is shown in **figure 2**. Channels extend up to and often through convergent **areas** of thick colluvial deposits. The channels in the steep canyons have bedrock floors. In the main valley the channel is incised into a broad, several meter thick deposit of alluvium and colluvium. Radiocarbon dating in this **area** (Montgomery 1991), and elsewhere in the Bay area (Reneau et al. 1991) indicates that the **aggradation** of colluvium and alluvium here took place during the Holocene. A **variety** of direct and indirect evidence, gathered from historical accounts, recovered artifacts, and aerial photographs indicates that the channel in the main valley cut down and **formed** a terrace about 100 **yrs** ago **during** the **period** of most intense grazing and that many of the tributary channels were either formed or extended into the **upslope** colluvium at this time (Montgomery 1991).

As reported by Montgomery and Dietrich (1988, 1989, 1992), the drainage area to the mapped channel heads systematically decreases with increasing local slope (**figure 3**). For any particular slope, contributing area to the observed **channeled** heads ranges about one order of magnitude. The data for **channeled** and **unchanneled** valleys below and above the **channel** head suggest that the channel heads lie at a topographic threshold (**figure 3**), as might be expected **from** the threshold theories presented above.

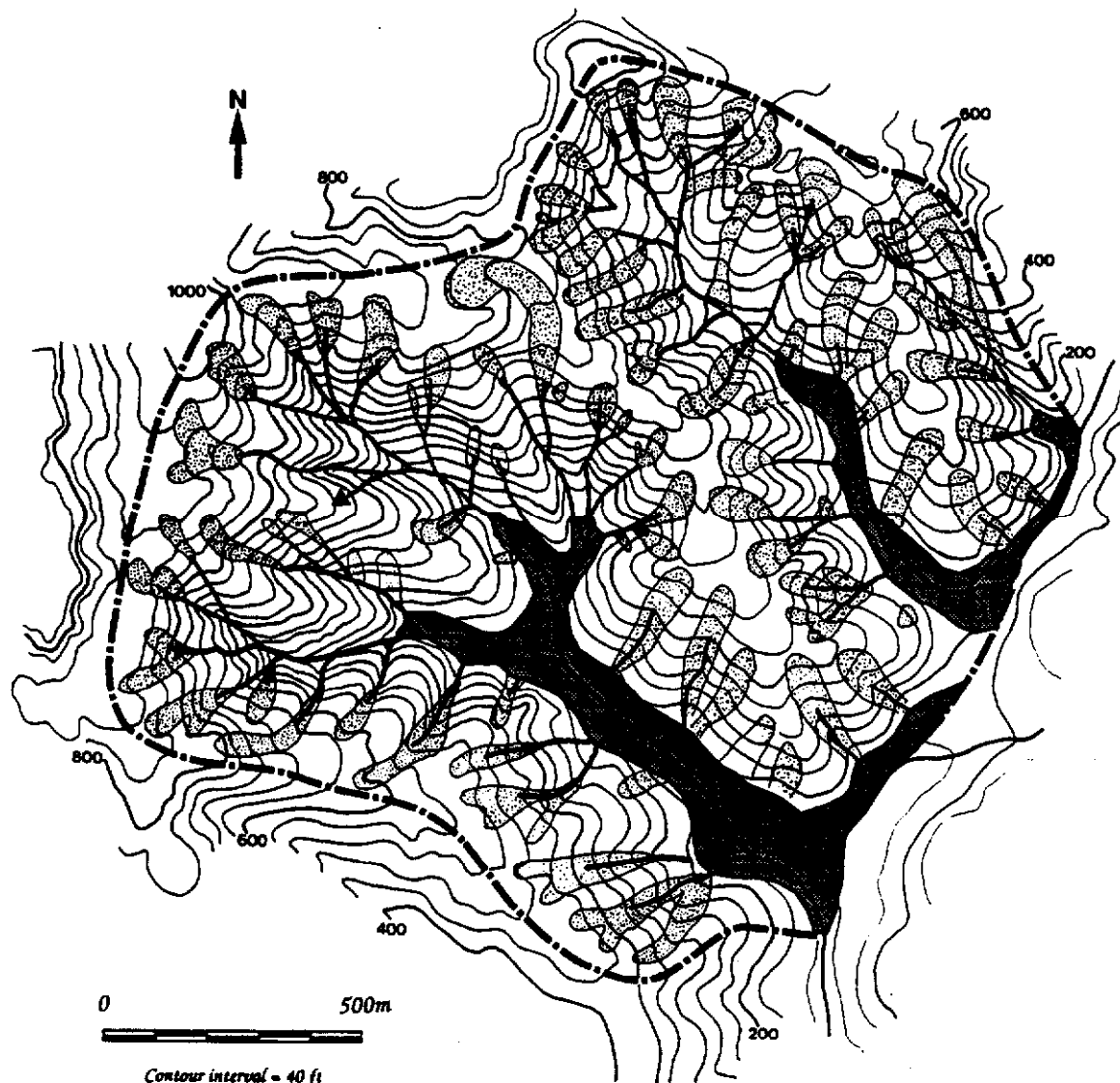


Figure 2. Map of the channel network (heavy solid lines), areas of thick colluvium (stippled area) and thick valley floor deposits of colluvium and alluvium (shaded area) in the Tennessee Valley study area of Marin County, California (modified from Montgomery and Dietrich 1989).

Field work in this area (Montgomery 1991) and a nearby site with similar topography, geology and vegetation (Wilson and Dietrich 1987; Wilson 1988) has demonstrated that shallow subsurface flow and saturation overland flow are the principal runoff mechanisms in response to rainstorms. By mid-winter when the ground has become sufficiently moist, storms delivering about 70 mm in about two days can cause extensive zones of saturation overland flow to form in the unchanneled and small channeled valleys. In the past few years, despite severe drought conditions, we have observed saturation overland flow extend over 100 m above the present channel heads in the lower gradient valleys. When this occurs, the water above the head typically runs very clear, carrying

little or no sediment. In the channels just downstream, however, we have observed freshly scoured banks and local levee deposits on the grass where the small channels (<20 cm wide) have shoaled, causing water to spill onto the surrounding surface. One intensively monitored abrupt channel head a few meters high has migrated upslope at about 20-40 cm per year for at least the past 3 yrs (Montgomery 1991). Both seepage erosion, which leads to undermining and wall collapse, and saturation overland flow, which removes collapsed material once it falls over the head cut, are responsible for erosion.

In 1986, during monitoring of runoff at an unchanneled valley north of this site, 40 cm of rain fell in 11 days, producing saturation overland flow

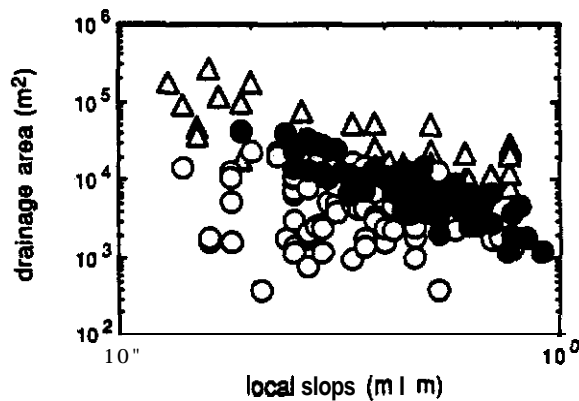


Figure 3. Drainage area and local ground slope for channels (triangles), channel heads (solid circles), and unchanneled surfaces (open circles) in the study area shown in figure 2 {modified from Montgomery and Dietrich 1992}.

over 100 m in length (essentially to the divide). The grass was bent down by the flow and, locally at the upslope tip of the small channel and the downslope end of the valley, the overland flow had a Froude number >1.0 , although no obvious surface erosion occurred. Measurements of the runoff produced during this storm revealed that it had roughness properties compatible with a laminar flow description, i.e., the calculated roughness varied inversely with Reynolds number, yielding a K (as defined above) of about 10,000 (Wilson 1988, p. 109). Despite this large Reynolds number, the data gave no indication of reaching a constant roughness. We suspect that the flow was indeed turbulent, but the momentum defect caused by the vegetation resulted in a turbulent eddy diffusion coefficient that did not vary with height above the bed, giving a laminar-like flow resistance relationship.

As saturation overland flow is largely confined to convergent zones along valley axes, erosion on the surrounding hillslopes is primarily due to processes not involving surface runoff, i.e., mass-wasting processes. Shallow landslides involving just the soil-mantle are common in this area. Due to the dense brush in the steep canyon areas, it is difficult to map all the scars, even in the field. Some of these scars are probably several decades old based on the vegetation cover and sharpness of the edges, and in other cases, where bedrock is near the surface, it is difficult to define a discrete failure area. The scars are commonly only 5 to 10 m across and about twice as long. Using aerial photographs and field inspection, we mapped 39 landslide scars in the 1.2 km² larger catchment of the two shown in figure 2. The scars are most commonly found

on the steeper footslopes and at the downstream end of small steep, unchanneled valleys. Given the uncertainty in mapping these subtle features when we compare the observed and predicted pattern of landsliding, we will interpret the mapped scars as indicating areas of mass instability, rather than as discrete points of failure.

On the gentler hillslopes and on the ridges, sediment transport occurs primarily by biogenic transport associated with the burrowing activity of animals (Reneau et al. 1988; Black and Montgomery 1991). Given the minor role of water in transporting soil, downslope transport by this biogenic activity is probably largely slope dependent. Perhaps the well-defined hilltop convexities in this area, as would be expected from a slope dependent transport law (Gilbert 1909), attest to this process.

Topographic Analysis

Prediction of the full extent of the channel network in a landscape using the above threshold theories requires digital elevation data of sufficiently high resolution that the finest scale source-area basins can be quantitatively analyzed. At least for our field area (but probably in general), the digital elevation model (DEM) from the United States Geological Survey 7.5' quadrangle was useless. Although elevations were digitized every 25 m along north-south lines in this DEM, the individual profiles were 150 m apart, and the data were interpolated to a rectangular array of data points spaced 30 m apart (Bauer and Anderson unpub. data). As shown by Bauer and Anderson and clearly visible by inspection of a topographic map generated from the data, this DEM (made available for the first time in January 1992) cannot resolve valleys with wavelengths <1000 m with much accuracy. Given the general tendency for channel networks to extend into fine-scale valleys in steep terrain [Montgomery and Dietrich 1988, 1989; Dietrich and Dunne 1993] we question whether analyses based on USGS DEM's can be used to infer channel networks or the transition from hillslope to channel-driven erosion processes.

As an alternative, we took advantage of specially flown, low-elevation high resolution black and white photographs to generate our own DEM. Several mapped ground features were used to control registration of the digital coordinates. Elevation data were obtained at a density of about every 10 m for the 1.21 km² catchment from stereo digitization of the photographs. The low canopy cover permitted clear ground visibility, and we selected data points to capture topographic change rather than to

follow a regular grid. Elevation **error for** individual points we estimate to be ± 0.5 m, horizontal error is about ± 3 m.

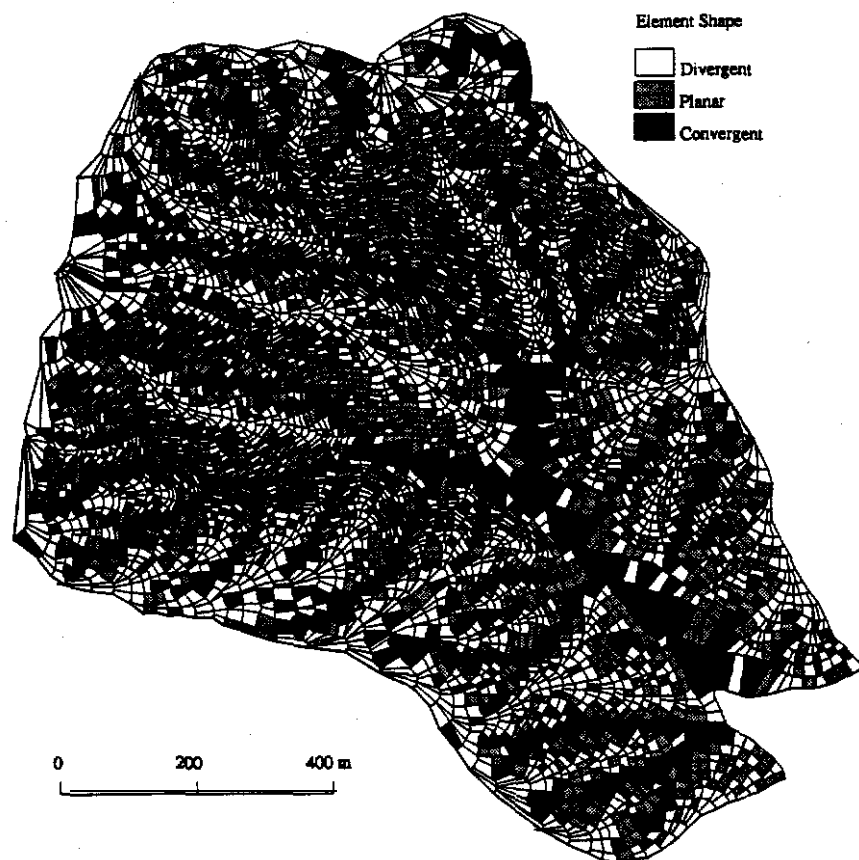
For the simple steady-state threshold of erosion theories described above, any digital terrain model that enables one to compute local a/b and M with reasonable accuracy should be sufficient. As many have found, however, grid-based analyses so far tend to produce undesirable artifacts (e.g., Fairfield and Leymarie 1991). To avoid this problem and to analyze landscape morphology in a manner strongly tied to its hydrologic response, we have relied on the digital terrain model, TOPOG (O'Loughlin 1986; Moore et al. 1988b; Vertessy et al. 1990).

TOPOG grids the data points, smooths the data to remove sinks, draws contours and then lines roughly normal to the contours (minimum distance lines) that extend up from low elevations to ridges. These lines are approximately the flow lines for shallow subsurface and overland flow, and the combination of two adjacent flow lines intersecting two successive contours divides the land surface into distinctly shaped elements. For each element, the total contributing area, a , can be calculated and the ratio a/b from the bottom contour length of the element. The local slope, M , is the

sine of the **gradient** from the contour interval divided by the average length of the flow lines **joining** them in an element.

In order to link runoff and erosion processes to landscape morphology, we took advantage **of** the element shape created by TOPOG to classify each element into divergent, planar, and convergent morphology. We used the simple criterion that if $(b_2 - b_1)/(b_2 + b_1)$ exceeded a set percentage change, the element fell into one of **the** three categories. Here b_1 and b_2 are the contour length of the **upslope** and downslope sides of the element, respectively. This percentage change is somewhat arbitrary. We chose the smallest values estimated to be relatively free of artifacts of the model (< -0.10 is convergent, > 0.10 is divergent, otherwise planar) to resolve the fine-scale topography. Figure 4 shows the spatial distribution of the three element types for our map representation of our site with 5 m contour intervals and average spacing between the "flow lines" of about 20 m. This combination of element size and criterion for shape distinction successfully shows the valley axes as convergent and the ridge lines as divergent. The relative distribution of divergent and planar elements is, however, clearly dependent on flow line spacing and contour interval relative to the **crite-**

Figure 4. Spatial pattern of convergent, planar, and divergent topographic elements in the larger, 1.2 km² catchment in figure 2 [modified from Dietrich et al. 1992].



tion. If the percentage change requirement is held constant, then with decreasing spacing between the flow lines and resultant narrowing of the elements, the planar elements spread **upslope** at the expense of divergent ones, leaving **just** the triangular elements where the flow lines terminate along the ridge line. The extent of the convergent elements is much less sensitive to the size of the element.

Land surface morphology **classified** in this manner captures an aspect of both the form **of the surface** and its likely hydrologic behavior. The contour lines create a smoothed representation of the surface, and in combination with the relatively broadly spaced flow lines this tends to emphasize the relative hydrologic convergence as compared to the local detailed shape of the ground surface. We will use element classification to guide evaluation of **T/q** as shown below.

In order to make comparisons with **our** channel initiation theory, we have also **classified** convergent elements as channeled or unchanneled. Channeled elements were identified by tracing the observed channel network (figure 2) onto a computer-generated map of the catchment. We found that nearly all of the "channeled" elements fell within the observed range of topographic threshold for **channel** heads of $(a/b)S^2 = 200$ m to $(a/b)S^2 = 25$ m reported by Montgomery and Dietrich (1992) (figure 5) (here S is the $\tan \theta$). This excellent agreement between field-determined values of **a/b** and **$\tan \theta$** and that calculated from the DEM for channeled portions of the landscape strongly supports the use of the DEM as an accurate representation of the actual ground surface. Only where the threshold relations are projected to steep slopes where channels **do not** occur in the field do the planar and unchanneled elements also fall within this range. We will discuss this later.

Further evidence of the reliability of the data comes from comparing the computed **alb** and slope data using TOPOG with that from a completely different grid-based digital terrain model developed by Bauer (pers. comm. 1992). For all elements, the average of the logarithm of **a/b** is 58.9 m using TOPOG and 59.0 using Bauer's model. The average slope of the elements is 23.4° using TOPOG, **whereas** the **average** slope using Bauer's model **is** 22.5°. **In** both cases the standard deviations were essentially identical. This suggests that artifacts peculiar to a particular digital terrain model are minimum.

Building upon the characteristic form concept popularized by Kirkby (1971), Willgoose (1989) has suggested that in a slope-area analysis of the kind

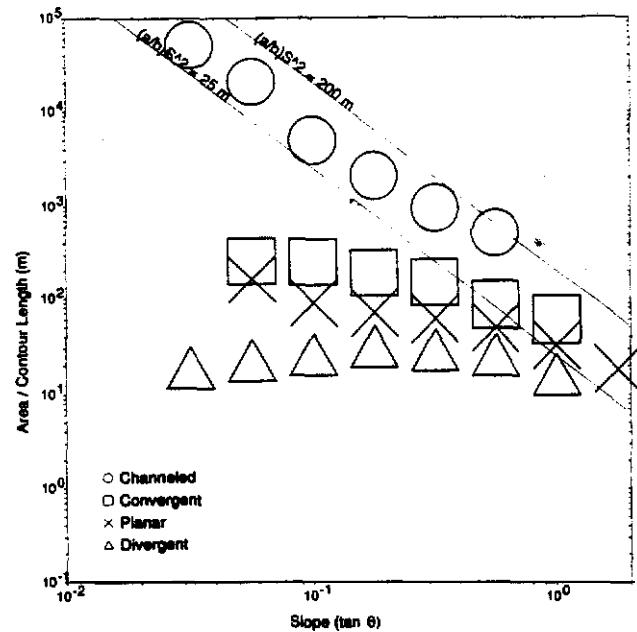


Figure 5. Comparison of the area per unit contour length versus ground slope data generated from the digital terrain model, TOPOG, with the upper and lower limit (solid lines) of channel head data given in figure 3. A total of 5632 elements were classified by shape. Channeled convergent elements were identified using the network map in figure 2. Symbols represent the average of the log values of **alb** for uniform log classes of ground slope. Individual data points are shown in Dietrich et al. (1992).

in figures 2 and 5, hillslopes should show a systematic increase in contributing area with increasing slope (a convex profile), because hillslope form is presumably set by slope-dominated transport processes. Channeled portions of the landscape should show a systematic decrease in slope with increasing drainage area because of the importance of water runoff as well as slope in the transport process (a concave profile), and the length of the hillslope would be reflected in a distinctive inflection point on a area-slope or slope-area graph of elements derived from a digital terrain model. Tarboton et al. (1991) have subsequently claimed to observe this inflection point in their analysis of digital elevation data, but this may be an artifact of their analysis of low resolution USGS DEM's. Furthermore, an innovative theoretical analysis based on stability theory by Loewenherz (1991a, 1991b) suggests that the channel head may extend **upslope** of the inflection point. While there is a clear change in the contributing area-slope relation associated with the transition from divergent to convergent elements (figure 5), there is no simple inflection in our data.

Threshold Analysis

The thresholds of saturation (equation 2), slope stability (equation 4), and erosion by saturation overland flow (equations 10 and 11) are functions of a/b and M ; hence the derived threshold equations can be readily compared with the observed distribution of element types. This comparison can place significant constraints on the **appropriateness** of the threshold and, in effect, permits a rational approach for evaluating the parameters in each of the threshold theories. In fact, given the assumption of steady-state runoff, such a comparison may be the only reasonable way to **parameterize** fully these theories.

Threshold of Saturation. All three thresholds are controlled at least partly by the ratio of transmissivity to runoff rate (T/q). In the threshold of saturation (equation 2) T/q is the slope of the line relating a/b to M . **There are at least three ways to assess $\{T/q\}$.** Field measurements, such as pump tests on **piezometers**, can provide estimates of T , and q can be selected from precipitation records. Given the high spatial variability of T and the uncertainty of what exactly q is [because of the steady-state assumption], this method of assessing T/q cannot be used. Based on an intensive hydrologic study near our field site (Wilson 1988), we estimate the transmissivity to be about $17 \text{ m}^2/\text{d}$ and, surprisingly, not to vary **significantly** with topographic position [hollow versus ridge] because of the dominance of the high conductivity of the surface soil. This estimate must still **be** considered extremely crude, but without some other constraint, we have no rational way of choosing a **significant** steady-state q to drive the erosion thresholds.

Another method, which at least would help evaluate the general validity of the model, would be to map in a watershed the farthest **upslope** extent of saturated areas developed from a large precipitation event and determine whether this position has a similar value of $a/(bM)$ throughout the basin, as expected from equation (2). We have attempted to do this, but because of an extended drought in California, we have had very little **opportunity** to make observations. It is also difficult to locate field observations with the precision necessary to identify which element it belongs to in the digital terrain model. The last significant overland flow event was in March of 1989 after a roughly 0.08 m rainfall. For six different hollows, it appears the $a/(bM)$ value for the farthest **upslope** extent of surface saturation ranged from 200 to at least 2000 m, with four of the points apparently

falling between 500 to 1000 m. If T is roughly $17 \text{ m}^2/\text{d}$, then q in this case would be 0.034 to 0.068 m/d. No landslides occurred during this event, but some of the smallest **upslope** channel tips did scour, and a carefully monitored channel head advanced about 0.4 m upslope .

A third method to estimate T/q , and one that seems most appropriate for a general threshold of erosion investigation, is to use the landscape morphology to place constraints on the possible value of T/q . Based on both field observations and what we would expect from simple physical intuition, we would not expect the divergent elements, which are almost exclusively found on the ridges, to experience saturation. Furthermore, the lower gradient convergent elements making up channeled and **unchanneled** valleys ought to become saturated during events large enough to cause **landsliding** or **channelization** by saturation overland flow. Figure 6 shows the saturation threshold line for three values of T/q plotted against the various element types. Clearly, a value of about 350 m for T/q causes nearly all divergent elements to be unsaturated while nearly all of the convergent and channeled ones are saturated (figure 6) [see Dietrich et al. [1992] for comparison with individual data points]. The vast majority of the planar elements are also predicted to be unsaturated, which seems reasonable. This value of T/q would require a q of 0.05 m/d if T is $17 \text{ m}^2/\text{d}$. To judge whether an 0.05 m/d roughly steady-state runoff is possible, we used the simple analytical model of Lida (1984) to estimate that it would take roughly 9 days for a 59 m long planar slope (approximate mean slope length here) to reach steady-state with a transmissivity of $17 \text{ m}^2/\text{d}$ and rainfall of 0.05 m/d . A storm about this magnitude (0.40 m) and duration occurred near here in 1986 [Wilson 1988]. The maximum precipitation recorded in 10 days at a rain gage in this general area is 1.1 m (California Dept. Water Resources 1981). Figure 7 shows the extent of ground water saturation for steady-state runoff and a T/q of 350 m . The saturated region, with few exceptions, is **confined** to the valley network of channeled and **unchanneled** convergent topography. Some of the long triangular saturated patches along the divide are clearly artifacts of the model, but otherwise the predicted saturated topography appears consistent with field observations.

Although we cannot conclude that we knew with any precision an appropriate value of T/q , the above analyses place significant constraint on it. The estimated value of 350 m is not unreasonable, based on field observations. In the analysis to follow, we will take T/q **as fixed** and evaluate the

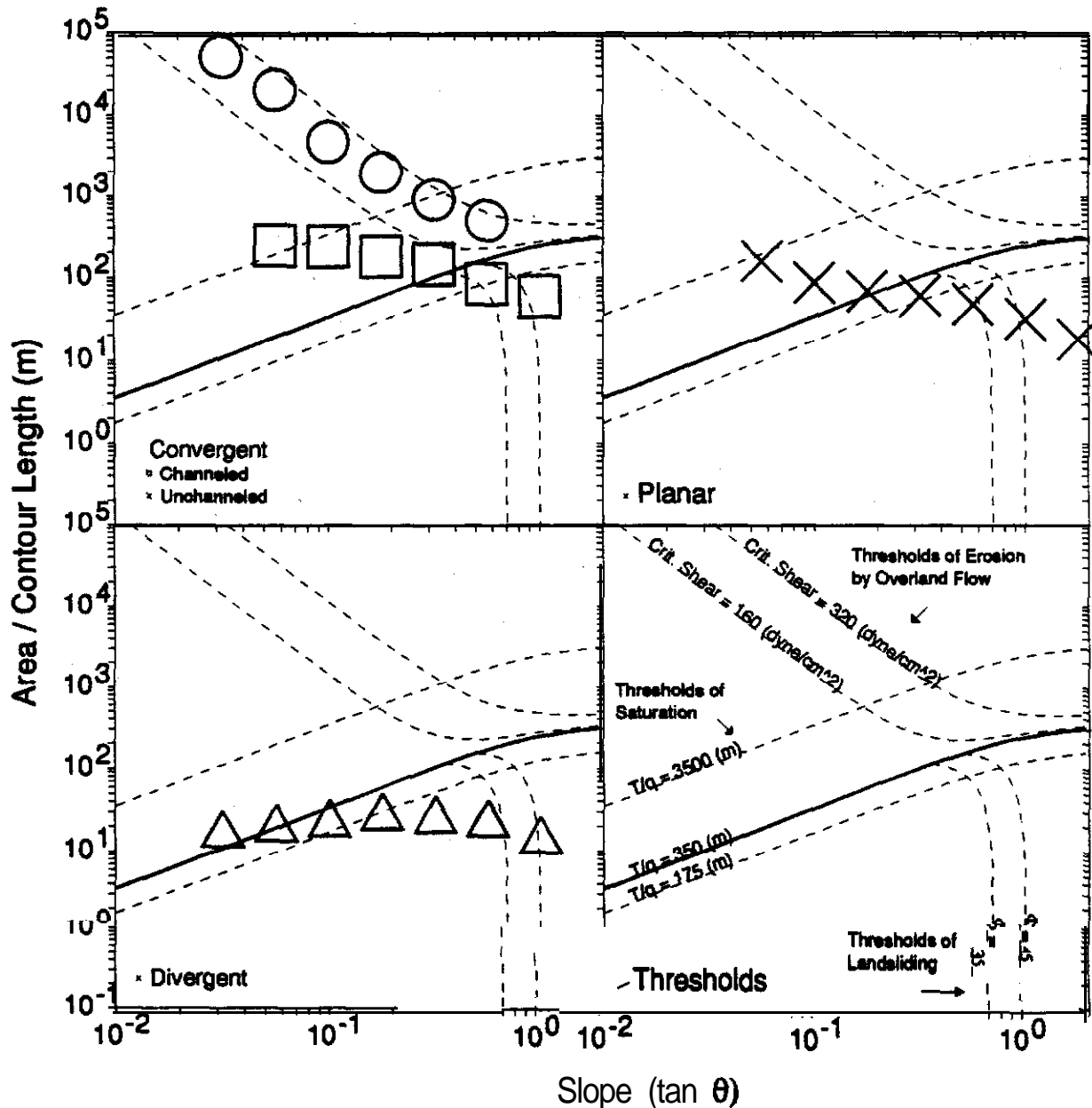


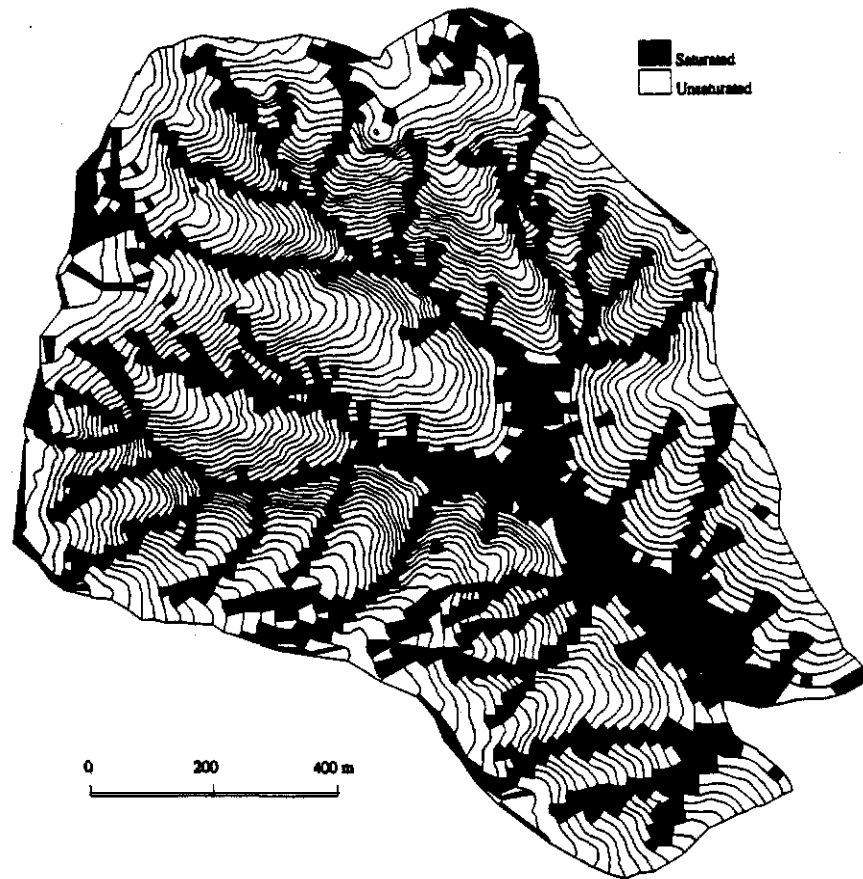
Figure 6. Comparison of threshold theories with digital terrain data of the Tennessee Valley catchment (modified from Dietrich et al. 1992).

other parameters in the two **erosion** threshold theories.

Slope Stability Threshold. Given the assignment of T/q to a value of 350 m, the slope stability threshold (equation 4) has two remaining parameters. The ratio of wet soil bulk density to water density is about 2, based on bulk density measurements by Reneau (1988) in nearby areas. Previous studies (Reneau et al. 1984; Reneau and Dietrich 1987; Reneau 1988) in the Bay area suggest that for the coarse-textured soils in the field area, the angle of internal friction ϕ can be as high as 45° and is likely to lie between 40 and 45°. These soils are

generally cohesionless although the roots of the grass and coyote brush would add a slight apparent cohesion. This strength contribution has been ignored here. In figure 6, we show the position of the slope stability threshold for the possible range of ϕ from 35° to 45°. The lower bound of the angle of internal friction predicts many divergent elements and a large number of planar elements to be unstable, a prediction not consistent with our field observations, in which most of the current landslide scars are found in convergent areas, some in planar, and none in divergent ones. Hence, this lower bound appears to be too low. Very few elements

Figure 7. Predicted Pattern of ground saturation (black area) for the T/q value of 350 m during steady state runoff.



are steeper than 45° , perhaps because of the chronic instability at this gradient; hence a ϕ of 45° is probably too high.

Figure 8 shows the pattern of predicted areas of instability and observed landslide scars for a ϕ of 40° . Nearly all of the mapped landslide scars (35 of 39 scars) fall within the area of predicted instability. Many of the sites predicted to be unstable are actually places of bedrock outcrop, where the model does not strictly apply. Bedrock outcrop would, nonetheless, be expected where landslide frequency exceeds soil production rate, so this prediction is not inconsistent. Evaluation of this landslide model is more extensively carried out elsewhere [Montgomery and Dietrich unpub. data]. It seems fair to conclude that there is reasonable support for the slope stability threshold at this site and that the parameters in the model are fairly well constrained.

Threshold Of Erosion by Saturation Overland Flow. The threshold of erosion {and presumably channelization} by saturation overland flow (equations 10 and 11) has three additional parameters, the roughness (K) or friction factor (f), the critical boundary shear stress (τ_c) and the runoff (q) (as compared to T/q). Field observations indicate that

even at Reynolds numbers as high as 20,000 the roughness varies inversely with Reynolds number (Wilson 1988, p. 109); hence equation (11) is more appropriate to use here. Measurements by Wilson [1988] on typical grass cover not **subject** to cattle **grazing** in this area gives a roughness coefficient of about 10,000. The value of K would have been lower during the period of heaving grazing in the last century.

The magnitude of the critical boundary shear stress is much more difficult to **define**. Wilson (1988) observed shear stresses in excess of 200 **dyne/cm²** without noticeable incision into the grass turf, although active scour and sediment transport did occur in the channels just downstream of their points of inception. We can use the observed crude separation of channeled and **un**channeled convergent elements as a guide for parameter selection. Reid (1989) summarized available literature on critical boundary shear stresses in overland flow and concluded that a well-vegetated mat would have a value in excess of 1000 **dynes/cm²**. Given a K of 10,000, if equation (11) is plotted to separate **un**channeled from channeled elements, then q would have to be about 1.5 m/d for this high critical boundary shear stress. This

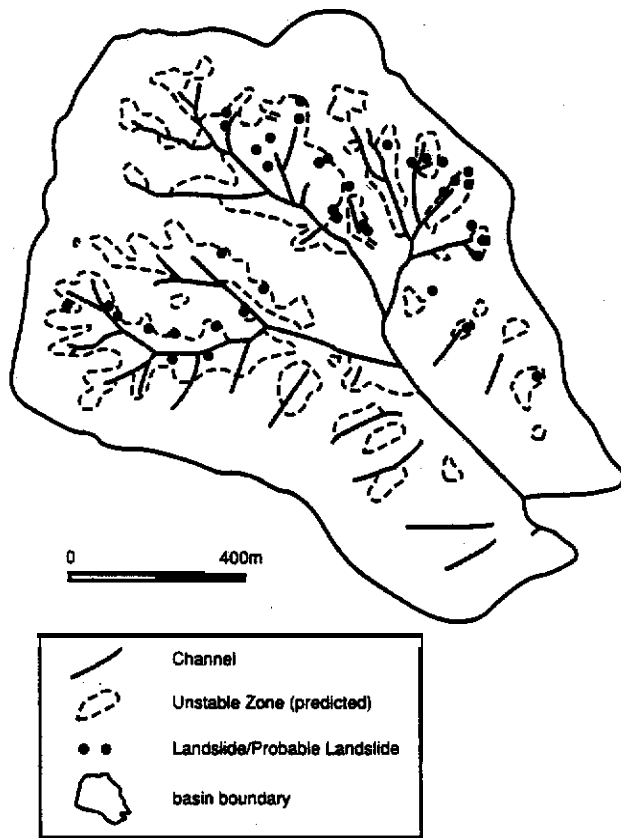


Figure 8. Predicted and observed pattern of shallow landslides for a T/q of 350 m, and an angle of internal friction of 40° .

value of runoff is absurd and points to the necessity that the critical boundary shear stress be lower, as K may not be significantly larger and the second term in equation (11) involving T/q is not significant. We assume, as have Reid (1989) and many others, that channel instability occurs when critical boundary shear stress is reduced due to vegetation disturbance by grazing, fire, trampling or some other effect.

If we use $T/q = 350$ m, $q = 0.05$ m/d, and $K = 10,000$ then according to the available data in figure 6, the critical boundary shear stress would be about 160 to 320 dyne/cm^2 , reasonable values for disturbed, poorly vegetated surfaces [Reid 1989]. The two threshold lines are nearly identical to the lines defining the upper and lower limit to the channel head locations (figure 5). The value of critical shear stress is reasonably well constrained because the term involving T/q for most of the range of interest is insignificant and because the value of K and q are probably known to within an order of magnitude. This uncertainty in K or q is equivalent to slightly more than a factor of 2 uncertainty in the critical boundary shear stress because a/b

varies with $(\tau_c)^3$. This finding is testable by field experiments directed toward evaluating critical boundary shear stress.

It has been observed by some that rill initiation is associated with supercritical flows. We have observed supercritical saturation overland flow at channel heads in our study area and perhaps the altered resistance and flow velocity under supercritical conditions is important to channel initiation as well. Using equations (6) and (9), we find that the Froude number is 1.0 for laminar overland flow when

$$a/b = (T/q)M + Kv/2qM. \quad (12)$$

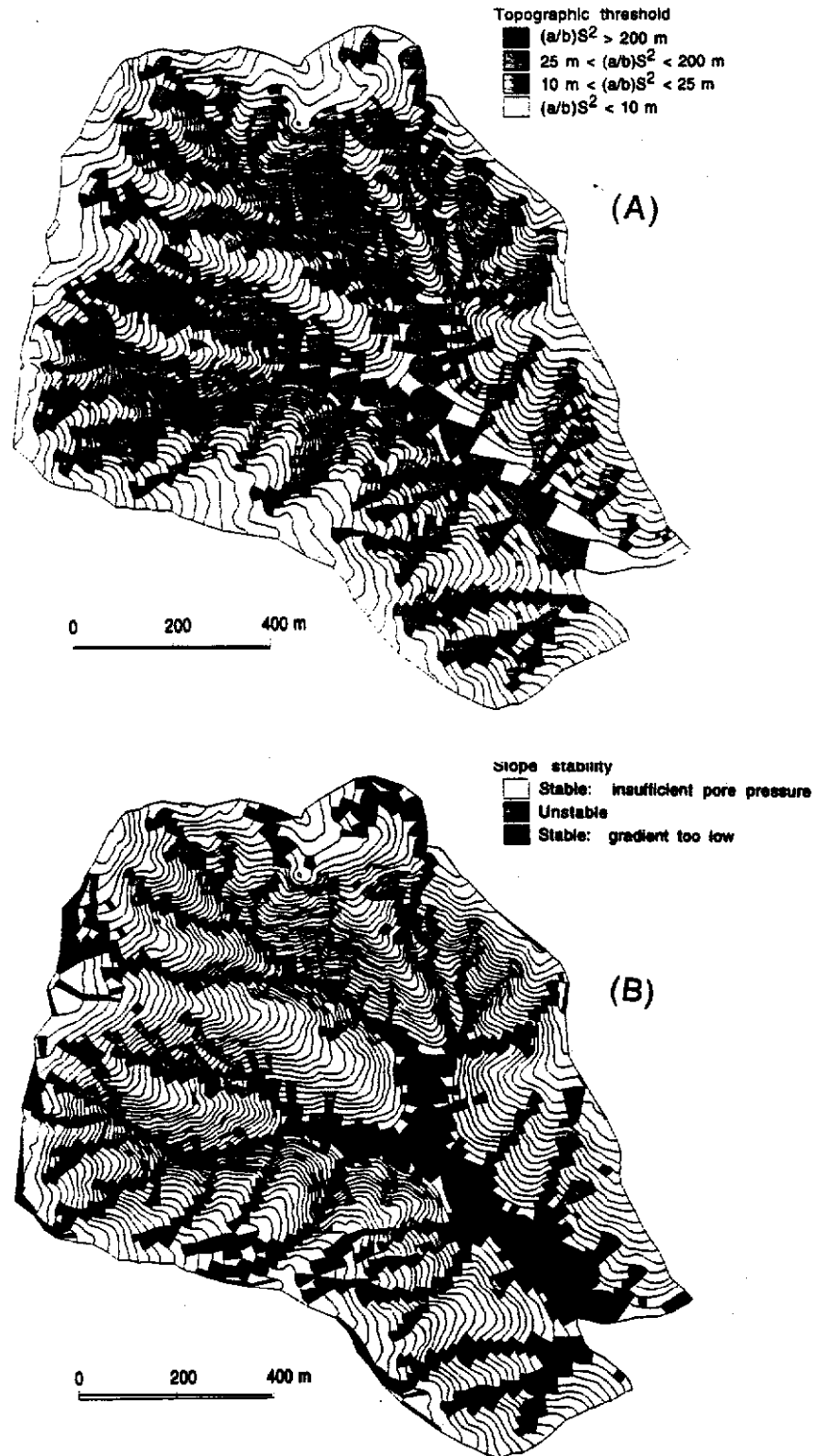
For the range of slopes 0.1 to 1.0, equation (12) plots close to but mostly above the line labelled $\tau_c = 320$ dyne/cm^2 in figure 6, when K in equation (12) is assumed equal to 1000 (a value that may be typical of grazed grass, Dunne and Dieuch 19801). This implies that K would have to be at least 10 times smaller for a significant number of the channel heads to experience flows at or above supercritical conditions. If K were 1000 and critical boundary shear stress were 149 dyne/cm^2 , the threshold line of equation (11) would be identical to that shown for $K = 10,000$ and $\tau_c = 320$ dyne/cm^2 . Reduction of vegetation cover, which decreases K and τ_c , may increase the tendency for overland flow to incise both because the critical boundary shear stress is more likely to be exceeded and because the flow will tend to become supercritical. It is worth noting that for $K = 1000$ to correspond to the lower line in figure 6, which lies below the channel heads, τ_c would have to equal only 74 dyne/cm^2 , and channel head erosion would not be affected by supercritical conditions. This low value of critical shear stress seems unlikely, however, even under intense grazing.

Channel Network Analysis

Figure 9A shows the field-mapped channel network and the distribution of $(a/b)S^2$ for our study site, revealing a strong correspondence between the extent of the mapped network and the observed range of $25 \text{ m} \leq (a/b)S^2 \leq 200 \text{ m}$ for channel heads. Not a single channel head extends below this range, suggesting not only a strong topographic threshold to channel initiation but also excellent agreement between field data and the results of the digital terrain analysis.

Four other attributes of this comparison warrant attention. Nine of the first-order tributaries do not connect to the higher order channels. This observa-

Figure 9. Comparison of observed channel network with: (A) the empirical topographic threshold based on field observations at the channel head (modified from Montgomery and Dietrich 1992); (B) the pattern of areas predicted to be subject to shallow landsliding.



tion strongly suggests that the tributary channels are not driven by instability originating at the junction with a higher order channel junction. A threshold theory for channel initiation should presumably also explain why channels are discontinuous. The second feature we note is that only the

elements in the narrow bedrock canyons of the steeper tributaries have $(a/b)S^2$ values in excess of the channel head threshold range. Why don't higher-order channels well downslope from the channel head also have such high values? Is this an artifact of the insensitivity of the analysis? Field

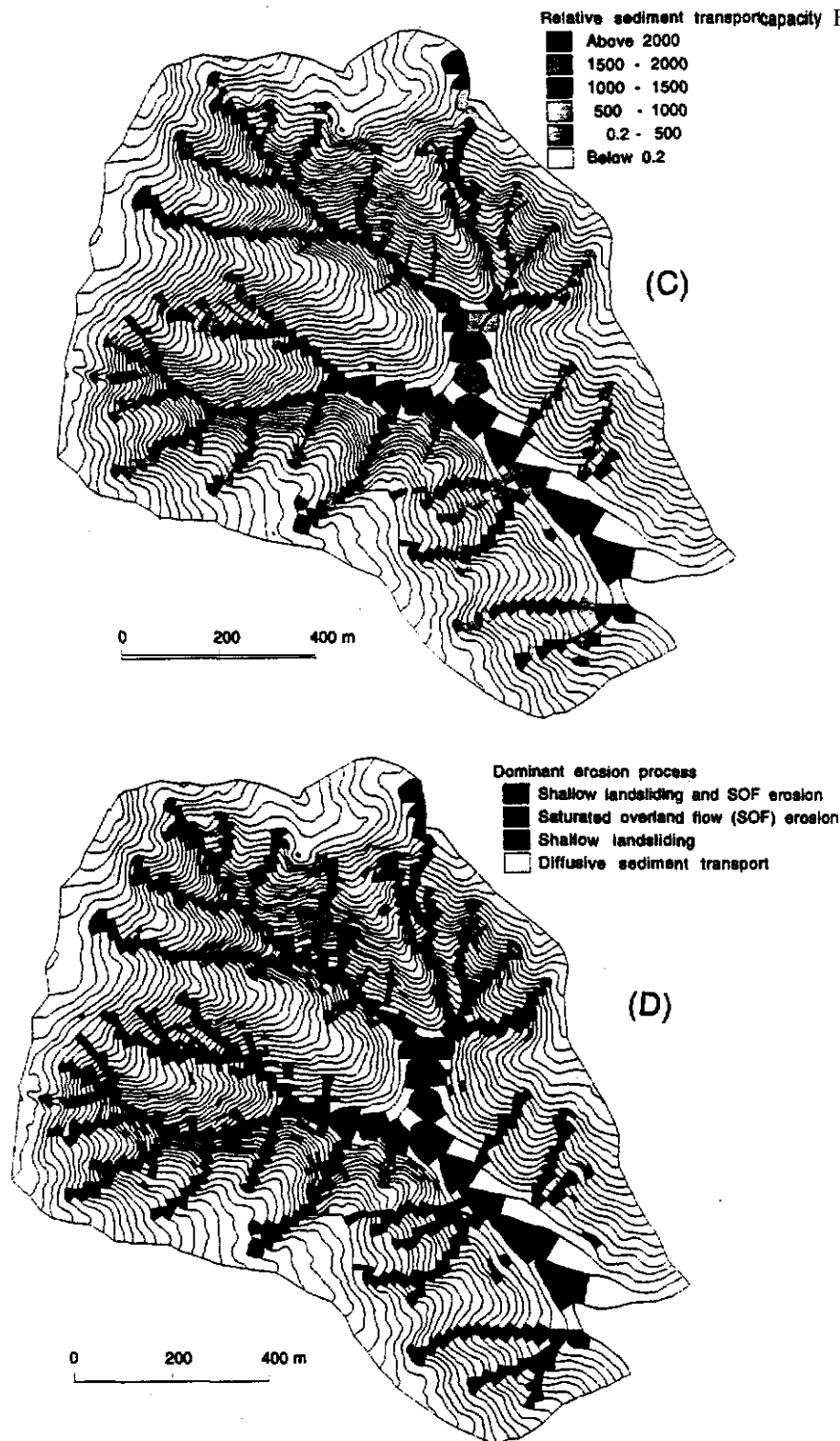


Figure 9. (Continued) (C) the pattern of relative sediment transport capacity by overland flow calculated from $q_s = (\tau_b - \tau_c)^{1.5}$ with τ_c equal to 160 dyne/cm²; and (D) spatial pattern of dominant erosion processes.

observations suggest otherwise. As shown in figure 2, the lower gradient valleys in the field area contain thick deposits of alluvium and colluvium, whereas the narrow bedrock canyons show little or no evidence of stored sediment. Analysis of landuse and landscape change in this area (Montgomery 1991) indicates that the main low gradient

channel network into which the steeper uplands drain only entrenched into its floodplain after introduction of intensive cattle grazing. Based on observations nearby in one of the only watersheds never subject to cattle grazing, it is reasonable to suggest that the low gradient channels may not have been continuous before disturbance. Our abil-

ity to **analyze** this problem is limited because the elements in the low gradient valleys are quite large and the local hydraulics within an element associated with a channel are likely to be quite different than that estimated from the element as a whole. Nonetheless, the field observations and topographic analysis suggest a tendency for the low gradient valleys to aggrade with poorly defined channels when unaltered by **landuse**.

The third and fourth features of figure 9A have to do with the unchanneled elements within or near the threshold range of channel initiation. While none of the channel heads extend below the $(a/b)S^2$ of 25 m, many elements lying above this value are unchanneled. Most of these elements form distinct linear patches on the **steep** side slopes of the bedrock canyons and lie in subtle hollows. Empirically we would argue that these elements lie in areas prone to channelization, but either because of local variations in such properties as saturated conductivity and friction angle or, and more likely, because of a tendency for diffusive sediment transport to fill in channels here the sites lack mappable channels. If these elements lie above the erosion threshold, the latter interpretation seems most plausible. The fourth feature, and one that Montgomery and Dietrich (1992) emphasized, is the tendency for elements **with** the value of $(a/b)S^2$ just below 25 m to lie at the topographic transition from valley to ridge. Montgomery and Dietrich (1992) argue that this strongly suggests that ridge and valley development and ultimately their spacing is influenced by the threshold of channel initiation. To be consistent, the erosion theories described above should not predict surface instability **upslope** of these elements.

Figure 9B shows the pattern of elements predicted to be unstable for a T/q of 350 m and a ϕ of 40° and their relationship to the channel network. As discussed above, these parameters are reasonably well constrained by topographic analysis and observations; nonetheless, there remains **significant** uncertainty about the full extent of the potentially unstable ground. The comparison with the channel network shows that nearly half of the channel heads lie in or just below areas predicted to be above the slope stability threshold. The vast majority of the unstable elements, however, do not drain directly to a channel head nor lie on the path of a channel. Hence, while landsliding can contribute to channel head advance **upslope**, the tendency for landsliding alone is not sufficient to maintain a channel. On the other hand, many of these **unchanneled**, but unstable elements do correspond to the elements either within the channeled range of

$(a/b)S^2$ or just below it (compare with figure 9A). These observations indicate that the linear patches of unchanneled elements within the channel head range shown in figure 9A correspond to unstable areas that just lack sufficient runoff to maintain a channel.

In figure 9C, the pattern of relative sediment transport capacity $(\tau_b - \tau_c)^{1.5}$ is mapped and compared with the observed channel network. Although channel incision is expected to occur once a critical boundary shear stress is exceeded (and possibly supercritical flow **occurs**), if the divergence of the boundary shear **stress** and thereby sediment transport field is negative downslope, **aggradation** and smothering of any channelization tendency is likely. In comparing the excess relative sediment transport capacity with the observed channel network it is worth remembering how approximate the parameters are in the boundary shear stress model and the large scale of the element relative to the size of the channel. Nonetheless, the similarity throughout the *basin* of results for 35 different tributaries for a single set of parameters supports the mechanistic interpretation proposed here.

In most of the tributaries, the channel head lies slightly downslope of the point where the boundary shear stress exceeds the critical value for saturation overland flow erosion. The other channel heads generally correspond to sites where **landsliding** predominates. Relative sediment transport increases downstream along the channel network, but for all nine discontinuous tributaries, the downstream end of the channel corresponds to the reach where the relative sediment transport declines downslope. A decline in the downslope direction also occurs along the network where the channels leave the narrow canyons and enter the broad valley, in agreement with the historical tendency for deposition to occur in the lower valley and possibly have only a poorly **formed** channel. This seems to provide strong support for the general structure of our model.

Most of the unchanneled elements that lie within the channel head range of $(a/b)S^2$ and along the valley axes are predicted to be unstable due to saturation overland flow erosion (compare 9C,A). Although this is good correspondence between the threshold theory and the observed topographic threshold, it does not explain why these elements remained **unchanneled**. One simple answer, **which** presumes the model to be reasonably accurate, is that the assumed critical boundary shear stress and roughness are slightly incorrect for application of this model to the field observations. Figure 10

shows the effect of changing the critical boundary shear stress by **only** a factor of two. Because of the third power dependency on critical boundary shear stress in the threshold model, a huge difference in the extent of **channel** network (elements **above** the critical boundary shear stress) is predicted with small changes in τ_c . This implies that the difference between observed and predicted channel network in figure 9 C is explicable by a small modification of the τ_c . Unfortunately, for the purposes of field verification of this erosion threshold model, this result suggests that critical boundary shear stress is an important parameter which is virtually unknowable at the level necessary to test model predictions. While it will be useful to determine whether τ_c is 1000 or 100 **dyne/cm²** from field experiments, we will likely not be able to characterize it for an entire basin to within 50%. Hence, like saturated conductivity or transmissivity, critical boundary shear stress, even though it has a **smaller** range of values, may not be a parameter that can be sufficiently well-known from just field observations and **an** "effective" value must be estimated from response of the system as a whole.

If we accept the general validity of the saturation overland flow erosion threshold model, then our model results clearly demonstrate that changes in land use or climate that alter the **surface** resistance to erosion should have a dramatic effect on the stability of the channel network. Cattle grazing in this area reduced the critical boundary shear stress and caused significant expansion of the channel network (**figure 10**).

Figure **9D** summarizes the spatial significance of different erosion processes predicted from the threshold theories. It shows the ridge lines dominated by diffusive (slope-dependent) sediment transport processes that feed sediment to **landslide**-prone planar and subtle convergent slopes bordering the ridges and valley sides. Surface **runoff** in the larger valleys then conveys the sediment further downstream. Mapping of process dominance, as shown in **figure 9D**, should prove useful **in** catchment sediment budget studies. A more formidable task is the development of sediment transport laws supported with field observations that permit routing of sediment down hillslopes and along the channel network.

Conclusions

With the development of digital terrain models **capable** of analyzing large sets of digital elevations, it is now possible **both** to quantify the detailed topography of landscapes and to explore **process-**

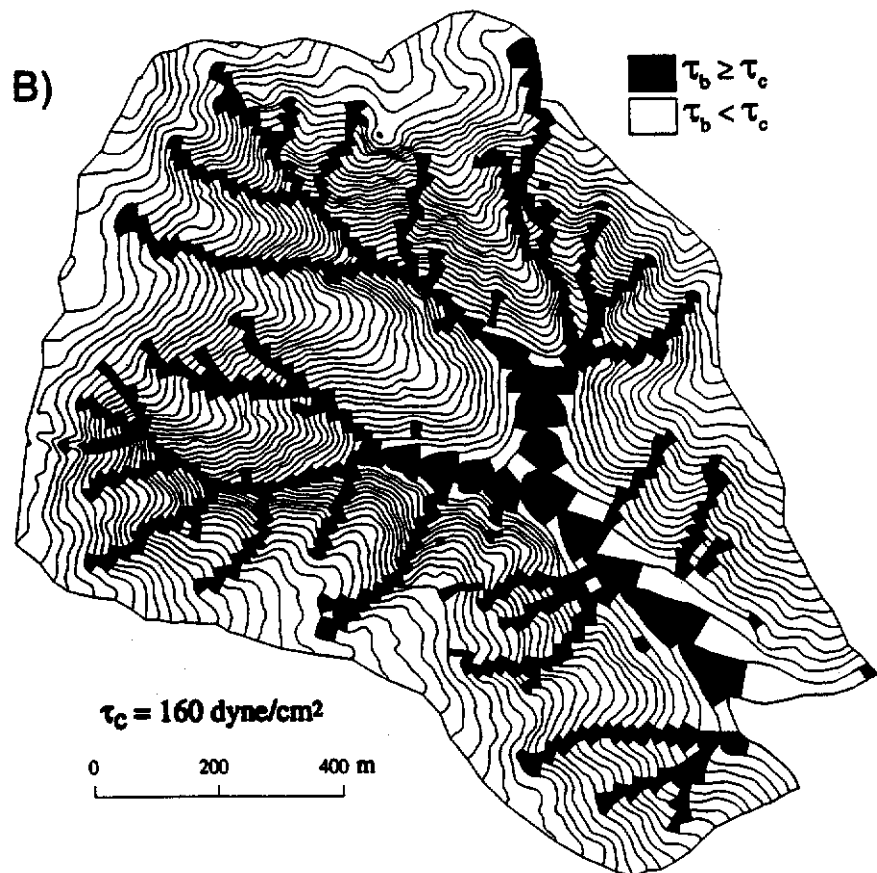
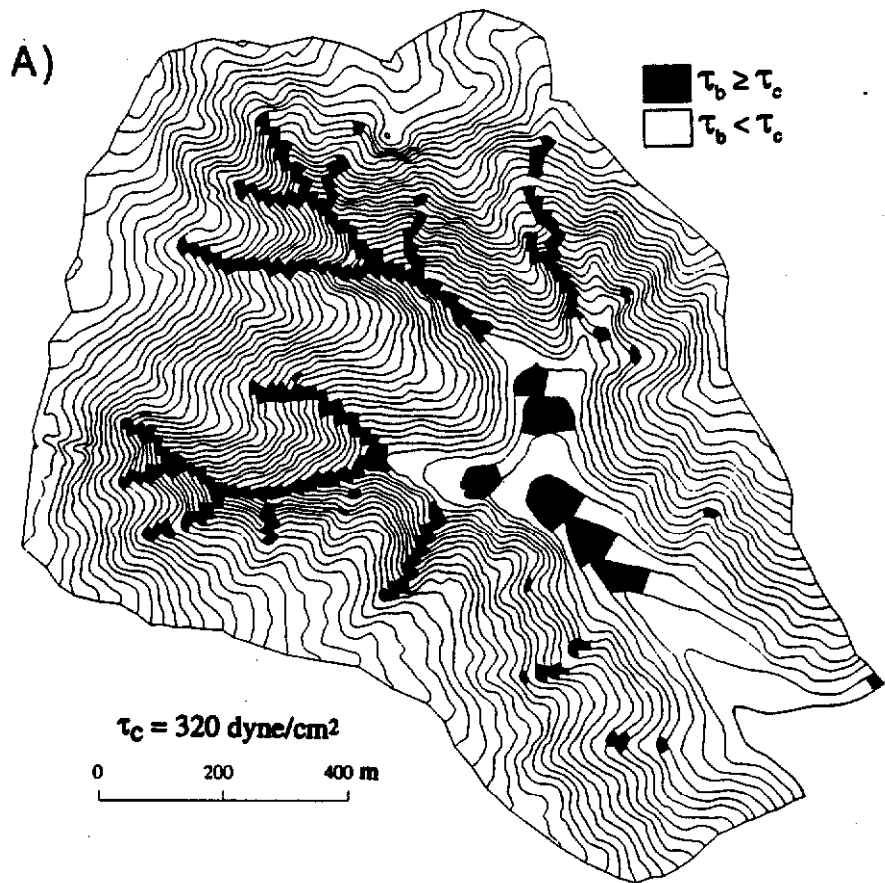
based models in explaining mappable features. One of the most useful features to map is the channel network. We have shown that it can be used to place significant constraint on erosion theories. **Parameterization** of such theories may be quite difficult because of the high spatial variability of the controlling parameters and the sensitivity of the model outcome to their values. Instead of relying on field observations alone for evaluation of the parameters, the topography and the extent of the observed channel network itself can be used to determine the parameters. But once **such** a calibration is done, application elsewhere is needed to validate the model.

Despite this limitation, the comparison between the threshold theory of saturation, erosion by saturation overland flow, and threshold of slope instability and the observed topography and extent of the channel network in our field area suggests several conclusions. The **upslope** extent of the channel network is controlled by a combination of slope instability and erosion by saturation overland flow. These two thresholds have very different *a/b* to *M* relationships and should not be represented by a single function, as **some** may choose when **examining** the empirical data. Although seepage erosion may also be important, our analysis **suggests** that it is not required. While slope instability contributes to channel head advance, it alone does not control the tendency for **channelization**: overland flow appears to be required. Hence, there are many steep areas bordering the channeled valleys that cross the topographic threshold for **channelization**, but remain **unchanneled** because only shallow **landsliding occurs**. In other, steeper environments with greater relief, perhaps debris flow scour from landsliding can act to cut channel-like features, thus reducing the importance of overland flow. Application of our model to locations in Oregon and Washington support this interpretation.

The threshold of erosion by saturation overland flow varies as the third power of critical boundary **shear** stress. Consequently, the extent of the channel network incised by erosive overland flow varies dramatically with changes in surface resistance. This helps explain the widespread **gullying** in the grazing land surrounding the San Francisco Bay and probably many other areas where overland flow is important in channel incision.

Application of the models proposed here to other landscapes with similar erosion processes will require high resolution digital elevation models to capture the topographic control on runoff and erosion mechanisms. The models proposed here should be quite general to landscapes where

Figure 10. Area predicted to be eroded by saturation overland flow for a critical boundary shear stress of (A) 320 dyne/cm² and (B) 160 dyne/cm². This pattern corresponds to the two threshold lines shown in figure 6.



shallow subsurface and saturation overland flow runoff mechanisms predominate. For **model evaluation**, detailed mapping of the **channel** network and location of landslide scars is essential. Such data are rarely available at present.

ACKNOWLEDGMENTS

This research was supported by National Science Foundation Grant EAR-8917467, Grant TFW-FY92-010 from the CMER and SHAMW commit-

tees of the Washington State Timber/Fish/Wildlife agreement, and Australian Center for Catchment Hydrology (Wilson). We thank the U.S. Department of Agriculture Forest Service, Pacific Southwest Region, Engineering Staff for providing access to an analytical stereo plotter for generating the digital elevation data. Rob Reiss conducted the TOPOG simulations and generated the plots used here. This paper was greatly improved by the **generous** comments of three anonymous reviewers, and by Keith **Loague** and Mary Power.

REFERENCES CITED

- Beven, K.**, and **Kirkby, M. J.**, 1979, A physically based variable contributing **area** model of basin hydrology: *Hydrol. Sci. Bull.*, v. 24, p. 43-69.
- Black, T.**, and **Montgomery, D. R.**, 1991, **Sediment transport by** burrowing mammals, **Marin County, California**: *Earth Surf. Proc. Landforms*, v. 16, p. 163-172.
- California** Department of Water Resources, 1981, Rain-fall-depth duration frequency.
- Dietrich, W. F.**, and **Dunne, T.**, 1993, The channel head, *in* **Beven, K.**, and **Kirkby, M. J.**, eds., *Channel Networks Hydrology*: **Chichester**, Wiley, p. 175-219.
- ; **Wilson, C. J.**; **Montgomery, D. R.**; **McKean, J.**; and **Bauer, R.**, 1992, Erosion thresholds and land surface morphology: *Geology*, v. 20, p. 675-679.
- Dunne, T.**, 1978, Field studies of hillslope flow processes, *in* **Kirkby, M. J.**, ed., *Hillslope Hydrology*: **Chichester**, Wiley, p. 227-293.
- , 1980, Formation and **controls** of **channel networks**: *Prog. Phys. Geog.*, v. 4, p. 211-239.
- , 1990, Hydrology, mechanics, and geomorphic implications of erosion by subsurface flow, *in* **Higgins, C. G.**, and **Coates, D. R.**, eds., *Groundwater geomorphology: the role of subsurface water in earth-surface processes and landforms*: **Geol. Soc. America Spec. Paper** 252, p. 1-28.
- , and **Aubry, B. F.**, 1986, Evaluation of Horton's theory of **sheetwash** and **rill** erosion on the basis of field experiments, *in* **Abrahams, A. D.**, ed., *Hillslope Processes*: Boston, Allen and **Unwin**, p. 31-53.
- , and **Dietrich, W. E.**, 1980, Experimental study of Horton **overland flow on** tropical **hillslopes**; 1. Soil conditions, **infiltration** and **frequency of runoff**; 2. **Hydraulic characteristics** and **hillslope hydrographs**: *Zeits. fur Geomorph. Suppl.* Band 35, p. 40-80.
- Fairfield, H.**, and **Leymarie, P.**, 1991, Drainage networks **from** grid digital elevation models: *Wat. Resour. Res.*, v. 27, p. 709-717.
- Gilbert, G. K.**, 1909, Convexity of hilltops: *Jour. Geology*, v. 17, p. 344-350.
- Horton, R. E.**, 1945, Erosional **development** of streams and their drainage basins: *Geol. Soc. America Bull.*, v. 56, p. 275370.
- Iida, T.**, 1984, A hydrological **method** of estimation of the topographic effect on the **saturated throughflow**: *Jap. Geomorph. Union Trans.*, v. 5, p. 1-12.
- Kirkby, M. J.**, 1971, Hillslope **process-response** models based on the continuity equation: *Inst. Brit. Geog. Spec. Pub.* 3, p. 15-30.
- , 1978, **Implications** for sediment **transport**, *in* **Kirkby, M. J.**, ed., *Hillslope Hydrology*: **Chichester**, Wiley, p. 325-364.
- Loewenherz, D. S.**, 1991a, Stability and the initiation of **channeled** surface drainage: a reassessment of the **short wavelength** limit: *Jour. Geophys. Res.*, v. 96, p. 8453-8464.
- , 1991b, Stability and the role of length **scale**-dependent material transport in the initiation and development of surface drainage networks: Unpub., Ph.D. dissertation, University of California, Berkeley.
- Montgomery, D. R.**, 1991, Channel initiation and landscape evolution: Unpub. Ph.D. dissertation, University of California, Berkeley.
- , and **Dietrich, W. E.**, 1988, Where do channels begin!: *Nature*, v. 336, p. 232-234.
- , and ———, 1989, Source **areas**, drainage density, and **channel** initiation: *Water Resour. Res.*, v. 25, p. 1907-1918.
- , and **Dietrich, W. E.**, 1992, Channel initiation and the problem of **landscape** scale: *Science*, v. 255, p. 826-830.
- Moore, I. D.**, **Burch, G. J.**, and **MacKenzie, D. H.**, 1988a, Topographic effects on the distribution of surface soil water and the location of ephemeral gullies: *Trans. Am. Soc. Agric. Eng.*, v. 31, p. 1098-1107.
- , **O'Loughlin, E. M.**, and **Burch, G. J.**, 1988b, A contour-based topographic model for hydrological and ecological applications: *Earth Surf. Proc. Landforms*, v. 13, p. 305-320.
- O'Loughlin, E. M.**, 1986, Prediction of surface saturation **zones** in natural **catchments** by topographic analysis: *Water Resour. Res.*, v. 22, p. 794-804.
- Rantz, S. E.**, 1968, **Average** annual precipitation and runoff in **north** coastal **California**, U.S. *Geol. Survey Hydro. Atlas* 298: scale 1: 1,000,000.
- Reid, L. M.**, 1989, Channel **incision** by **surface** runoff

- in grassland **catchments**: Unpub. **Ph.D.** dissertation, University of Washington, Seattle.
- Reneau, S. L.**, 1988, Depositional and **erosional** history of hollows: application to landslide location and **frequency**, long-term erosion rates, and the effects of climatic change: Unpub. **Ph.D.** dissertation, University of California, Berkeley, 328 p.
- ; **Dietrich, W. E.**; **Wilson, C. J.**; and **Rogers, J. D.**, 1984, **Colluvial** deposits and associated landslides in the northern S. F. Bay Area, California, USA: **Proc. Fourth Int. Sym. Landslides** (Toronto), p. 425-430.
- , and ———, 1987, Size and location of colluvial landslides in a steep forested landscape: **Int. Assoc. Hydrol. Sci. Pub.** 165, p. 39-48.
- ; ———; **Donahue, D. J.**; **Jull, A. J. T.**; and **Rubin, M.**, 1990, Later **Quaternary** history of **colluvial** deposition and erosion in hollows, central California Coast **Ranges: Geol. Soc. America Bull.**, **v.** 102, p. 969-902.
- Slattery, M. C.**, and **Bryan, R. B.**, 1992, Hydraulic conditions for rill incision under simulated rainfall: a laboratory experiment: **Earth Surf. Proc. Landforms**, **v.** 17, p. 127-146.
- Smith, T. R.**, and **Bretherton, F. P.**, 1972, Stability and conservation of mass in drainage basin evolution: **Water Resour. Res.**, **v.** 8, p. 1506-1529.
- Tarboton, D. G.**; **Bras, R. L.**; and **Rodriguez-Iturbe, I.**, 1991, On the extraction of channel networks from digital elevation data: **Hydro. Proc.**, **v.** 5, p. 81-100.
- Vertessy, R. A.**; **Wilson, C. J.**; **Silburn, D. M.**; **Connolly, R. D.**; and **Ciesiolka, C. A.**, 1990, Predicting erosion **hazard** areas using digital terrain analysis: **Int. Assoc. Hydrol. Sci. Pub.** 192, p. 298308.
- Wahrhaftig, C.**, 1984, Structure of the **Marin** Headlands Block, **California**: a **progress** report, in **Blake, M. C., Jr.**, ed., **Franciscan Geology of Northern California: Soc. Econ. Paleont. Mineral. Pacific Coast Sec.**, **v.** 43, p. 31-50.
- Willgoose, G. R.**, 1989, A physically based channel network and **catchment** evolution model: Unpub. **Ph.D.** dissertation, Massachusetts Institute of Technology, Cambridge, MA.
- ; **Bras, R. L.**; and **Rodriguez-Iturbe, I.**, 1991, A coupled channel network **growth** and hillslope evolution model: **Water Resour. Res.**, **v.** 27, p. 1671-1702.
- Wilson, C. J.**, 1988, Runoff and pore pressure development in hollows: Unpub. **Ph.D.** dissertation, University of **California**, Berkeley, 284 p.
- , and **Dietrich, W. E.**, 1987, The contribution of bedrock **groundwater** flow to storm **runoff** and **high** pore pressure development in hollows: **Int. Assoc. Hydrol. Sci.**, **v.** 165, p. 49-59.
- Yalin, M. S.**, 1972, **Mechanics of Sediment Transport**, Pergamon Press, 290 p.

Appendix 3

Channel Network Source Representation using Digital Elevation Models

DAVID R. MONTGOMERY

*Department of Geological Sciences and Quaternary Research Center
University of Washington
Seattle, Washington 98295*

EFI FOUFOULA-GEORGIU

*St. Anthony Falls Hydraulic Laboratory
Department of Civil and Mineral Engineering, University of Minnesota
Minneapolis, Minnesota 55414*

ABSTRACT

Methods for the identification of the sine, or scale, of hillslopes and the extent of channel networks from digital elevation models (**DEM's**) are examined critically. Theoretically, a constant critical support area, the method most commonly used at present for channel network extraction from **DEM's**, is more appropriate for depicting the hillslope/valley transition than for identifying channel heads. Analysis of high-resolution **DEMs** confirms that a constant contributing area per unit contour length defines the extent of divergent topography, or the hillslope scale, although *there* is considerable variance about the average value. In even moderately-steep topography, however, a DEM resolution finer than the typical 30 m by 30 m grid size is required to accurately resolve the hillslope/valley transition. For many **soil-**mantled landscapes, a slope-dependent critical support area is both theoretically and empirically more appropriate for defining the extent of channel networks. Implementing this method for overland flow erosion requires knowledge of an appropriate proportionality constant for the drainage area-slope threshold controlling channel initiation. Several methods for estimating this constant from DEM data are examined, but acquisition of even limited field data is recommended. Finally, the hypothesis is proposed that an inflection in the drainage area-slope relation for mountain drainage basins reflects a transition from steep **debris-flow-**dominated channels to lower-gradient **alluvial** channels.

INTRODUCTION

The problem of identifying the actual extent of the channel network from digital elevation models (**DEMs**) is of considerable geomorphic and hydrologic importance, given the widespread use of **DEMs** in simulation models. Physically-based models of hydrologic and erosional processes require differentiation between the runoff generation and erosion mechanisms that operate on hillslopes and in channels. For example, channel network extent directly affects the simulated hydrologic response of a catchment because it determines both hillslope travel distances and network link lengths and thus hydrologic response functions [e.g., **Rodriguez-Iturbe** and **Valdes**, 1979; **Gupta et al.**, 1980]. Consequently, accurate estimation of network source locations is important for accurate runoff prediction using these methods. Identification of network sources is thus of fundamental importance in landscape-scale geomorphic and hydrologic analyses.

A variety of methods exist for automatically extracting channel networks from **DEMs** [e.g., **Mark**, 1983; 1988; **O'Callaghan** and **Mark**, 1984; **Band**, 1986; **Morris** and **Heerdegen**, 1988; **Smith et al.**, 1990], but little attention has been paid to the accuracy of network source representation. The most common method of extracting channel networks from **DEMs** is to specify a critical support area that defines the minimum drainage area required to initiate a channel [e.g., **Band**, 19%; 1989; **Zevenberger** and **Thome**, 1987; **Morris** and **Heerdegen**, 1988; **Tarboton et al.**, 1988; **Lammers** and **Band**, 1990; **Gardner et al.**, 1991]. In practice, this threshold value often is selected on the basis of visual similarity between the extracted network and the blue lines depicted on topographic maps. However, **Morisawa [1957]**, and later **Coffman** and others [1972], demonstrated that blue line networks provide only a poor representation of channel networks observed in the field because they do not depict first-order channels, as well as many second and third-order channels. Other methods used to simulate network source locations include the degree of contour indentation, or **crenulation** [e.g., **Strahler**, 1952; **Morisawa**, 1957; **Lublowe**, 1964; **Smart** and **Surkan**, 1967; **Howard**, 1971; **Abrahams**, 1980], and a minimum slope [e.g., **Shreve**, 1974]. Two general methods have been used to simulate network sources in digital terrain models: a constant threshold area [e.g., **O'Callaghan** and **Mark**, 1984; **Band**, 1986; **Mark**, 1988; **Tarboton et al.**, 1991] and a slope-dependent critical support area [e.g., **Dietrich** et al., 1992;

1993]. This paper critically examines these approaches and suggests modifications to existing procedures and interpretations.

THEORETICAL BASIS FOR ESTIMATING CRITICAL SUPPORT AREAS

Models that predict either constant or slope-dependent thresholds assume different criteria for channel initiation. Assuming that channel heads represent a transition in the dominant sediment transport process implies a constant critical support area, whereas assuming that channel heads represent an erosional threshold leads to a slope-dependent critical support area. These models and their development are discussed in greater detail elsewhere [Dietrich and Dunne, 1993; Montgomery and Dietrich, in press]. Below we outline key assumptions and briefly **discuss** model development and application to the problem of predicting network source locations from digital elevation data.

Constant Threshold

The logic behind a constant critical support area descends from ideas originally developed by Gilbert [1877; 1909]. Essentially, the hypothesis holds that slope-dependent sediment transport on hillslopes gives rise to convex slopes, whereas discharge- and slope-dependent sediment transport in channels gives rise to concave slope profiles. A series of workers developed this hypothesis into the proposition that channel heads correspond to the transition from convex to concave slope profiles [e.g., Kirkby, 1971; 1980; 1986; Smith and Bretherton, 1972; Tarboton et al., 1992].

These models are based on coupling the continuity equation with distinct sediment transport laws for hillslope and **fluvial** processes. In general, sediment transport may be considered to reflect the availability of sediment for transport and the competence of the transporting medium. Thus in most cases, the sediment transport rate (q_s) will be a function of the slope (s), discharge (q), and, if transport capacity **exceeds** sediment supply, the production rate of transportable material (p):

$$q_s = f(s, q, p) \quad (1)$$

For soil-mantled landscapes, many workers exclude p from (1) and formulate a general sediment transport equation as

$$q_s = k q^n s^m \quad (2)$$

where k , n , and m are constants [e.g., **Kirkby**, 1971; 1980; 1986; Ahnert, 1976; 1987; 1988; Tarboton et al., **1992**].

In most landscape evolution models, sediment transport by hillslope and **fluvial** processes involve different parameter values. Models for hillslope sediment transport [e.g., Davison, 1889; Gilbert, 1909; Culling, 1963; **Kirkby**, **1971**] generally assume that $n=0$, and the most widely used formulation for geomorphic modeling is the linear diffusion model ($m=1$):

$$q_s = k_1 s \quad (3)$$

where k_1 is an **erosional** diffusivity. **Fluvial** sediment transport is a function of both discharge and slope, and most workers assume that $n>1$ and $m=2$ for channel processes.

A number of workers have shown that equilibrium slope **profiles** for a slope-dependent transport law are convex, which requires that slope increases with either distance from the drainage divide, or drainage area [e.g., Davison, 1889; Gilbert, 1909; Culling, 1963; **Kirkby**, 1971; 1980; **1986**]. Transport laws with both slope and discharge dependency, on the other hand, result in concave equilibrium slope profiles [e.g., Gilbert, 1877; **Kirkby**, **1971**; 1980; 1986; Smith and Bretherton, **1972**]. Smith and Bretherton [**1972**] further showed that concave slope profiles occur where

$$\partial q_s / \partial q > q_s / q \quad (4),$$

and that convex slope profiles result when the opposite inequality is satisfied. They then showed that concave surfaces are unstable to lateral perturbation, whereas convex surfaces are stable. Smith and Bretherton [**1972**] also proposed a general sediment transport law for both **fluvial** and hillslope processes where

$$q_s = k_1 s + k_2 q^n s^m \quad (n > 1; k_1, k_2 > 0) \quad (5)$$

and argued that channel heads correspond to the transition from convex to concave slopes. Kirkby [1980; 1986] substituted contributing area per unit contour length (a) for discharge in equation (4) and also suggested that the channel head was coincident with a transition from convex slopes where $\partial q_s / \partial a > q_s / a$ to concave slopes where $\partial q_s / \partial a < q_s / a$. Tarboton and others [1992] further proposed that the channel head corresponds to a transition from hillslopes where $\partial s / \partial a > 0$ to channels where $\partial s / \partial a < 0$. However, the transition from convex to concave slope profiles commonly coincides with the transition from divergent to convergent topography, suggesting that these models are more appropriate for representing controls on valley development than for channel initiation [Dietrich and Dunne, 1993; Montgomery and Dietrich, in press] (Figure 1). No data are presently available, however, with which to directly test this hypothesis.

Slope-Dependent Threshold

Models for a slope-dependent critical support area assume that the channel head represents an erosional threshold, an assumption similar to Horton's [1945] hypothesis for drainage network evolution. This assumption requires that the channel head represents a change in sediment transport processes, rather than a spatial transition in process **dominance**. Another key assumption in this approach is that the channel head is associated with erosion initiation, an expectation that will not **be** met, for example, in landscapes where sheetwash erosion occurs. Field observations in humid, soil-mantled landscapes, however, generally support the association of **channel** heads with a change **in** sediment transport processes [Dietrich and Dunne, 1993; Montgomery and Dietrich, in press].

A general model for sediment transport with a threshold control on channelization is given by

$$q_s = k_1 s \quad a < a_{cr} \quad (6a)$$

$$q_s = k_1 s + k_2 q^n s^m \quad a \geq a_{cr} \quad (6b)$$

where a_{cr} is the critical contributing area for channel initiation [Dietrich and Dunne, 1993; Montgomery and Dietrich, in press]. Essentially, this formulation argues that sediment transport occurs by slope-dependent processes **upslope** of a critical contributing area per unit contour **length**, whereas discharge-dependent processes also transport sediment downslope of the channel head.

The critical contributing area per unit contour length required to initiate a channel may be estimated from simple models of channel initiation processes. Field observations and measurements suggest that these processes include overland flow, seepage, piping, and landsliding [e.g., **Kirkby** and Chorley, 1967; Dunne, 1980; Jones, 1987; Montgomery and Dietrich, 1988; 1989; in press; **Dietrich** and Dunne, **1993**]. Models for channel initiation by overland flow and shallow landsliding predict inverse relations between critical support area and local slope.

Channel initiation by overland flow may be assumed to occur where the basal shear stress of the flow (τ_b) exceeds the critical shear stress of the ground surface (τ_{cr}). For a steady-state rainfall intensity (q_r) a laminar flow model predicts that the critical contributing area required for $\tau_b > \tau_{cr}$ is given by

$$a_{cr} = C / (\tan\theta)^2 \quad c = f(\tau_{cr}^3, q_r^{-1}) \quad (7)$$

where θ is the local slope [Dietrich et al., 1992; 1993; Montgomery and Dietrich, in press]. Thus, smaller drainage areas are needed to initiate channels on steeper slopes. Rearranging equation (7), channels may be defined using the criterion of $a(\tan\theta)^2 \geq C$. The absolute value of the proportionality constant C depends on both ground surface (τ_{cr}) and climatic (q_r) properties.

An analogous model for channel initiation by shallow landsliding is derived from combining a model for shallow **throughflow** and the **infinite-slope** stability model. This simple hybrid model for cohesionless soils predicts that

$$a_{cr} = (T/q_r) \sin\theta (\rho_s/\rho_w) [1 - (\tan\phi/\tan\theta)] \quad (8)$$

where T is the soil transmissivity, ρ_s and ρ_w are the bulk density of the soil and water, and ϕ is the friction angle of the soil [Montgomery and Dietrich, in press]. This relation predicts a non-loglinear relation between the critical support area and local slope and is only valid for steep slopes where $\tan\theta \geq [(\rho_s - \rho_w) / \rho_s] \tan\phi$.

The available field data on channel head locations in landscapes where overland flow and landsliding are the dominant channel-initiation processes support the general form of equations (7) and (8) [Montgomery and Dietrich, in press]. In mountainous landscapes, the transition from landslide to overland-flow-dominated channel initiation occurs at $\tan\theta \approx 0.5$. However, for most of this paper we will consider only channel initiation by overland flow, as expressed by (7). The reader interested in channel initiation in steeper landscapes is referred to discussions presented elsewhere [Dietrich et al., 1986; 1987; Montgomery and Dietrich, 1989; in press; Dietrich and Dunne, 1993]. Identification of an appropriate value for C is a major impediment to implementing the overland flow model for channel network extraction from DEMs, as this parameter should vary with both rainfall and critical shear stress of the ground surface, the latter reflecting both soil properties and the type and density of vegetation cover.

APPLICATION OF METHODS

Each of the preceding hypotheses may be correct under different circumstances and over different time scales. In landscapes where rainsplash and sheetflow occur, for example, channel heads may indeed coincide with a spatial transition in process dominance. In many soil-mantled landscapes, however, a threshold model for channel initiation is more appropriate. Montgomery and Dietrich [in press] proposed that a continuity based approach, like that employed to argue for a constant a_{cr} , is most appropriate for modeling valley development over geologic time (e.g., $10^4 - 10^6$ yr) whereas a threshold-based approach is most appropriate for modeling channel head locations over shorter, geomorphic time scales (e.g., $10^2 - 10^3$ yr). Thus, these hypotheses need not be viewed as competing ideas, rather they are complementary. Below we examine methods for implementing these criteria and test their appropriateness for locating channel network sources

against high-resolution DEM data from an area in which the channel network has been mapped in the field.

The effect of spatial variability of slope on channel network extent is one primary difference between channel networks defined by constant and slope-dependent thresholds. Using a slope-dependent threshold, drainage density is greater in steeper portions of a catchment, as is found in natural landscapes. For the case of a catchment with little spatial variability in slope, the constant and slope-dependent threshold methods converge and predict similar channel networks. In relatively small, or homogeneous basins the channel networks defined by these methods may not differ significantly. Differences between the two methods should increase with basin size and geologic complexity.

Constant Threshold

The theory equating a channel head with the transition from **slope**-dependent hillslope transport to slope and discharge-dependent **fluvial** transport [e.g., Smith and Bretherton, 1972; **Kirkby**, 1980; **Willgoose**, 1989; Tarboton et al., 1992] predicts that the channel head is associated with a change in the relation between local slope and drainage area (or **discharge**). Tarboton and others [**1991; 1992**] developed this criterion **into** a method for determining network source locations from digital elevation data. We show below that, as proposed, **their** method is inconsistent with the theory and predicts anomalously large hillslope sizes. We also show that a similar approach, reformulated in more appropriate terms, provides a reasonable estimate of the scale of the transition from convergent to divergent topography, or the **hillslope/valley** transition.

The method proposed by Tarboton and others [**1991; 1992**] consists of the following operations. First, a critical support area is assumed and a channel network is extracted from a DEM. This is then repeated for a number of support areas. Next, one generates a plot of link slope (the average channel slope between two confluences) versus the drainage area at the downstream end of the link for each link in the extracted channel networks. Finally, the individual link values are averaged and the “appropriate” critical support area is determined from an inflection in the composite drainage area-slope relation for the averaged data.

Each of these steps presents either conceptual or procedural problems. First, the method identifies an inflection in the drainage area-slope relation, rather than the reversal from a positive to inverse relation predicted by the theory. Although a reversal **is** seen in some data sets, the drainage area at which it occurs depends upon the support area initially assumed to extract the channel network (see Figure 9 of Tarboton and others [1991]). Consequently, Tarboton and others [1991] chose instead to relate an inflection observed in some data sets to the scale of channel initiation and offered an argument to explain that this inflection represented **the relation** expected from “noisy” DEM data.

The use of the link slope presents further problems. First, it requires that a channel network be extracted from the DEM. In other words, the search for an appropriate support area is constrained to be **within** a previously defined channel network. Furthermore, link slopes introduce systematic biases into the data. This occurs because the link slope is defined as the elevation difference between the upper and lower confluences bounding the link divided by the length of the link. For a slope profile on which the gradient is not constant, the average slope of a channel link is a function of the length of the link. However, the length of individual links within a catchment depends upon the threshold area used to define the channel network. **Link** slopes then depend on the threshold used to extract the channel network, which probably explains the threshold size control on the reversal in the drainage area-link slope relation.

Another problem with the proposed method **is** a consequence of common flow-routing algorithms in grid-based digital terrain models. The traditional method of directing flow from one grid cell, or pixel, into one of its eight neighbors does not allow for the representation of divergent flow [e.g., Moore et al., 1988; Freeman, 1991]. In essence, flow is allowed to converge into valleys, but not to diverge on hillslopes, resulting in preferential flow partitioning along the cardinal and diagonal directions of the grid matrix in divergent topography [e.g., Freeman, 1991; Fairfield and Leymarie, 1991]. This **artefact** makes it difficult to represent, let alone distinguish, the transition from convergent to divergent topography. A number of newer algorithms for representing divergent flow have been

developed [Freeman, 1991; Quinn et al., 1991; Cabral and Burges, 1992], but are not yet widely implemented.

This **artefact** of representing hillslopes with linear, rather than divergent, flow allows a simple check on the hillslope lengths implied by the method of Tarboton and others [1991; 1992]. The drainage area contributing to a pixel at **the** base of a divergent hillslope will be equal to the width of the pixel multiplied by the **upslope** distance to the drainage divide. Conversely, the hillslope length will equal the drainage area at the hillslope/valley transition divided by the pixel width. The inflection in the link slope plots of Tarboton and others [1991; 1992] occurs at drainage areas of 10^5 to 10^6 m². For a pixel size of 30 m, this implies hillslope lengths on the order of 3.3 to 33 km. Field surveys indicate that typical **hillslope** lengths are on the order of **10's** to 100's of meters, but in low-gradient semi-arid landscapes hillslope lengths may approach 1 km [T. Dunne, unpublished data]. Thus, the drainage **area-slope** relation noted by Tarboton and others [1991; 1992] is related to something other than the hillslope/valley transition.

In order to be more consistent with the theory outlined above, we formulate our analyses in terms of local slopes, which in a grid-based DEM may be best approximated by the slopes for individual grid elements, or pixels. Figure 2 shows plots of drainage area versus local slope for two U.S.G.S. 30 m **DEMs**. Prior to averaging, there is tremendous scatter apparent in the data, but the averaged plot for the South Fork Smith **River**, California, (Figure **2A**) reveals an inflection at a drainage area of approximately 1 km². **Plots** constructed with the link-averaging technique also show this inflection. The Smith **River** is in rugged mountainous terrain and a typical 1 km² watershed in this area is shown in Figure 3. The drainage area associated with the inflection in the drainage area-slope relation (the "hillslope" scale of Tarboton and others [1991;1992]) roughly corresponds to the outlet of this basin, which contains a magnitude 17 valley network. The reversal predicted by the theory is not readily apparent in Figure **2A**, but could be reflected in the two smallest data points at a drainage area of about 2×10^{-3} km², which would imply a hillslope length of 67 m. Extensive field experience in the coastal mountains of southern **Oregon** and northern California provides the basis for concluding that this provides a reasonable estimate of hillslope lengths in this area.

A similar plot of drainage area versus local slope for the Schoharie Creek catchment reveals a reversal at an area of $6 \times 10^{-3} \text{ km}^2$, but no inflection at larger areas (Figure 2B). The pixel width of 30 m thus implies a hillslope length of 200 m. The Schoharie Creek watershed is a low-gradient area and, although we have no field experience in this region, this estimate of the hillslope length seems reasonable.

It appears then that we must explain two distinct changes in the drainage area-slope data derived from digital elevation models; a reversal at very small drainage areas, and an inflection in the relation at local slopes of about 0.2 to 0.3. We chose to examine this question with high-resolution (2 m grid) DEMs of areas in which the channel network previously was mapped in the field [Montgomery and Dietrich, 1989; 1992]. The DEM of the Tennessee Valley area near San Francisco, California, was generated from low-altitude stereo aerial photographs for use in geomorphic process modeling [Dietrich et al., 1992; 1993]. Consequently, the DEM was generated at a resolution sufficient to capture the divergent form of the hillslopes in this catchment. In order to allow comparison with more typical resolution data, we also examine results obtained using the U.S.G.S. 30 m grid size DEM for a larger area that contains the catchment covered by high-resolution data. For both data sets, drainage areas and local slopes were calculated using the eight neighbor method for flow partitioning.

The plot of the averaged drainage areas versus local slope for the 30 m data (Figure 4A) exhibits an inflection at a drainage area of about 10^{-1} km^2 and a reversal suggested by the averaged values for individual pixels at a drainage area of about $3 \times 10^{-3} \text{ km}^2$. The hillslope length implied from the inflection is 6.6 km; that implied by the reversal is 100 m. For comparison, the length of the entire watershed covered by the high-resolution data is about 1 km. A similar plot from the high-resolution DEM also exhibits a pronounced inflection at a drainage area of about 10^{-1} km^2 (Figure 4B). In this case, however, a well-defined reversal in the trend of the averaged data occurs at 10^{-4} km^2 , corresponding to a hillslope length of 50 m.

We used a digital terrain model capable of representing topographic divergence to test whether the transition from divergent to convergent topography coincides with the reversal apparent in the drainage area-slope relation. The digital terrain model TOPOG [O'Loughlin, 1981; 1986] was used

to divide the catchment into a series of topographic elements defined by the intersection of contours and orthogonal flow lines and to calculate the slope and contributing area per unit contour length for each element. In a modification of the **criteria** used by **Dietrich** and others [1992], we divided elements into divergent and convergent classes based on the **ratio** of the length of the lower and upper contours bounding the element. The lower contour is longer for divergent elements and shorter for convergent elements. Plots of drainage area versus slope for elements in both the Tennessee Valley area and similar high-resolution data from **Mettman** Ridge in coastal Oregon [Montgomery and Dietrich, in press] both reveal a general reversal from a positive to a negative relation coincident with the transition from divergent to convergent slopes (Figure 5). In both cases, there is tremendous data scatter and most of the data cluster around the hillslope/valley transition. The transition from divergent to convergent elements for both data sets occurs at a contributing area per unit contour length of 30 - 50 m, essentially equal to the hillslope length suggested by analysis of the high-resolution grid-based **DEM**. Field mapping of channel networks and surveyed slope profiles in both of these areas [Montgomery and Dietrich, 1988; 1989; 1992] confirms that these values provide reasonable estimates of hillslope lengths, indicating that when used with sufficient resolution, a constant support area is appropriate for defining the **hillslope/valley** transition.

Slope Dependent Threshold

The available field data from arid to temperate environments indicate that the drainage area required to initiate a channel is a function of the local slope, except in locations where bedrock properties control channel head locations [Montgomery and Dietrich, in press]. Channel heads in Tennessee Valley define a slope-dependent transition from unchanneled to channeled valleys (Figure 6), implying **that** the channel network could be defined given the appropriate threshold. Although landsliding dominates channel initiation on the steepest slopes in this area, the regression of drainage area (**A_{cr}**) against local slope for data from channel heads yields

$$A_{cr} = 1,790 \tan \theta^{-1.84} \quad (r^2 = 0.68) \quad (9)$$

where A_{cr} is in square meters. This relation is similar to that predicted by equation (7) [Montgomery, 1991].

The field-mapped channel network greatly exceeds the network defined by blue lines on the U.S.G.S. 7.5' quadrangle (Figure 7), as the blue line network depicts only two first-order channels in this magnitude 36 watershed. In contrast, the channel network defined by $C \geq 2000 \text{ m}^2$ reasonably approximates the field-mapped channel network, indicating that equation (7) may be used to delineate the channel network, given appropriate constraints on C.

Based on field data from three study areas in California and Oregon, Montgomery [1991] reported that

$$C \approx 10^6 / R_a \quad (10)$$

where C is in square meters and R_a is mean annual rainfall in millimeters. Although this relation suggests a convenient method for estimating an appropriate value of C, it is important to recognize that the critical shear stress is also a major determinant of C. For example, field data from an arid, dissected alluvial fan in Nevada [Repka, unpublished data] indicate significantly smaller source areas than in any of the semi-arid to humid study areas mapped by Montgomery and Dietrich [1988; 1992], documenting that changes in the critical shear stress due to variations in ground cover may dominate the value of C. Thus, simple correlation of C with mean annual rainfall, as in equation (10), is unjustified. Unfortunately, there is no theory for predicting the value of C directly from either drainage area or slope, the primary topographic attributes that may be derived from a DEM.

Dietrich and others [1993] presented a method for approximating C that involves estimating τ_{cr} and calibrating q_r against observed hydrologic response. For the Tennessee Valley area, the steady-state rainfall required to saturate convergent areas of the landscape provides a reasonable estimate of q_r [Dietrich et al., 1993]. Given that C is a function of the 3rd power of τ_{cr} , the predicted extent of the channel network is extremely sensitive to the assumed value of τ_{cr} [Dietrich et al., 1993]. When τ_{cr} and q_r may be estimated with some confidence, then this technique may be used to simulate channel

network source locations. **In** many potential applications, however, appropriate values of these parameters will be unknown.

Several other approaches allow estimation of channel network extent using a slope-dependent threshold. Montgomery and **Dietrich [1992]** presented evidence that, in a landscape where channel head locations may reflect a long-term average position, the variance in channel head locations effectively defines the limit to convergent topography, and thus the hillslope size. They showed that portions of the landscape where $a(\tan\theta)^2$ was just less than necessary to sustain a channel essentially surround the valley network. Thus, if channel networks are defined using smaller and smaller thresholds, then eventually numerous channels should branch from the sides of channels and generate a “feathering” of channels extending into planar or divergent hillslopes (Figure **8**). Consequently, one criterion for defining the extent of the channel network is to use the smallest value of C that does not result in development of significant feathering along the low-order channels in a basin’s headwaters.

We calculated interior-link, exterior-link and source-basin lengths and areas for channel networks extracted from the Schoharie Creek and Tennessee Valley data using different thresholds to examine whether statistical properties of channel networks are useful for estimating C . **Abrahams [1984]** reviewed previous network studies and **concluded** that the ratio of the mean interior to mean exterior link length (L_i/L_e) was approximately equal to unity in natural channel networks. Analyses of ratios of interior and exterior link lengths from networks defined with differing threshold areas indicate that these properties do not change systematically with the imposed threshold (Figure **9A**). Although this ratio varies, it remains generally close to unity. This reflects the inter-dependence of the number and lengths of network links. A smaller source area results in **an** almost equal increase in the number of interior and exterior links and decreases the mean length of both populations. Consequently, this ratio is rather insensitive to the source area used to define the network and, therefore, does not provide useful constraints on network extent.

Link area ratios (A_e/A_s and A_i/A_s), on the other hand, may be more useful. **Montgomery [1991]** found that for channel networks in small basins mapped in the field mean exterior-link drainage area was just less than twice

the mean source area ($A_e/A_s \approx 2$). The mean exterior and interior link areas for the Schoharie Creek catchment converge to the empirical values of twice the source-area size at $C = 8,000$ to $16,000 \text{ m}^2$ (Figure 9B). For the Tennessee Valley catchment, this occurs at $C = 500 \text{ m}^2$ (Figure 9B). Probability distribution functions (PDF's) of interior-link, exterior-link, and source-basin lengths and areas vary with the threshold used to define the channel network. For the C values examined, the PDF's for source and network properties in the Schoharie Creek catchment appear most similar for $C = 16,000 \text{ m}^2$ and the analogous PDF's for networks extracted from the high-resolution Tennessee Valley DEM appear most similar at $C = 1,000$ to $2,000 \text{ m}^2$. Although there is no unique value of C predicted by examination of network statistical properties, such procedures may provide rough estimates of appropriate values to use for channel network extraction from DEMs.

The approaches discussed above entail the implicit assumption that the channel network is in long-term equilibrium with the land surface upon which it is developed. In reality, channels at any given time could start anywhere within the valley network. In badland landscapes, for example, channels may extend onto hillsides in a manner resembling the feathering discussed earlier. In some landscapes extensive dry valleys record significant climatic variations. Furthermore, previous land-sculpting processes, such as glaciation, may control channel network architecture. Realistically, if the objective is an accurate description of the contemporary channel network extent, then there is no proven substitute for collecting some field data on channel head locations. A threshold of the form $a_{cr}(\tan\theta)^2$ could be fit to even minimal field data and then used to extrapolate the channel network extent in similar areas.

DISCUSSION

While a reversal in the drainage area-slope relation correlates with the hillslope/valley transition, what controls the inflection observed in the averaged drainage area-slope relation for some data sets? Where it is present, the inflection in the drainage area-slope plots of Figures 2 and 4 occurs at gradients between 20 and 30%. Each of the inflections identified in the figures presented in Tarboton and others [1991] occur in this same gradient range. In the Tennessee Valley study basin, the inflection also is apparent in the

analysis of high-resolution **DEMs** (Figure 4), indicating that it is not a consequence of poor fine-scale resolution of commercially-available **DEMs**. The drainage area at **which** this inflection occurs ($\approx 10^{-1} \text{ km}^2$) correlates well with the transition from either colluvium-floored channels, or those with a discontinuous veneer of alluvium overlying bedrock, to lower-gradient channels within alluviated valleys. Field mapping of channels in mountain drainage basins in Oregon and Washington indicates that a transition from debris-flow-dominated to alluvial channels occurs in **this** gradient range [Montgomery, unpublished data] and corresponds to a change in the drainage area-slope relation observed within the channel network. **Seidl** and **Dietrich [1992]** report a change in the drainage area-slope properties of tributary junctions derived from topographic maps of the Oregon Coast Range at gradients of about 20% and **argue that** this transition reflects a change in the dominant erosional mechanism from debris-flow to **fluvial** processes. We suggest that the inflection observed in the drainage area-slope relation derived from **DEMs** reflects this transition in valley-incision processes.

The results presented above suggest a schematic illustration of landscape partitioning into drainage area and slope regimes **that** define hillslopes, unchanneled valleys, and debris-flow-dominated and alluvial channels (Figure 10). Hillslopes are defined by topographic divergence and hillslope size may be approximated by a constant drainage area. Unchanneled valleys occupy the lowest gradients for a given drainage area. The boundary between unchanneled valleys and **fluvial** channels is defined by a **slope-dependent threshold** that reflects both critical shear stress and climate. The data available at present suggest that channels on slopes in **excess of** 20 to 30% are debris-flow dominated. Thus, we would not expect to see this inflection in the averaged drainage area-slope relation for low to moderate-gradient landscapes. This model for landscape partitioning suggests that boundaries between debris-flow-dominated and alluvial channels and between hillslopes and valleys can be estimated from **DEMs**, but that **the** extent of the channel network cannot. Other considerations, such as those developed above, are necessary to approximate the locations of channel heads from **DEMs**.

CONCLUSIONS

Theories for valley development and channel initiation respectively predict constant and slope-dependent critical support areas. Both theories are supported by field data. The extent of topographically-divergent hillslopes, and thus the extent of the *valley* network, corresponds to a change in sign of the relation between local slope and contributing area per unit contour length. This transition is readily derivable from digital elevation data, but a higher resolution grid size may be required than the 30 m data commonly available. The extent of debris-flow-dominated channels also can be determined from an inflection in the drainage area-slope relations derived from a DEM. In contrast, the extent of the contemporary channel network cannot be directly determined from drainage area-slope relations extracted from **DEMs**. Field data, even if limited, on the drainage area-slope relation for channel heads is the best method for determining appropriate values of parameters defining channel network extent.

Acknowledgements

This work was supported by grant TFW **FY92-010** from the SHAMW committee of the Washington State Timber/Fish/Wildlife agreement, NSF grant **CES-8957469**, and the Minnesota **SuperComputer** Institute (**MSI**). We thank Harvey Greenberg and Keith Helmlinger for computational and graphics support, Jim **McKean** for generating the high-resolution data of Tennessee Valley, and Bill **Dietrich** for conversations that stimulated our thinking. **Mariza Costa-Cabral** and an anonymous reviewer provided valuable critiques of the manuscript.

REFERENCES

- Abrahams, A. D., Channel link density and ground slope: *Ann. Am. Assoc. Geol.*, **70**, 80-93, 1980.
- Abrahams, A. D., Channel networks: A geomorphological perspective, *Wat. Resour. Res.*, **20**, 161-188, 1984.
- Ahnert, F., Brief description of a comprehensive three-dimensional process-response model of **landform** development, *Zeit. f. Geomorph.*, N. F., **Suppl. Bd. 25**, 29-49, 29-49, 1976.
- Ahnert, F., Approaches to dynamic equilibrium in theoretical simulations of slope development, *Earth Surf. Proc. and Land.*, **12**, 3-15, 1987.
- Ahnert, F., Modelling **landform** change, in *Modelling Geomorphological Systems*, edited by M. G. Anderson, John Wiley & Sons, Ltd., pp. **375-400**, 1988.
- Band, L. E., Topographic partition of watersheds with digital elevation models, *Wat. Resour. Res.*, **22**, 15-24, 1986.
- Band, L. E., A terrain-based watershed information system, *Hydrol. Proc.*, **3**, 151-162, 1989.
- Cabral, M. and S. J. Burges, DEMON: A new method for the automated extraction of contributing areas and drainage networks from rectangular **DEMs**, *EOS, Trans. Am. Geoph. U.*, **73 (43)**, 202-203, 1992.
- Coffman, D. M., E. A. Keller, and W. N. Melhom, New topologic relationship as an indicator of drainage network evolution, *Wat. Resour. Res.*, **8**, 1497-1505, 1972.
- Culling, W. E. H., Soil creep and the development of hillside slopes, *J. Geol.*, **71**, 127-161, 1963.
- Davison, C., On the creeping of the soil-cap through the action of frost, *Geol. Mag.*, **6**, 255, 1889.
- Dietrich, W. E., C. J. Wilson, and S. L. Reneau, Hollows, colluviurn, and landslides in soil-mantled landscapes, in *Hillslope Processes*, edited by A. D. Abrahams, pp. 361-388, Allen and Unwin, London, 1986.
- Dietrich, W. E., S. L. Reneau and C. J. Wilson, Overview: "zero-order basins" and problems of drainage density, sediment transport and hillslope morphology, *Int. Assoc. Hydrol. Sci. Pub.* **165**, 49-59, 1987.

- Dietrich, W. E., and Dunne, T., The channel head, in *Channel Network Hydrology*, edited by K. Beven and M. J. Kirkby, pp. 176-219, J. Wiley and Company, 1993.
- Dietrich, W. E., C. J. Wilson, D. R. Montgomery, J. McKean, and R. Bauer, Erosion thresholds and land surface morphology, *Geology*, 20, 675-679, 1992.
- Dietrich, W. E., C. J. Win, D. R. Montgomery, and J. McKean, Analysis of erosion thresholds, channel networks and landscape morphology using a digital terrain model, *J. Geol.*, 101, 259-278, 1993.
- Dunne, T., Formation and controls of channel networks, *Prog. in Phys. Geog.*, 4, 211-239, 1980.
- Fairfield, J., and P. Leymarie, Drainage networks from grid digital elevation models, *Wat. Resow. Res.*, 27, 709-717, 1991.
- Freeman, T. G., Calculating catchment area with divergent flow based on a regular grid, *Computers & Geosciences*, 17, 413-422, 1991.
- Gardner, T. W., K. C. Sasowsky, and R. L. Day, Automated extraction of geomorphic properties from digital elevation data, *Zeit. für Geomorph.*, Suppl. 80, 57-68, 1991.
- Gilbert, G. K., 1877, *Geology of the Henry Mountains*: U. S. Geographical and Geological Survey, 160p.
- Gilbert, G. K., The convexity of hill tops, *J. Geol.*, 17, 344-350, 1909.
- Gupta, V. K., E. Waymire, and C. Y. Wang, A representation of an instantaneous unit hydrograph for geomorphology, *Wat. Resow. Res.* 16, 855-862, 1980.
- Horton, R. E., Erosional development of streams and their drainage basins; hydrophysical approach to quantitative morphology, *Geol. Soc. Am. Bull.*, 56, 275-370, 1945.
- Howard, A. D., Simulation of stream networks by headward growth and branching, *Geograph. Anal.*, 3, 29-50, 1971.
- Jenson, S. K. and J. O. Dominique, Extracting topographic structure from digital elevation data for geographic information system analysis, *Photogramm. Eng. Remote Sensing*, 54, 1593-1600, 1988.
- Jones, J. A. A., The initiation of natural drainage networks, *Prog. Phys. Geog.*, 11, 207-245, 1987.

- Kirkby, M. J., Hillslope process-response models based on the continuity equation, *Inst. Brit. Geog. Spec. Pub.* 3, 15-30, 1971.
- Kirkby, M. J., The stream head as a significant geomorphic threshold, in *Thresholds in Geomorphology*, edited by D. R. Coates and J. D. Vitek, pp. 53-73, Allen and Unwin, London, 1980.
- Kirkby, M. J., A two-dimensional simulation model for slope and stream evolution, in *Hillslope Processes*, edited by A. D. Abrahams, pp. 203-222, Allen and Unwin, London, 1986.
- Kirkby, M. J. and R. J. Chorley, Throughflow, overland flow and erosion, *Bull. Int. Assoc. Sci. Hydrol.*, 12, **5-21**, 1967.
- Lammers, R B., and Band, L. E., Automatic object representation of drainage basins: *Computers & Geosciences*, 16, 787-810, 1990.
- Leopold, L. B., and Maddock, T., The hydraulic geometry of stream channels and some **physiographic implications**, U.S. *Geol. Surv. Prof. Pup.* 252, 1953.
- Lublowe, J. R., Stream junction angles in the dendritic drainage pattern, *Am. J. Sci.*, **262, 325-29**, 1964.
- Mark, D. M., Automated detection of drainage networks from digital elevation models, *Auto-Carto*, **6**, 169-178, 1983.
- Mark, D. M., Network models in geomorphology, in *Modelling Geomorphological Systems*, edited by M. G. Anderson, John Wiley & Sons, Inc., 1988.
- Montgomery, D. R., Channel initiation and landscape evolution [dissert.], University of California, Berkeley, **421p.**, 1991.
- Montgomery, D. R., and W. E. Dietrich, *Where do channels begin?*, *Nature*, 336,232-234,1988.
- Montgomery, D. R., and W. E. Dietrich, Source areas, drainage density and channel initiation, *Wat. Resow. Res.*, 25, 1907-1918, 1989.
- Montgomery, D. R., and W. E. Dietrich, Channel initiation and the problem of landscape scale, *Science*, **255, 826-830**, 1992.
- Moore, I. D. and R B. **Grayson**, Terrain-based catchment partitioning and runoff prediction using vector elevation data, *Wat. Resour. Res.*, 27, **1177-1191**, 1990.
- Moore, I. D., E. M. **O'Loughlin**, and G. J. **Burch**, A contour-based topographic model for hydrological and ecological applications, *Earth Surf. Proc. & Land.*, 13, 305-320, 1988.

- Morlsawa, M. E., Accuracy of determination of stream lengths from topographic maps, *Amer. Geophys. U. Trans.*, 38, **86-88**, 1957.
- Morris, D. G. and R. G. Heerdegen, Automatically derived catchment boundaries and channel networks and their hydrological applications, *Geomorphology*, 1, 131-141, 1988
- O'Callaghan**, J. and D. M. Mark, The extraction of drainage networks from digital elevation data, *Comput. Vision Graphics Image Process.*, 28, 323-344, 1984.
- O'Loughlin**, E. M., Saturation regions in catchments and their relation to soil and topographic properties, *J. Hydrol.*, 53, **229-246**, 1981.
- O'Loughlin**, E. M., Prediction of surface saturation zones in natural catchments by topographic analysis, *Wat. Resow. Res.*, 22, **794-804**, 1986.
- Quinn, P., K. Beven and O. Planchon, The prediction of hillslope flow paths for distributed hydrological modeling using digital terrain models, *Hydrol. Proc.*, 5, 59-79, 1991.
- Rodriguez-Iturbe, I., and J. B. Valdes, The geomorphologic structure of hydrologic response, *Wat. Resow. Res.*, 15, 1409-1420, 1979.
- Seidl, M., and W. E. Dietrich, The problem of channel incision into bedrock, in *Functional Geomorphology*, edited by K.-H. Schmidt and J. de Ploey, Catena Supplement 23, pp. 101-124, Catena-Verlag, Cremlingen, 1992.
- Shreve, R. L., Variation of mainstream length with basin area in river networks, *Wat. Resour. Res.*, 10, 1167-1177, 1974.
- Smart, J. S., and A. J. Surkan, The relation between mainstream length and area in drainage basins, *Wat. Resow. Res.*, 3, **963-974**, 1967.
- Smith, T. R. and F. P. Bretherton, Stability and the conservation of mass in drainage basin evolution, *Wat. Resow. Res.*, 8, 1506-1529, 1972.
- Smith, T. R., C. Zhan and P. Gao, A knowledge-based, two-step procedure for extracting channel networks from noisy DEM data, *Computers & Geosciences*, 16, 777-786, 1990.
- Strahler, A. N., Hypsometric (area-altitude) analysis of erosional topography, *Geol. Soc. Am. Bull.* 63, **1117-1142**, 1952.
- Tarboton, D. G., R. L. Bras, and I. Rodriguez-Iturbe, The fractal nature of river networks, *Wat. Resour. Res.*, 24, **1317-1322**, 1988.

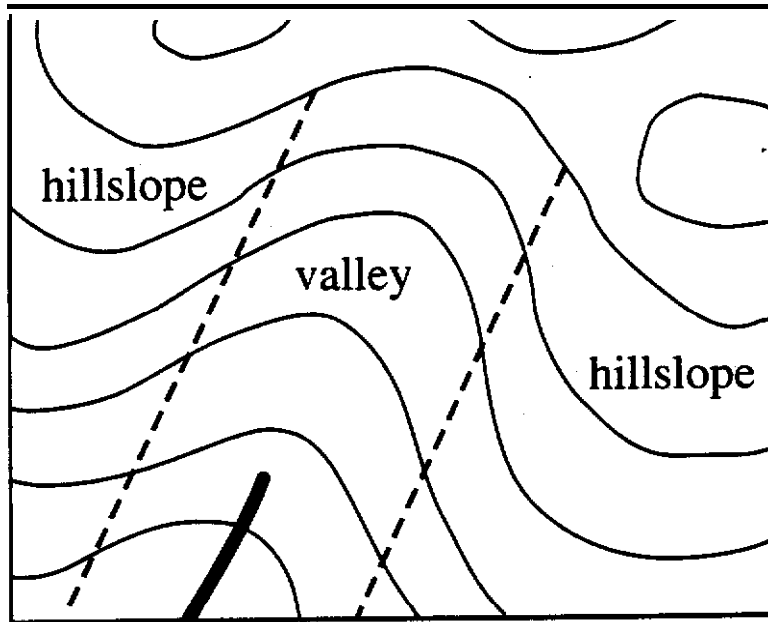
- Tarboton, D. G., R. L. Bras, and I. Rodrlquez-Iturbe, On the extraction of channel networks from digital elevation data, *Hydrol. Proc.*, 5, 81-100, 1991.
- Tarboton, D. G., R. L. Bras, and I. Rodrlquez-Iturbe, A physical basis for drainage density, *Geomorphology*, 5, 59-76, 1992.
- Willgoose, G. R., A physically based channel network and catchment evolution model [**dissert.**], Massachusetts Institute of Technology, Cambridge, Massachusetts, **464p.**, 1989.
- Zevenbergen, L. W., **and** C. R. Thome, Quantitative analysis of land surface topography, *Earth Surf. Proc.*, 12, 47-56, 1987.

FIGURE CAPTIONS

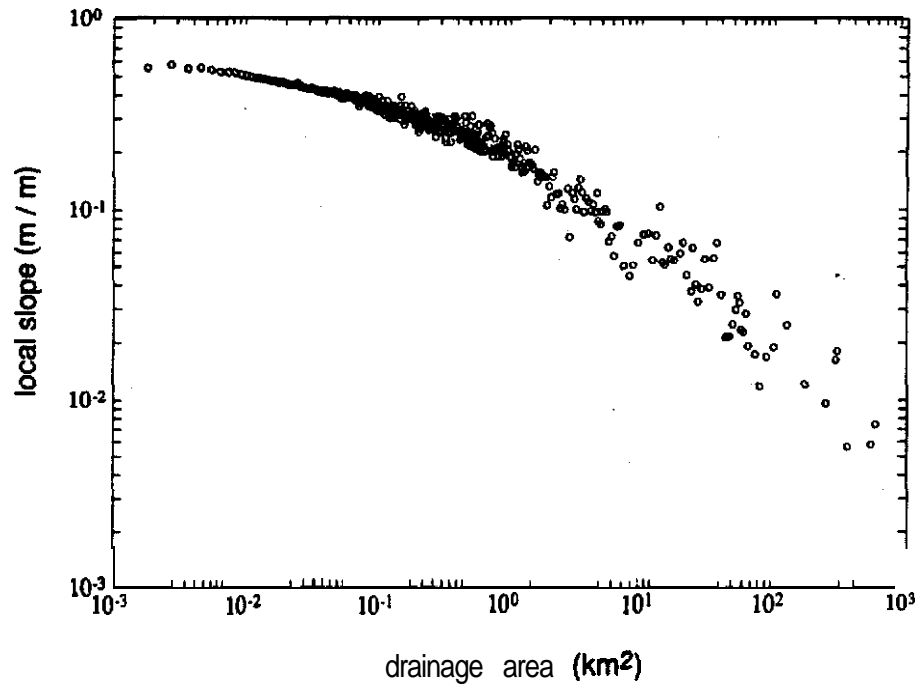
- 1 Schematic topographic map illustrating distinctions between hillslopes, valleys, and channels. Hillslopes are areas of topographic divergence; valleys are areas of topographic convergence. Dashed lines indicate transition from hillslopes to valleys. A channel (thick black line) is a morphologic feature defined by sediment transport concentrated within definable banks. Channels typically begin some distance down valley axes from drainage divides.
- 2 Plots of local slope versus drainage area for averaged data from all pixels for U.S.G.S. 30 m DEM's of **A)** South Fork Smith River, California, and **B)** Schoharie Creek, New York.
- 3 Portion of U.S.G.S. Ship Mountain 7.5' topographic quadrangle showing a typical 1 km* watershed in the South Fork Smith River drainage basin. Solid lines indicate valley network defined by areas of convergent topography.
- 4 Plots of drainage area versus local slope for averaged data from the Tennessee Valley area of **Marin** County, California, for **A)** a portion of U.S.G.S. Point Bonita 7.5' quadrangle DEM data and **B)** high-resolution data for a sub-basin of the area covered **by** the U.S.G.S. data.
- 5 **Plots** of local slope **versus contributing** area per unit contour length for each topographic element generated by TOPOG [O'Loughlin, 1986] from high-resolution DEM data from **A)** Mettman Ridge, Oregon, and **B)** Tennessee Valley, California. Data from divergent elements are shown as crosses, data from convergent elements are shown as circles. Linear band of data in Figure **5B** is an **artefact** of flow tube architecture and has no physical significance.
- 6 Plot of drainage area versus local slope for data from field mapping in the Tennessee Valley catchment. Triangles are from channels, solid

circles are from channel heads, and open circles are from unchanneled valleys. Data from Montgomery and **Dietrich [1992]**.

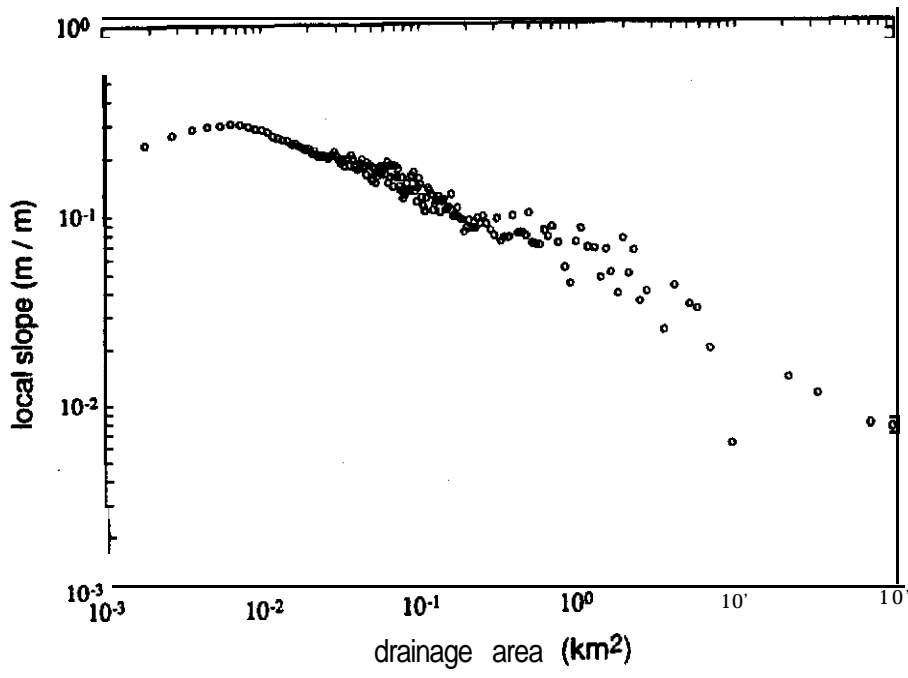
- 7 Comparison of channel networks determined for the Tennessee Valley watershed by field mapping (top), blue lines depicted on **U.S.G.S.** Point Bonita 7.5' quadrangle (middle), and $A_{cr}(\tan\theta)^2 = 2,000 \text{ m}^2$ (bottom).
- 8 Maps of the Schoharie Creek channel network defined using A) $A_{cr}(\tan\theta)^2 = 64,000 \text{ m}^2$, B) $A_{cr}(\tan\theta)^2 = 16,000 \text{ m}^2$, C) $A_{cr}(\tan\theta)^2 = 4,000 \text{ m}^2$, and D) $A_{cr}(\tan\theta)^2 = 2,000 \text{ m}^2$. Note the "feathering" along low-order channel in the lower (steeper) portions of the catchment in C and D.
- 9 A) Ratio of mean interior to exterior **link** length versus C [$A_{cr}(\tan\theta)^2$] for Schoharie Creek (open circles) and Tennessee Valley (solid circles). B) Ratio of mean link area to mean source area for exterior (solid) and interior (open) links from Schoharie Creek (squares) and Tennessee Valley (circles).
- 10 Schematic illustration of relations between drainage area and local slope depicting **hillslope/valley** transition and channel initiation criteria. Note that the trend of the averaged data [wide shaded line] for a catchment will vary between landscapes and watersheds.



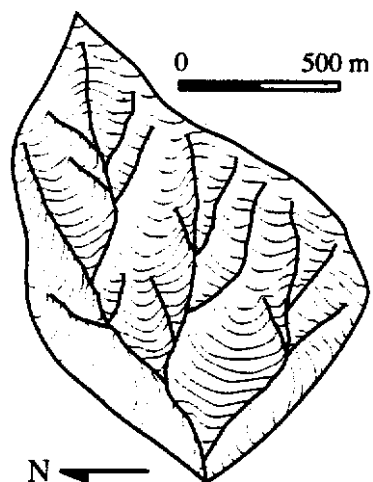
Montgomery and Foufoula Figure 1



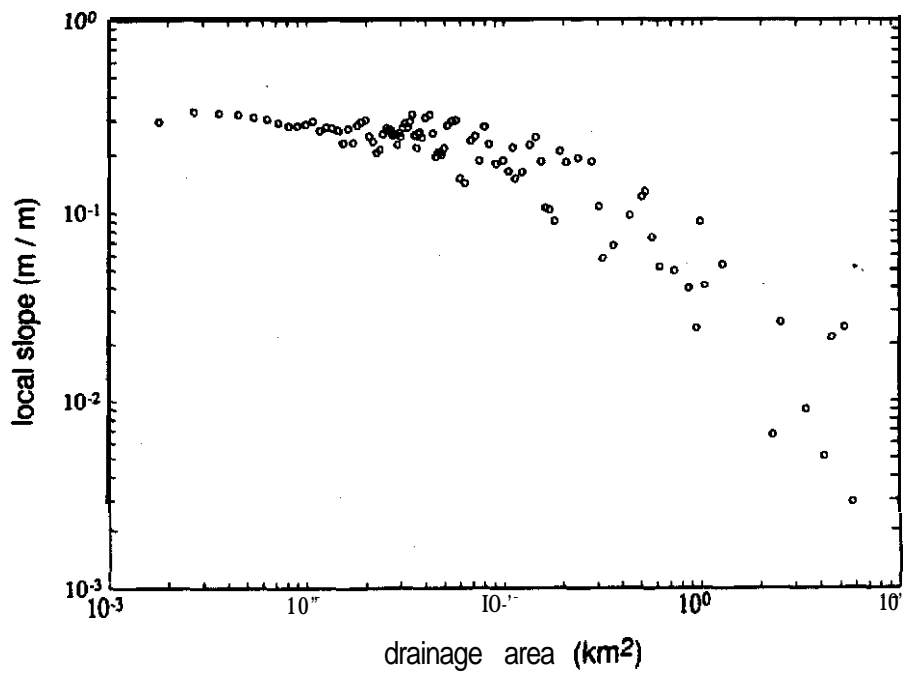
Montgomery and Foufoula Figure 2A



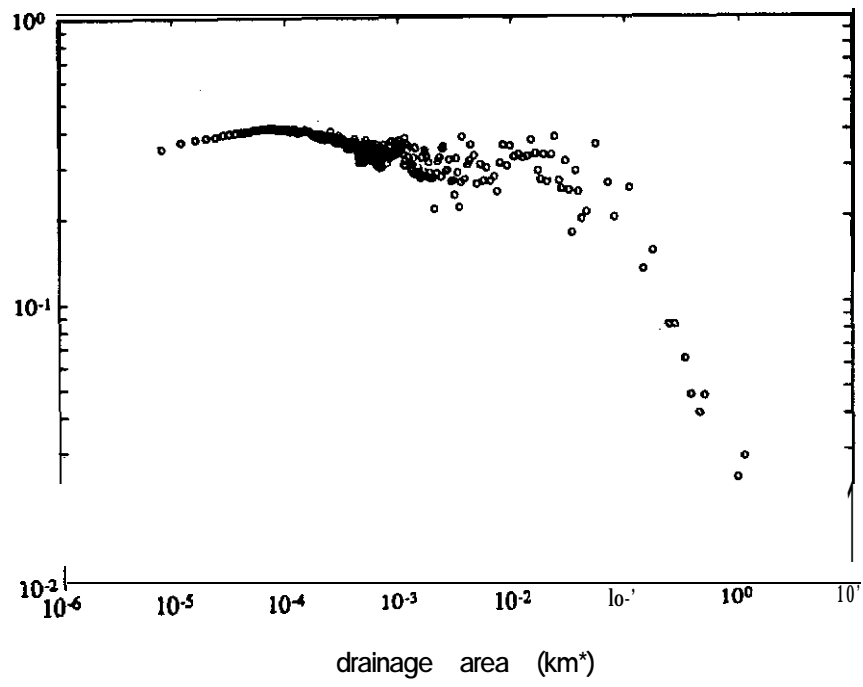
Montgomery and Foufoula Figure 2B



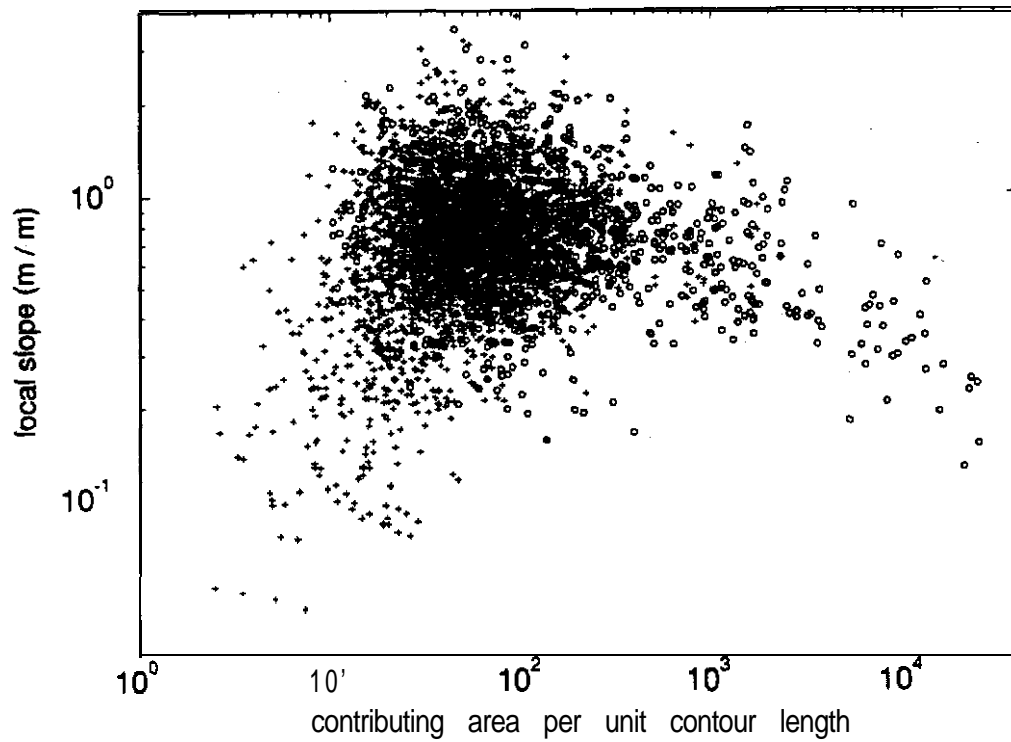
Montgomery and Foufoula Figure 3



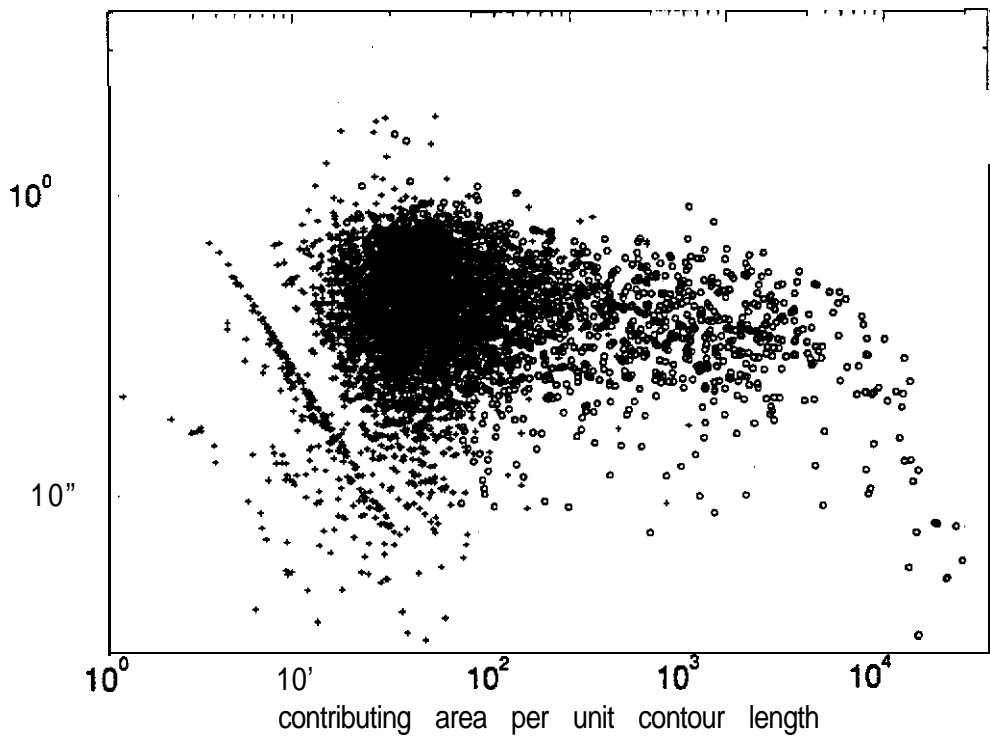
Montgomery and Foufoula Figure 4A



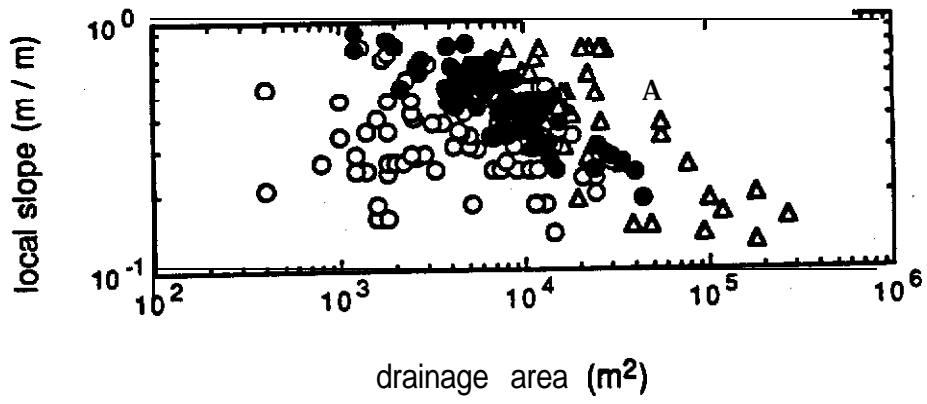
Montgomery and Foufoula Figure 4B



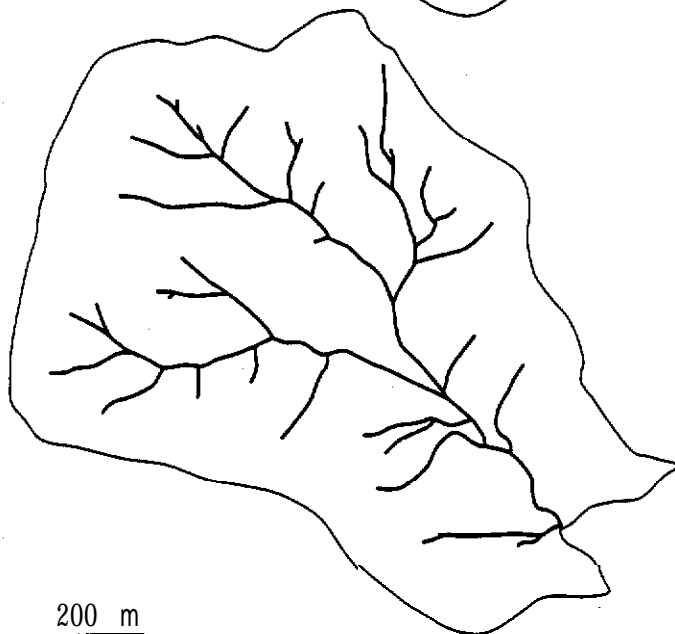
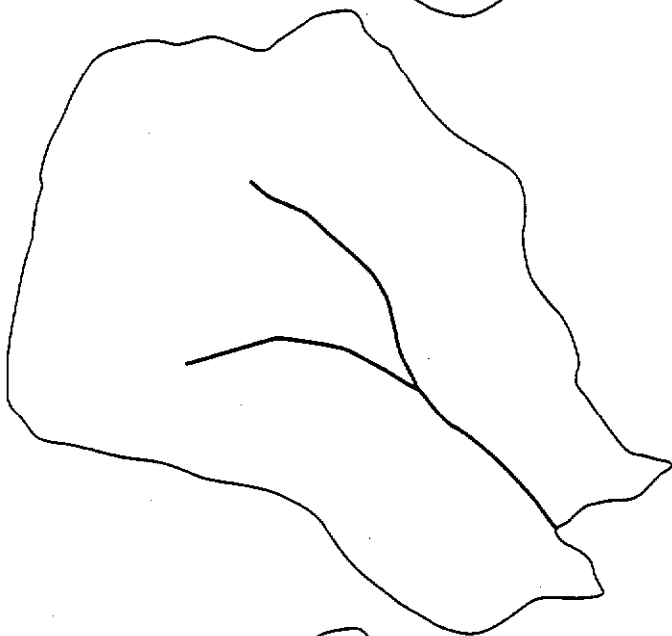
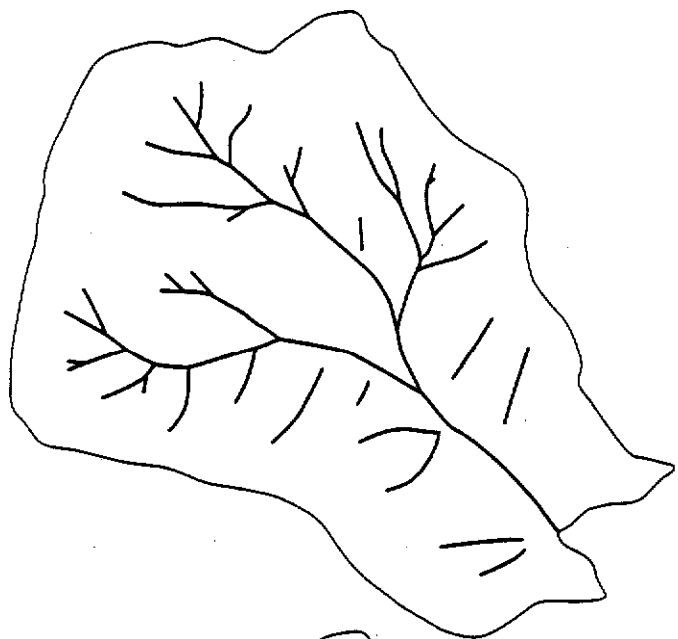
Montgomery and Foufoula Figure 5A



Montgomery and Foufoula Figure 5B



Montgomery and Foufoula Figure 6



200 m

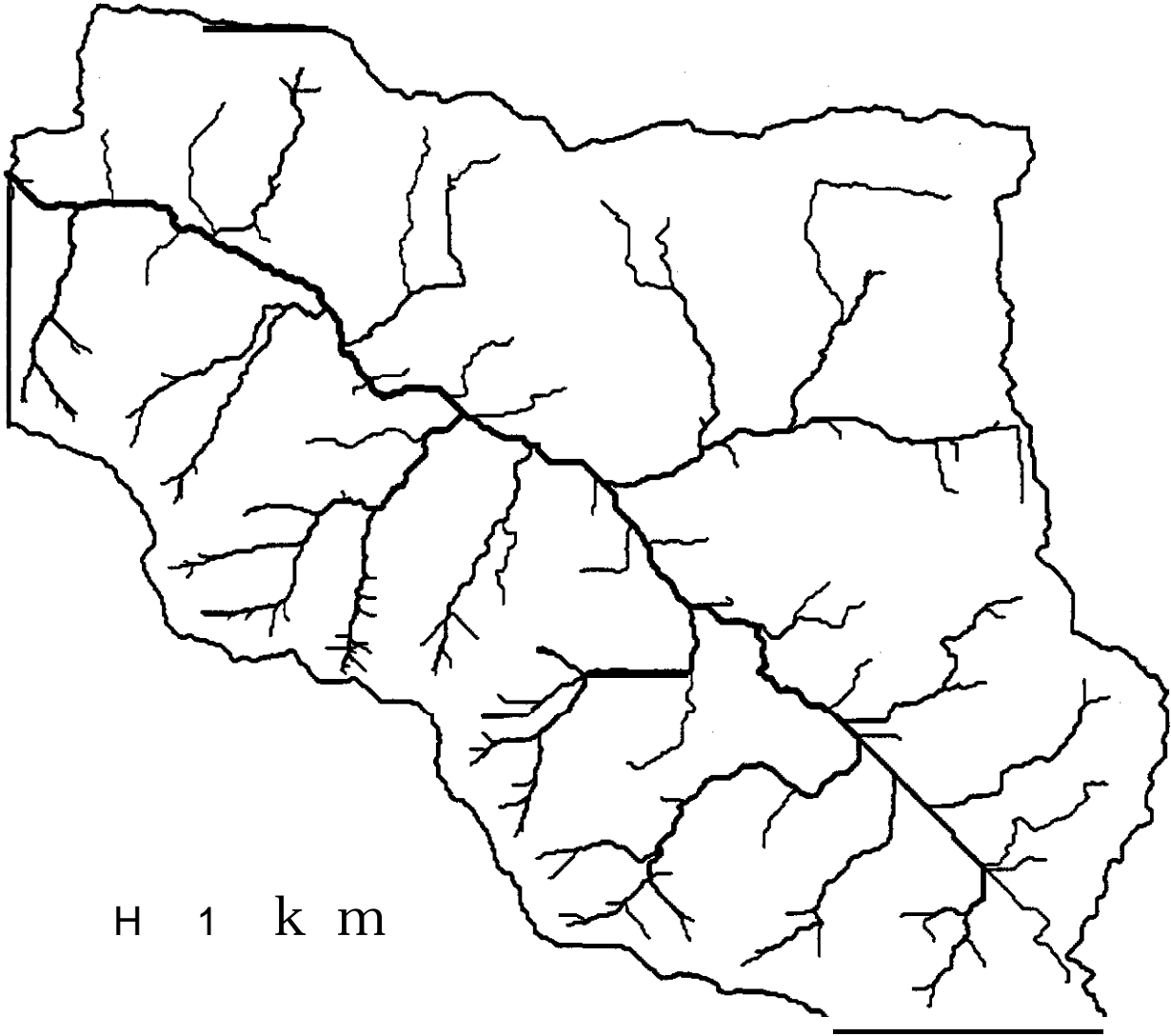
Digital Elevation Model Grid **Size**, Landscape Representation
and Hydrologic Simulations

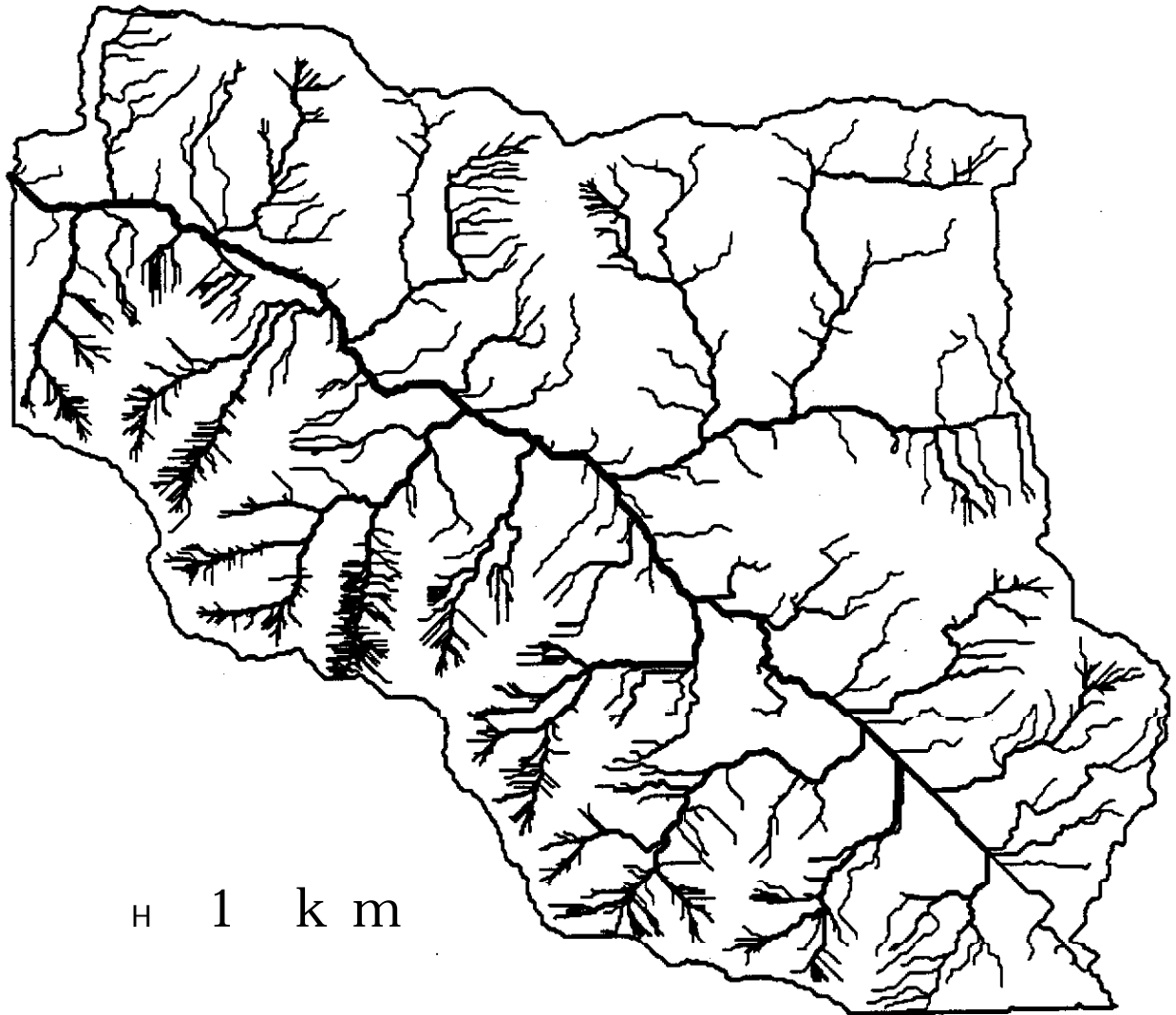
revised submission to Water Resources Research

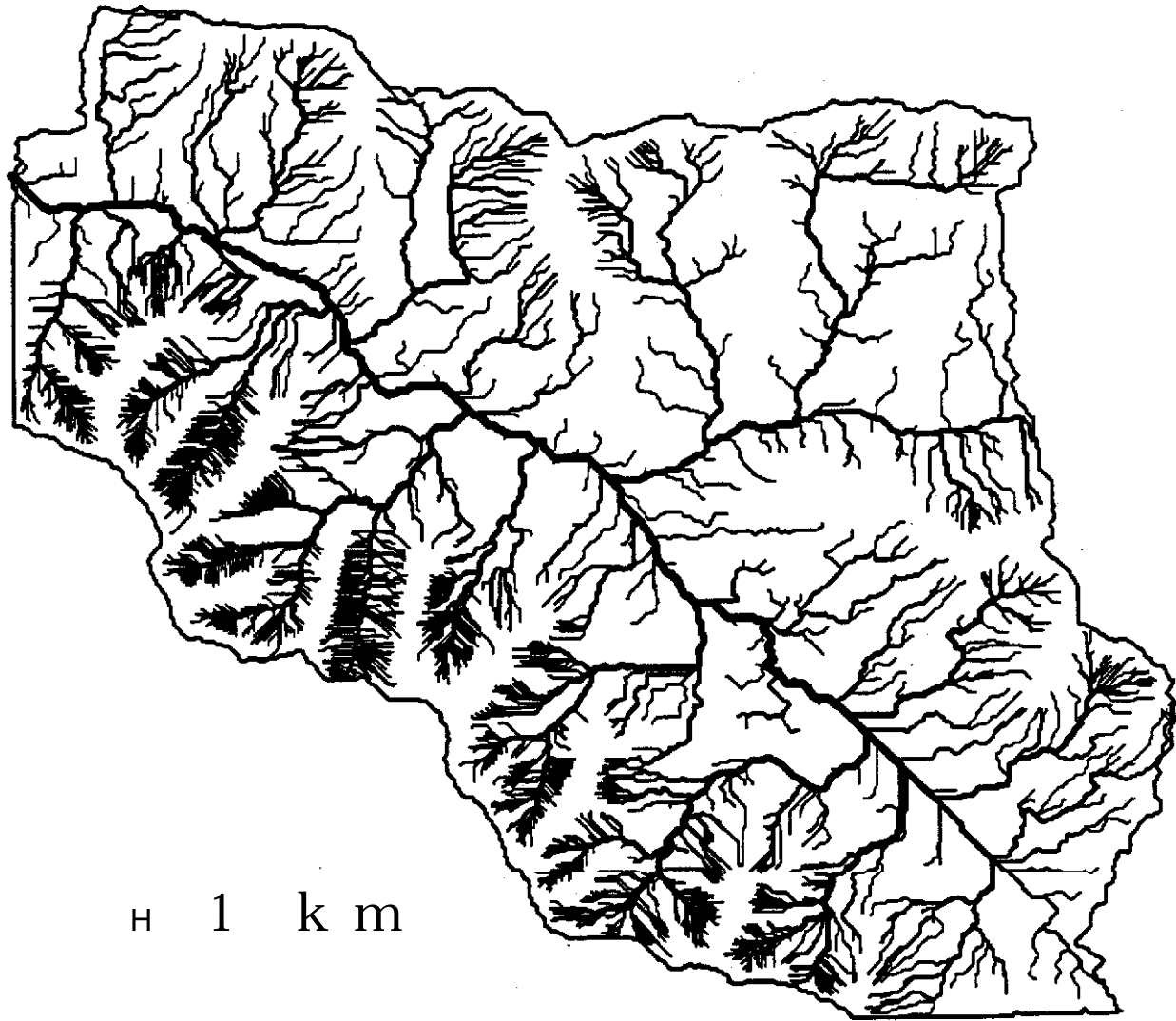
WEIBUA **ZHANG** AND DAVID R. MONTGOMERY
Department of Geological **Sciences**,
University of Washington, Seattle, WA 98195

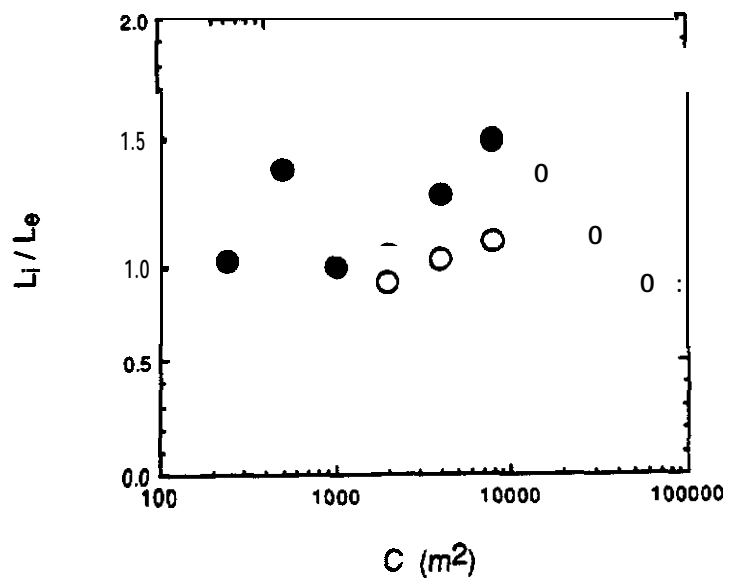
ABSTRACT

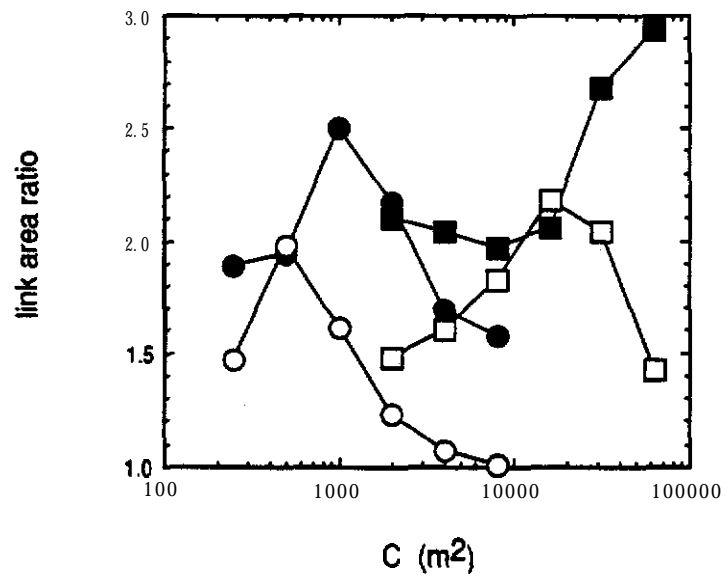
High-resolution digital **elevation** data **from** two small catchments in the western United States are used to examine the effect of digital elevation model (DEM) grid size **on** the portrayal of the land surface and hydrologic **simulations**. Elevation data were gridded at 2, 4, 10, 30, and 90 m scales to generate a series of simulated landscapes. Frequency distributions of slope (**tanB**), **upslope** drainage area per unit contour length (a), and the topographic index (a/tanB) were calculated for each grid size model. Frequency distributions of **a/tanB** were then used in **O'Loughlin's [1986]** criterion for predicting zones of surface saturation for a given catchment wetness and in **TOPMODEL [Beven and Kirkby, 1979]** for simulating hydrographs in response to 4-hr storms of various intensities and initial baseflows. For both catchments, DEM grid size significantly affects computed topographic parameters and hydrographs. While channel routing dominates hydrograph characteristics for large catchments, grid-size effects are important for physically-based models of runoff generation and surface processes. When interpreting models of hydrologic and geomorphic processes, it is imperative to recognize limitations imposed by both the original data and imposed grid size. For the



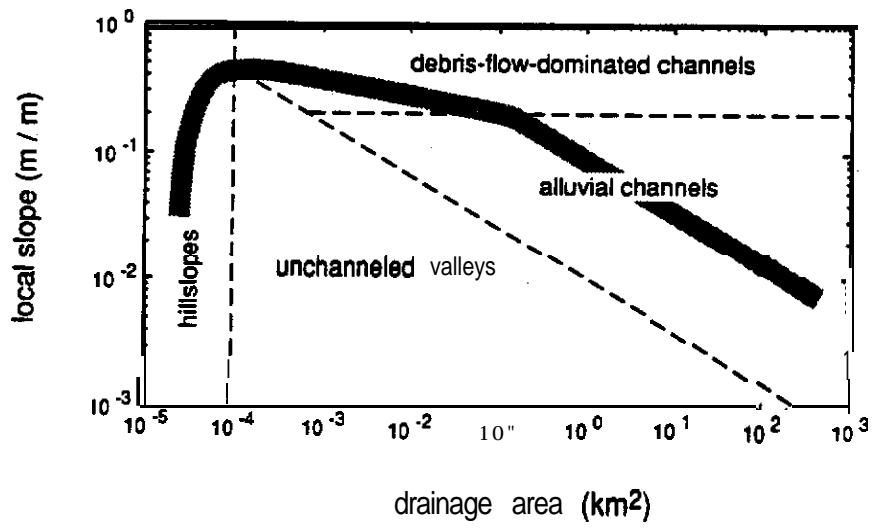








Montgomery and Foufoula Figure 9B



Montgomery and Foufoula Figure 10

Appendix 4

Digital Elevation Model Grid **Size**, Landscape Representation
and Hydrologic Simulations

revised submission to Water Resources Research

WEIBUA **ZHANG** AND DAVID R. MONTGOMERY
Department of Geological **Sciences**,
University of Washington, Seattle, WA 98195

ABSTRACT

High-resolution digital **elevation** data **from** two small catchments in the western United States are used to examine the effect of digital elevation model (DEM) grid size **on** the portrayal of the land surface and hydrologic **simulations**. Elevation data were gridded at 2, 4, 10, 30, and 90 m scales to generate a series of simulated landscapes. Frequency distributions of slope (**tanB**), **upslope** drainage area per unit contour length (a), and the topographic index (a/tanB) were calculated for each grid size model. Frequency distributions of **a/tanB** were then used in **O'Loughlin's [1986]** criterion for predicting zones of surface saturation for a given catchment wetness and in **TOPMODEL [Beven and Kirkby, 1979]** for simulating hydrographs in response to 4-hr storms of various intensities and initial baseflows. For both catchments, DEM grid size significantly affects computed topographic parameters and hydrographs. While channel routing dominates hydrograph characteristics for large catchments, grid-size effects are important for physically-based models of runoff generation and surface processes. When interpreting models of hydrologic and geomorphic processes, it is imperative to recognize limitations imposed by both the original data and imposed grid size. For the

moderately- to steep-gradient topography of our study areas, a 10 m grid size provides a substantial improvement over 30 m and 90 m data, but 2 m or 4 m data provide only marginal additional improvement. For many landscapes, a 10 m grid size presents a rational compromise between increasing resolution and data volume for simulating geomorphic and hydrological processes.

INTRODUCTION

Predicting spatial patterns and rates' of runoff generation and many geomorphic processes requires both a hydrologic model and characterization **of** the land surface. Most physically-based models of hydrologic and geomorphic processes rely on either **spatially-**distributed or lumped characterizations of local slope and the **upslope** drainage area per unit contour length [e.g., Beven and **Kirkby**, 1979; **O'Loughlin**, 1986; Famiglietti and Wood, 1990; Vertessy et al., 1990; **Dietrich** et al., 1992, **1993**] and digital elevation models (**DEMs**) commonly are used for such characterization in a wide variety of scientific, engineering, and planning applications. Although the increasing availability of **DEMs** allows rapid analysis of topographic attributes over even large drainage basins, the degree to which DEM grid size affects the representation of the land surface and hydrological modeling has not been **examined** systematically.

Digital elevation data are stored in one of several formats: as point elevation data on either a regular grid or triangular integrated **network**, or as vectorized contours stored in a digital line graph. Each of these formats offers advantages for certain applications, but the grid format is used most widely. Several recent studies explored

the effect of DEM grid size on landscape representation [Hutchinson and Dowling, 1991; Jenson, 1991; Panuska et al., 1991; Quinn et al., **1991**]. These studies showed that distributions of topographic attributes derived from a DEM depends to some degree on grid size across a range of scales. None of these studies, however, systematically analyzed the effect of grid size on either the statistical characterization of the land surface, or simulated hydrologic response using topographically-driven models. In this **paper**, we assess how grid size affects topographic representation, derived topographic attributes, and hydrological simulations for two small catchments using high-resolution digital elevation data. In contrast to previous studies, we grid the same elevation data at several different scales in order to isolate the effect of grid size on landscape representation.

STUDY AREAS

The study catchments are located at Mettman Ridge near Coos Bay, Oregon, and Tennessee Valley in **Marin** County, California (Figure 1). Previous field investigations determined the nature and distribution of geomorphic and hydrologic processes in each catchment. **High-** resolution digital elevation data were generated for testing DEM-based process models in these catchments [Dietrich et al., 1992; **1993**]. Field mapping in each catchment reveals that the high resolution data provides a reasonably-accurate portrayal of the land surface.

Mettman Ridge

The Mettman Ridge catchment occupies 0.3 km^2 of an area in which previous field mapping documented the extent of the channel network and land surface dissection [Montgomery, 1991; Montgomery and Dietrich, **1992**]. Channel head locations in this area are controlled primarily by shallow debris flows from small unchanneled valleys [Montgomery and Dietrich, **1988**]. The catchment is highly dissected with hillslope lengths on the order of 30 m. Slopes of 30' - 40' are common and there are a substantial number of slopes that locally exceed 45'.

A **1:4,800** scale **topographic basemap** derived from low-altitude aerial photographs taken prior to timber clearing was used as the source of digital elevation data. The **basemap** was scanned and vectorized using an automated routine to reproduce contours identical to those on the original topographic map. Although several discrepancies were noted between this map and the ground surface, here we assume that this data provides an accurate portrayal of the land surface (Figure **2a**).

Tennessee Valley

The Tennessee Valley catchment occupies 1.2 km^2 in which previous field mapping also documented **the extent** of the channel network and landscape dissection [Montgomery and Dietrich, 1989; **1992**]. Shallow landsliding dominates sediment transport in steep hollows and side slopes, diffusive transport dominates on divergent noses, and saturation overland flow and channel processes dominate sediment transport in lower-gradient valleys [Dietrich et al., **1993**]. The catchment is rhythmically dissected, with hillslope lengths on the

order of 50 m. The topography of the Tennessee Valley catchment is less steep than that of the Mettman Ridge catchment; slopes of 20' - 30' are common and slopes in excess of 40' are **rare**:

Digital elevation data were obtained from low-altitude aerial photographs using a stereo digitizer at a density about every 10 m [Dietrich et al., 1992]. The spot elevations **were** gridded to generate a 5 m contour interval map of the catchment (Figure 2b). Field inspection reveals that the data provide an excellent portrayal of the land surface.

METHODS

Spot elevation data for the Mettman Ridge and Tennessee Valley catchments were gridded at scales of 2, 4, 10, 30, and 90 meters using the grid module of Arc/Info, with gridded elevations recorded to the nearest centimeter. Cumulative frequency distributions of three topographic attributes, local slope (**tanB**), **upslope** drainage area per unit contour length, (a) , and the topographic index **$\ln(a/\tan B)$** , were calculated for each DEM of the two study catchments using the model of Jenson and Domingue [1988]. Their model defines the downslope flow direction for each cell corresponding to the orientation of the neighboring cell of lowest elevation. The local slope of the cell is then calculated based on the elevation difference between cells. Definition of the spatial distribution of flow directions allows determination of the total number of the cells that direct flow to each cell, and thus **upslope** drainage areas. The **upslope** drainage area per unit contour length is the **upslope** drainage area divided by the grid cell dimension calculated for the center of the cell. Local

slope and upslope drainage area per unit contour length were used to calculate $\ln(a/\tan B)$ for each grid cell. Although the assignment of all flow to a single downslope grid cell distorts flow paths in both divergent topography and for slopes oriented at angles other than the eight cardinal directions [Quinn et al., 1991], the algorithm has been widely used in many topographic models [e.g., Marks et al., 1984; Band, 1986; Jenson, 1991]. Several workers [e.g., Quinn et al., 1991; Cabral and Burges, 1992; Lea, 1992] recently proposed algorithms for multiple-downslope-flow directions that are more suitable for representing flow on divergent hillslopes. While we are eager to explore these newer algorithms, this study does not examine their influence on topographic representation.

Hydrologic simulations employed the steady-state model TOPOG [O'Loughlin, 1986] to examine patterns of surface saturation and TOPMODEL [Beven and Kirkby, 1979] to predict runoff production to short-duration storms. The soil hydraulic parameters used in the simulations were estimated from field measurements [Montgomery, 1991]. Model simulations explored the effect of DEW grid size on simulated hydrologic response.

LANDSCAPE REPRESENTATION

The cumulative frequency distributions of slope, upslope drainage area per unit contour length, and $\ln(a/\tan B)$ were determined for each grid size model. These distributions reflect changes in both the mean and local values of these topographic attributes. Comparison of these distributions allows direct assessment of the influence of grid size on landscape representation.

Slope

Cumulative slope distributions are sensitive to DEM grid size (Figure 3), but are more so for the steeper Mettman Ridge catchment than for the moderate-gradient Tennessee Valley catchment. For both study areas, the percent of the catchment steeper than a given slope systematically decreases as the DEM grid size increases, and the largest effect is **for** the steepest portions of the catchments.

The effect of grid size on the cumulative slope distribution is much larger for the Mettman Ridge catchment. For this case, the mean slope reduces from 0.65 for the 2 m grid size model to 0.41 for the 90 m grid size model (Figure 3a). While this result is consistent with those of previous studies [Jenson, 1991; Panuska et al., 1991], the **effect** of DEM grid size in this case is more pronounced. Grid size influence on slope distributions is less pronounced for the Tennessee Valley catchment (Figure 3b). The mean slope is 0.34 for the 2 m grid model, and reduces to 0.29 for the 90 m grid **size model**. For both study areas, these distributions suggest that grid sizes smaller than 10 m yield only marginal improvement in slope representation. Since the slope of a grid cell represents an average slope for the area covered by the cell, increasing DEM grid size should result in decreasing ability to resolve the slope characteristics of the landscapes, especially for highly-dissected landscapes with short, steep hillslope. Thus, **one would** expect that the effect of **DEM** grid size on slope is greater for steeper and more dissected topography, as illustrated by our **analysis of** the study catchments.

The cumulative slope distribution for the 10 m and 30 m grid size models of the Mettman Ridge catchment are stepped, **while** distributions for both largest grid size and smallest grid sizes are smoother. We suspect that this reflects two things: the relation between the grid size and the hillslope length scale and the small number of grid cells in this catchment using a large grid size. If the sampling grid size is on the order of the hillslope length, then any slopes that are in phase with the topography may be repeatedly sampled while other intermediate slopes are filtered out. Such a sampling bias would introduce steps into the cumulative distribution curves. The observed steps occur using 10 and 30 m grid sizes that are on the order of the hillslope length. The number of samples may also affect the smoothness of the distribution curve, as fewer samples should result in a more discontinuous cumulative distribution. For the Tennessee Valley catchment, the hillslope length is larger and the **number** of samples is greater. Therefore, we should expect the Tennessee Valley catchment distributions to be smoother than the Mettman Ridge catchment distributions.

Upslope drainage area per unit contour length

Cumulative distributions of **upslope** drainage area per unit contour length derived from a **DEM** are sensitive to grid size (Figure 4). Larger grid sizes **bias** in favor of larger contributing areas, with comparable effects in both catchments. For the Mettman Ridge catchment, the mean **upslope** drainage area per unit contour length increases from 20 m for a 2 m grid size to 102 m for a 90 m grid size. In the Tennessee Valley catchment, the mean **upslope** drainage area per

unit contour length increases from 19 m for a 2 m grid size to 120 m for a 90 m grid size.

For each grid size, a single pixel defines **the smallest** possible value of the **upslope** drainage area per unit contour length. The algorithm used to compute the **upslope** drainage area per unit contour length determines this minimum value. Thus, the grid size defines where the cumulative frequency distributions of this topographic parameter reach 100% of the catchment area. While it is intuitive that larger grid size limits the resolution of fine-scale topographic features, the effect on both the mean and local specific catchment areas is significant for topographically-driven hydrologic and surface process models.

Topographic-Index

The topographic-index $\ln(a/\tan B)$ is an important component of many physically-based geomorphic and hydrologic models, as it reflects the spatial distribution of soil moisture, surface saturation, and runoff generation processes [e.g., Beven and **Kirkby**, 1979; **O'Loughlin**, 1986; Moore et al., **1986**]. Derivation of frequency distributions of **$\ln(a/\tan B)$** is the first step for hydrological simulations in most topographically-driven hydrologic models.

Grid size significantly affects the cumulative frequency distributions of **$\ln(a/\tan B)$** (Figure 5). Decreasing grid size shifts the cumulative distribution toward lower values of **$\ln(a/\tan B)$** , with the greatest effect on smaller values. Again, computed frequency distributions systematically converge toward that of the finest grid size, with a systematic decrease in the mean **$\ln(a/\tan B)$** with

decreasing grid size. For the Mettman Ridge catchment, the mean $\ln(a/\tan B)$ increases from 3.4 m for a 2 m grid size to 5.6 m for a 90 m grid size. In the Tennessee Valley catchment, the mean $\ln(a/\tan B)$ increases from 4.0 for a 2 m grid size to 6.2 for a 90 m grid size. The influence of grid size on both mean and local values of $\ln(a/\tan B)$ demonstrates the potential for affecting topographically-based hydrologic models based on this parameter.

The effect of grid size on spatial patterns of $\ln(a/\tan B)$ is even more striking (Figure 6). Detailed features that appear on finer-grid DEMs are obscured on coarser-grid DEMs, with a progressive loss of resolution for both the drainage network defined by the higher values of $\ln(a/\tan B)$ and hillslopes associated with the lower values of $\ln(a/\tan B)$. Degradation of these important geomorphic features affects the simulation of runoff production and geomorphic processes in topographically-driven models.

HYDROLOGIC SIMULATIONS

We used the models TOPOG [O'Loughlin, 1986] and TOPMODEL [Beven and Kirkby, 1979] to investigate the effect of grid size on hydrologic simulations. We examined both representation of saturated areas within a catchment using TOPOG and the influence on hydrographs calculated using TOPMODEL for a range of reasonable rainfall intensities and baseflows for the study catchments.

Surface Saturation

Many hydrological, geomorphological and ecological phenomena are closely related to the behavior of the variable saturation area within

a catchment. Field experiments document that accurate prediction of zones of surface saturation is important for understanding and modeling runoff generation [e.g., Dunne and Black, **1970a, b**; Anderson and Burt, 1977; Wilson and Dietrich, **1987**]. The sufficient condition for the development of local surface saturation in a catchment is that the accumulated water flux from **upslope** drainage exceeds the capacity of the soil profile to transmit the flux. By assuming a steady state drainage condition, **O'Loughlin [1981, 1986]** expressed the condition for surface saturation at any location *in* a catchment as

$$\frac{a}{\tan B} \geq \frac{\bar{T}A_t}{Q_o} \quad (1)$$

where \bar{T} is the mean soil transmissivity of the catchment, A_t is the total catchment area, and Q_o is the runoff rate from the catchment. The term on the **right hand** side of the equation is the ratio of the transmissivity of the saturated soil column to the drainage flux per unit area. **O'Loughlin [1986]** defined this ratio as the average wetness state of a catchment (W). The total saturated area for a given catchment wetness is simply the sum of all the local areas which have values of $a/\tan B \geq W$.

Following the criterion for surface saturation defined by **(1)**, the effect of DEM grid size on the computed saturation area can be directly examined using the cumulative distribution of **$\ln(a/\tan B)$** . For a given wetness condition, predicted saturation areas for both catchments increase with increasing grid size. For example, in the **Mettman** Ridge Catchment, a wetness condition of $W = 180 \text{ m}$ predicts a saturated area equal to about 13% of the total catchment area for a **2**

m grid spacing; 32% for a 30 m grid spacing; and 50% for a 90 m grid spacing. The Tennessee Valley catchment exhibits a similar, although less pronounced, relation between grid size and saturated area for a **given** wetness condition.

Catchment Resuonse Durins a Storm Event

We used **TOPMODEL** [Beven and **Kirkby**, 1979; Beven **1986**] to explore the effect of DEM grid size on the simulated hydrologic response of each catchment to a simple short-duration rainfall event. The model predicts the distribution of soil moisture and the associated runoff processes on the basis of surface topography and soil properties. A critical assumption of the model is that locations with **similar** topography and soil properties, defined by $(a/T \tan B)$ where T is the local soil transmissivity, will respond in a hydrologically identical way to **the same** input. By assuming a spatially-uniform recharge rate and a quasi-steady subsurface response, Beven and **Kirkby [1979]** derived a function relating local soil moisture storage to the topographic-index of a catchment as

$$S = \bar{S} + m \{ \lambda - \ln(a / \tan B) - m(\delta - \ln(T)) \} \quad (2)$$

where S is the local soil moisture deficit, **\bar{S}** is the mean soil moisture of the basin, m is a parameter that characterizes the decrease **in** soil conductivity with soil depth, and λ and δ are the mean values of $\ln(a/\tan B)$ and **$\ln(T)$** for the catchment. For locations where **$S > 0$** , the soil **moisture store is** not filled, and therefore, there is

no surface saturation. For locations with $S \leq 0$, the soil moisture capacity is full, and surface saturation occurs.

The model computes both the relative amount of subsurface runoff and saturation overland runoff, as well as the spatial distribution of these runoff processes. During a model simulation, the mean soil moisture deficit of a catchment at time t , \bar{S}_t , is calculated using the following moisture-accounting equation:

$$\bar{S}_t = \bar{S}_{t-1} + (q_{t-1} - r) \Delta t \quad (3)$$

where q is the total catchment runoff at time $t-1$ divided by the catchment area, r is the net recharge rate into the soil column, and Δt is the computation time step. The updated S at all points in the catchment are then computed using equation (2). Any area with a soil **moisture deficit** larger than the incremental precipitation in a unit time step will only produce subsurface runoff, while those areas with a soil **moisture deficit** smaller than the incremental precipitation in a unit time step, or those saturated at the previous time step will produce both subsurface and saturation excess runoff. The subsurface flow rate q_b of the catchment is calculated by

$$q_b = e^{-(\lambda-\delta)} e^{-\bar{S}/m} \quad (4)$$

The saturation excess runoff q_o is the sum of excess soil moisture and direct precipitation that falls on the saturated areas. This is expressed as

$$q_o = \frac{1}{A_t} \int_{A_s} \left\{ \frac{-S}{\Delta t} + r \right\} dA \quad (5)$$

where A_t is the total catchment area and A_s is the area of the catchment with surface saturation (i.e., $S \leq 0$). Total runoff, q , at any time step is the **sum** of subsurface and surface runoff. The topographic index $\ln(a/\tan B)$ determines both the flow rates and spatial distribution of subsurface and surface runoff. While the equation **for** saturation excess flow is related to both the distribution form and mean, λ , the equation for subsurface flow is only related to the mean. Therefore, the response of equations (4) and (5) differs in their sensitivity to DEM grid-size influence on the distribution of the $\ln(a/\tan B)$.

We first examine the simulated subsurface hydrologic response using equation (4) without considering either surface flow, or interactions between surface and subsurface flow paths. This illustrative example **may** approximate conditions of small initial **baseflow** and rainfall in steep catchments. **For** this case, it is shown that by adjusting the initial values of the **mean** soil deficit, \bar{S} , the model will produce the same runoff hydrographs with different distributions of $\ln(a/\tan B)$.

Given any two mean values of topographic indexes, λ_1 and λ_2 , we have the following **baseflow** equations

$$q_{b1} = e^{-(\lambda_1 - \delta)} e^{-\bar{S}_1/m} \quad (6)$$

$$q_{b2} = e^{-(\lambda_2 - \delta)} e^{-\bar{S}_2/m} \quad (7)$$

The necessary condition for $q_{b1} = q_{b2}$ requires that \bar{S}_1 be related to \bar{S}_2 according to the following function

$$(\bar{S}_2 - \bar{S}_1) = m (\lambda_2 - \lambda_1) \quad (8)$$

Once the initial values of mean soil moisture deficit is set according to the functional relation given by equation (8), the relation will hold for all time steps during a storm, leading to an identical hydrograph. In other words, DEM grid size does not affect the computed hydrographs using only the subsurface flow equation. This demonstrates that the subsurface flow component of **TOPMODEL** depends only on the mean values of **ln(a/tanB)**.

In the following, we examine the effect of **DEM** grid size on simulated hydrologic response considering both subsurface and saturation excess flow. In our simulations, soil parameters were assumed spatially uniform so that the effect of topography is isolated. We used values of **70 mm** and **360 mm/hr** for the parameter m and surface hydraulic conductivity, respectively. For simplicity, we only calculated runoff production and ignored flow routing in channels. Simulations were conducted with four rainfall intensities (5, 10, 50 and 100 **mm/hr**) and five initial **baseflow** conditions (1, 2.5, 3.5, 4.5 and 9.5 mm/day) for total of twenty model runs. The lowest simulated rainfall intensity (**5 mm/hr**) occurs frequently in these areas and the highest simulated rainfall intensity (**100 mm/hr**) represents a hypothetical extreme event. At most times, the antecedent base flow rates for the study areas is less than 4 mm/day.

Grid size significantly affects computed hydrographs (Figure 7). To quantitatively examine these results., we normalized peak discharges computed with different grid size models by the corresponding peak discharges computed from the 90 m DEM. A plot of normalized peak

discharge verses grid size for a 4-hr duration and 10 **mm/hr** rainfall at various antecedent base flow rates (Figure 8) illustrates the effect of DEM grid scale on the computed peak discharge. For both catchments, peak discharges computed with a 2 **m** grid size range from roughly 5 - 40% **of** those computed with a 90 **m** grid size.

In general, the computed peak discharge increases with increasing grid size. However, there are some deviations from this trend, especially for the Mettman Ridge catchment. Further examination reveals that the deviations in Figure **8a** reflect the non-systematic variation with the grid size of the back-calculated **mean** initial soil moisture deficit . **For a** given initial baseflow, the mean soil moisture deficit generally decreases as the grid size increases, but there is a deviation from this trend at a 30 **n** grid size, where the initial mean **soil moisture** deficit is larger than that of 10 **m** grid size. With a larger moisture deficit and **therefore**, a smaller saturated area, the runoff production rate will be smaller. For the Tennessee Valley catchment, both the computed initial mean soil moisture deficit and peak discharge vary much more systematically with grid size.

The grid size effect on simulated peak discharge also varies with the initial **baseflow** and rainfall intensity. As the initial **baseflow** increases, the effect **of** grid size on the computed peak discharge decreases (Figure 8). The effect of rainfall intensity is more complex (Figure 9). Within a rainfall intensity range of 5 to 10 **mm/hr** for the Mettnan Ridge catchment and 5 to 50 **mm/hr** for the Tennessee Valley catchment, the difference between the peak discharge from grid sizes smaller than 90 **m** and that **from** a 90 **m** grid increases with the

rainfall intensity. As rainfall intensity further increases, however, the difference between peak discharges for the grid sizes less 90 m and those of 90 m grid reduces. This result is expected considering that in extreme cases of 1) no surface saturation under a very small rainfall intensity and 2) a complete surface saturation under a very large rainfall intensity: peak discharge should be the same for all grid size models. The curves in Figure 9 should converge at very high and low rainfall intensities.

Within a range of reasonable rainfall intensities (e.g., less than 50 **mm/hr**), differences between peak discharges computed **with** some grid sizes are small. The results for all the cases show that peak discharge differences are less than 5% for grid sizes smaller than 30 m for the Tennessee Valley catchment, while for the Mettman Ridge catchment the difference is less than 8% for grid sizes smaller than 10 m. Figure 9 are results simulated with an initial **baseflow** of 2.5 mm/day. This suggests that there is a DEM grid size beyond which computed hydrologic response is insensitive to grid size, and that this grid size is approximately 10 m for Tennessee Valley catchment and 4 m for the Mettman Ridge catchment.

DISCUSSION

The analyses presented above are **based** on the single-direction flow-partitioning algorithm. This algorithm does not resolve hillslope divergence, introducing artifacts that influence cumulative frequency distributions of a and **tanB**. Quinn et al. [1991] showed that for the same grid size the single-direction algorithm yields higher values of local slope, and therefore lower **$\ln(a/\tan B)$** , than a

multiple-direction algorithm. This effect was most pronounced for steeper hillslope areas. Quinn et al. [1991] also illustrated that DEM grid size influences the distribution of $\ln(a/\tan B)$ for multiple-direction algorithms, with the percent of area having larger $\ln(a/\tan B)$ increasing with grid size. Thus, the flow-partitioning algorithm also affects topographic representation, in addition to the grid size dependence documented in this paper.

Implications for modelino surface processes

The effect of DEM size on the distribution of derived slopes has important implications for geomorphic modeling and land management decisions based on such models. Consider the problem of predicting areas prone to shallow landsliding. Models of slope instability involve relations between the ground surface slope, relative soil profile saturation, and properties of the soil. The results presented earlier (Figure 3) indicate that the total area predicted to be unstable will decrease with increasing grid size, as modeled slopes will be progressively less steep and, therefore, more stable. Thus, it is important to use a DEM with a grid size appropriate for both the landscape and the process being modeled.

This has implications for interpreting process-based geomorphic models. In particular, the effect of grid size on the representation of slope and contributing areas will affect models using slope or area-dependent sediment transport laws. For a slope-dependent transport law, the lower slopes reflected in a 90 m DEM require commensurate increases in the diffusivity. Similar calibration would be required for area and slope-dependent transport laws. While a

coarse-grid DEM may be most practical for modeling large-scale geomorphic processes, the coefficients incorporated in transport laws at such scales are not analogous to those measured in field studies.

Implications for Hydrologic Simulations

These results also have important implications for topographically-driven hydrologic simulations. For example, simulated zones of surface saturation for wetland delineation using steady-state models, such as TOPOG, reflect DEM resolution; coarser-resolution DEMs predict more extensive saturated areas for the same catchment wetness. This effect will also affect prediction of the spatial distribution of runoff processes, and the associated material transport processes over a land surface.

Our results also highlight other problems for hydrologic modeling. Although the topography of natural landscapes varies across scales from mountain ranges to micro-scale perturbations on the order of centimeters, near-surface (subsurface and surface) runoff processes are governed by neither the finest-, nor the coarsest-scale topography within a landscape. Rather they are governed by processes acting over intermediate scales. If the DEM grid size is too large, then many topographic features, such as hollows, low-order channels, and the surrounding hillslopes may not be resolved. We suggest that the most appropriate DEM grid size for topographically-driven hydrologic models is somewhat finer than the hillslope scale.

Another implication is for flood forecasting in a drainage basin. For this case, the crucial variables are the peak discharge and runoff volume. Our results indicate that with the same values for soil

parameters, but different DEM grid sizes the magnitude of the peak runoff rate, and therefore the runoff volume, predicted in response-to a given storm may differ significantly. However, these results are only for runoff production and hydrographs at the basin mouth also will reflect the routing of flow through the basin channel network. The effect of grid size should be smaller for a large drainage basin where runoff hydrographs are dominated by channel routing. Even so, the influence of DEM grid size on predicted runoff production is an important consideration for interpreting hydrological simulations using a topographically-driven model.

A particularly intriguing implication is for calibration and validation of dynamic physically-based hydrologic models. All hydrological models make simplifying assumptions, and only approximate real hydrologic systems. In practice, calibration is required to obtain acceptable correspondence between field results and model simulations. Calibrated parameters for a particular catchment are then used for hydrological forecasting either for the same catchment, or for a different catchment with similar physical properties. However, our results show that DEM grid size, rainfall intensity, and initial baseflow all affect simulated hydrographs computed with the same set of parameter values. Consequently, TOPMODEL, at least, is inherently unvalidatable and model calibrations are grid size specific.

Appropriate Grid Size

The results of our study invite the question of what defines an appropriate grid size for simulations of geomorphic and hydrologic

processes using topographically-driven models. This question is best examined in two parts: the relation between land surface and the spot elevation data used to create a DEM and that between grid size and the original spot elevation data.

The data used to create a DEM are a filtered representation of landscape sampled at some regular or irregular interval to build a collection of elevation data. The spacing of the original data used to construct a DEM effectively limits the resolution of the DEM. Construction of a grid finer than the spacing of the original data involves interpolation between data points. Any additional topographic information obtained in this manner essentially reflects the interpolation algorithm. The relation of the original elevation data to the land surface is a crucial, but often neglected, characteristic of a DEM. This is a problem with many commercially-available DEMs. While there are data collection strategies that could optimize landscape representation (e.g., dense topographic sampling in areas of complex topography and sparse sampling in areas with simple topography), the average spacing of the data used to derive a DEM provides a guide to the grid size that would take full advantage of the original spot elevation data, and thus provide the most faithful landscape representation.

We have shown that grid size significantly influences representation of a land surface. We suggest that the length scale of the primary landscape features of interest provides a natural guide to an appropriate grid size. The most basic attribute of many landscapes is the division into topographically divergent hillslopes and convergent valleys. Resolution of hillslopes and valleys is important

for modeling many surface processes and the average hillslope length reflects differences in geology, climate conditions, and **landscape-**forming processes. A grid size smaller than the **hillslope** length is necessary to adequately simulate processes controlled by land form. The **most** appropriate grid size for simulation models is best scaled in reference to the process being modeled. For example, a coarser (e.g., 90 m) grid size may be most appropriate for modeling **orogenic** processes over large areas and long **time scales**. In low-gradient, low-roughness topography, where hillslopes are the order of **100's meters**, a coarse grid size (**i.e., 30 - 90 m**) may provide a reasonable representation of land form .

Our results imply that it is unreasonable to use a 30 m or 90 m grid size to model hillslope or runoff generation processes in moderately- to steep-gradient topography without **some** modification of the process model. A 10 m grid is a significant improvement over 30 m and 90 m grid sizes. However, finer grid sizes provide comparatively little additional resolution. For modeling surface processes in many landscapes, a 10 m grid size presents a rational compromise between increasing spatial resolution and data handling requirements. The results presented above document that it is essential to consider the effects of DEM grid size when interpreting DEM-based simulations of surface processes.

CONCLUSIONS

The grid size of a DEM significantly affects both the representation of the land surface and hydrologic simulations based on this representation. As grid size decreases, landscape features are

more accurately resolved, but faithful representation of a land surface by a DEM depends on both grid size and the accuracy and distribution of the original survey data from **which the** DEM was constructed. If grid size decreases beyond the resolution of the original survey data, then the accuracy of the land surface representation of the DEM not only does not increase, but interpolation errors may be introduced. These results have important, implications for simulations of hydrologic and geomorphic processes in natural landscapes. In particular, we suggest that agencies creating **DEMs** adopt higher standards to make their products useful to emerging applications. Soon, our ability to model surface processes will **be** limited primarily by data quality and the variability of natural processes, rather than our modeling ability or computer capabilities. We suggest that a grid size of 10 m would suffice for **most** applications of geomorphic and hydrologic modeling.

Acknowledgments

This research was supported by NASA grant **NAGW-2652A**, NSF grant **IRI91-17094** and grant TFW **FY92-010** from the SHAMW and CMER committees of the Washington State Timber/Fish/Wildlife agreement. We thank Harvey Greenberg for technical support, Susan Jenson for making her topography analysis model available to us, and Bill Dietrich, Tom Dunne, and Romy Bauer for discussions on subjects related to the study.

REFERENCES

- Anderson, M. G. and T. P. Burt, Automatic monitoring of soil moisture conditions in a hillslope spur and hollow, *J. Hydrol.*, 33, 27-36, 1977.
- Band, L. E., Topographic partition of watershed with digital elevation modes, *Water Resour. Res.*, **22(1)**, 15-24, 1986.
- Beven, K., and M.J. **Kirkby**, A physically based, variable contributing area model of basin hydrology, *Hydrol. Sci. Bull.*, 24, 43-69, 1979.
- Beven, K., Runoff production and flood frequency in catchment of order n: An alternative approach, in *Scale Problem in Hydrology*, V.K. Gupta et al. (eds.), Reidel Publishing Company, 107-131, 1986.
- Cabral, M. and S. J. Burges, DEMON: A new method for automated extraction of contributing areas and drainage networks from **rectanglar DEMs**, *Trans. Am. Geophys. Union*, EOS Supplement **73(43)**, 202-203, 1992.
- Dietrich, W. E., C. J. Wilson, D. R. Montgomery, J. **McKean**, and R. Bauer, Erosion thresholds and land surface morphology, *Geology*, 20, 675-679, 1992.
- Dietrich, W. E., C. J. Wilson, D. R. Montgomery and J. **McKean**, Analysis of erosion thresholds, channel networks, and landscape morphology using a digital terrain model, *Journal of Geology*, **101(2)**, 259-278, 1993.
- Dunne, T. and R. G. Black, An experimental investigation of runoff production in permeable soils, *Water Resour. Res.*, **6(5)**, 478-490, 1970a.

Dunne, T and R. **G.** Black, Partial area contributions to storm runoff in a small New England watershed, Water Resour. Res., **6(5)**, 1296-1311, 1970b.

Famiglietti, J.S. and E.F. Wood, Evapotranspiration and runoff from large land areas: Land surface hydrology for atmospheric general circulation models, Surveys in Geophysics, 12, 179-204, 1990.

Hutchinson, M. F. and T. I. Dowling, A continental hydrological assessment of a new grid-based digital elevation model of Australia, Hydrol. Processes, **5(1)**, 45-58, 1991.

Jenson, **S. K.** and J. **O.** Domingue, Extracting topographic structure from digital elevation data for geographic information **system** analysis, Photogramm. Eng. Remote Sensing, **54(11)**, 1593-1600, 1988.

Jenson, S. K., Applications of hydrologic information automatically extracted from digital elevation models, Hydrol. Processes, **5(1)**, 31-44, 1991.

Lea, N. J., An aspect driven kinematic routing algorithm, Overland Flow and Erosion Mechanics, eds., A. J. Parsons and A. D. Abrahams, Chapman and Hall, New York, 393-407, 1992.

Marks, D. M., J. Dozier and J. Frew, Automated basin delineation from digital elevation data, Geo-Processing, 2, 299-311, 1984.

Montgomery, D. **R.**, Channel initiation and landscape evolution (dissert.), University of California, Berkeley, **421p.**, 1991.

Montgomery, D. R., and W. E. Dietrich, Where do channels begin?,

Nature, 336, 232-234, 1988.

Montgomery, D. R., and W. E. Dietrich, Source areas, drainage density, and channel initiation, Water Resour. Res, **25(8)**, 1907-1918, 1989.

Montgomery, D. R., and W. E. Dietrich, Channel initiation and the problem of landscape scale, Science, 255, 826-830, 1992.'

Moore, I. D., S. M. Machay, P. J. Wallbrink, G. J. Burch and E. M. O'Loughlin, Hydrologic characteristics and modeling of a small forested catchment in southeastern New South Wales: Prelogging condition, J. Hydrol., 83, **307-335**, 1986.

O'Loughlin, E. M., Saturation regions in catchments and their relation to soil and topographic properties, J. Hydrol., 53, 229-246, 1981.

O'Loughlin, E. M., Prediction of surface saturation zones in natural catchments by topographic analysis, Water Resour. Res., **22(5)**, 794-804, 1986.

Panuska, J. C., I. D. Moore, and L. A. Kramer, Terrain analysis: Integration into the agriculture **nonpoint** source (AGNPS) pollution model, J. Soil and Water Conserv., **46(1)**, 59-64, 1991.

Quinn, P., K. Beven and O. Planchon, The prediction of hillslope flow paths for distributed hydrological modeling using digital terrain models, Hydrol. Processes, **5(1)**, 59-79, 1991.

Vertessy, R. A., C.J. Wilson, D.M. Silburn, R. D. Connolly, and C. A., Ciesiolka, Predicting erosion hazard areas

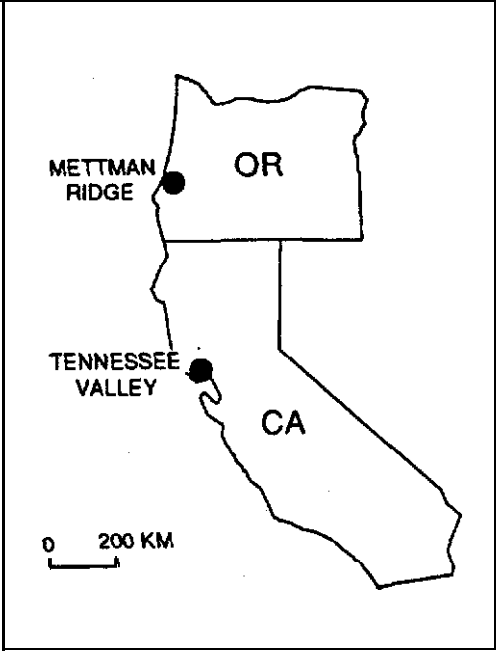
using digital terrain analysis, International Association of Hydrological Sciences, Publication 192, pp. 298-308, 1990.

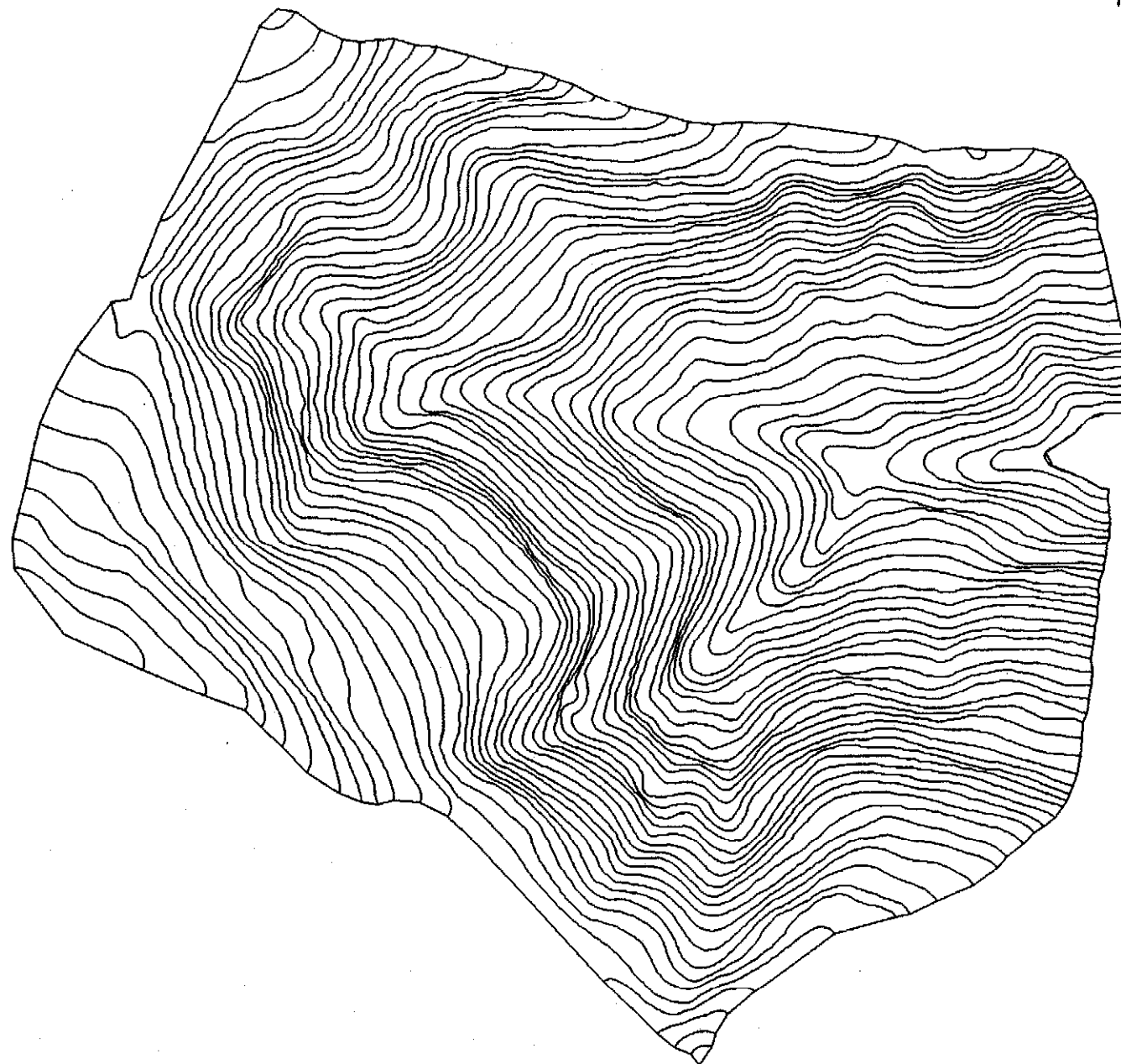
Wilson, C. J. and W. E. Dietrich, The Contribution of Bedrock Ground Water Flow to Storm Runoff and High Pore Pressure Development in Hollows, in proceedings of The International Symposium on Erosion and Sedimentation in the Pacific Rim, R. L. Beschta, T. Blinn, G. E. Grant, G. G. Ice and F. J. Swanson, editors, International Association of Hydrological Sciences, Publication 165, 49-59, 1987.

Figure Captions:

1. Location map of the study catchments.
2. Contour map of the a) Mettman Ridge and b) Tennessee Valley catchments.
3. Cumulative frequency distributions of slope derived for different DEM grid sizes. a) Mettman Ridge: b) Tennessee Valley.
4. Cumulative frequency distributions of the **upslope** drainage area per unit contour length for different DEM grid sizes. a) Mettman Ridge; b) Tennessee Valley.
5. Cumulative frequency distributions of the topographic index, $\ln(a/\tan B)$, for different DEM grid sizes. a) Mettman Ridge: b) Tennessee Valley.
6. Maps showing the spatial distribution of the topographic index $\ln(a/\tan B)$ for four different DEM grid sizes: 4 m, 10 m, 30 m and 90 m. Darker shades represent larger $\ln(a/\tan B)$. a) Mettman Ridge: b) Tennessee Valley.
7. Runoff hydrographs for different DEM grid sizes under different rainfall and initial **baseflow** conditions. a) Mettman Ridge catchment under 5 **mm/hr** rainfall and 3.5 mm/day initial baseflow; b) Mettman Ridge catchment under 100 **mm/hr** rainfall and 3.5 mm/day initial baseflow; c) Tennessee Valley catchment under 5 **mm/hr** rainfall and 3.5 mm/day initial baseflow; d) Tennessee Valley catchment under 100 **mm/hr** rainfall and 3.5 mm/day initial baseflow.
8. Computed peak discharge vs. DEM grid size for a given rainfall intensity (10 **mm/hr**) and different initial baseflows. The peak discharges are normalized to those of the 90 m grid size. a) Mettman Ridge: b) Tennessee Valley.


9. Computed peak discharge vs. DEM grid size for a given initial **baseflow** (2.5 mm/day) and different rainfall intensities. Peak discharges are normalized to those of the 90 **m grid** size.
- a) **Mettman** Ridge: b) Tennessee Valley.

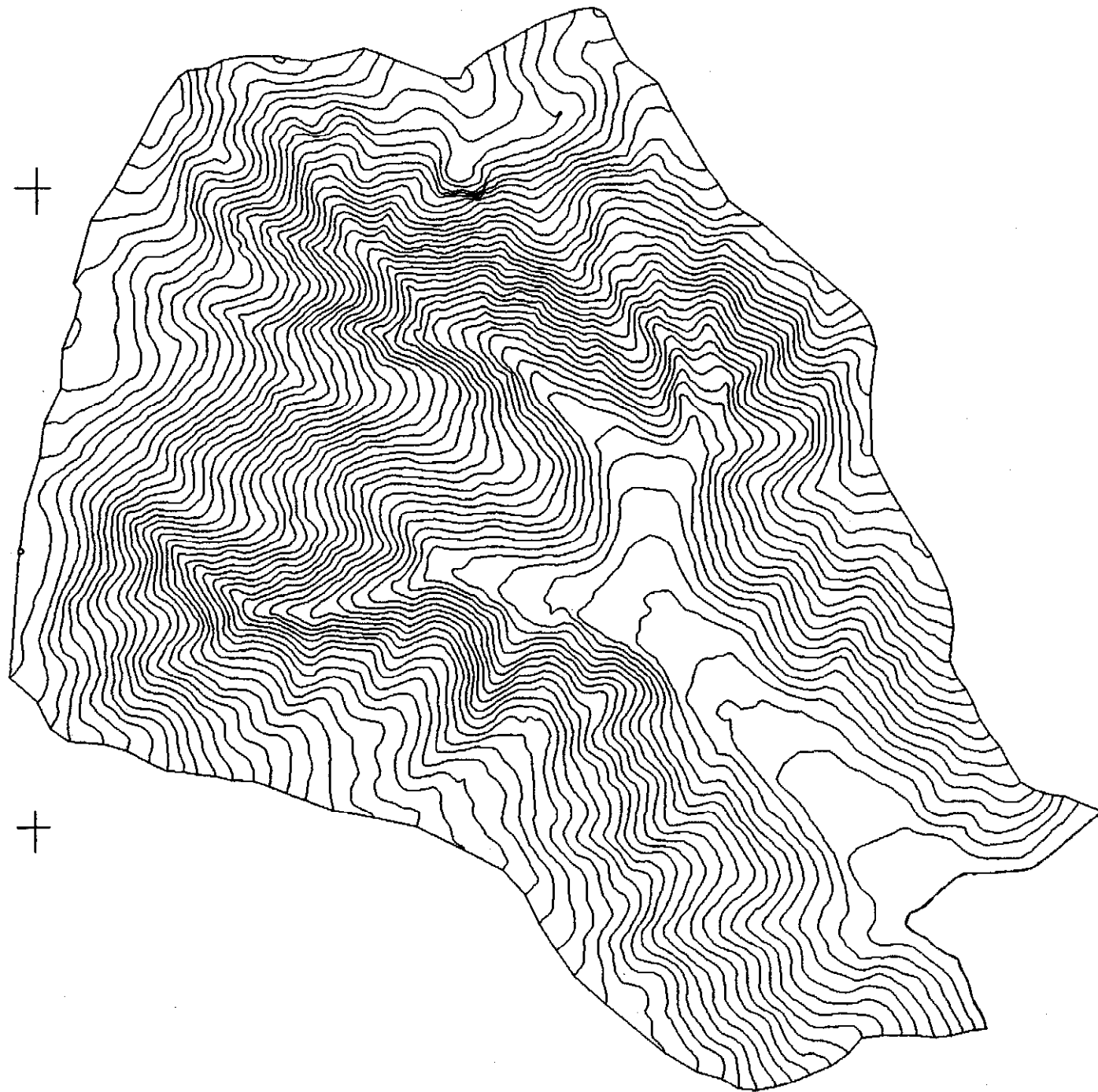




Pickable files:

Other files:
net.sbd
net.scn


100.0 meters



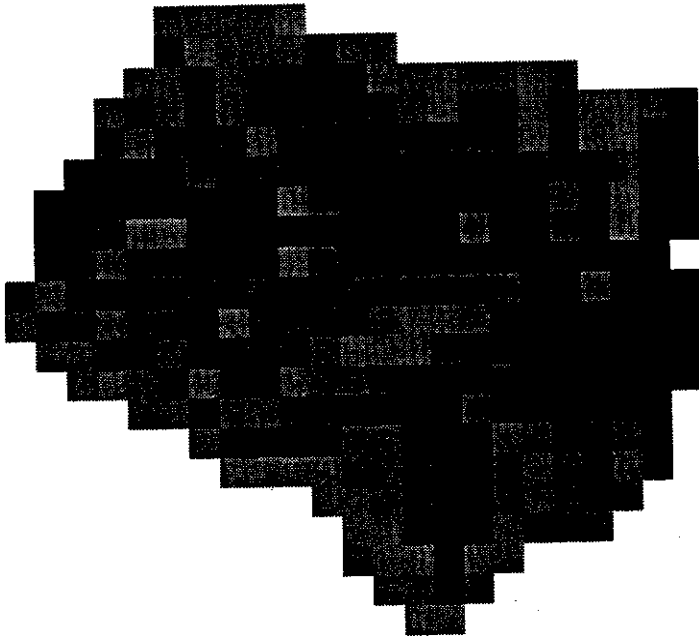
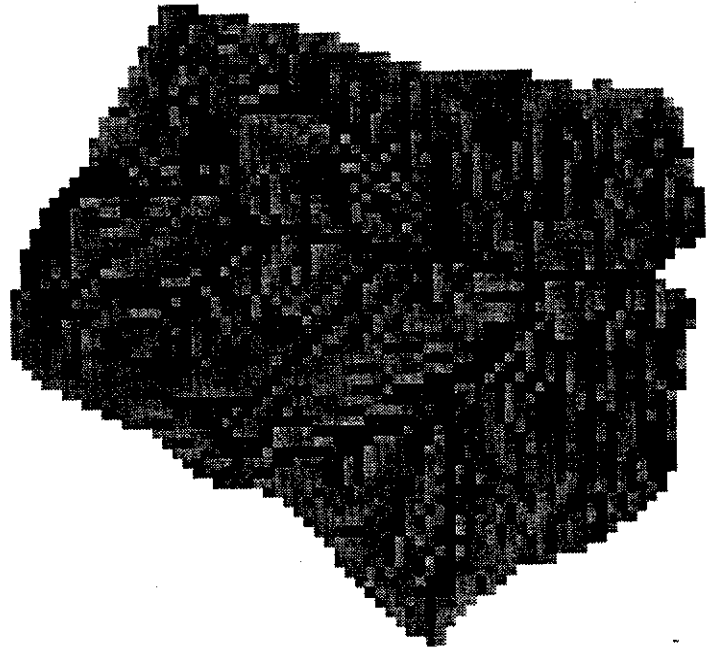
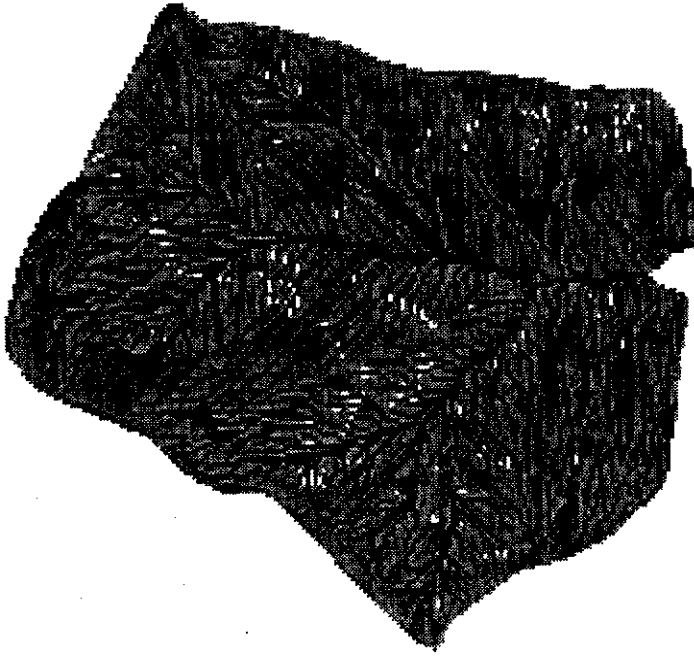
Pickable files:

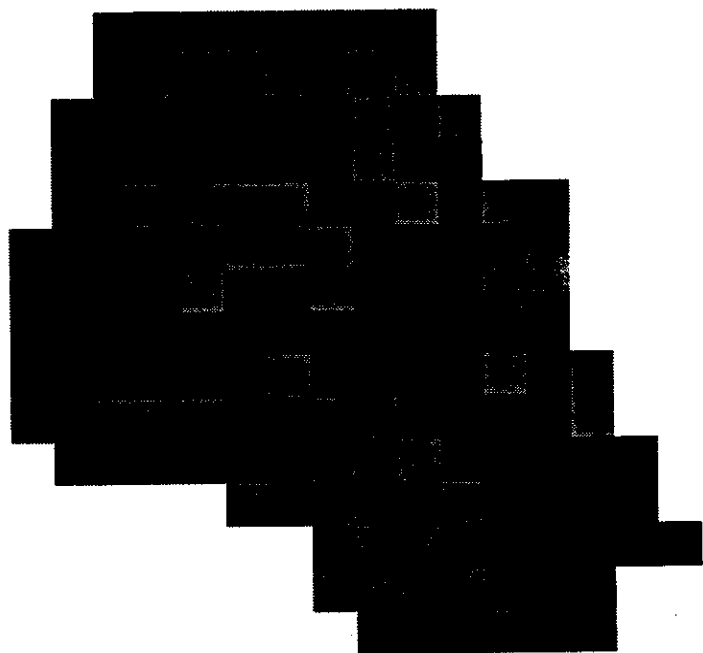
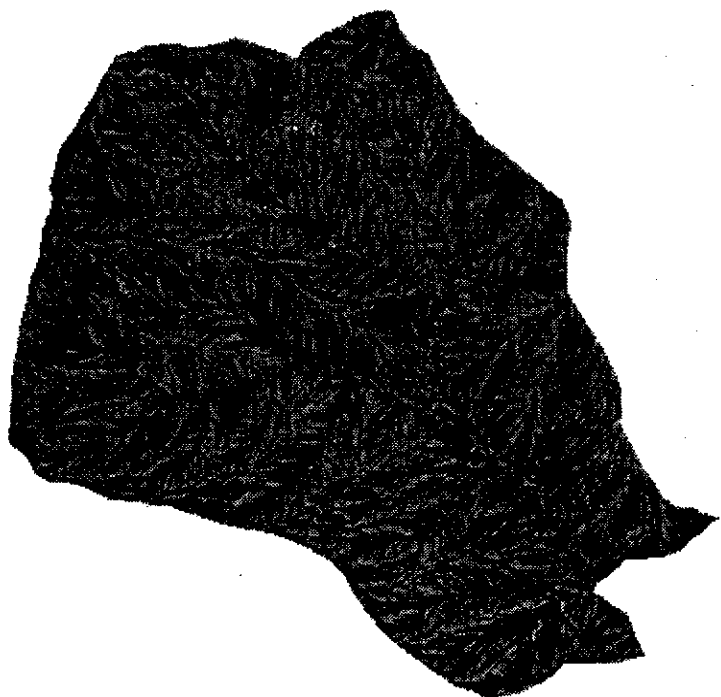
Other files:

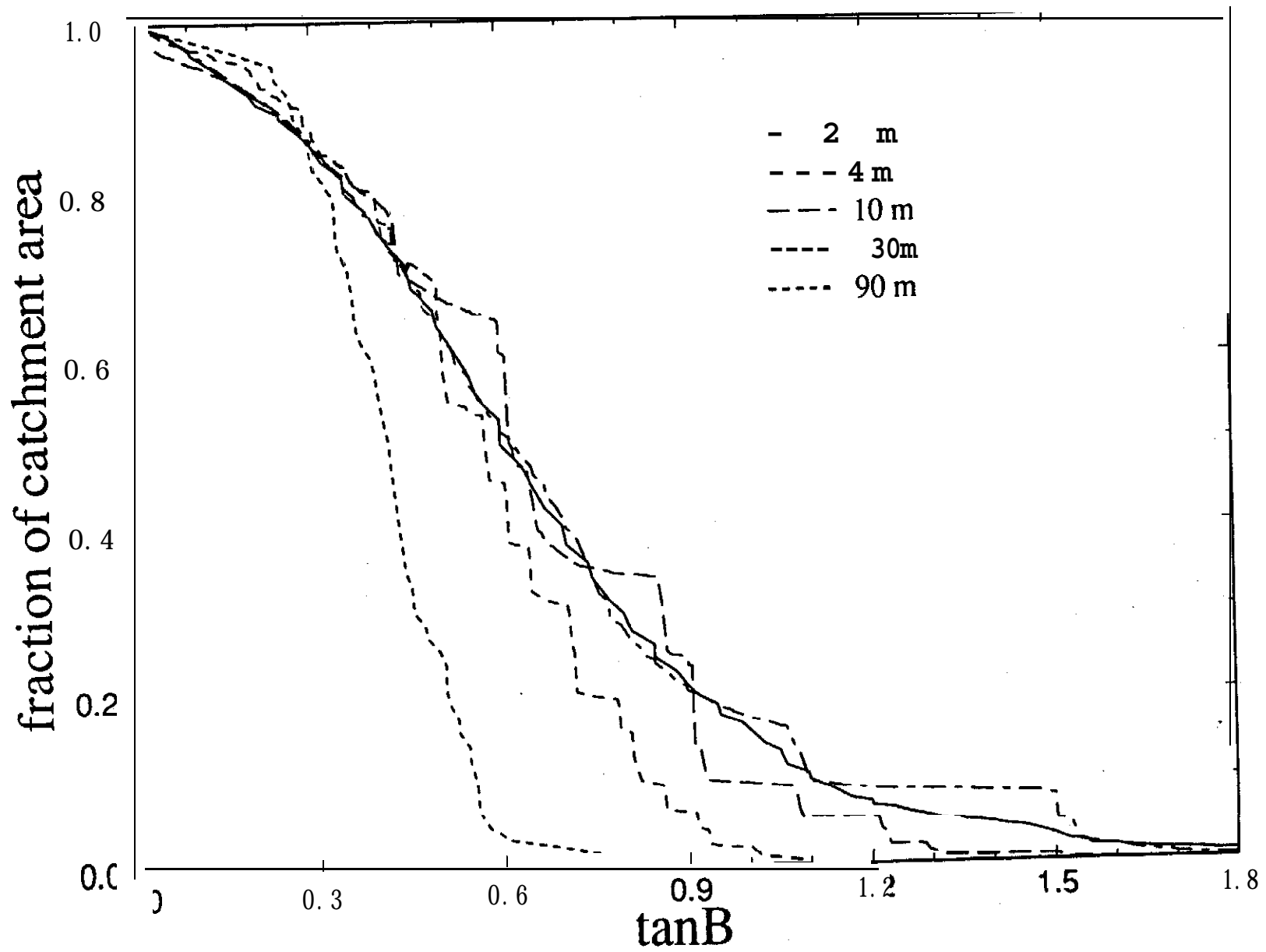
tv.scn

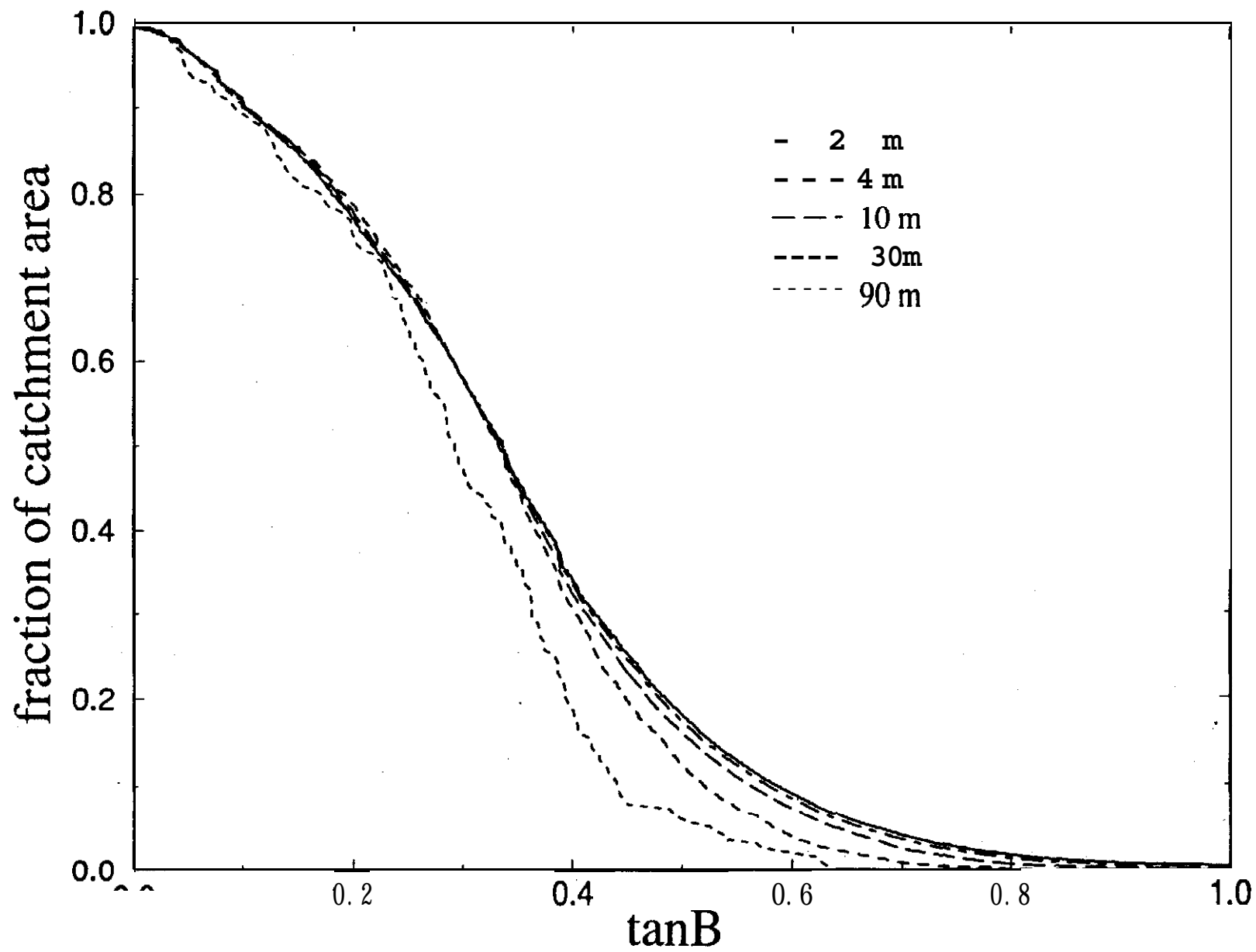
tv.sbd

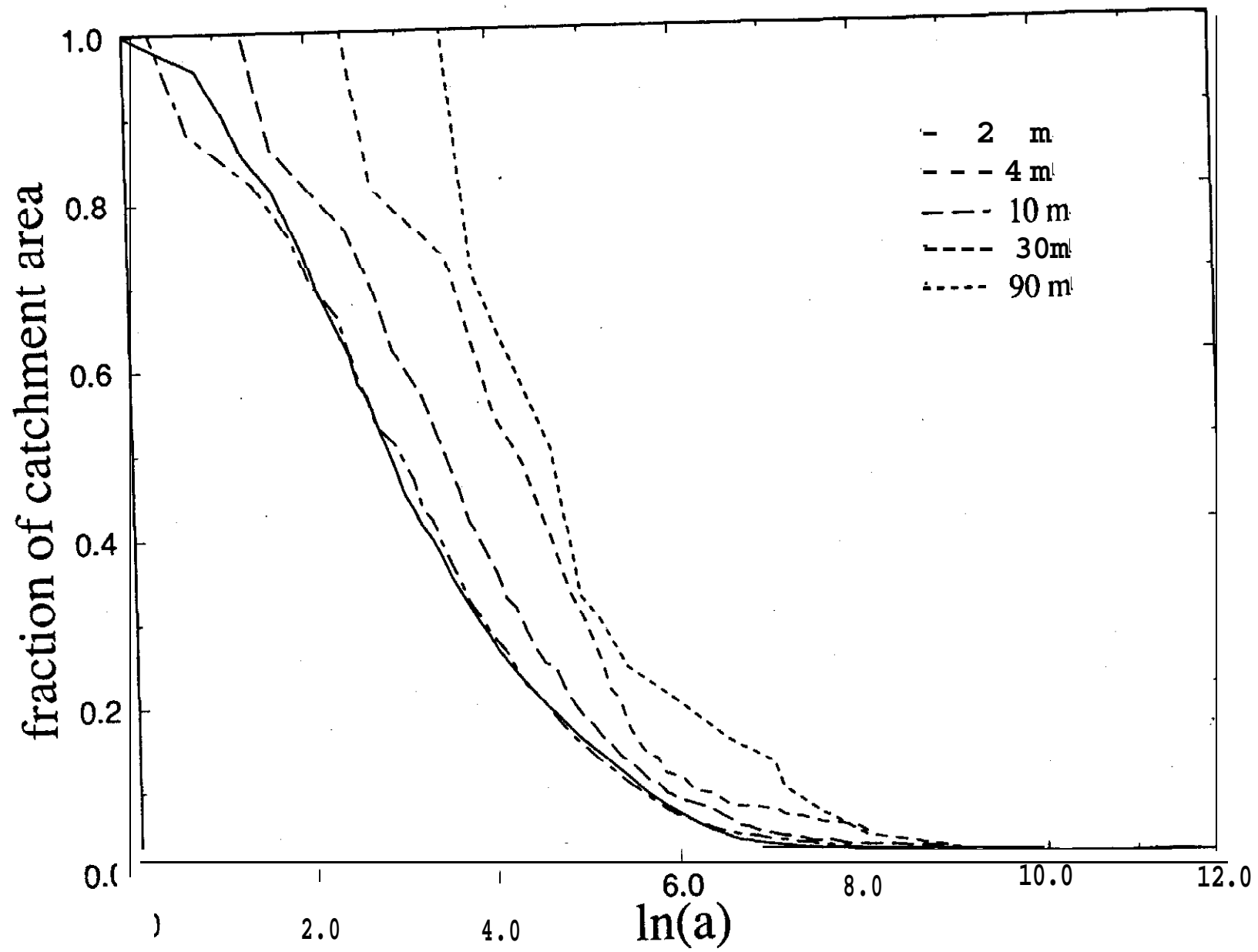
200.0 meters

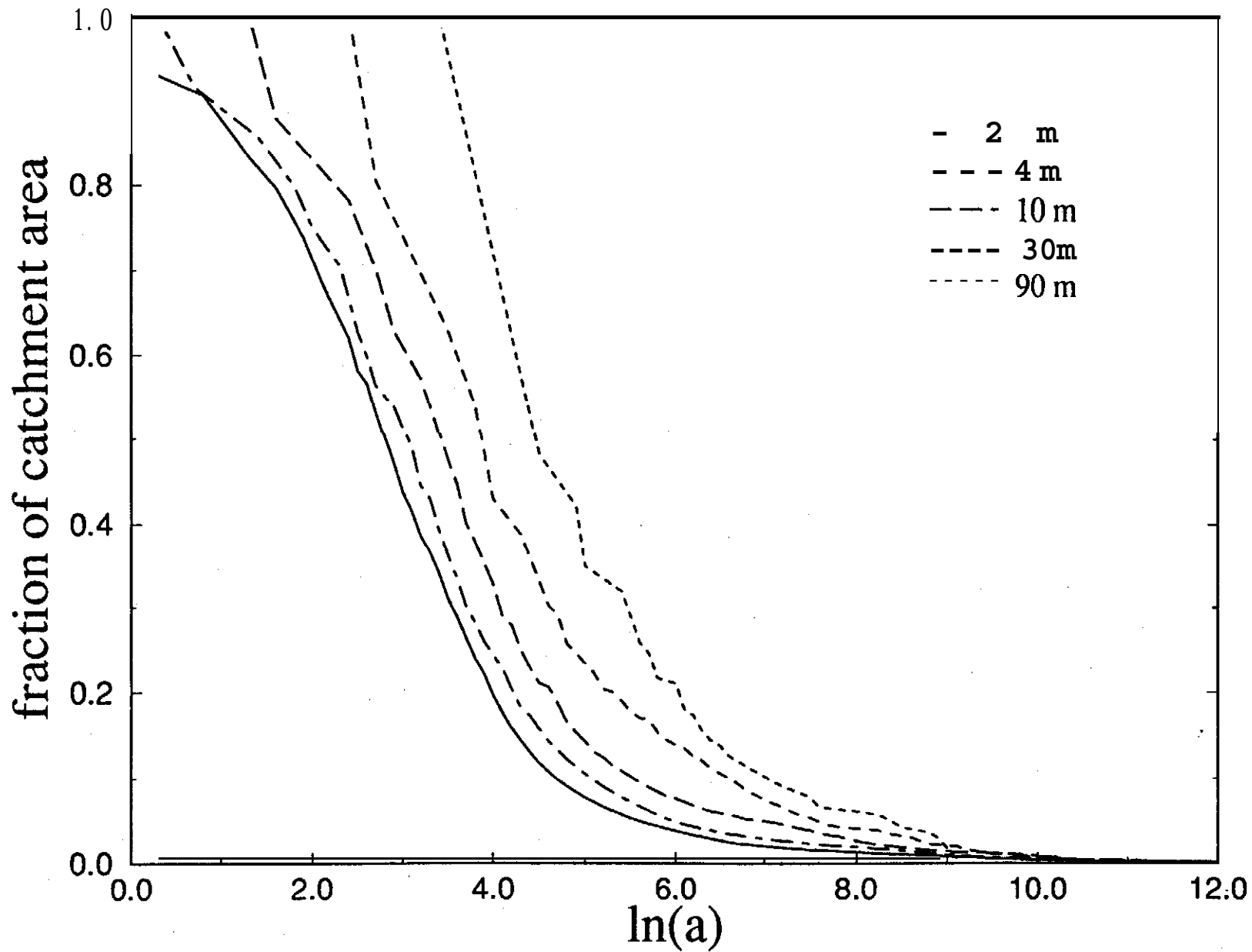


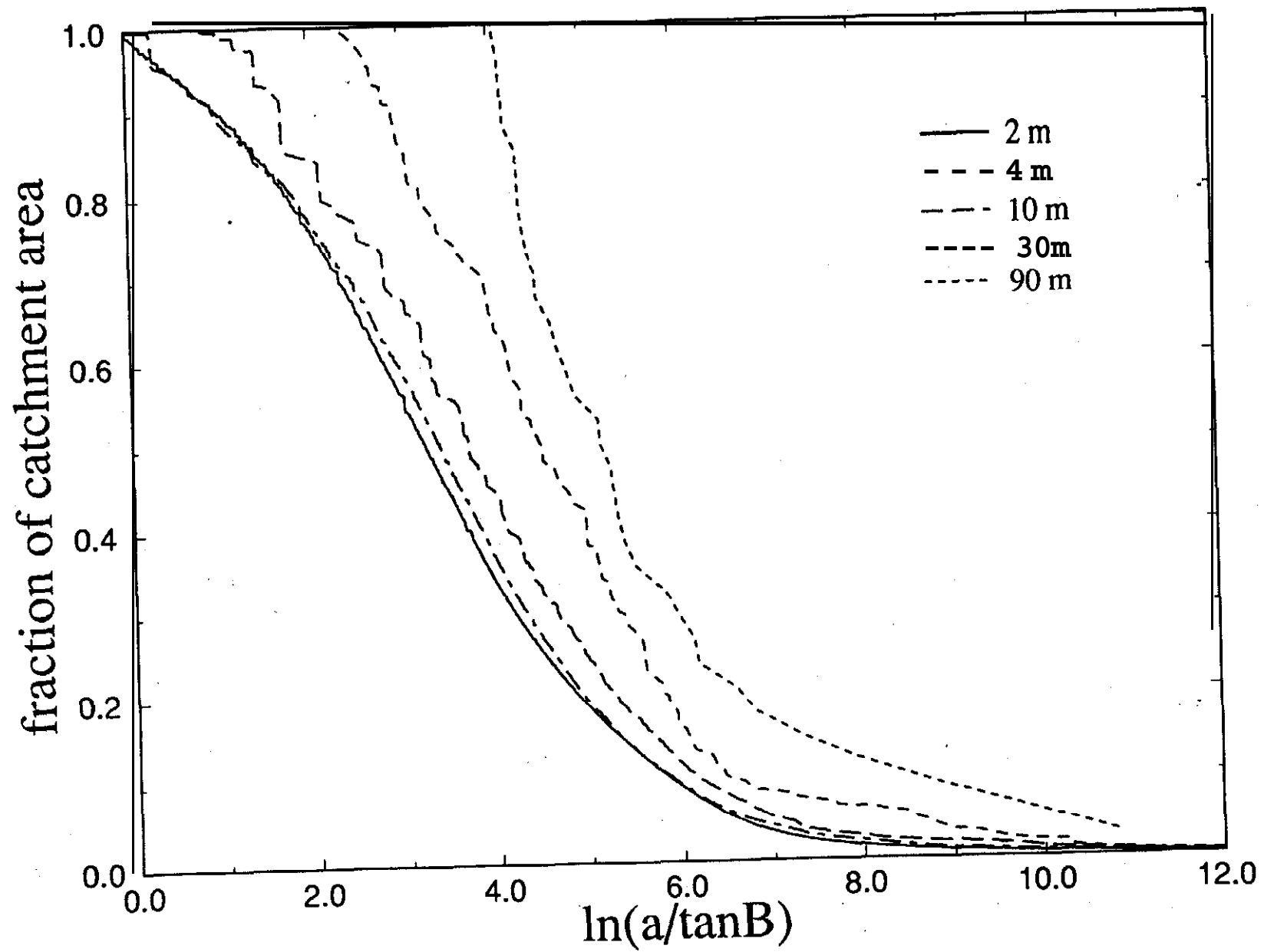


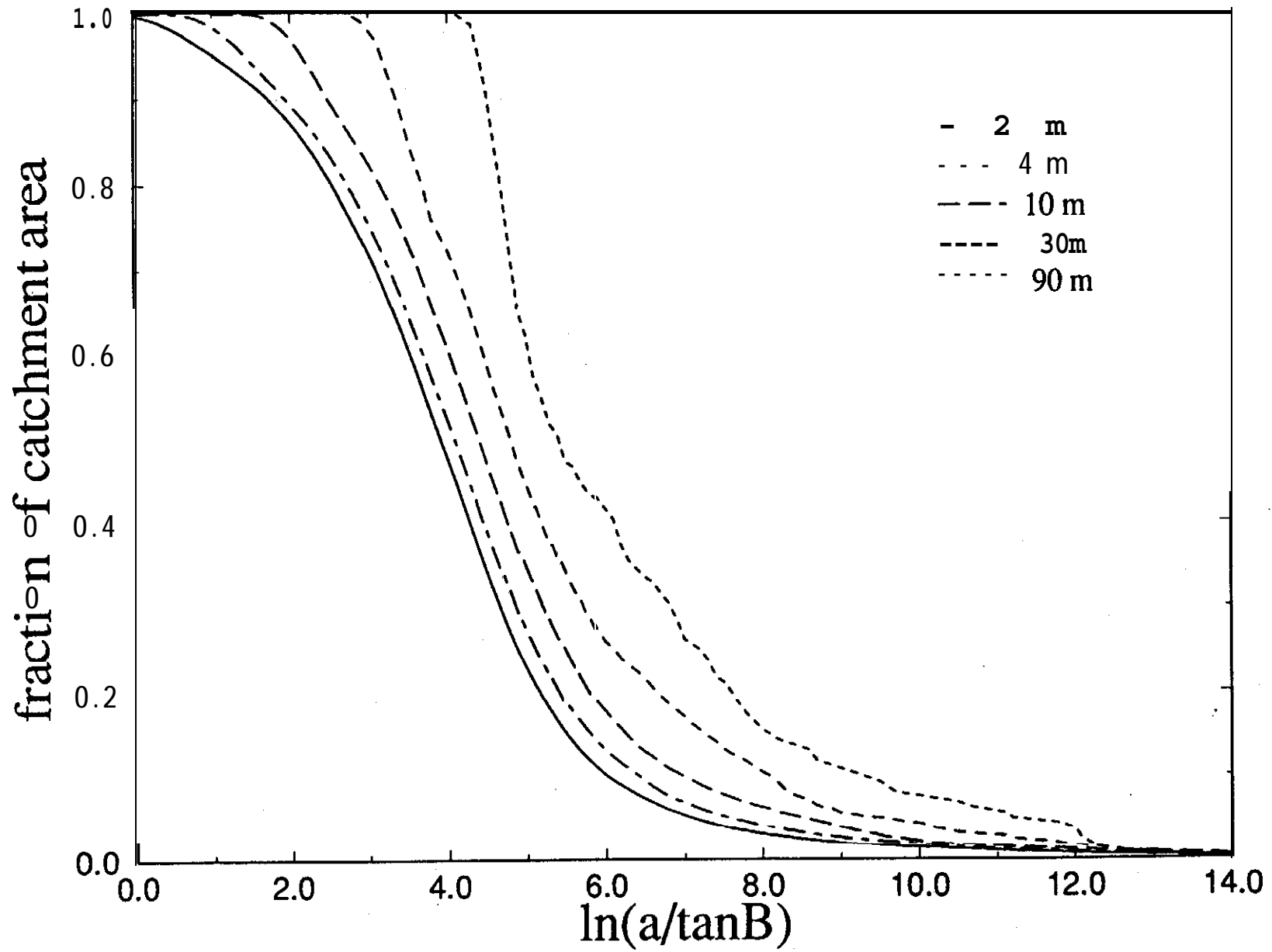


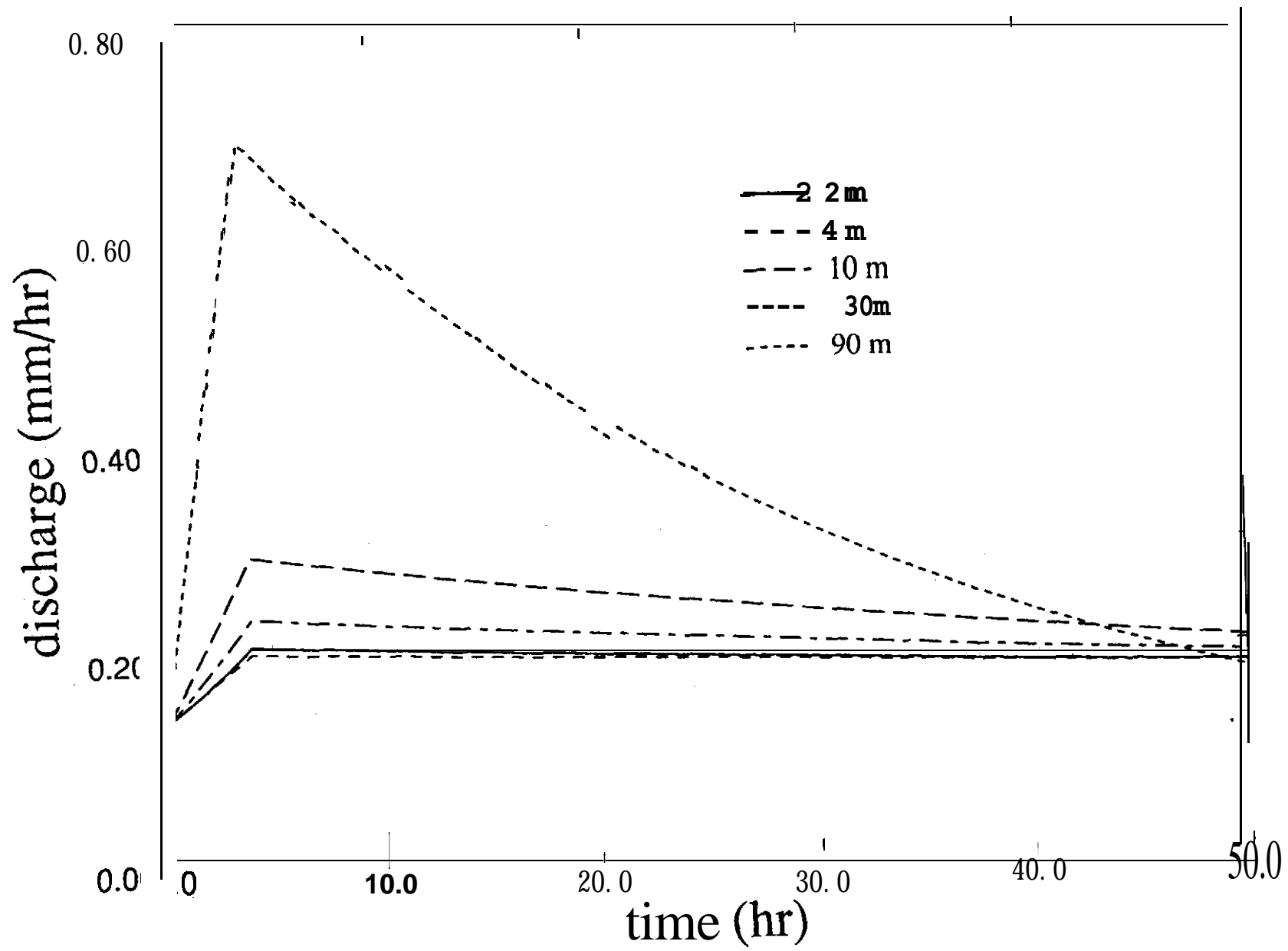


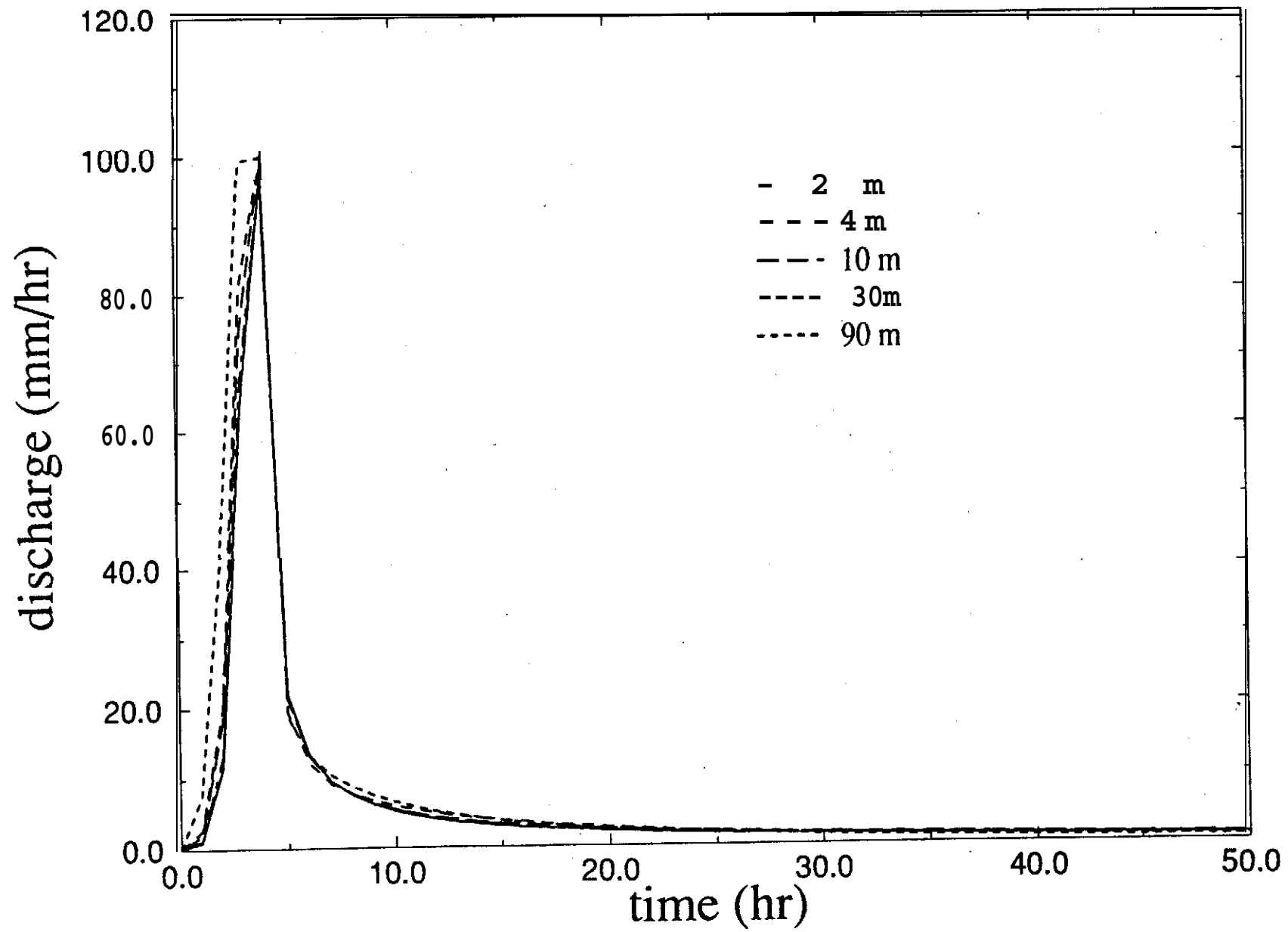


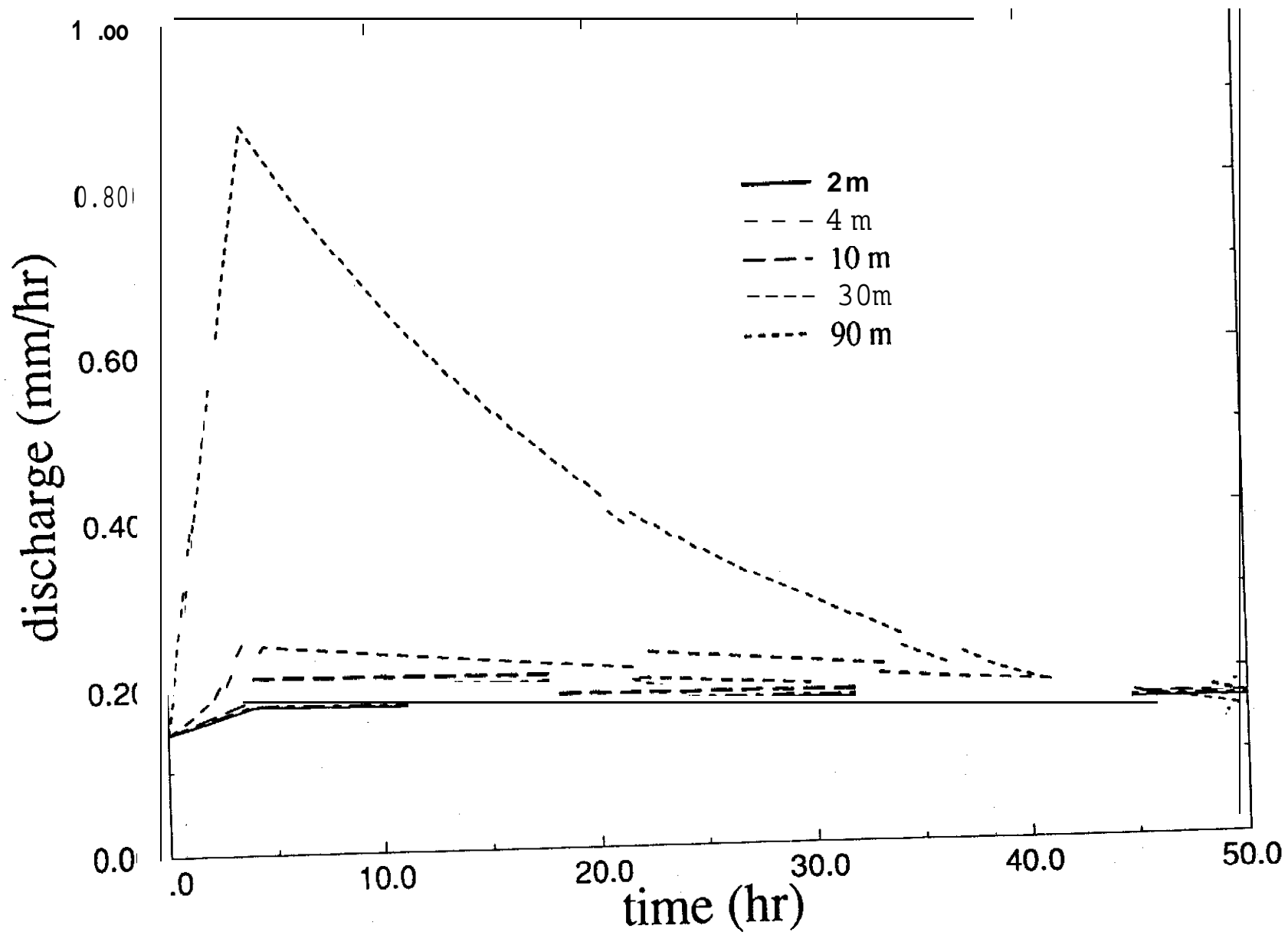


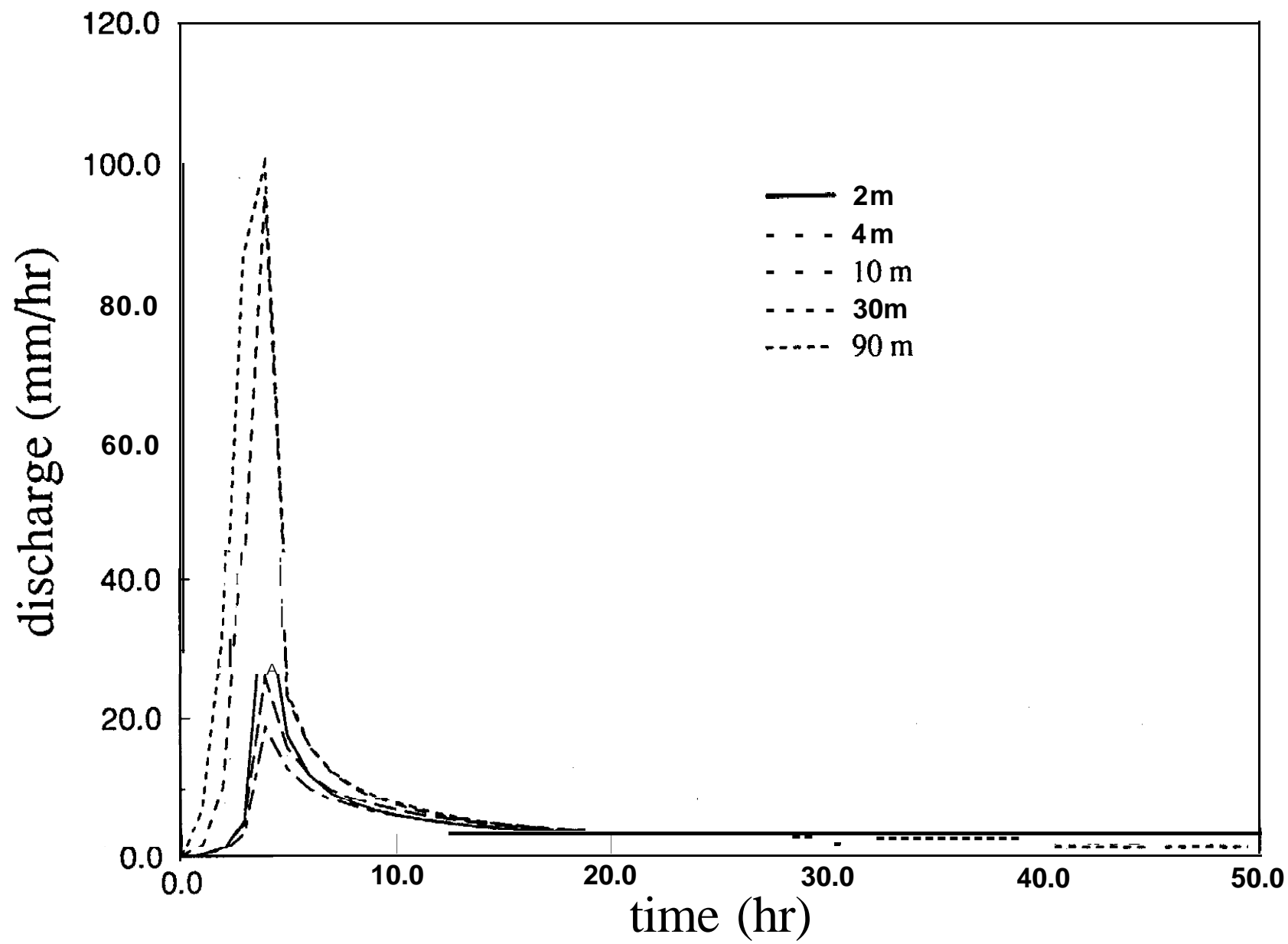


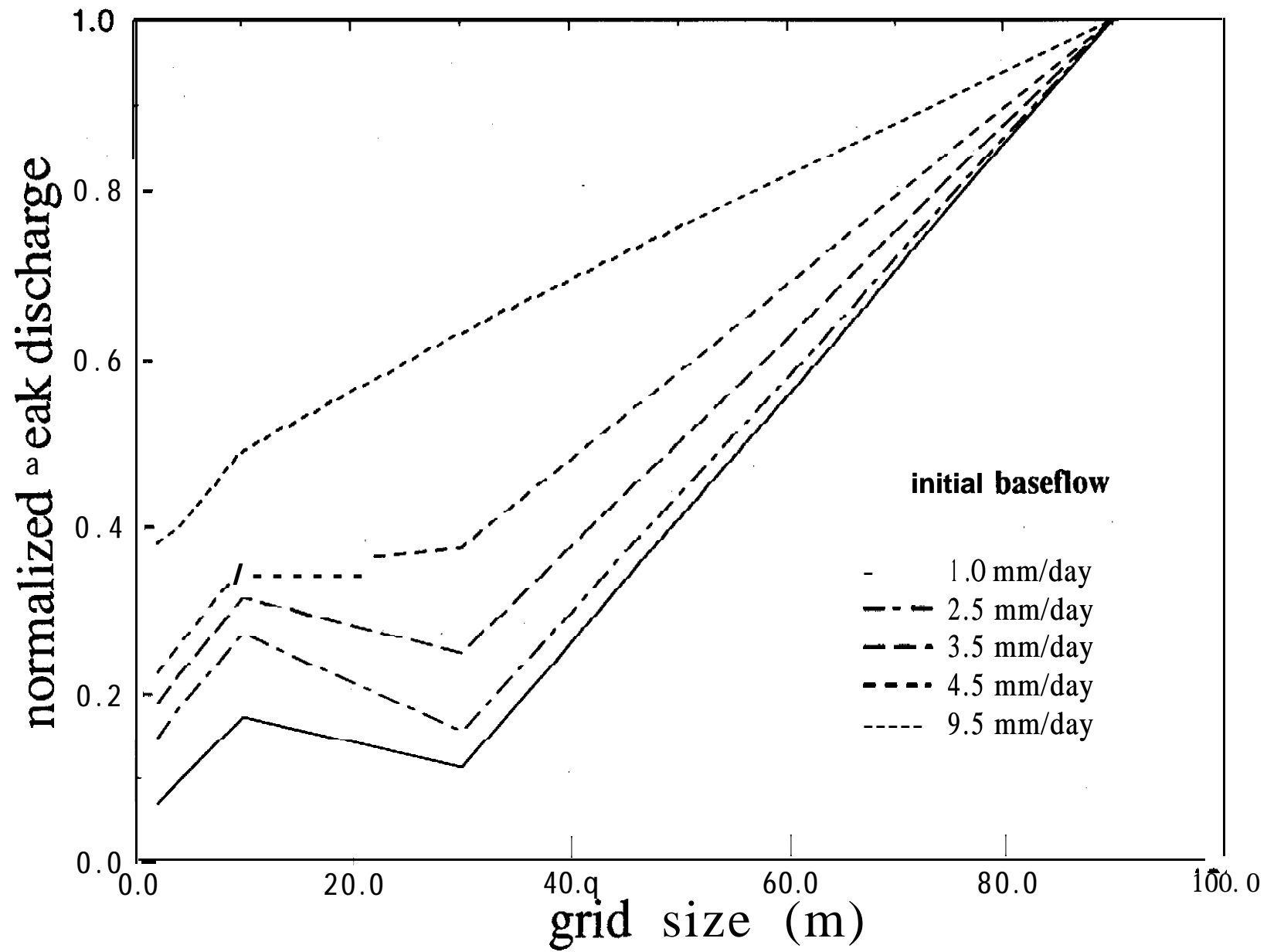


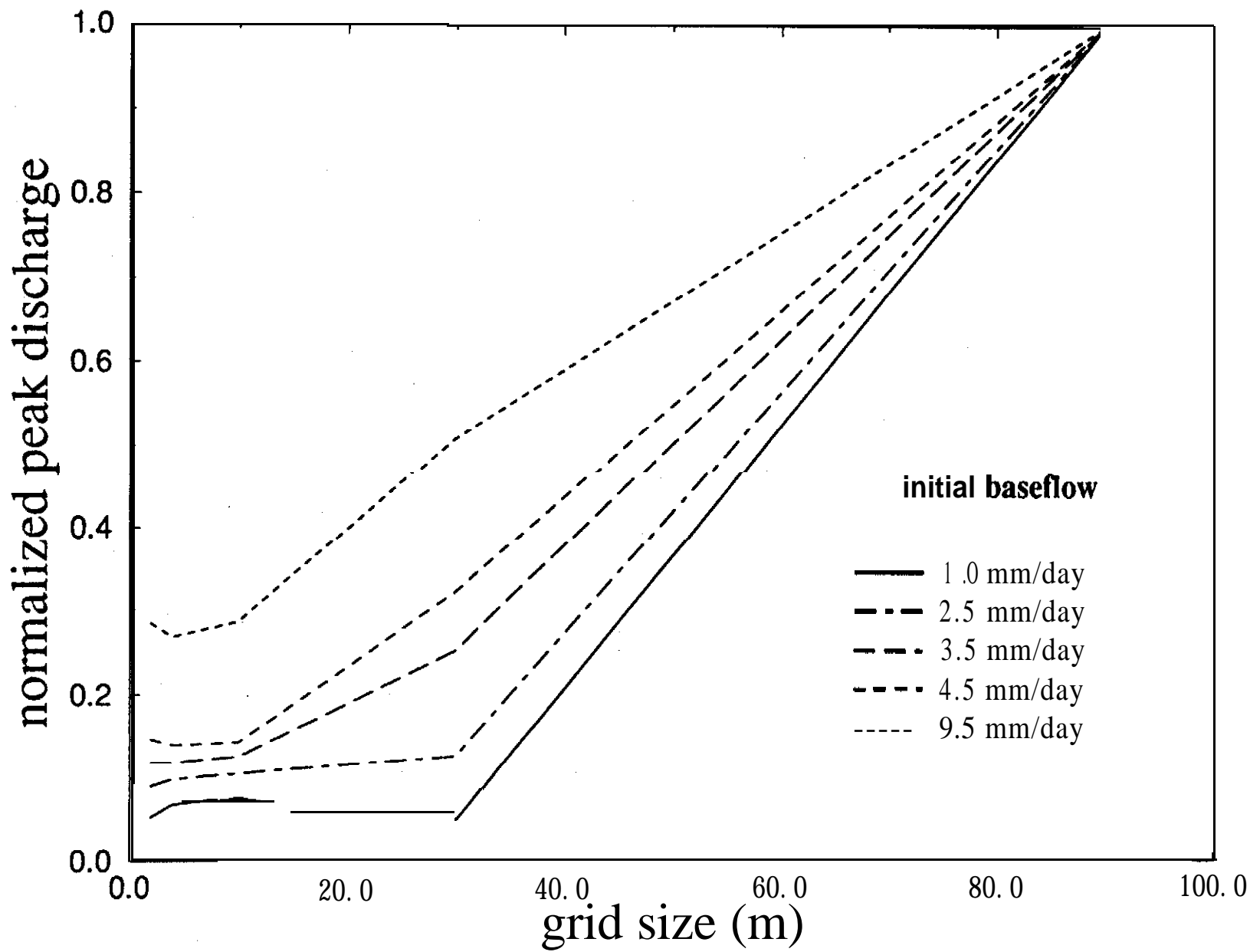


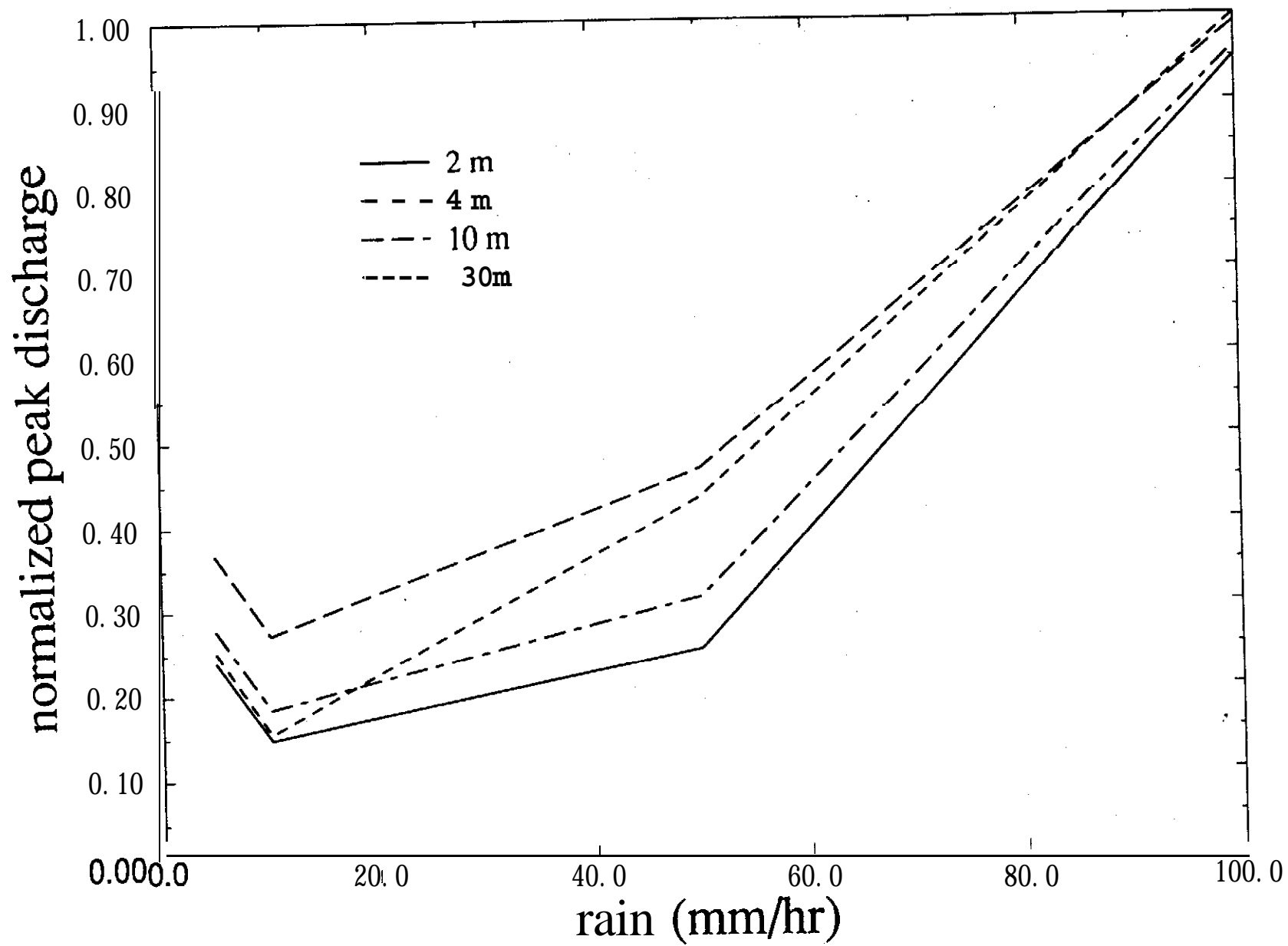


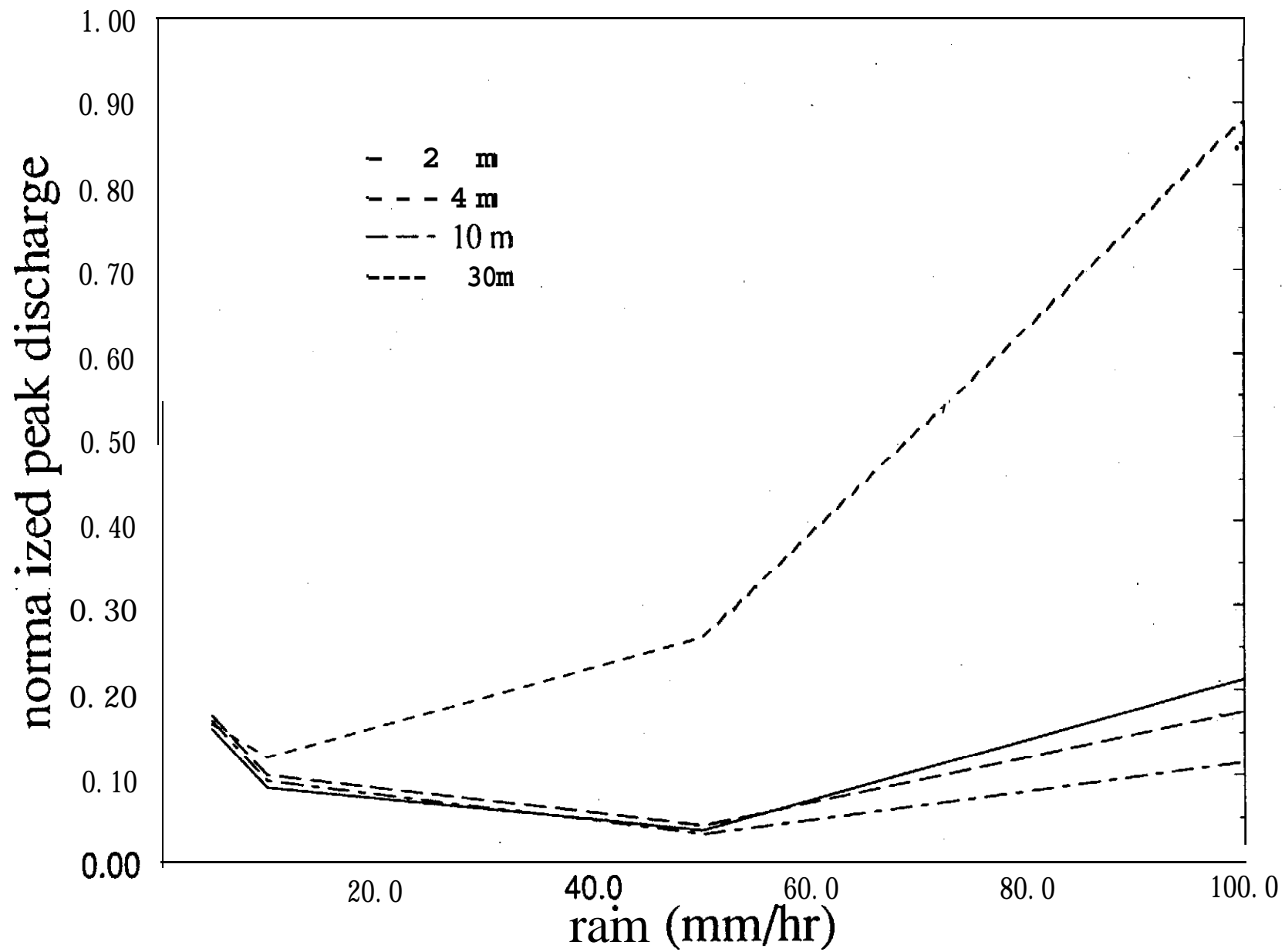












Road **Surface** Drainage, Channel Extension, and Slope Stability

David R. Montgomery

Department of Geological Sciences and Quaternary Research Center
University of Washington, Seattle, WA 98195

revised submission-to Water Resources Research

ABSTRACT

Simple models for contributing area-ground slope thresholds for channel initiation by landsliding and overland flow are fitted to data from field surveys of road drainage concentration in three study areas in the western United States. Fitted threshold models predict the general form of the boundary **on** a plot of drainage area versus local ground slope between data fields for locations where road drainage is associated with either landsliding, channel extension to the road, or no observable geomorphic effect. Landsliding occurs at the greatest drainage areas on steep slopes; locations with no observable geomorphic effect have **the smallest** drainage areas for a given slope. Comparison with data from previous studies in these areas indicates that the drainage area required to support a channel head is smaller for road-related runoff than for undisturbed slopes, reflecting the lower infiltration capacity and thus greater runoff production per unit area on road **surfaces**. In each of these study areas, road drainage concentration increases the effective length of the channel network and strongly **influences the** distribution of erosional processes. Drainage concentration from **ridgetop** roads also may cause **both** landsliding and integration of the channel and road networks. Calibration of threshold theories for road drainage-induced erosion & rough limited field reconnaissance provides criteria for road design that would minimize direct impacts on downstream channel systems.

INTRODUCTION

Road building results in a wide variety of environmental impacts. Although virtually all road surfaces alter both drainage patterns and runoff generation, the geomorphic impact of **road** construction has received little attention in a quantitative theoretical framework. Significant road-related environmental impacts include destabilization of side-cast material and downslope hillslopes (Figure 1), gullying and channel network expansion, as well as increased downstream sediment loads, altered streamflow and channel adjustments [see Furniss et al. (1991) for a recent review]. For example, many previous workers established that erosion rates from road surfaces and road-related landslides are many times greater than from undisturbed areas [e.g., Megahan and **Kidd**, 1972; Swanson and Dyrness, 1975; Beschta, 1978; Rice et al., 1979; **McCashian** and Rice, 1985; Reid and Dunne, 1984; Schroeder and Brown, 1984; Amaranthus et al., 1985; Anderson and Potts, **1987**]. Each of these impacts can result from the concentration of runoff generated on road surfaces and rerouting of intercepted subsurface discharge.

Differences in runoff generation from road surfaces and natural slopes are well known. Road surfaces are less permeable and act as a source of rapid runoff, increasing both rates and volumes of runoff [Megahan, **1972**]. Road runoff thus effectively generates greater peak discharges than an equivalent natural drainage area. Road surfaces concentrate and deliver runoff to specific locations; ditches on the in-board side of roads intercept both surface and shallow subsurface runoff from **upslope** areas and route road drainage to culverts or other drainage locations [e.g., Megahan, 1972; Burroughs et al., **1972**]. These drainage alterations and diversions may alter channel network pattern, extent, and processes.

Concentration of road drainage can have several direct geomorphic effects; 1) increased discharge may be insufficient to modify sediment transport, and thus have

no identifiable geomorphic impact, 2) the discharge increase may be sufficient to initiate or enlarge a channel and 3) the concentrated discharge may contribute to slope instability on steep slopes below the drainage outfall. Sediment transport, channel initiation, and shallow slope instability are each strongly influenced by local slope and surface or subsurface discharge. This paper compares models for erosion initiation by shallow landsliding and overland flow with data from field surveys of road drainage concentration in three study areas in the western United States. The methodology outlined provides a process-based framework for assessing the impact of road systems on channel extension and landsliding.

THEORY

Threshold theories for channel initiation and slope stability [e.g., Horton, 1945; Schaefer, 1979; **Dietrich** et al., 1986; 1992; Montgomery and Dietrich, 1989; 1994; Willgoose et al., **1991**] provide a context within which to analyze erosional impacts of drainage modification. The essential principle underlying these theories is that erosion occurs once sufficient surface or subsurface discharge accumulates on a steep enough slope to overcome the erosional resistance of the ground. Many factors influence the specific timing and location of erosion by these processes including the intensity and duration of rainfall and temporal variations in the contribution of vegetation to soil strength. However, threshold models for the spatial distribution of erosion by these processes may be developed in terms of drainage area (as a surrogate for discharge), ground slope, and soil properties (e.g., critical shear stress, bulk density, and friction angle). More detailed derivations of these models and discussions of their assumptions and limitations are presented elsewhere [Montgomery and Dietrich, 1989; 1994; in press; **Dietrich** et al., 1992; **1993**].

The overland flow model considers a critical shear stress to control channel initiation. The critical shear stress, τ_{cr} , is given by

$$\tau_{cr} = \rho_w g (D \sin\theta)_{cr} \quad (1)$$

where ρ_w is the density of water, g is **gravitational** acceleration, D is the flow depth, and θ is the ground slope. Following Montgomery and **Dietrich (1994)**, the discharge per unit contour length for Horton overland flow (precipitation in excess of the infiltration capacity of the soil) in response to a steady-state rainfall is given by

$$q = (R - I)a = u D \quad (2)$$

where R is the rainfall rate, I is the infiltration capacity of the ground surface, a is the **upslope** contributing area per unit contour length, and u is the flow velocity. The flow velocity also is related to slope and surface roughness. For laminar flow, this may be expressed as

$$u = (2 g D \sin\theta q / k v)^{1/2} \quad (3)$$

where k is a dimensionless surface roughness coefficient and v is the kinematic viscosity. For turbulent flow, the flow velocity may be related to flow depth and slope by the well known Manning equation

$$u = (1/n) D^{2/3} \sin\theta^{1/2} \quad (4)$$

where n is a roughness coefficient. The critical drainage area, a_{cr} , required to **initiate** erosion (and thus, we assume, a channel) can be derived from equations (1-4) and is given by

$$a_{cr} \propto \frac{\tau_{cr}^3}{(R - I) \sin^2 \theta} \quad (5)$$

for **laminar** flow and

$$a_{cr} \propto \frac{\tau_{cr}^{5/3}}{(R - I) \sin^{7/6} \theta} \quad (6)$$

for turbulent flow. Each of these equations predicts an inverse critical area-slope relation; a greater drainage area is required to initiate a channel on a gentler slope. Since road construction generates a topographic surface with a decreased infiltration capacity, equations (5) and (6) predict that channel initiation by runoff generated on road surfaces requires smaller drainage areas than for undisturbed ground.

Analogous topographic controls on shallow landsliding may be developed through coupling simple hydrologic and slope-stability models (see Montgomery and Dietrich [1989; 1994, in press] and **Dietrich** and others [1992; 1993]). The coupled model essentially relies on an expression for the convergence of shallow **throughflow** to predict the depth of saturation, which is then input into the **infinite-slope** stability model. Following **Dietrich** and others [1993], the model assumes infiltration of steady-state rainfall and runoff by shallow subsurface flow through cohesionless soil overlying less **conductive** bedrock. The ratio of subsurface flow to that which would occur at soil saturation is

$$\frac{R a}{T \sin \theta} = \frac{h}{z} \quad (7)$$

where b is the contour length across which the subsurface flow drains, T is the soil **transmissivity** at soil profile saturation, h is the local thickness of saturated flow, and z is the soil thickness. The infinite slope stability model for cohesionless soils can be expressed as

$$h / z = (\rho_s / \rho_w) [1 - (\tan \theta / \tan \phi)] \quad (8)$$

Substitution of (6) into (7) yields an expression for the critical drainage area per unit contour length required to initiate a shallow landslide:

$$a_c = (T/R) \sin \theta (\rho_s / \rho_w) [1 - (\tan \theta / \tan \phi)] \quad (9)$$

This equation is only valid for steep slopes where $\tan \theta \geq [(\rho_s - \rho_w) / \rho_s] \tan \phi$, which generally can be approximated by **$\tan \theta > 0.5$** Montgomery and Dietrich, **1994**].

Equation (9) predicts a steeper, non-loglinear inverse critical area-slope relation than models for channel initiation by overland flow. Increased volumes or rates of water delivery to unchanneled valleys would decrease the critical area for debris-flow initiation by effectively increasing the steady-state rainfall.

Equations (5), (6), and (9) predict different drainage area-slope relations for channel or landslide initiation. Comparison of field mapped channel networks in natural landscapes (i.e., no road drainage influence) with **topographic** thresholds defined using digital elevation models indicate that such thresholds can be used to define drainage area-slope relations below which channels do not develop

[Montgomery and Dietrich, 1992]. These relations provide testable hypotheses for examining the effect of road drainage concentration on the stability of natural landscapes.

STUDY AREAS AND METHODS

Road alignments and drainage patterns in each of the study areas were mapped onto topographic **basemaps** in three study areas in the western United States; an area near Oiler Peak in the southern Sierra Nevada, California, Mettman Ridge in the Oregon Coast Range, and Huelsdonk Ridge on the Olympic Peninsula, Washington (Figure 2). Previous field mapping of channel network extent in portions of the Southern Sierra and Mettman Ridge study areas that are uninfluenced by road drainage documented drainage area-slope thresholds defining **channeled** and unchanneled portions of the landscape [Montgomery and Dietrich, 1988; 1992]. Additional field mapping reveals similar relations for channeled and unchanneled locations in the Huelsdonk Ridge study area. The pattern of drainage diversion in the southern Sierra study area was used to estimate **upslope** contributing areas for discharge points both with and without drainage modifications. Field maps were used to determine contributing drainage areas for the Huelsdonk Ridge study areas. In the Mettman Ridge study area, the drainage area contributing to discharge concentration points and the ground slope immediately downslope were measured using a tape measure, stadia rod, and hand level. In each study area, ground slopes were measured in the field at every point where road drainage was concentrated.

Mapping road drainage and determining contributing areas for discharge points is subject to considerable inaccuracy because of uncertainty associated with partitioning road surface runoff to different potential discharge points. Reid [pers. **comm.**], for example, estimated that surface mapping of road drainage was accurate to about $\pm 30\%$ of the actual contributing area when conducted at times when

runoff was not occurring. She also found that mapping road surface drainage patterns during or immediately after runoff-producing events improved the **accuracy** of contributing area estimates to about ± 10 %. I concur and estimate that the drainage area data for road surfaces collected in this study should be considered to have an accuracy of roughly $\pm 10-30$ %.

Southern Sierra Nevada, California

The drainage system associated with a paved two-lane highway near Oiler Peak provides an example of the effects of road drainage diversions on gully development and channel network expansion. The area **is** underlain by deeply weathered granitic rocks with thick colluvial soils developed in topographic hollows. Slopes are gentle and vegetation consists of open oak forest and grasslands. The road system is located significantly downslope from the drainage divide. Road cuts truncate colluvial fills in topographic hollows and weathered bedrock in noses and divert both surface and subsurface flow into an inboard ditch system that drains through culverts into natural drainage courses.

Culvert locations and drainage diversions were mapped along a 2 km stretch of road. Drainage areas both prior and subsequent to road construction were determined from the mapped pattern of drainage diversions, which significantly altered the channel network in the mapped area. For example, at one mapped location a deeply-incised gully begins downslope of a culvert outfall that receives drainage from **upslope** diversions. The natural channel head is a gradual incision located 200 m down valley and that has been stranded and effectively abandoned by **gully** incision.

Incision of previously unchanneled valley bottoms resulting from road drainage concentration has integrated the road and channel networks, allowing the road surface to act as an extension of the channel network. Within the area shown

in Figure 3, four hollows (A,C,E, & G) lost drainage area through road drainage diversions. **In** each of these cases, the channel begins significantly downslope of the road. In contrast, three hollows (B,D, & F) receive additional drainage from the road system and the channels begin at or immediately downslope of culverts. In the area shown, integration of these channels with the road drainage network increased the total channel length by about 570 m, which increased the effective drainage density (here used in the sense of the channel density of Montgomery and **Dietrich [1994]**) from 5.2 km^{-1} to 8.7 km^{-1} (170% of the natural **drainage density**). For the whole 1.2 km^2 basin in which the extent of the channel network was mapped, integration of the road and channel networks increased the drainage density from 2.8 km^{-1} to 4.4 km^{-1} (160% of the natural drainage density). These estimates do not include the length of new channels incised between culverts and previous channel heads. Larger channels in this area are entrenched in **colluvial/alluvial** valley fills, with a series of three terraces preserved along the main channel. Cultural artifacts recovered from within these alluvial terraces indicate that the entrenchment is historic, Downstream channel entrenchment in this area may further reflect the effects of historic grazing activity, which caused channel entrenchment in other parts of California (see Cooke and Reeves **[1976]** and Montgomery **[1991]**).

Road drainage also influences the threshold for channel initiation in this area. The transition from channeled to **unchanneled** slopes exhibits the same inverse form for both natural and road-altered drainage (Figures **4A&B**), but less drainage area appears to be required to initiate a channel for hollows receiving road drainage (Figure 4C). A test for the equivalence of regression models for the **log**-transformed data for channeled locations [Berenson et al., **1983**] allows rejection of the hypothesis that the two population models are coincident ($\alpha=.05$). These results **imply** that road drainage has not altered channel initiation mechanisms (in this case

overland flow) and support the hypothesis that the impervious paved road surface generates runoff equivalent to that of a larger natural area.

Huelsdonk Ridge, Washington

Recently-constructed logging roads on Huelsdonk Ridge provide an example of the effect of **ridgetop** road drainage on channel network extension and slope stability. Steep **clearcut** slopes drain to narrow tributary channels that empty into a wide alluviated **valley** along the South Fork Hoh River. These steep slopes are divided into rhythmically-spaced hollows and noses. Most of the landslides in this area originate in topographic hollows **and** landslide inventories from historical aerial photographs indicate that the rate of landslide initiation increased dramatically following road construction and clear-cutting [Schlichte, 1991].

A 7.8 km stretch of the gravel road system along Huelsdonk Ridge was mapped onto a **1:4800** scale topographic **basemap**. Road drainage divides, culverts, and other locations where road drainage discharged onto the slopes were mapped. Road surface widths measured in the field consistently were 5.6 m. As is typical throughout the Pacific Northwest (Figure 5), **ridgetop** road drainage generally is focused into the heads of topographic hollows. Drainage areas **contributing** to each discharge point were calculated as the product of the contributing road length and the road width. The local slope immediately downslope of the discharge point was measured from the topographic **basemap**. Each discharge point was classified as either not influencing erosion, causing channel formation immediately downslope of the road margin, or associated with a debris-flow scar.

Data from these classes appear to define distinct fields on a plot of drainage area versus slope (Figure 6). Data from locations where road drainage does not influence downslope erosion (unchanneled) plot at the lowest drainage areas and slopes. Data from locations where road drainage initiates a channel (channeled) plot at higher drainage areas. Road drainage-associated landslides plot at the highest

drainage areas and steepest slopes. Although the sample sizes are small, the significance of this **interpretation** is supported by Komolgorov-Smirnov tests [Sprent, **1989**] of the null hypothesis that each of the variables (drainage area and slope) for each of the samples (unchanneled, channeled, and landslide) are drawn from populations with identical distributions. The slope distributions for channeled and landslide data differ ($\alpha=.05$), whereas the null hypothesis cannot be rejected ($\alpha=.05$) for comparison of unchanneled and either channeled or landslide data. Drainage area distributions differ significantly ($\alpha=.05$) for comparison of unchanneled and either channeled or landslide data, but are not significantly different ($\alpha=.05$) for comparison of channeled and landslide data. These tests allow us to conclude that unchanneled sites have significantly smaller drainage areas than either channeled or landslide sites, and that landslide sites are steeper than channeled sites.

These data also are consistent with the form of relations predicted by equations (6) and (9), as fitted relations essentially define boundaries between data fields (Figure 6). Channeled and unchanneled data are reasonably segregated by

$$A = 400 / \sin\theta \quad (10)$$

a relation close to the form predicted for channel initiation by turbulent overland flow, such as might be expected where road drainage is discharged onto natural slopes. Landsliding sites only occur on slopes where $\tan\theta > 0.5$ and the lower bound to the data for sites of observed landsliding is well fit by adjusting the steady-state rainfall in equation (9) using estimates of $T = 65 \text{ m}^2/\text{day}$, $\rho_s = 1800 \text{ kg/m}^3$, and $\phi = 45^\circ$ derived from field measurements (see Montgomery and **Dietrich** [in press] for further discussion). These observations suggest that adverse erosional impacts associated with **ridgetop** road construction could be minimized by a drainage, system

designed to keep the contributing area at discharge locations below the range for the channeled data in Figure 6.

Mettman Ridge, Oregon

The forest road system on Mettman Ridge provides another example of the effect of **ridgetop** road drainage on erosional processes. The gravel road system is located on narrow ridge crests separating steep slopes, which are divided by regularly-spaced hollows that indent **ridgetop** drainage divides. Consequently, road drainage commonly is discharged into the heads of topographic hollows. Road surface widths measured in the field consistently were 3.5 m. Landslides are a major channel initiation mechanism in this area [Montgomery and Dietrich, **1988**] and landslide-related sediment transport accelerated dramatically after road building and forest clearance, with most of the increase coming from failures associated with road drainage concentration or logging landings [Montgomery, **1991**].

A total of 3.2 km of the gravel road system was mapped onto **1:4800** scale topographic **basemaps** (Figure 7). Road drainage flow directions, drainage divides, culverts, and other points of drainage concentration were mapped immediately after rainfall observed to produce copious runoff from road surfaces. In many cases, distinct channels on either side of the road crown drained to opposite sides of a ridge. Moreover, flow down the road surface sometimes bypassed culverts. Road surface area was allocated to each discharge point based on field measurements, mapping, and estimates. Again each discharge point along surveyed road segments was classified according to the association of the discharge point with either no apparent geomorphic effect, channel extension to the drainage outfall, or debris-flow scars. Integration of the **ridgetop** road network with the channel network in the three Mettman Ridge basins mapped in the previous studies would increase the drainage density from 9.9 **km⁻¹** to 12.2 **km⁻¹** (123% of the original drainage density).

Data from Mettman **Ridge** exhibit general relations similar to the Huelsdonk Ridge data (Figure 8). Locations where drainage concentration has no observable geomorphic effect plot at the **smallest** drainage areas and slopes. **Locations** where road drainage initiates a channel plot at higher drainage areas and slopes, while those locations where road drainage is associated with landsliding plot at the highest drainage areas and are restricted to steep slopes (i.e., $\tan\theta > 0.5$). Again sample sizes are small, but these interpretations are supported by Komolgorov-Smirnov tests [Sprent, 1989] of the null hypothesis that each of the variables are drawn from populations with identical distributions. In this case, the distributions of drainage area data for unchanneled locations differ ($\alpha=.05$) from both channeled and unchanneled data, while the null hypothesis cannot be rejected ($\alpha=.05$) for comparison of channeled and landslide data. Slope distributions differ significantly ($\alpha=.05$) for comparison of landslide and either channeled or unchanneled data, but are not significantly different ($\alpha=.05$) for comparison of channeled and unchanneled data. These tests allow us to **conclude** that unchanneled sites have smaller drainage areas than **channeled** or landslide sites, and that the population of landslide sites is steeper than those for both channeled and unchanneled sites.

Equations (6) and (9) also provide reasonable predictions of the boundaries to unchanneled, channeled, **and** landslide data from the Mettman Ridge road drainage survey (Figure 8). The lower bound to the data from channeled road drainage locations along Mettman Ridge can be approximated by

$$A = 100 / \sin\theta \quad (11)$$

This is significantly lower than for the Huelsdonk Ridge data, presumably reflecting differences in climate (rainfall intensity and duration) and soil properties.

(infiltration capacity and critical shear strength) between these study areas. This

difference illustrates that a single relation is not applicable to all landscapes. Appropriate relations need to be developed for application in different areas. Again, equation (9), fitted by adjusting the rainfall rate and using field derived estimates of $T = 65 \text{ m}^2/\text{day}$, $\rho_s = 1800 \text{ kg/m}^3$, and $\phi = 45^\circ$, provides a reasonable lower bound to data from sites of observed landsliding (Figure 8).

Comparison of data from road drainage surveys with data generated from a field survey of channel head locations in this area of Mettman Ridge [Montgomery and Dietrich, 1992] reveals that overland flow-initiated channel heads associated with road drainage plot at lower drainage areas than undisturbed channel heads (Figure 9). This presumably reflects the lower infiltration capacity for road surfaces than for natural slopes. Many steep channel heads in this area are associated with small landslide scars [Montgomery and Dietrich, 1988; 1992]. Contributing areas for road-related landsliding plot within the range of natural data. The mechanism for initiating landsliding involves infiltration of runoff and lateral subsurface flow convergence, which should decrease hydrologic differences between road-related and natural contributing areas of similar size. The small sample size of the available data preclude greater exploration of this issue.

DISCUSSION

The lower-limit to the data for channel initiation by overland flow and landsliding from road drainage concentration is consistent with the general forms predicted by equations (6) and (9). The relations reported above apply only to geomorphic impacts on locations immediately downslope of roads; they do not consider a wide array of other road-related impacts that warrant further research. These include more detailed assessments of the integration of road and channel networks, the attendant effects on downstream hydrologic and geomorphic response, and the influence of sediment eroded from road surfaces on substrate sizes

in downstream channels. Each of these effects depends on the integration of the channel **and road** networks, which itself depends on continuing incision **downslope** to existing channels. Such integration is to be expected for the cases of landsliding or drainage to existing channel crossings. In contrast, overland flow delivered from a road to a previously unincised slope may cause incision, but subsequently infiltrate into colluvial deposits. However, the resulting increase in the downslope subsurface discharge may destabilize the channel head and cause channel extension. Integration of the road and channel networks thus may reflect an interplay of these mechanisms.

The data reported here have important implications for assessing current road designs. **Ridgetop** roads are presently recommended as a means to avoid direct road connection to channels and construction of potentially unstable fill berms across low-order channels [e.g., Fumiss et al., **1991**]. Ridgetops, however, are generally indented at the heads of valleys and thus **ridgetop** road drainage typically is focused into and, as the data presented here show, may destabilize **unchanneled** valleys. While recent improvements in road construction practices (e.g., **end-hauling**) should decrease some road-related impacts, road drainage concentration may still trigger slope instability and integrate channel and road networks.

The survey results reported here suggest that incorporation of empirical drainage area-slope thresholds into road drainage designs would help to minimize adverse affects of road drainage concentration. This requires determination of the relation appropriate for the area of interest from field surveys. Fortunately, such surveys are simple and are **not** time consuming. For example, collection of the data from Heulsdonk Ridge required two people for one day; acquisition of the Mettman **Ridge** data required two people for two days. Collection of the necessary data entails a fraction of either the cost of repairing a single landslide, or the value associated with resource loss.,

For a road of constant width, the drainage area-slope threshold defines a relation between the maximum road length, L, and the gradient of the slope onto which road drainage is discharged. Equations (5), (6), and (9) indicate that the specific relations should reflect the road surface material (infiltration capacity), rainfall characteristics, and soil properties (critical shear stress, friction angle, bulk density, and transmissivity). For the Huelsdonk Ridge data, the empirical relation is approximated by

$$L = 70 / \sin\theta \quad (12)$$

and for the Mettman Ridge data by

$$L = 30 / \sin\theta \quad (13)$$

(Figure 10). These relations highlight the need to include in evaluations of road-related environmental impacts both the frequency along a road that drainage is discharged and the gradient of the slope onto which it is discharged. At present, management regulations generally prescribe culvert spacing based either on delivery of road runoff to natural drainages or a design culvert spacing that varies with **the road** gradient (e.g., Washington Administrative Code **222-24-025**). Road designs or codes that do not take both drainage frequency and ground slope into consideration do not adequately address the potential for downslope geomorphic impacts from road drainage concentration..

CONCLUSIONS

Road construction fundamentally alters the hydrologic and erosional processes operating in a drainage basin. Sufficient concentration of road drainage is

associated with expansion of the channel network (and integration of the channel and road networks) and landsliding in steep terrain. Many existing road designs, including **ridgetop** roads, inadequately address geomorphic **impacts of** road construction, but simple changes in road design that would prevent drainage concentration could minimize road-related adverse impacts on slope stability and downslope stream channels. Collection of field data to calibrate theoretical thresholds for erosion initiation could be used to generate empirical relations for allowable drainage concentration **that** could reduce road drainage-related impacts.

Acknowledgements

This work was supported by grants TFW **FY92-010** and TFW **FY94-004** from the SI-IAMW committee of the Washington State Timber-Fish-Wildlife agreement. I also appreciate discussions with Leslie Reid on the accuracy of road drainage surveys. Field and office **discussions with** Bill **Dietrich** helped motivate this work. Kevin Schmidt, Tamara Massong, and Carolyn Trayler provided field assistance. A copy of the unpublished report by Schlichte **[1991]** can be obtained on request from either the author or from the Forest Land Management Division of the Washington State Department of Natural Resources in Olympia, Washington.

strength characterization provides a simple method to refine and supplement both the data available on geologic maps and the predictions made by GIS analyses.

REFERENCES

Selby, **M.J.**, 1980, A rock mass strength classification for geomorphic purposes: with tests from Antarctica and New Zealand: *Zeitschrift für Geomorphologie*, vol. 24, no. 1, p. 31-51.

FIGURE CAPTIONS

Figure 1. Plot of transects for Chuckanut Formation showing characteristic rock mass strength ratings with respect to topographic relief development. Landslide sites, enclosed by open circle, typically have lower strengths than neighboring stable hillslopes.

Figure 2. Plot of rock mass strength rating vs. topographic height of hillslope for Chuckanut Formation. Landslide sites are constrained below a rock mass strength value of 69.

Figure 3. Plot of rock mass strength rating vs. topographic gradient of hillslope for Chuckanut Formation. Landslide sites are constrained below a rock mass strength value of 69.

- their Habitats*, edited by W. R. Meehan, pp. 297-323, American Fisheries Society, Bethesda, 1991.
- Horton, R. E., Erosional development of streams and their drainage basins; Hydrophysical approach to quantitative morphology, *Geol. Soc. Am. Bull.*, **56**, **275-370**, 1945.
- McCashion**, J. D. and R. M. Rice, Erosion on logging roads in northwestern California, *J. For.*, **81**, **23-26**, 1983.
- Megahan, W. F., Subsurface flow interception by a logging road in mountains of central Idaho, *National Symposium on Watersheds in Transition*, 350-356, 1972.
- Megahan, W. F., and **Kidd**, W. J., Effects of logging and logging roads on erosion and sediment deposition from steep terrain: *J. Forestry*, **70**, **136-141**, 1972.
- Montgomery, D. R., *Channel Initiation and Landscape Evolution*, unpublished Ph.D. **dissertation**, Dept. of Geology and Geophysics, University of California, Berkeley, California, **421p.**, 1991.
- Montgomery, D. R. and W. E. Dietrich, Where do channels begin?, *Nature*, **336**, **232-234**, 1988.
- Montgomery, D. R. and W. E. Dietrich, Source areas, drainage density, and channel initiation, *Waf. Resour. Res.*, **25**, p. 1907-1918, 1989.
- Montgomery, D. R., and W. E. Dietrich, **Channel** initiation and the problem of landscape scale, *Science*, **255**, **826-830**, 1992.
- Montgomery, D. R., and W. E. Dietrich, Landscape dissection and drainage **area-slope** thresholds, in *Theory in Geomorphology*, edited by M. J. **Kirkby**, pp. 221-246, John Wiley & Sons, Chichester, 1994.
- Montgomery, D. R. and W. E. Dietrich, *in press*, A physically-based model for the topographic control on debris flow initiation, *Wafer. Resources Research*.

- Reid, L. M., and T. Dunne, Sediment production from forest road surfaces, *Wat. Resow. Res.*, 20, 1753-1761, 1984.
- Rice, R. M., Tilley, F. B., and Datzman, P. A., A watersheds response to logging and roads: South Fork of Caspar Creek, California, 1967-1976: U.S. Dept. of Agriculture, Forest Service, *Res. Pup. PSW-146*, 12p., 1979.
- Schaefer, M. G., *The Zero Order* Watershed, Unpublished Ph.D. dissertation, University of Missouri-Rolla, Rolla, Missouri, 69p., 1979.
- Schlichte, K., *Aerial photo interpretation of the failure history of the Huelsdonk Ridge/Hoh River area*, unpublished report, Washington State Department of Natural Resources, 17p., 1991.
- Schroeder, W. L., and G. W. Brown, Debris torrents, precipitation, and roads in two coastal Oregon watersheds, in *Proceedings of the Symposium on the Effects of Forest Land Use on Erosion and Slope Stability*, Honolulu, Hawaii, p. 117-122, 1984.
- Swanson, F. J., and Dyrness, C. T., Impact of **clear-cutting** and road construction on soil erosion by landslides in the western Cascade Range, Oregon: *Geology*, 3, 393-396, 1975
- Willgoose, G. R, Bras, R. L., and Rodriguez-Iturbe, I., A coupled channel network growth and **hillslope** evolution model: 1. Theory: *Wat. Resow. Res.*, 27, 1671-1684, 1991.

FIGURE CAPTIONS

- 1 Road-related landsliding in the central Washington Cascades.
- 2 Location map for the study areas.
- 3 Map of a portion of the Southern Sierra Nevada study site showing effect of road drainage diversions on the extent of the channel network; channels represented by black **lines**, colluvial deposits in topographic hollows by gray shading, and road drainage by arrows. Contour interval is in feet.
- 4 Plot of drainage area versus local slope for channeled (solid circles) and unchanneled locations (open circles) in the Southern Sierra Nevada study site. for A) natural drainage and B) road-related drainage diversions. C) Similar plot showing channeled data for natural (open triangles) and **road-related** drainage (solid triangles).
- 5 A) Landslide on the Olympic Peninsula, Washington, associated with drainage concentration along a **ridgetop** road. B) Schematic illustration of **ridgetop** road drainage concentration into topographic hollows. Landslides represented by gray shading; channels by black lines. Modified from a sketch by W. E. Dietrich.
- 6 Contributing road drainage area vs. slope at the discharge point for the **ridgetop** road system on Huelsdonk Ridge. Locations immediately downslope of the discharge point were either unchanneled (open circles), channeled (solid circles), or a debris-flow scar (triangles). Lines indicate fitted

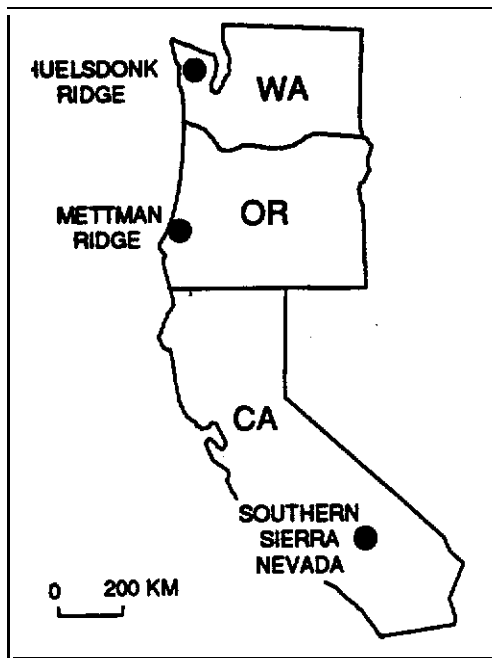
predictions of the models for turbulent overland flow (inclined line) and for landsliding (curve); dashed vertical line indicates lower limit to applicability of landslide model.

- 7 Map of a portion of the Mettman Ridge study area showing road drainage patterns, landsliding (black shading), channels (black lines), and colluvial deposits (gray shading). Contour interval is in feet.
- 8 Plot of contributing road drainage area versus local slope at discharge points for the Mettman Ridge study area for unchanneled locations (open circles), channels extending to the drainage outfall (solid circles), and landslides immediately downslope of the drainage outfall (triangles). Lines indicate fitted predictions of the models for turbulent overland flow (inclined line) and for landsliding (curve); dashed vertical line indicates lower limit to applicability of landslide model.
- 9 Plot of contributing area versus local slope for channeled **data** for natural channel heads (open triangles) and for both road drainage-related landslides (solid triangles) and channel extension (solid circles).
- 10 Plot of contributing road length vs. ground slope at the point of drainage concentration for **A)** Huelsdonk Ridge and **B)** Mettman Ridge. Solid lines represent equations (12) and (13); data are for unchanneled locations (open circles), channels extending to the drainage outfall (solid circles), and landslides immediately downslope of the drainage outfall (triangles).

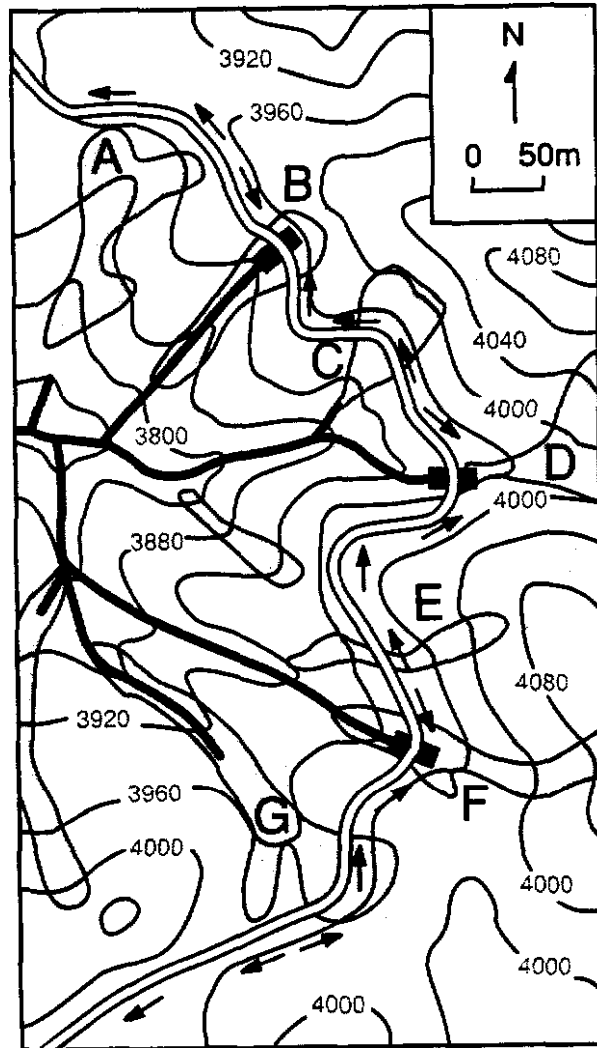


Montgomery

Figure 1

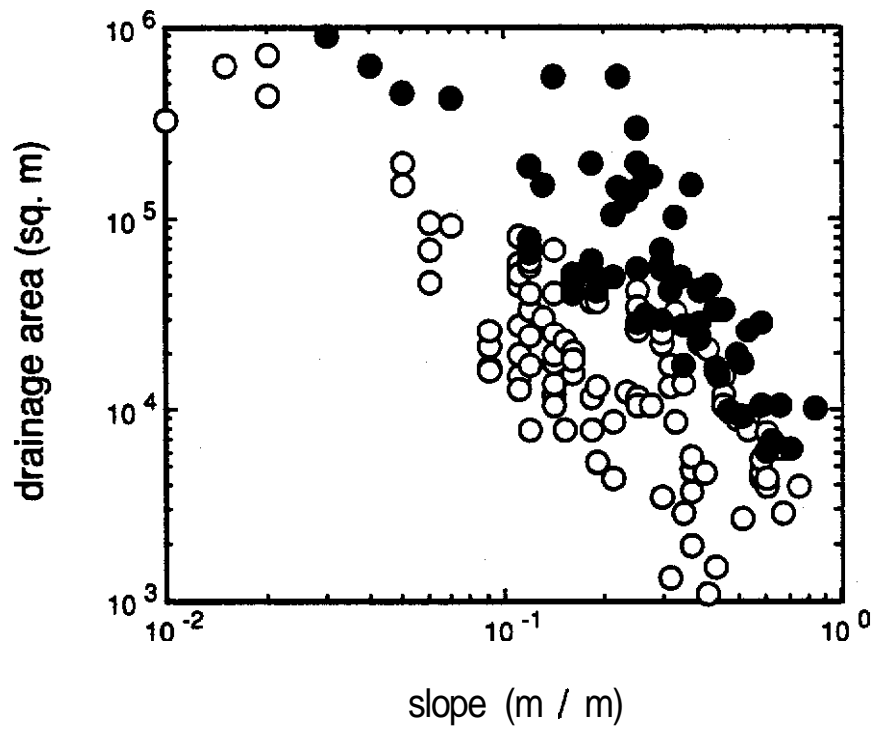


Montgomery Figure 2

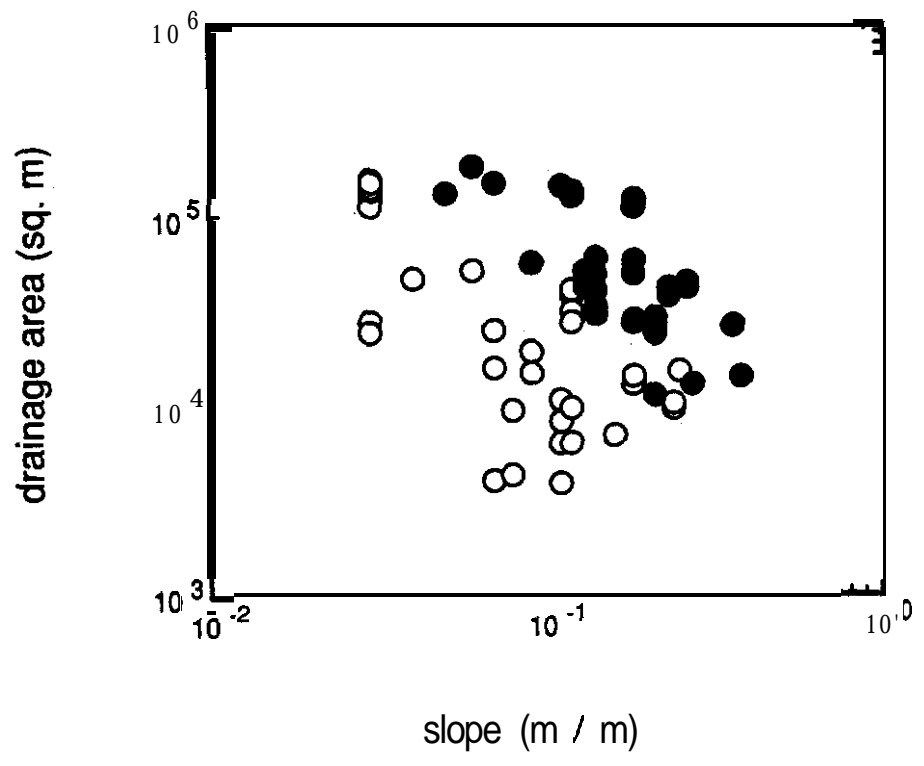


Montgomery Figure 3

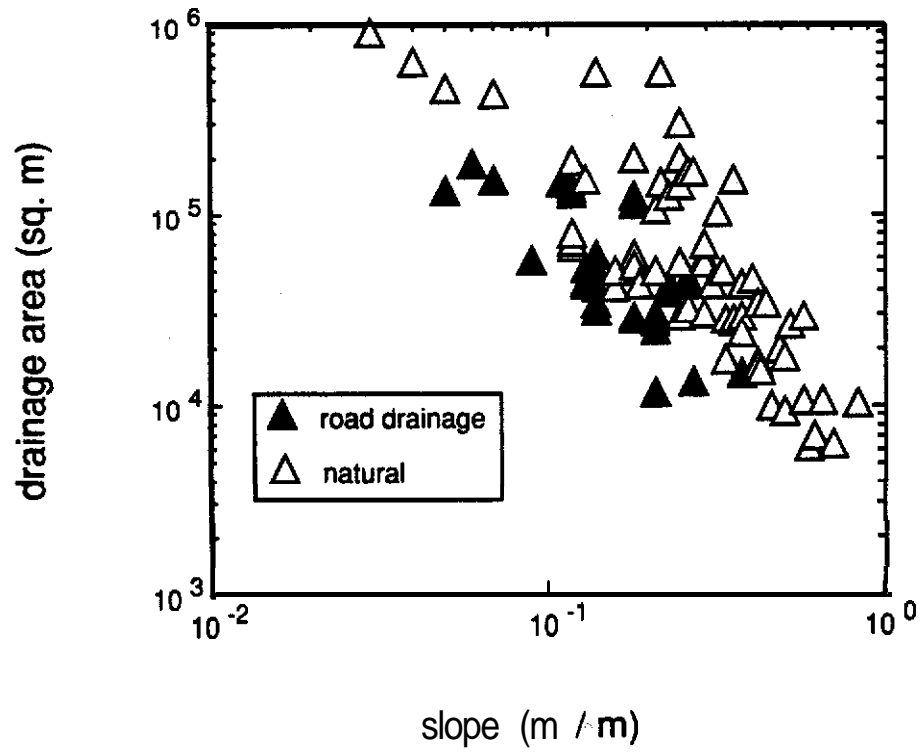
A



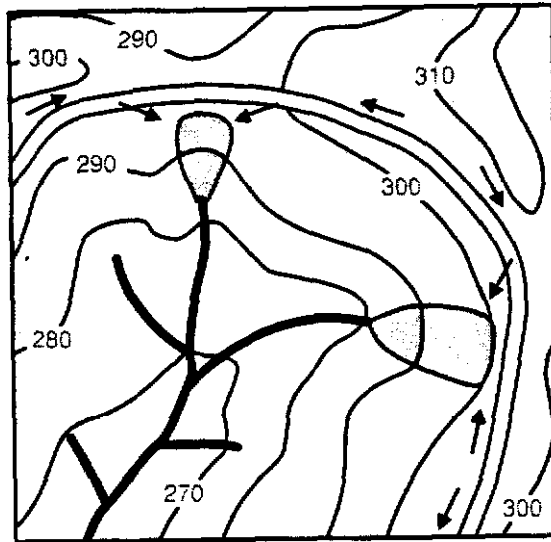
B



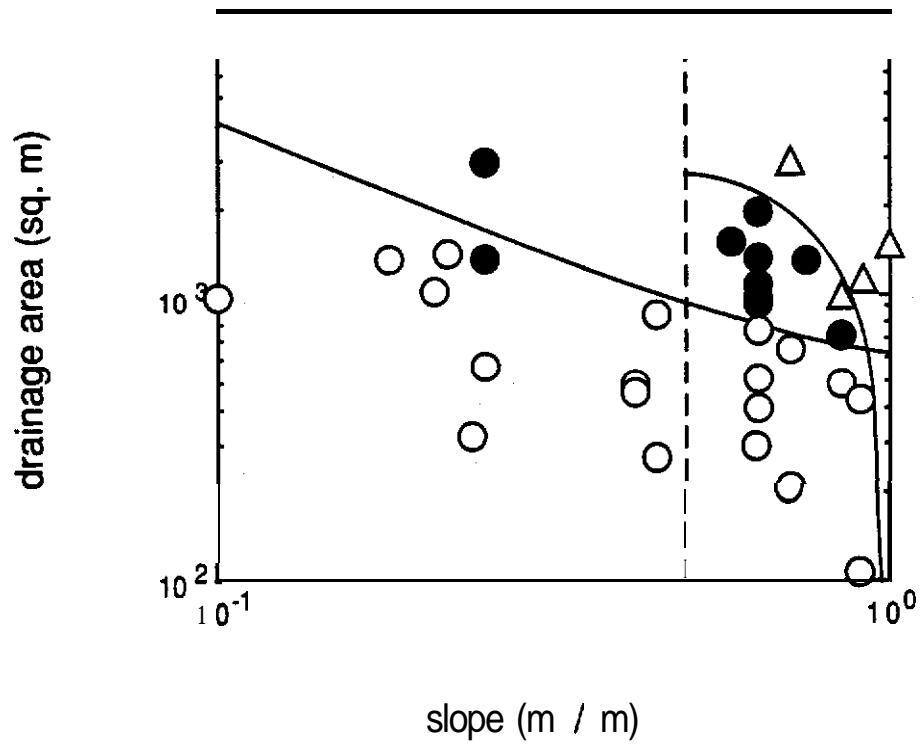
C

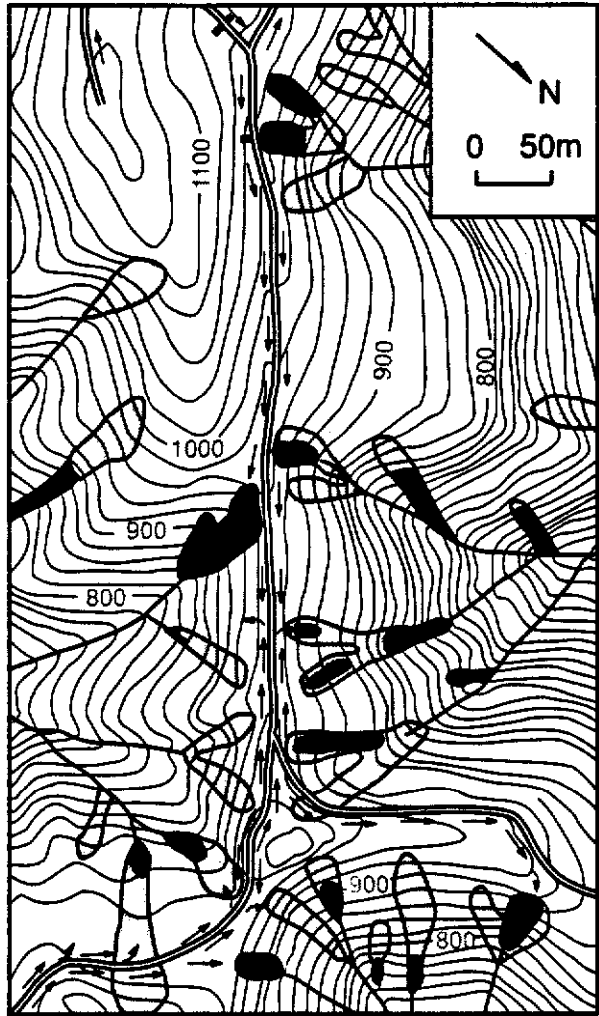






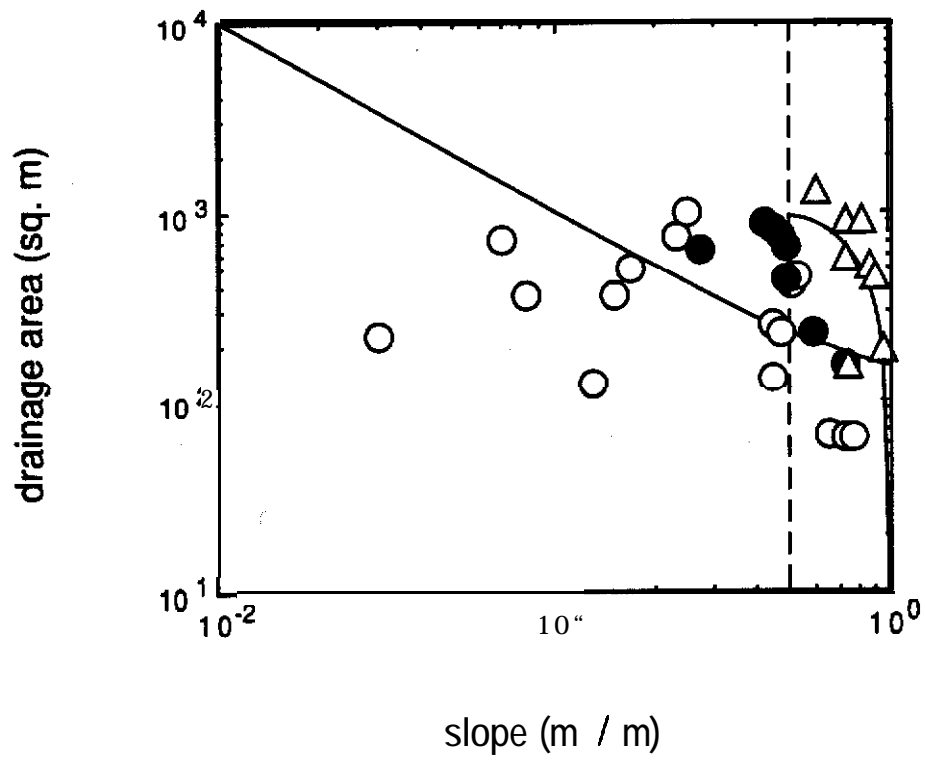
Montgomery Figure 5B

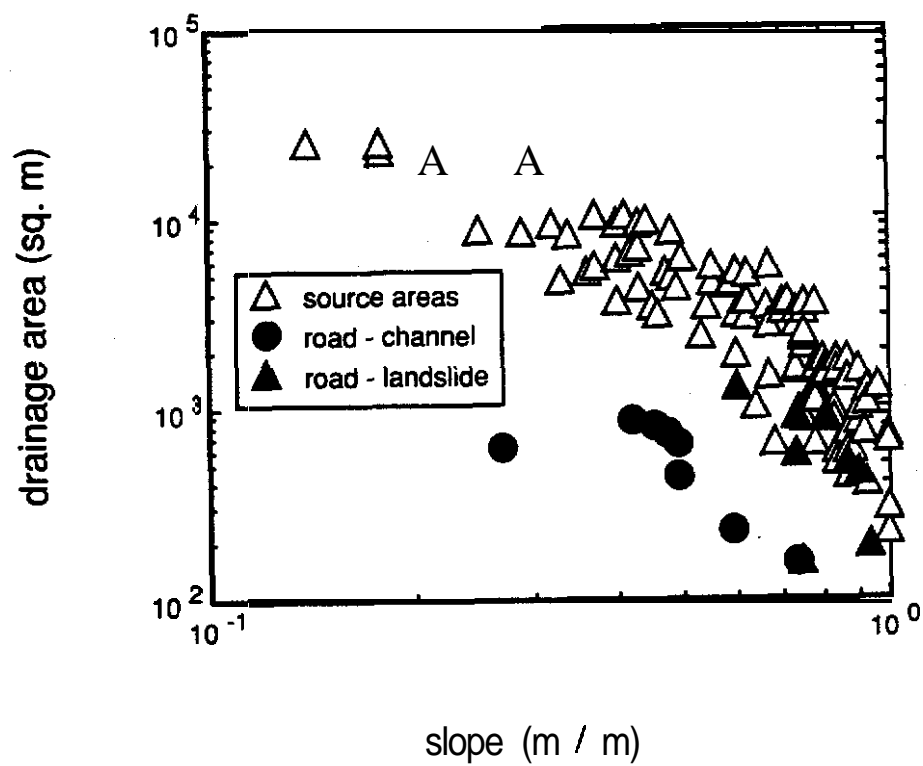


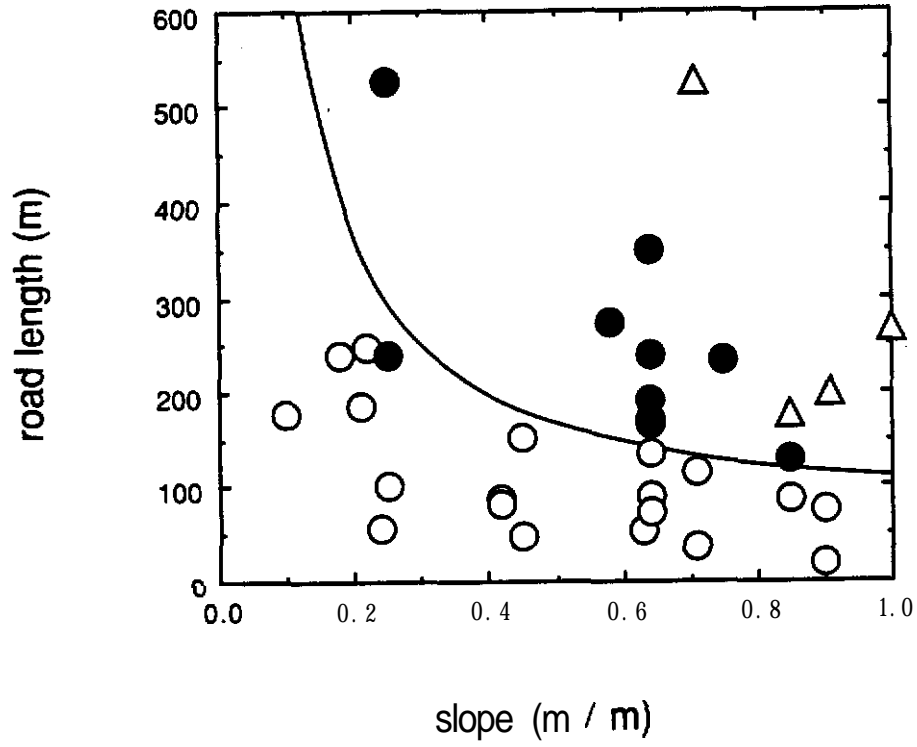


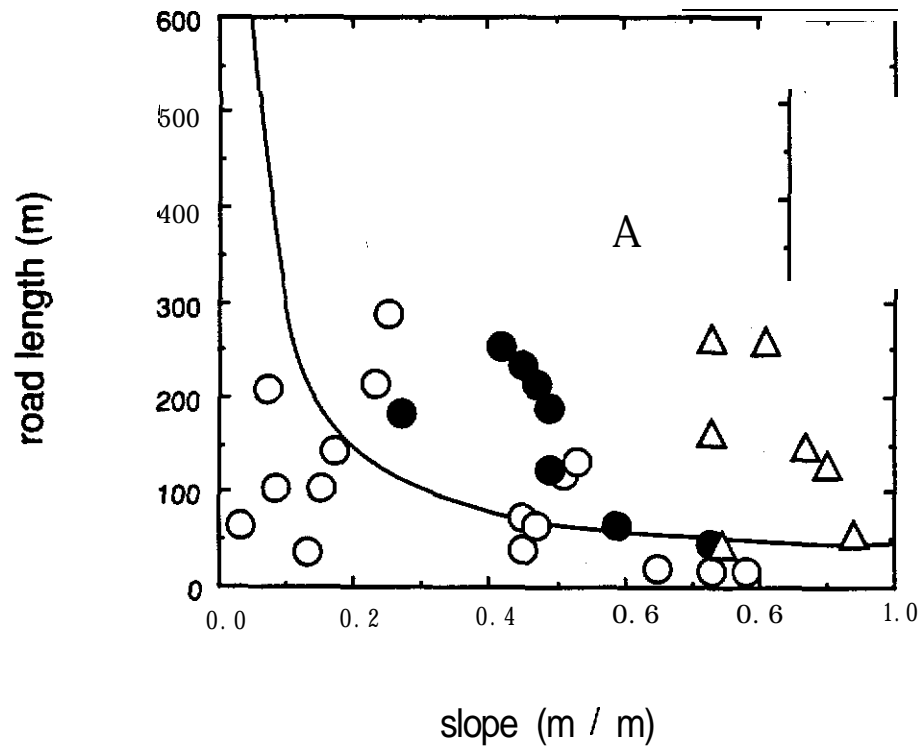
Montgomery

Figure









Appendix 5



Channel Bed Coarsening by **Salmonid** Spawning:
Feedback Mechanism for Population Stability

David R. Montgomery¹, N. Phil Peterson²,
John M. **Buffington**¹, David **Schuett-Hames**³, and Thomas P. **Quinn**²

1 Dept. of Geological Sciences and Quaternary Research Center, University of Washington, Seattle, WA 98195

2 School of Fisheries, University of Washington, Seattle, WA 98195

3 Northwest Indian Fisheries Commission, 6730 Martin Way E., Olympia, WA 98506

Rapidly declining salmon populations are forcing reexamination of fisheries and land management in the Pacific Northwest and are propelling proposals for widespread habitat restoration. We present evidence suggesting a feedback mechanism for population decline of mass-spawning species whereby reduced spawning activity decreases the shear stress necessary for bed mobilization, which, in turn, increases scour and decreases embryo survival. This feedback mechanism implies that it may become increasingly difficult to maintain or rehabilitate a declining population.

Dramatic **declines** of Pacific salmon (*Oncorhynchus* spp.) in the northwestern United States have led to the application of the Endangered Species Act to certain populations (1) and concern that many other populations are also in jeopardy or are already extinct (2). While these declines reflect the

combined influences of dam construction, overfishing, and habitat degradation, isolating these influences has proven extremely difficult, in part because it is difficult to link habitat change to population-level response (3). Recent proposals for extensive habitat restoration programs (4) assume that the availability of high-quality habitat is the factor limiting populations.

Although habitat degradation may lead to population decline in salmon and other organisms, the response to habitat restoration efforts is more complex. One complication is that animals may play an active role in the creation and maintenance of their own habitat. Beaver dams are probably the most widely recognized example of this phenomena (5), but burrowing activity (6) and grazing (7) provide additional examples. Although the sorting of stream gravels during spawning and the construction of gravel redds and egg pockets is well-known (8), neither fisheries biologists nor geomorphologists have explored how spawning activity changes channel processes (9). We present evidence of a feedback between digging behavior associated with salmon spawning and channel bed mobility. This feedback could make it increasingly difficult to reverse accelerating salmon population declines because decreased spawning activity makes the channel bed more susceptible to scour, in turn leading to higher embryo mortality.

Anadromous salmon are spawned in freshwater, migrate to sea after a variable period of freshwater residence, spend several years at sea, then return and spawn either in their natal or a nearby stream. Each female constructs a redd consisting of several egg pockets in the channel bed by turning on her side and rapidly undulating her tail and body. After eggs are released and fertilized, the **female** buries them while simultaneously excavating another egg pocket immediately upstream (10). This action coarsens the channel bed by sweeping the finer particles into the water column where they are transported

downstream. Females defend these nests from encroachment, but under high densities some may superimpose their nests on those of earlier spawners. Such superimposition is widely accepted as a major cause of **density-dependent mortality** (11) and fisheries managers generally attempt to prevent overly high densities of salmon from reaching spawning areas by manipulating fishing pressure. In the absence of superimposition, most embryo mortality is thought to occur from poor water circulation associated with fine sediment filling inter-gravel pore spaces (8) and scour **from** high flow events (12). Contrary to the assumption that high salmon densities are undesirable for the status of the population, observations collected during a two-year study indicate that **mass-spawning activity** alters channel morphology in ways that may reduce the probability of bed mobility and thus the vulnerability of the eggs to scour.

Kennedy Creek is a gravel-bed pool-riffle type channel (13) flowing into the south end of Puget Sound, Washington (Figure 1) that supports a run of chum salmon (*O. keta*). The stream reach discussed here has a **bankfull** width and depth of approximately 10.8 m and 0.42 m, respectively, and a **reach-average** slope of 0.0047. Observations during fall 1990 indicated that spawning occurred across the entire bed surface, coarsening the bed material, filling pools, and excavating bar margins. The following year, similar effects of spawning on channel morphology were documented through repeated surveying immediately prior to and after spawning and through pebble counts during spawning activity. Surveys were conducted using a digital theodolite and pebble counts were conducted using Wolman's standard methodology (14).

Pebble counts conducted during spawning activity documented the magnitude of **channel bed surface** coarsening. Measurements were collected at unspawned locations in the channel, and immediately downstream of egg

pockets in locations observed to be representative of the channel bed in general **after** mass spawning activity. Spawning activity increased the median grain size (d_{50}) of material on the channel bed from 22 mm to 30 mm (Figure 2). The coarse end of both the spawned and unspawned grain size distributions is similar; bed coarsening occurred by the selective removal of fine particles, producing better sorted gravels.

The critical boundary shear stress required to mobilize the surface grains of a gravel-bed channel (τ_{bc}) can be estimated from the bed surface d_{50} . This critical shear stress for general bed mobility (15) is given by

$$\tau_{bc} = \tau_{c50}^* (\rho_s - \rho_w) g d_{50} \quad (1)$$

(16), where τ_{c50}^* is the dimensionless critical shear stress for the median grain size, ρ_s and ρ_w are the densities of sediment and water, respectively, and g is gravitational acceleration. Expressing τ_{bc} in terms of the average depth-slope product

$$\tau_{bc} = \rho_w g D S \quad (2)$$

where D is the flow depth and S is the water surface slope, the critical depth of flow necessary to mobilize the bed can be calculated from (1) and (2). There is little consensus among investigators, however, regarding values of τ_{c50}^* for heterogeneous gravel beds (17).

The Shields shear stress (0.056) (16) provides a maximum estimate of τ_{c50}^* , but is likely to be an overestimate, as it characterizes homogeneous beds which have higher critical shear stress values due to greater friction angles (18). A second estimate of τ_{c50}^* (0.054) can be made from (1) and (2) by assuming

that in a self-formed channel the unspawned bed grain sizes are adjusted to **bankfull** conditions of depth (0.42 m) and slope (0.0047). However, this second τ^*_{c50} value is also likely to be an overestimate. In a forested channel the undisturbed bed grain sizes may reflect the additional influences of other roughness elements such as **bedforms** and large woody debris (19), which when included along with grain roughness in (1) effectively lower the above τ^*_{c50} estimate. Based on empirical data from similar channels in Western Washington (19) we estimate that τ^*_{c50} is 0.040 and that the other in-channel roughness elements have an “equivalent grain roughness” of 6 mm. This value of τ^*_{c50} and an “equivalent grain roughness” together with (1) and (2) predicts that the spawning-related increase in median grain size from 22 mm to 30 mm increased the critical flow depth for general bed mobilization from 100% (0.42 m) to 126% (0.53 m) of the **bankfull** flow depth (Figure 3). The duration of bed coarsening is uncertain and likely site specific, depending on the subsequent degree of fine particle distraintment and entrapment over the relatively rough spawned surfaces. Field observations at the study site suggest that the bed surface gradually fines during low-flow periods.

Spawning success is predicated on the depth of scour being less than the depth to which eggs are buried (20). Depth of scour in gravel-bed channels is related to the rate of **bedload** transport (21), which is in turn a function of both the peak flow depth and the duration of flow in excess of that required for bed mobility. Long-term records of discharge and scour depths are unavailable for Kennedy Creek, but the **bankfull** flow depth is generally considered to represent a condition of roughly annual to biennial bed mobilization in gravel-bed channels (22). Thus the increase in the critical flow depth indicates that spawning activity of salmon in Kennedy Creek should decrease the average

annual depth of scour, altering the channel in a way that increases the likelihood of their offspring surviving.

While we cannot yet rigorously assess the influence of this feedback mechanism on **salmonid** reproduction, additional data from Kennedy Creek suggest that it may be significant. Peak discharge in Kennedy Creek from November, 1991, to February, 1992, was approximately coincident with **bankfull** stage. Scour depths recorded by 104 scour chains ranged from 0 to 60 cm, with a mean of 13.4 cm. Forty egg-pockets measured during spawning activity ranged in depth from 9.8 to 48.9 cm, with a mean of 22.6 cm. While only a small proportion of the channel bed scoured to egg-pocket depths during this approximately **bankfull** event (Figure 4), the scour and egg pocket burial depth distributions indicate that even a minor increase in scour depths could have a major impact on the integrity of egg-pockets.

Our observations document that mass spawning increases channel bed stability through bed surface coarsening, which, in turn, may protect underlying egg pockets. Consequently, once a population declines, the bed may be more frequently scoured, decreasing the probability of embryo survival and leading to further population decline. Such a feedback **would** make it increasingly difficult to reverse a declining population trend, especially if the decline coincided with changes in land use that lead to more frequent or higher discharges or to bed surface fining (23). Based on these implications, we suggest that fishery managers prevent population decline before **critical** feedback levels are reached, and we recommend re-analysis of the conventional wisdom that compensatory biological processes will allow mass-spawning salmon populations to rebound from low levels. More fundamentally, these results illustrate the importance of feedback between physical processes and

biological activity in the maintenance of stream habitats and the **successful** proliferation of anadromous fishes.

REFERENCES AND NOTES

- 1 Federal Register, 56, 58619-58624 (1991); Federal Register, 57, 14653-14663 (1992).
- 2 W. Nehlsen, J. E. Williams, and J. A. Lichatowich, Fisheries (Bethesda), 16 (2), 4-21 (1991).
- 3 P. A. Bisson, T. P. Quinn, G. H. Reeves, and S. V. Gregory, in R. J. Naiman (editor), Watershed Management: Balancing Sustainability and Environmental Change, Springer-Verlag, New York, 189-232 (1992); L. B. Holtby and J. C. Scrivener, Canadian Special Publication of Fish- and Aquatic Sciences 10% 62-81 (1989).
- 4 F. H. Everest, J. R. Sedell, G. H. Reeves, and M. D. Bryant, American Fisheries Society Symposium 10, 68-77 (1991); N. B. Armantrout, American Fisheries Society Symposium 10, 136-149 (1991).
- 5 R. J. Naiman, J. M. Melillo, and J. E. Hobbie, Ecology, 67, 1254-1269 (1986); R. J. Naiman, C. A. Johnston, and J. C. Kelley, BioScience, 38, 753-763 (1988).
- 6 J. Grinnell, Journal of Mammology, 4, 137-149 (1923); G. W. Cox, Oecologie, 72, 207-210 (1987); T. A. Black and D. R. Montgomery, Earth Surface Processes and Landforms, 16, 163-172 (1991).
- 7 S. J. McNaughton, R. W. Ruess, and S. W. Seagle, BioScience, 38, 794-800 (1988).
- 8 D. W. Chapman, Transactions of the American Fisheries Society, 117, 1-21 (1988).

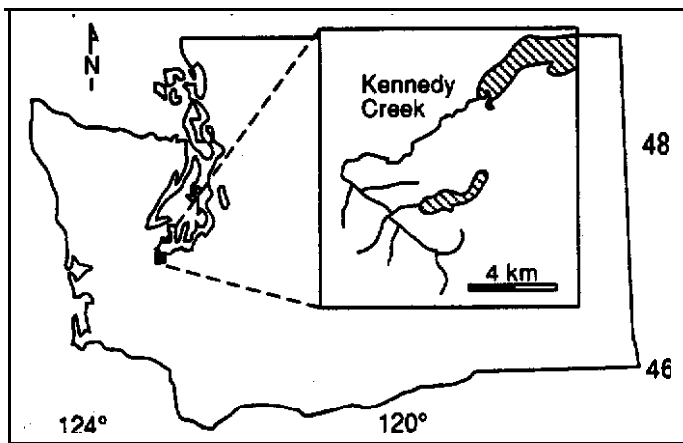
- 9 Floral influences on stream channels, on the other hand, are widely
 recognized. In particular, large woody debris strongly influences
 sediment storage and pool formation in channels in forested landscapes
 [B. H. Heede, Water Resources Bulletin, 8, 523-530 (1972); E. A. Keller
 and F. J. Swanson, Earth Surface Processes, 4, 361-380 (1979); M. P.
 Mosley, Earth Surface Processes and Landforms, 6, 571-579 (1981)].
- 10 C. Groot and L. Margolis, Pacific Univ. of British
 Columbia Press, Vancouver, B. C. (1991).
- 11 J. G. Hunter, Journal of the Fisheries Research Board of Canada, 16,
 835-886 (1959); W. J. McNeil, Journal of the Fisheries Research Board of
Canada, 21, 1385-1396 (1964).
- 12 T. E. Lisle, Water Resources Research, 25, 1303-1319 (1989).
- 13 D. R. Montgomery, J. M. Buffington, and T. Massong, EOS Transactions
of the American Geophysical Union, 73, 230-231 (1992).
- 14 M. G. Wolman, Transactions of the American Geophysical Union, 35,
 951-956 (1954).
- 15 Although some transport occurs at lower stages (W. L. Jackson and R. L.
 Beschta, Earth Surface Processes and Landforms, 7, 517-527 (1982)),
 general bed mobility typically occurs once the bed surface pavement is
 mobilized, exposing the underlying finer material that represents the
 composition of the channel bed load (G. Parker, P. C. Klingeman, and D.
 G. McLean, Journal of the Hydraulics Division, American Society of Civil
Engineers, 108, 544-571 (1982)).
- 16 A. Shields, Anwendung der Ähnlichkeitsmechanik und der
Turbulenzforschung auf die Geschiebebewegung, Translated by W. P.
 Ott and J. C. van Uchelen, California Institute of Technology, Pasadena,
 California (1936).

- 17 Shields (op. cit.) determined that for turbulent flow over homogeneous grains τ^*_c is a constant (0.056). Parker et al. (op. cit.) and others have demonstrated that for heterogeneous beds τ^*_c is a function of grain size relative to the median grain size of the sub-surface material, and that furthermore all grain sizes have essentially the same tb_c , rendering them “equally mobile”; nevertheless, for studies of initial motion of bed grains it seems more intuitively correct to define τ^*_c with respect to the surface material. In contrast to the “equal mobility” hypothesis, recent experiments corroborate traditional views of grain mobility by documenting size-selective grain entrainment (P.J. Ashworth and R.I. Ferguson, Water Resources Research, **25**, 627-634, 1969; P.R. Wilcock and B.W. McArdell, Water Resources Research, **29**, 1297-1312, 1993), but emphasize nevertheless approximate threshold conditions for general bed mobility and significant sediment transport (Ashworth and Ferguson, op. cit.).
- 18 Better sorting produces relatively rough beds with high inter-grain frictional resistance to mobility (J.M. Buffington, W.E. Dietrich, and J.W. Kirchner, Water Resources Research, **28**, 411-425, 1992).
- 19 J. M. Buffington (thesis in preparation):
- 20 T. E. Lisle and J. Lewis, Canadian Journal of Fisheries and Aquatic Science, **49**, 2337-2344 (1992).
- 21 W. W. Emmett and L. B. Leopold, Proceedings of the Federal Interagency Sedimentation Conference, U.S. Department of Agriculture Research Service Miscellaneous Publication 970, 399-409 (1963); L. B. Leopold, and W. W. Emmett, (1984); P. A. Carling (1987); M. A. Hassan, M. Church, and A. P. Schick, Water Resources Research, **27**, 503-511 (1991).

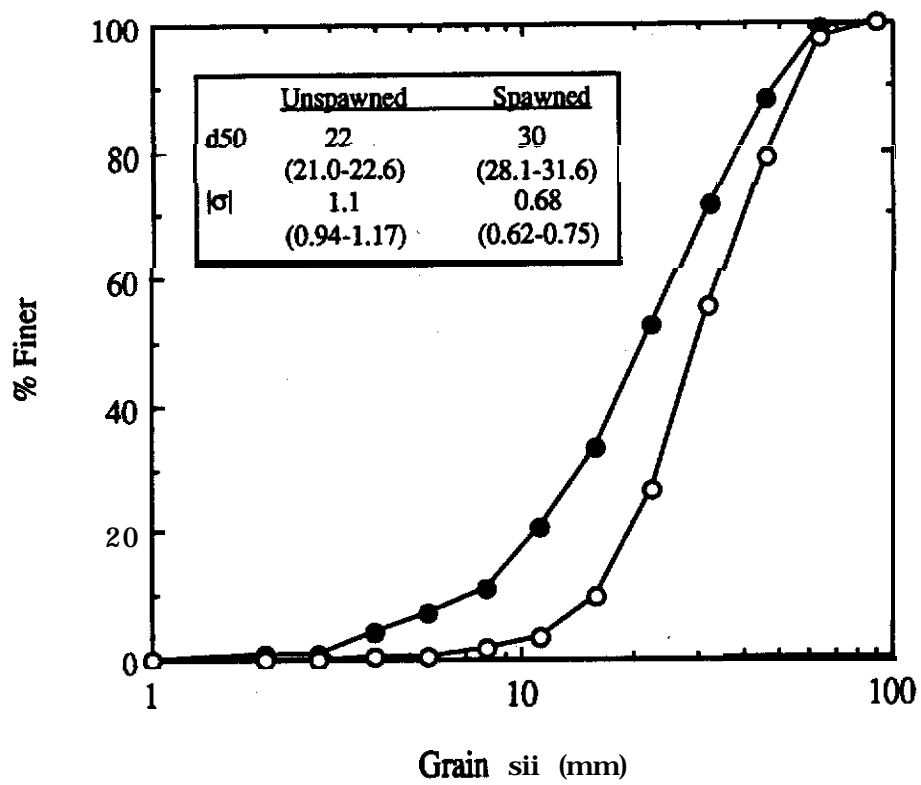
- 22 L. B. Leopold, M. G. **Wolman** and J. P. Miller, Fluvial Processes in Geomorphology, W. H. Freeman & Co., San Francisco, (1964); T. Dunne and L. B. Leopold, Water in Environmental Planning, W. H. Freeman & Co., New York, **818p.** (1978).
- 23 Many land management activities have the potential to alter the discharge regime or sediment supply of stream channels. Timber harvest may increase runoff during rain-on-snow events [R. D. Harr, Water Resources Research, 22, 1095-2000 (1986)]. Urbanization leads to increased peak discharges through faster runoff from an increase in impervious surfaces in a watershed [L. B. Leopold, U.S. Geological Survey Circular 554 (1968)]. Increased sediment supply may lead to bed surface fining [W. L. Jackson and R. L. Beschta, Water Resources Bulletin, 20, 527-533 (1984); W. E. Dietrich, J. W. Kirchner, H. Ikeda, and F. Iseya, Nature, 340, 215-217 (1989)], which would increase bed mobility through a decrease in the critical discharge.
- 24 After Blatt and others [H. G. Blatt, G. Middleton, & R. Murray, Origin of Sedimentary Rocks, Prentice-Hall, New Jersey, **782p.** (1980)].
- 25 This work was supported by grant **FY92-010** from the SHAMW and CMER committees of the Washington State Timber-Fish-Wildlife agreement. Anne **Biklé** helped with field work.

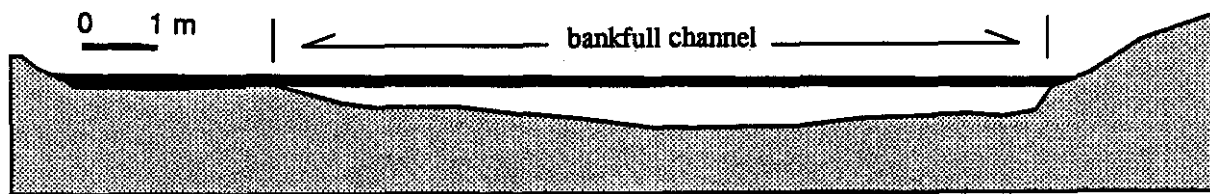
FIGURE CAPTIONS

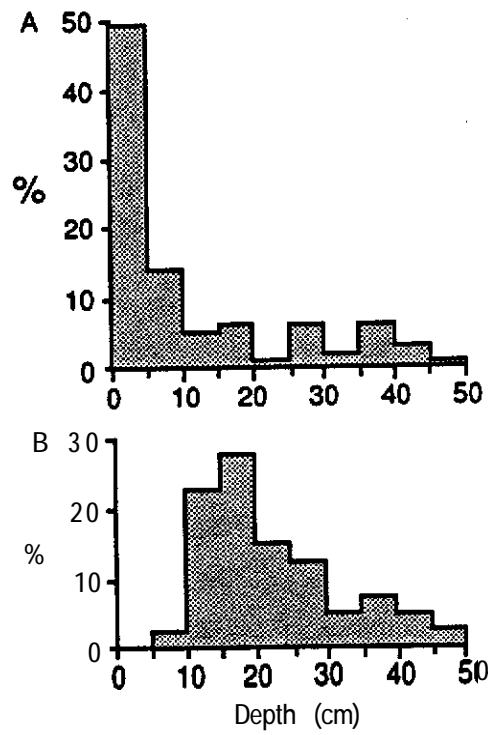
- 1 Map showing the location of Kennedy Creek in western Washington.
- 2 Cumulative size distributions of bed surface sediment for spawned (open circles) and unspawned (solid circles) locations sampled in Kennedy Creek on October 28, 1992. Distributions shown are composites of two pebble'counts of 100 grains each. Unpaired T-tests ($\alpha=.05$) 1) show that the means of the two unspawned samples are similar, 2) the means of the two spawned samples are similar and 3) the means of any combination of spawned and unspawned samples are significantly different. Simple averages and ranges are given for the median grain size (d_{50}) and the absolute value of the sorting parameter ($|\sigma|$) defined in terms of the phi grain size scale (24).
- 3 Cross-section of the study reach. Black area indicates the change in the calculated critical flow depth for bed mobility before and after spawning. No vertical exaggeration.
- 4 Normalized histograms of a) scour and b) egg burial depths for Kennedy Creek in 1991-92. Scour depths ($n = 104$) were determined from scour chains monitored through the winter season. Note that five percent of the scour chains recorded scour to greater than 50 cm depth. Egg burial depths ($n = 40$) were measured during spawning activity.



Montgomery et al. Figure 1







Appendix 6

Mountain-Scale Strength Properties, Deep-Seated Landsliding, and Limits to Local Relief

Kevin M. Schmidt and David R. Montgomery
Department of Geological Sciences, AJ-20
University of Washington
Seattle, WA. 98195

ABSTRACT

Controls on the size of mountains and the stability of bedrock slopes are only poorly constrained, but provide potentially important limits to the development of local relief. Large-scale mass wasting provides the most obvious limit to relief development. Simple models of slope stability indicate that susceptibility to mass wasting is a function of local relief, slope gradient, degree of saturation, and the strength of the material. Natural slopes, however, rarely attain heights close to the theoretical maximum predicted by intact rock strengths because of pervasive discontinuities such as faults, joints, and bedding planes. Thus, determining representative strength properties of a mountain or hillslope is difficult because such properties integrate both **material and structural discontinuities**, and may also be time dependent. While laboratory-derived strength properties may be applied on a site specific basis, alternative methods are necessary to describe representative geotechnical parameters over large spatial scales. We hypothesize that such integrated rock strength properties limit local relief development **and** effectively bound the site of stable hillslopes for mountain drainage basins in a given lithologic, climatic, and tectonic regime. Here we investigate this assumption using theory and field work for a study area in the northern Cascades.

STABILITY ANALYSIS

Simple force balances **in** a two-dimensional, limit equilibrium slope stability model can be applied to back-calculate the geotechnical properties implied by observed topographic relief. The sliding-wedge method of slope stability analysis (Culmann, 1866) predicts a limiting relation between hillslope gradient and ridge height by approximating a failure block as a wedge with a planar failure surface. The maximum stressed surface is then a plane passing through the toe of the slope (Spangler, 1960).

The force balance of shear stress and shear resistance for this geometric configuration leads to an equation for maximum slope height:

$$H = \frac{4c}{\gamma} \left\{ \frac{\sin \beta \cos \phi}{[1 - \cos(\beta - \phi)]} \right\} \quad (1)$$

where,

c = cohesive shear strength of rock

γ = unit weight of rock

β = hillslope angle measured with respect to horizontal

ϕ = internal friction angle

This technique has **been** applied to friable **loess** deposits in Iowa by **Lohnes and Handy (1968)**, to loess-derived alluvium in Tennessee **by Simon (1989)**, and to coastal bluffs composed of glacial deposits by **McGreal (1979)** but not in larger-scale bedrock landscapes. Other studies recognizing a slope/height limit to stable slopes include that of **Skempton (1953)** for clay strata in England and the work of **Grant-Taylor (1964)** on weathered **greywacke** in New Zealand.

Expanding on the simple relationship of the Culmann method, a more rigorous approach including the effects of ground water conditions, cleft and uplift pressures, is presented here in Figure 1 after **Hoek and Bray (1977)**. The analyses discussed here utilize this more detailed approach to back-calculate cohesion **and** friction angle **values** from observed topographic development. Development of topographic relief is a complex process controlled by erosional processes and the strength of material over long time scales. Thus, it is thought that the back-calculated strength parameters characterize in-situ strength properties representative of geologic formations over large spatial and temporal scales.

STUDY AREA

We measured the horizontal length and vertical height of slopes underlain by the strongly-bedded Eocene Chuckanut Formation, the Quaternary **glacio-fluvial** deposits forming channel banks in river valleys in northwestern Washington state, and the Darrington Phyllite. This area in the north Cascades was chosen **because** of numerous recognized bedrock landslides up to 1000 m in height as well as pronounced mass wasting along incised channel banks. Widespread landsliding argues for the

mobilization of peak strength values and thus the maximum relief development attributable to a unit. Landscapes with numerous large-scale landslides have developed their maximum strength, and thus back-calculated strength parameters are considered to reflect minimum values.

The Chuckanut Formation, a 6000 m thick package of subaerially-deposited sediments, is well suited for this study because of its wide extent as well as its propensity towards large-scale landsliding. Classified as one of the thickest fluvial sequences in North America (Johnson, 1982), this interbedded, well-cemented sandstone, shale and conglomerate extends from the low-relief topography around Bellingham, Washington east to the high-relief mountains just west of Mt. Baker in the Cascade Range (Figure 2). These Eocene rocks have been deformed into broad, northwest-plunging folds often truncated by local faults. Previous landslide identification by Fiksdal and Brunengo (1981) was supplemented with stereoscopic mapping of deep-seated landslides from color infrared aerial photographs onto 1:24,000 scale topographic maps.

Deeply-incised glacial deposits up to 150 m in thickness are ubiquitous along the mountain fronts in the northern Cascades. They locally form wide benches in the river valleys that are usually flat-topped. As with the Chuckanut Formation, we consider the sediments of the glacial benches as a homogeneous unit, even though it is composed of a varied sequence including stiff, laminated lacustrine clay, silt/sand outwash, and boulder till. Although slope failures in the glacial sediments are much smaller than those in the Chuckanut Formation, they represent a large source of sediment entering the adjacent channels (Kelsey, 1988). These slopes were field surveyed in the drainage basins of the Middle Fork of the Nooksack River, Clearwater Creek, Rocky Creek, and Boulder River.

RESULTS

CHUCKANUT FORMATION

Of the 204 measurements extending from ridge top to valley bottom in areas underlain by the Chuckanut Formation, 40 represent large-scale landslides. A plot of slope vs. height for these transects, including all deep-seated, bedrock landslide sites identified from aerial photograph analysis, suggests an arcuate upper bound (Figure 3). This limit to the local relief, assumed to be the maximum attainable based on the

widespread instability of the area, constrains back-calculated strength parameters. The geotechnical properties implied by fitting a threshold curve ($\phi=21^\circ$, $c=150$ kPa with $\gamma=25$ kN/m³) to the upper limit of the **observed data** are interpreted to approximate long-term effective values for the Chuckanut Formation as a whole.

Even under the **extreme assumption** of fully saturated conditions, many of the landslide sites lie below the predicted threshold of instability (Figure 3). This variance does not result solely from the decrease in slope gradient due to downslope movement of a landslide toe. Rather it reflects the treatment of the entire formation as one entity without **considering** the destabilizing effects of the geologic structure. A separation of the transects into the three structural categories of anti-dip slopes, dip slopes, and slopes trending parallel to fold axes results in a segregation of the data. Figure 4 reveals that the anti-dip **slopes** control the maximum relief development attained by the formation with threshold strength values of $\phi=21^\circ$, $c=165$ kPa. In contrast, the dip slopes define lower threshold strength values of $\phi=17^\circ$, $c=120$ kPa (Figure 5). The remaining sites, representing the specific condition of slopes trending **parallel to** fold axes, are even farther removed from the dip slope relief limit.

The present stability of some hillslopes above 750 m in height is partially explained by the buttressing of the lower slope profile with **glacio-fluvial** deposits. In these high-relief areas, much of the valley floor and lower portions of the adjacent hillslopes are covered with **up to** 150 m of glacial deposits. This added mass decreases the overall hillslope gradient and provides a downward force on the lower portion of the hillslope, thus increasing the relative stability of the underlying rock. While only 37% of the recognized landslide sites above 750 m are buttressed with glacial sediments, 80% of the currently stable sites have thick benches of glacial sediments buttressing their lower slopes. In addition, modeling carried **out** with the method-of-slices computer program "XSTABL" **suggests** that the presence of the glacial valley fills increase the relative factor of safety by about 30%. Therefore, these buttresses may allow higher ridges to be stable than would otherwise **be** possible.

GLACIAL DEPOSITS

A total of 178 transects were surveyed along four channels incised into **glacio-fluvial** deposits. **Stable** sites were defined **by** the presence of mature vegetation, *i.e.* moss, ferns, and conifers. Landslides were classified as slump failures only if the

landslide block, often with back-rotated trees, was still recognizable. The present, **post**-failure topographic profiles of slumps were measured. When possible, estimation of the pre-failure profiles also was obtained. On Figure 6. pre- and post-failure conditions are linked by tie-lines for those profiles where such reconstruction was possible. Exposed cliffs, lacking soil development, **vegetation**, an arcuate headscarp, and a defined failure block, were classified as inferred topple failures. The back-calculated threshold envelope yields strength values of $\phi=29^\circ$ and $c=20 \text{ kPa}$ with $\gamma=20 \text{ kN/m}^3$ for the stratigraphic package treated as a single unit. Because the model assumes hydrostatic conditions at saturation, the remaining failure sites positioned below the threshold for saturated conditions may be the result of excess pore pressures or seepage forces. Figure 7 shows a schematic representation of the effects of these forces and relative decrease in stability.

From field observations it appears as if shallow, **topple** failures **become** critical earlier in the downcutting phase followed later by an activation of slump failures. For example, only those reaches that have been over-steepened in meander bends produce well-developed slumps. Topple failures are commonly located at the beginning and end of meander bends while slumps are found at the apex of the bend, the location of maximum present undercutting and removal of failed material. It is inferred then that in high sinuosity reaches the full strength of the material composing the banks and locally the valley walls is mobilized.

The large number of failures with near-vertical slip surfaces can be explained by the state of equilibrium in an active Rankine state and the Navier-Coulomb criterion (Terzaghi, 1943). The state of tension adjacent to a free face such as a channel bank extends down to a critical depth depending on the cohesion, friction angle, and unit weight of the material. The maximum depth of tension is predicted by the relation: $\frac{2c}{\gamma} \tan\left(45 + \frac{\phi}{2}\right)$ Using the strength parameters back-calculated from the threshold curves, the predicted maximum depth of tension is 3.4 m. The observed maximum height of a vertical channel bank classified **as a topple** failure is 3.5 m.

Unstable, **deeply** incised reaches have high potential for impacting channels through rapid introduction of large volumes of sediment from bank failure (Kelsey, 1988). Recent work related to rain-on-snow events (Megahan, 1983; Harr, 1986; Berris and Harr, 1987) suggest that removal of timber in the transient snow zone can

significantly alter the hydrologic response of a basin. We caution that sites situated above the saturated threshold in Figure 6 may be considered potentially sensitive to changes in the hydrologic regime.

DARRINGTON PHYLLITE

The Darrington Phyllite, a relatively weak pre-Tertiary metamorphic rock, exhibits varying degrees of strength depending on its extent of weathering. Analysis of the strongly-bedded Chuckanut Formation revealed that stability is highly dependent on the underlying geologic structure. Similarly, examination of slopes underlain by Darrington Phyllite suggests that maturity of weathering, most developed in the inner gorges, dramatically alters material strength. Figure 8 depicts the relief development of weathered phyllite in the inner gorge of the Middle Fork of the Nooksack River downstream of the diversion dam and relatively unweathered rock above the inner gorge. The rock in the inner gorge is subjected to enhanced fracture intensity through mechanical weathering induced by the local topographic stress field (Miller, 1992). An increase in fracture density allows for increased hydraulic permeability and thus intensified chemical weathering. Consequently, rock comprising the inner gorge fails at much lower heights, for a given hillslope gradient, than the same unweathered rock (Figure 8) above the ground water flow field. Thus, rock strength will predictably differ through the landscape with the inner gorges identified as sites possessing weathered, weak rock.

COMPARISON OF BACK-CALCULATED AND LABORATORY-DERIVED PARAMETERS

Material properties obtained through analysis of bedrock slopes are lower than values typically derived from laboratory measurements on similar materials (Table 1). This discrepancy is rooted in problems of scale and the fact that rock masses are **discontinua**. Bieniawski and Van Heerden (1975) have shown that the strength of iron ore, diorite, and coal decrease considerably with increasing specimen size. A laboratory sample shears over a failure plane that is many orders-of-magnitude smaller in surface area than a natural **hillslope**. Smaller **samples** contain fewer discontinuities, and hence are stronger. Where few discontinuities are present, failure is forced to involve new crack growth. Therefore, small samples tested in the laboratory do not yield strength parameters directly applicable to the rock mass from

which the samples were taken. While back-calculated friction angle values are only slightly lower than those from laboratory tests, the cohesion values are substantially diminished. This relation is **supported** by the results of Cripps and Taylor (1981) which reports that the weathering of **mudrocks** is characterized by a several order-of-magnitude reduction of cohesion with a lesser reduction in friction angle. Cohesion decreases dramatically as the structural integrity of a rock is destroyed through weathering and fracturing into smaller pieces (Menci, 1965). Therefore, high cohesion values are to be expected in intact rock samples, whereas in heterogeneous materials the aggregate properties may be expected to reflect those of the weakest link in the mass. Also, the strain rate is many orders of magnitude less in a laboratory experiment. Taylor (1948) and Terzaghi (1955) have shown that the shear strength of clays decreases with increasing time of applied shear. Furthermore, back-calculated properties differ from laboratory-derived values in that they **reflect** all the destabilizing influences experienced by the slope, such as large magnitude earthquakes.

Back-calculated glacial deposit strength parameters are closer to those reported from laboratory experiments. This may reflect the hypothesized time-dependence of strength properties. The cohesion of these glacial deposits prior to weathering is low because they are nonlithified. Thus, the decrease in cohesion upon weathering will be minor relative to bedrock slopes.

WORK IN PROGRESS

Ongoing work includes incorporation of seismic accelerations into the wedge failure model. Paleo-seismic evidence and strong motion modeling (Heaton and Hartzell, 1989) indicate that the Puget Sound and Western Washington experience large magnitude earthquakes. Horizontal accelerations greater than **0.3g** on rock for a return interval of about 2,500 years 'are estimated' in the region of the study area (Perkins et al., 1980). Therefore, the hillslopes in the area studied have recorded several such events since the retreat of the continental ice sheet. Efforts to date some of the large-scale failures in the Chuckanut Formation may help to determine their triggering mechanism. For example, if dates of the sites studied match with previously recognized years of large magnitude earthquakes for the Puget Sound, a strong motion causal mechanism may be invoked.

A regional application of the limit-equilibrium stability model described here may be used to recognize and predict the locations of landslides over large spatial scales. The interpretation of a **landscape** with respect to the properties of topographic relief development and geologic structure lends itself **well** to a geographic information system (**GIS**) analysis. The next section, written by Dan Miller, describes the application of this approach in a **GIS** format.

SUMMARY

- The large-scale strength properties of bedrock slopes provide a limit to relief development that links the maximum stable height of mountains, deep-seated landsliding, and incision of the intervening valleys.
- Back-calculated strength **parameters** in areas where field observations indicate mobilization of the full strength of the material provide estimates of in-situ strength properties that incorporate the effects of material discontinuities and transient forces (e.g. seepage forces and seismic accelerations).
- The geomorphic problem of defining limits to local relief development and traditional engineering methods of determining material strength parameters operate at drastically different spatial and temporal scales,

CHUCKANUTFORMATION

- Structural control greatly influences local relief and the degree of instability. Dip slopes **and** slopes trending parallel to the trend of fold axes lie significantly below the threshold of maximum relief development indicated by anti-dip slopes.
- Buttressing of the lower slopes of mountain fronts by glacial benches may allow higher ridges above 750 m in relief to be stable than might otherwise be possible.

GLACIAL DEPOSITS

- The highest degree of instability is found in the apex of meander bends where the banks are over-steepened and failed material is actively removed.
- The predicted depth of tension in a vertical bank. 3.4 **m**, is in excellent agreement with the value of 3.5 m observed in the field.

. Those sites situated above the saturated threshold are most susceptible to changes in hydrologic response resulting from land management.

DARRINGTON PHYLLITE

- The extent of weathering greatly influences local relief and the degree of instability. Our observations suggest that certain predictable locations of the landscape, such as inner gorges, experience heightened strength degradation due to a high degree of chemical weathering, ground water focusing, and mechanical weathering arising from topographic stresses.

REFERENCES

Berris, S.N. and **Harr**, R.D. 1987. Comparative snow accumulation and melt during rainfall in forested and clear-cut plots in the western Cascades of Oregon: *Water Resources Research*, vol. 23. p. 135-142.

Bieniawski, Z.T. and **Van Heerden**, W.L., 1975. The significance of *in situ* tests on large rock specimens: *International Journal of Rock Mechanics and Mineral Science*, vol. 12, p. 101-113.

Cripps, J.C. and Taylor, R.K.. 1981. The engineering properties of mudrocks: *Quarterly Journal of Engineering Geology*, London, vol. 14, p. 325-346.

Culmann, C., 1866. *Graphische Statik*: Zurich.

Fiksdal, A.J. and Brunengo, M.J., 1981. Forest slope stability project phase II: Washington State Department of Ecology, **WDOE 8 I - 14, 62 p.**

Grant-Taylor, T.L., 1964. Stable angles in Wellington **greywacke**: *New Zealand Engineering*, vol. 19. p. 129-130.

Harr, R.D., 1986, Effects of clearcutting on rain-on-snow runoff in western Oregon: a **new** look at old studies: *Water Resources Research*, vol. 22, p. 1095-1100.

- Heaton, T.H. and Hartzell, S.H.**, 1989. Estimation of strong **ground** motions from hypothetical earthquakes on the Cascadia subduction zone. Pacific Northwest: Pure and Applied Geophysics, vol. 129, p. 13 **1-20** 1.
- Hoek. E. and Bray, J.W.. 1977, **Rock Slope** Engineering (2nd **ed**): Institute of Mining and Metallurgy, London.
- Johnson, **S.Y.**, 1982. Stratigraphy. sedimentology, and tectonic setting of the Eocene **Chuckanut** Formation. northwest Washington: Ph.D. dissertation, Department of Geological Sciences, University of Washington, Seattle Wa.
- Kelsey, H.M.**. 1988, Formation of inner gorges: Catena, v. 15, p. **433-458**
- Lohnes, R.A. and Handy. R.L., 1968, **Slope** angles in friable loess: The Journal of Geology. vol. 76, p. 247-258.
- McGreal, W.S.**. 1979, Factors promoting coastal slope instability in **southeast** County Down, N. Ireland: Zeitschrift fur Geomorphologie, vol. 23, p. **76-90**.
- Megahan. **W.F.**, 1983, Hydrologic effects of clearcutting and wildfire on steep granitic slopes in Idaho: Water Resources Research, vol. 19. **#3**, p. 81 1-8 19.
- Menci, V.**, 1965. Proportions of cohesion and of internal friction in the strength of rocks: Norwegian Geotechnical Institute Publication **#6** I. p. 17-19.
- Miller, D. J., 1992, **Cause** or consequence? The role of topographic form in the development of bedrock fractures: EOS. Transactions, American Geophysical Union, vol. 73. no. 43. p. **2** 12.
- Perkins, D.M.. **Thenhaus, P.C.**, Hanson, **S.L.**, Ziony, J.I., and S.T. **Algermissen**, 1980, Probabilistic estimates of maximum seismic horizontal ground motion on rock in the Pacific Northwest and the adjacent outer continental shelf: U.S. Geological Survey Open File Report 80-47 1.

Simon, A., 1989. Shear-strength determination and stream-bank instability in loess-derived alluvium, West Tennessee, USA, In: De Mulder and Hageman (eds) Applied Quaternary Research, Balkema. Rotterdam, p. 129- 146.

Skempton. A.W.. 1953. Soil mechanics in relation to geology: **Proceedings** of Yorkshire Geological Society, vol. 29. p.33-62.

Spangler, M.G.. 1960, Soil engineering (2nd ed): International Textbook Co.. New York, 483 p.

Taylor, **D.W.**, 1948. Fundamentals of Soil Mechanics: John Wiley and Sons, Inc., New York, 700 p.

Terzaghi. K., 1943. Theoretical Soil Mechanics: John Wiley and Sons, Inc., New York, 510 P

Terzaghi. **K.**, 1955. Influence of geological factors on the engineering properties of sediments, In: Economic Geology, Fiftieth Anniversary Volume 1905-1955, p. 557-618.

FIGURE CAPTIONS

Figure 1. Graphical representation and input parameters of plane failure stability model adapted from Hoek and Bray (1977). Because the geometry and thus the weight of the potential failure block is dependent on the position of the vertical tension crack, two versions are presented. Case **A**) with the headscarp in the upper slope surface is characteristic of failures in glacial material while case **B**) with the headscarp in the slope face is characteristic of bedrock failures in the Chuckanut Formation.

Figure 2. Index map showing location of Chuckanut Formation and surrounding pre-Tertiary rock. including the **Darrington Phyllite**, after Johnson (1982). The upper half of the figure is a schematic geologic map of the rectangular shaded area in the lower portion. B is Bellingham. G is Glacier. S is Seattle, and Vi is Victoria.

Figure 3. All site transects (**204** total) for the Chuckanut Formation plotted with respect to local topographic relief; 'height (**m**) vs. **hillslope** gradient (degrees).

Thresholds for both dry and completely saturated conditions are shown. Values reported to the right of threshold refer to friction angle in degrees and cohesion in **kPa**, i.e. (ϕ in degrees, c in **kPa**).

Figure 4. Anti-dip slope transects for the Chuckanut Formation plotted with respect to local topographic relief; height (**m**) vs. hillslope gradient (degrees). Values reported to the right of threshold refer to friction angle, $\phi = 21^\circ$ and cohesion, $C = 150$ **kPa**.

Figure 5. Dip slope transects for the Chuckanut Formation plotted with respect to local topographic relief; height (**m**) vs. hillslope gradient (degrees). Values reported to the right of threshold refer to friction angle, $\phi = 17^\circ$ and cohesion, $c = 120$ **kPa**.

Figure 6. Transects for glacial deposits surveyed with hand level, stadia rod, and tape plotted with respect to local topographic relief; height (**m**) vs. hillslope gradient (degrees). Values reported to the right of threshold refer to friction angle, $\phi = 29^\circ$ and cohesion, $c = 20$ **kPa**.

Figure 7. Schematic of figure 6 showing the spatial distribution of hillslope processes in context of topographic relief development. Sites located above the saturated threshold defined by the limit of topographic development may be highly susceptible to hydrologic changes within the watershed.

Figure 8. Transects for the Darrington Phyllite depicting both weathered and unweathered rock. The weathered phyllite in the inner gorge of the Middlefork of the Nooksack River is unstable at relatively low relief. Dashed line, at 180 **m**, represents maximum relief attained by weathered phyllite.

Table 1

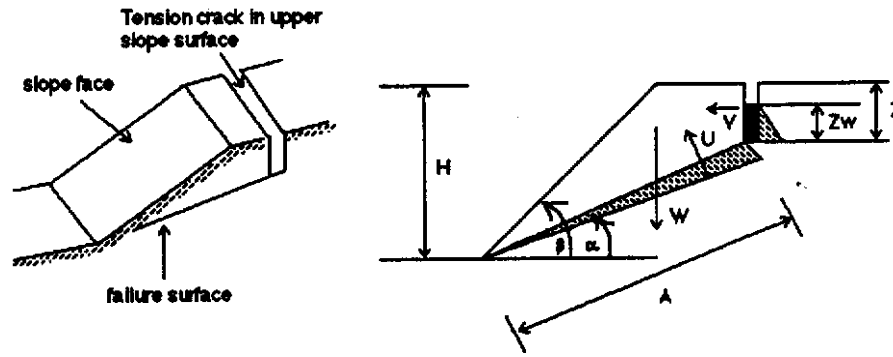
Comparison of Laboratory and Back-Calculated Strength Parameters

<u>Material</u>	<u>Friction Angle, ϕ (degrees)</u>	<u>Cohesion, C (kPa)</u>	<u>Source</u>
Hard sedimentary rock, ie. sandstone	35 • 45	10,000 • 30,000	Values Derived From Laboratory Experiments (from Hoek and Bray, 1977)
Soft sedimentary rock, ie. shale or coal	25 • 35	1,000 • 20,000'	
Stiff glacial clay	30 • 32	70 • 150	
Soft, slightly organic clay	22 -27	20 • 50	
Dense sand uniform size	32 • 40	0	

Chuckanut Formation Anti-dip slope	21	150	Values Derived From Empirical Relations (this study)
Chuckanut Formation Dip slope	1 7	120	
Glacial Sediments	29	20	

Plane Failure Model

Headscarp in Upper Slope Surface



Factor of safety, F , is the ratio given by the total force resisting sliding to the total force tending to induce sliding

$$F = \frac{cA + (W \cos \alpha - U - V \sin \alpha) \tan \phi}{W \sin \alpha + V \cos \alpha} \quad \text{where.}$$

$$A = (H \cdot z) \operatorname{cosec} \alpha \quad (\text{strip of unit thickness over which cohesion acts})$$

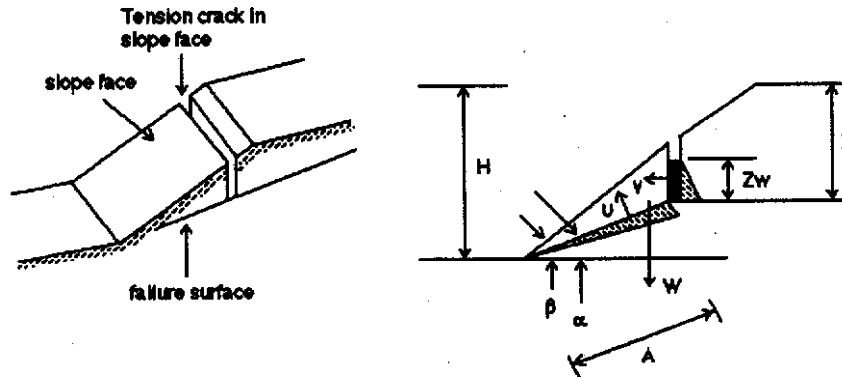
$$U = 1/2 \gamma_w z_w (H - z) \operatorname{cosec} \alpha \quad (\text{uplift force due to water pressure on the sliding surface})$$

$$V = 1/2 \gamma_w z_w^2 \quad (\text{de., pressure, uplift force due to water pressure in the tension crack})$$

For the tension crack in the upper slope surface,

$$W = 1/2 \gamma H^2 \left((1 - (z/H)^2) \cot \alpha - \cot \beta \right) \quad (\text{weight of the sliding block})$$

Headscarp in Slope Face



The weight of the sliding block becomes,

$$W = 1/2 \gamma H^2 \left[(1 - z/H)^2 \cot \alpha (\cot \alpha \tan \beta - 1) \right] \quad (\text{weight of the sliding block})$$

where,

c = cohesive shear strength of rock

ϕ = internal friction angle

γ = unit weight of rock

γ_w = unit weight of water

β = hillslope angle measured with respect to horizontal

α = failure plane angle measured with respect to horizontal

H = height of hillslope

Z = depth from top of hillslope to bottom of tension crack

Z_w = depth of water in tension crack

FIGURE 1. Graphical representation and input parameters of plane failure stability model adapted from Hoek and Bray (1977). Because the geometry and thus the weight of the potential failure block is dependent on the position of the vertical tension crack, two versions are presented. Case A) with the headscarp in the upper slope surface is characteristic of failures in glacial material while case B) with the headscarp in the slope face is characteristic of bedrock failures in the Chuckanut Formation.

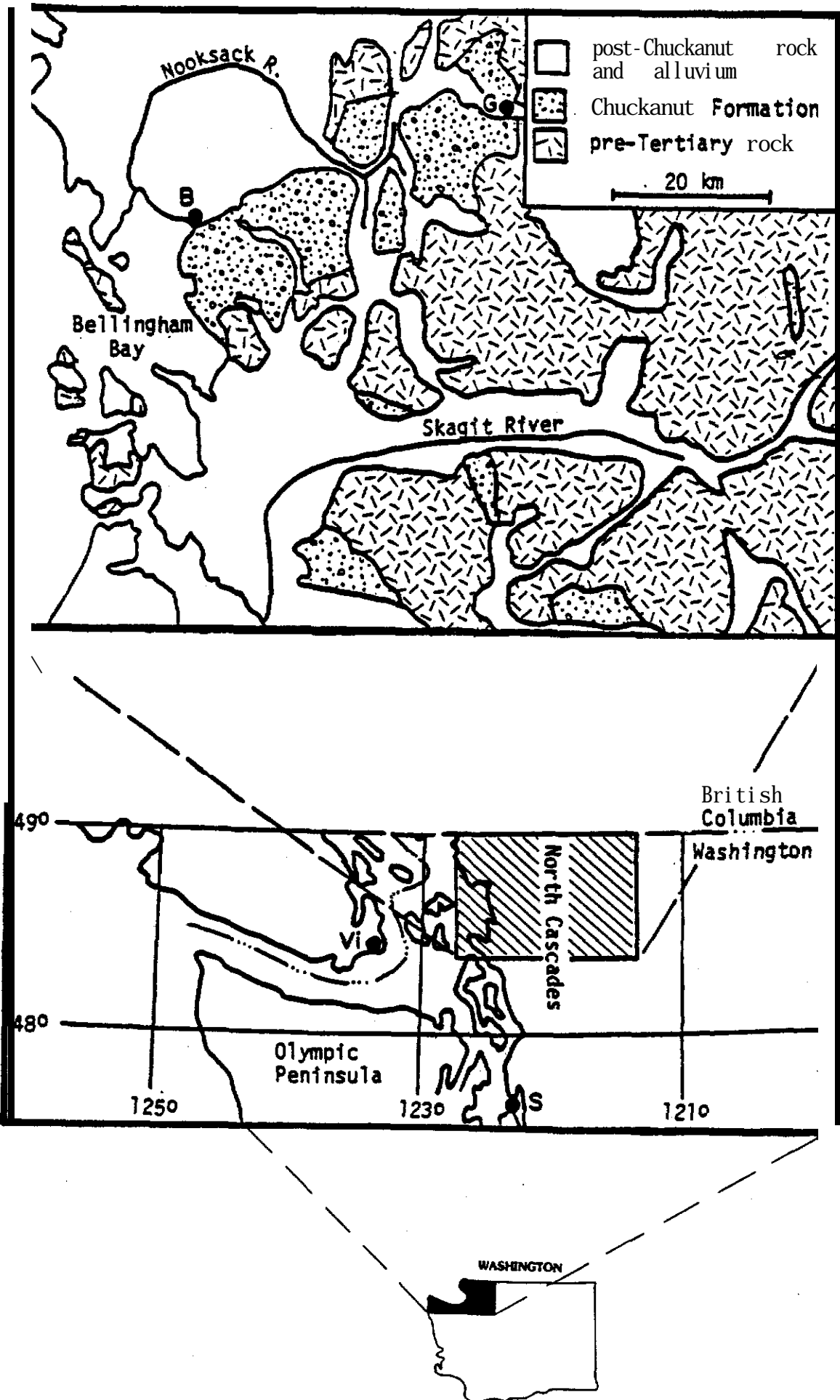


Figure 2

Figure 3
Chuckanut Formation

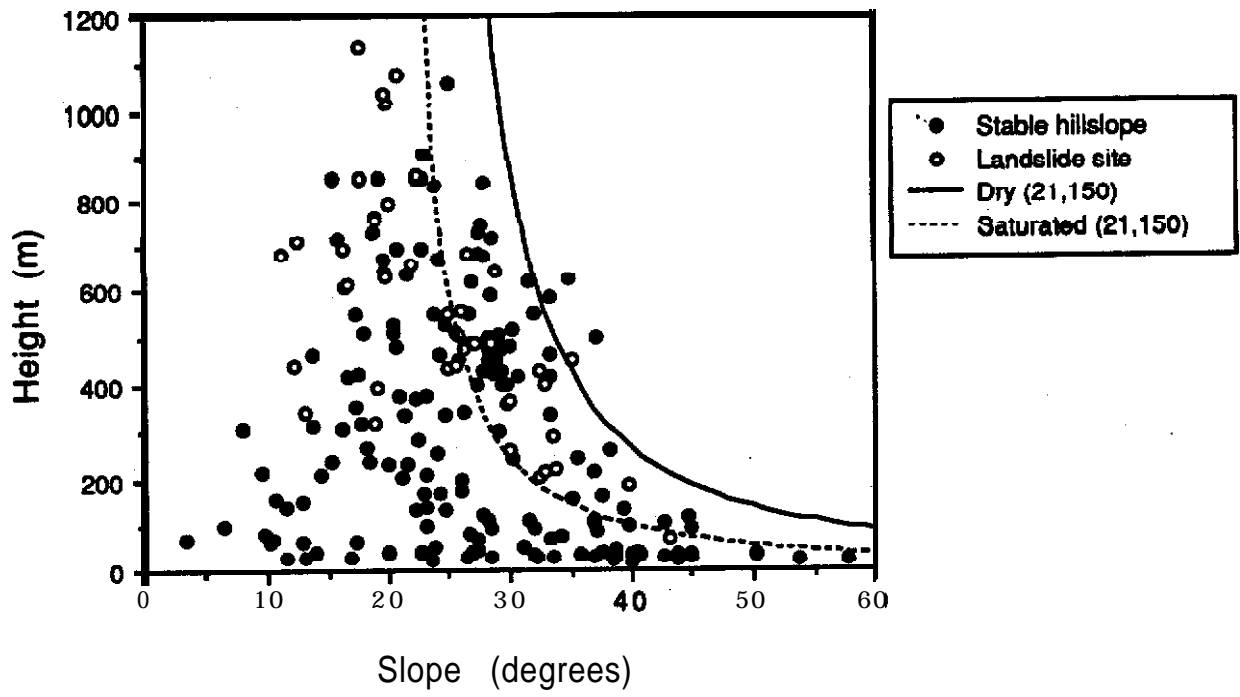


Figure 4

Chuckanut Formation

(Anti-dip slopes, dry and saturated thresholds)

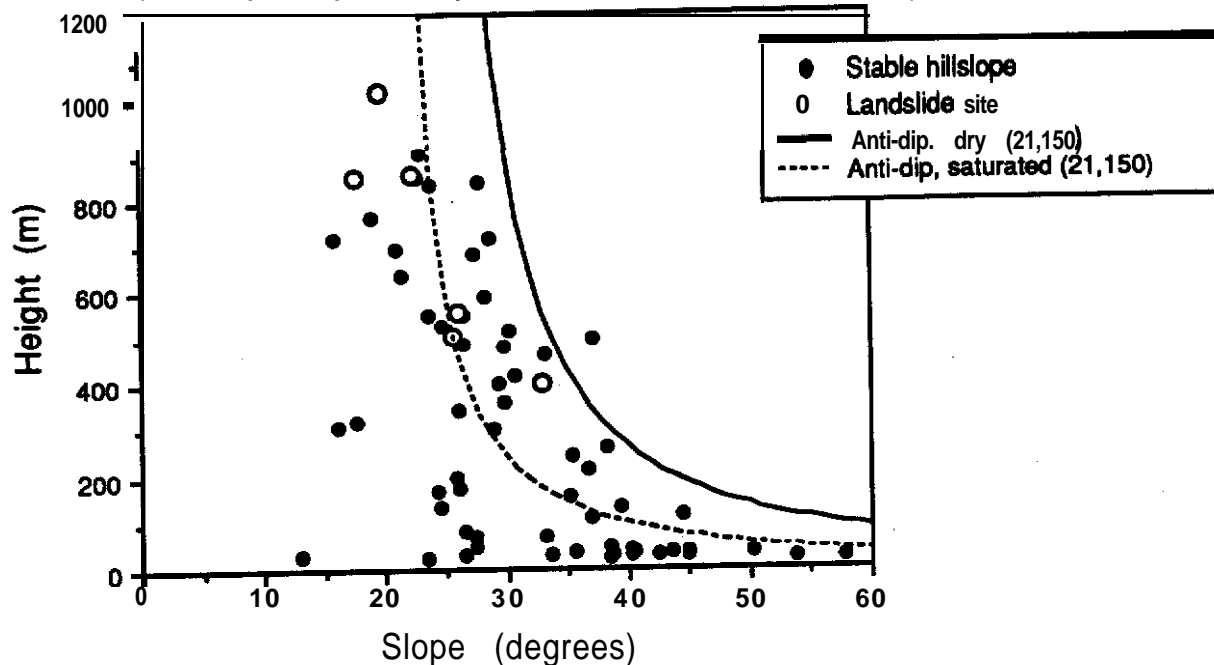


Figure 5

Chuckanut Formation

(Dip slopes, dry and saturated thresholds)

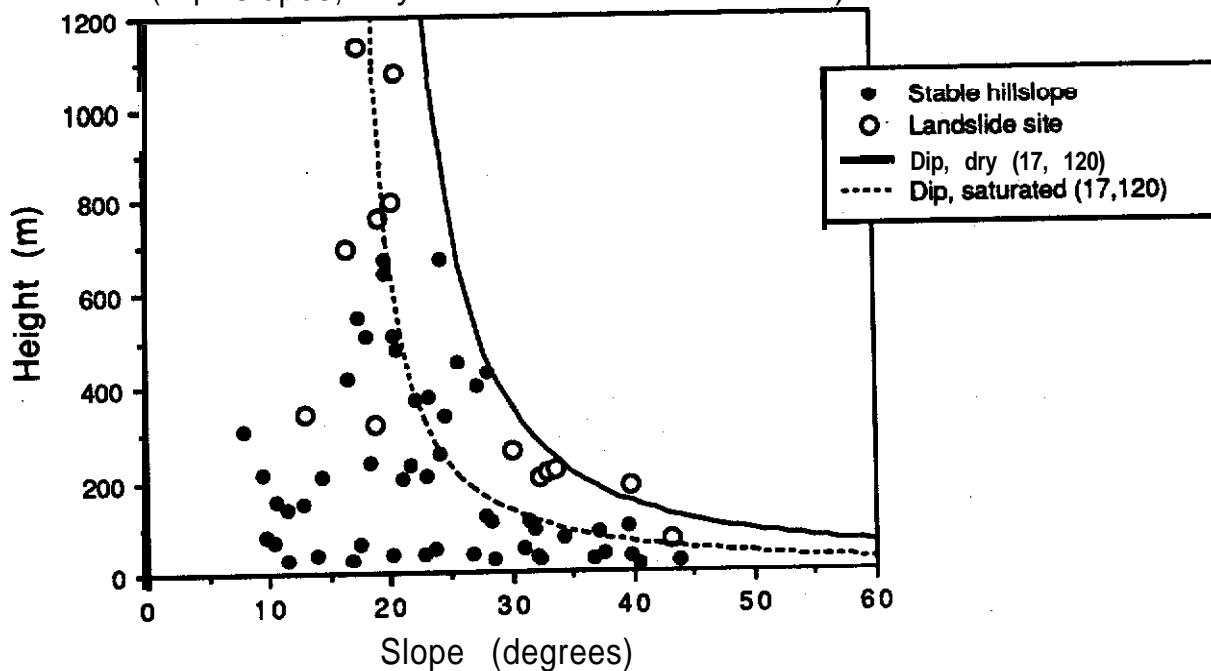


Figure 6
Glacial Deposits

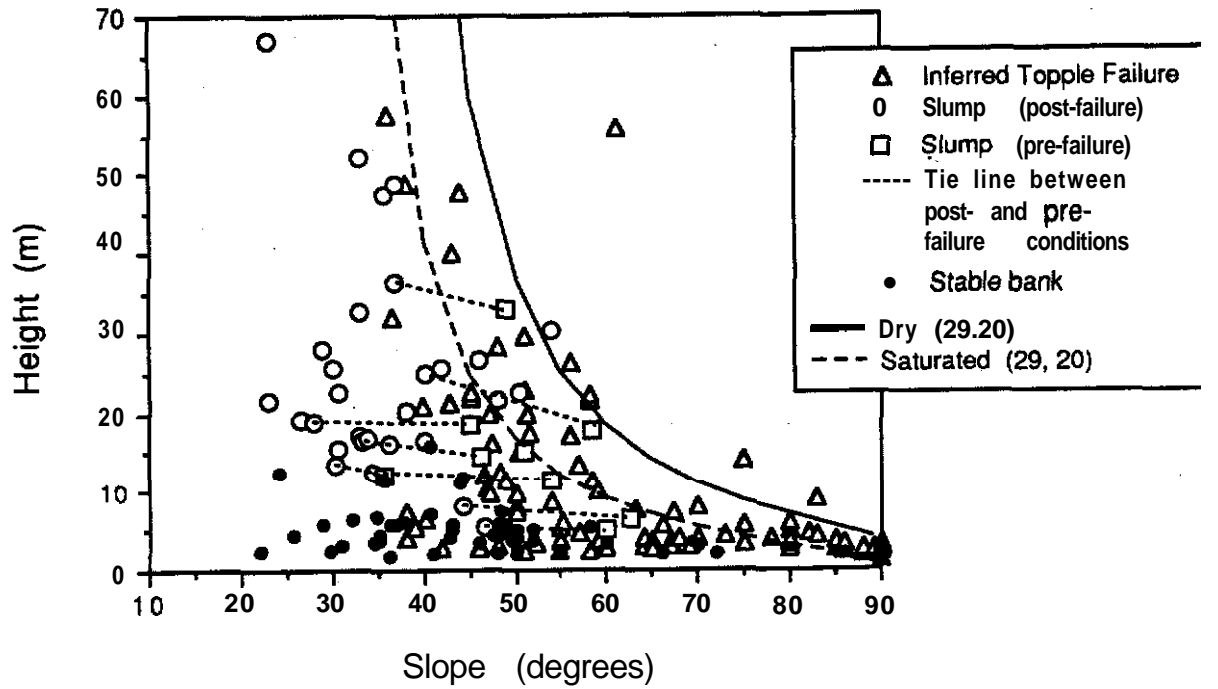


Figure 7: Relative Spatial Distribution of Hillslope Processes

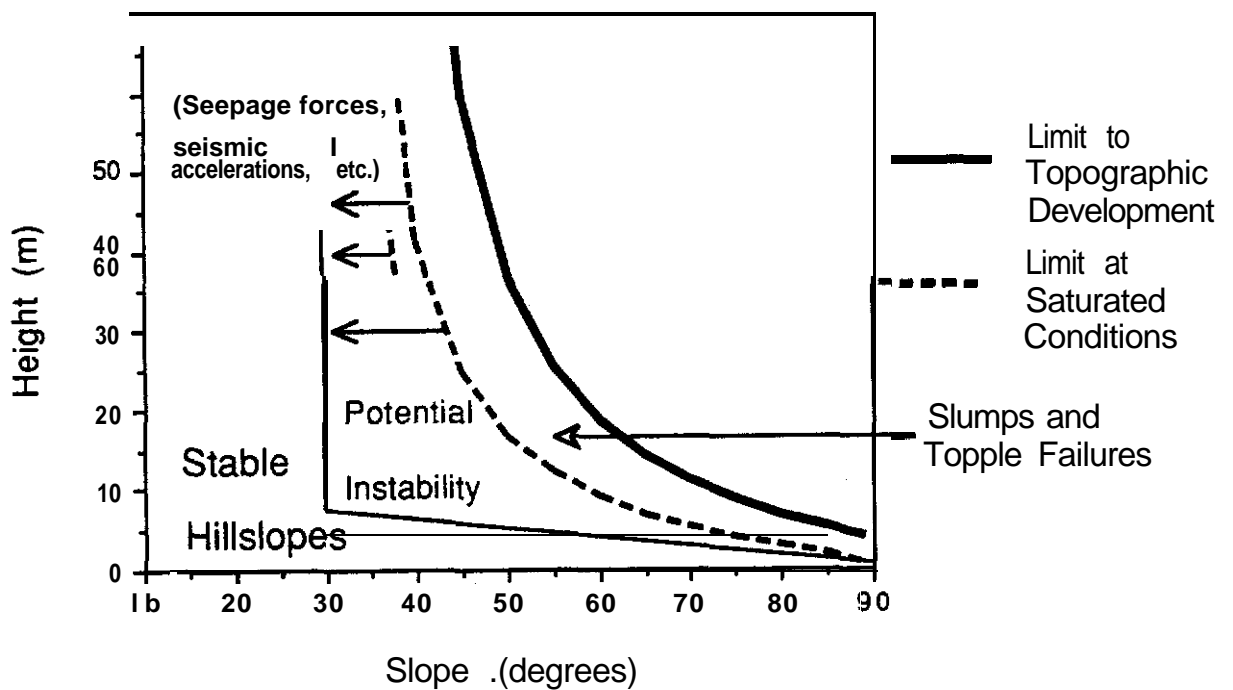
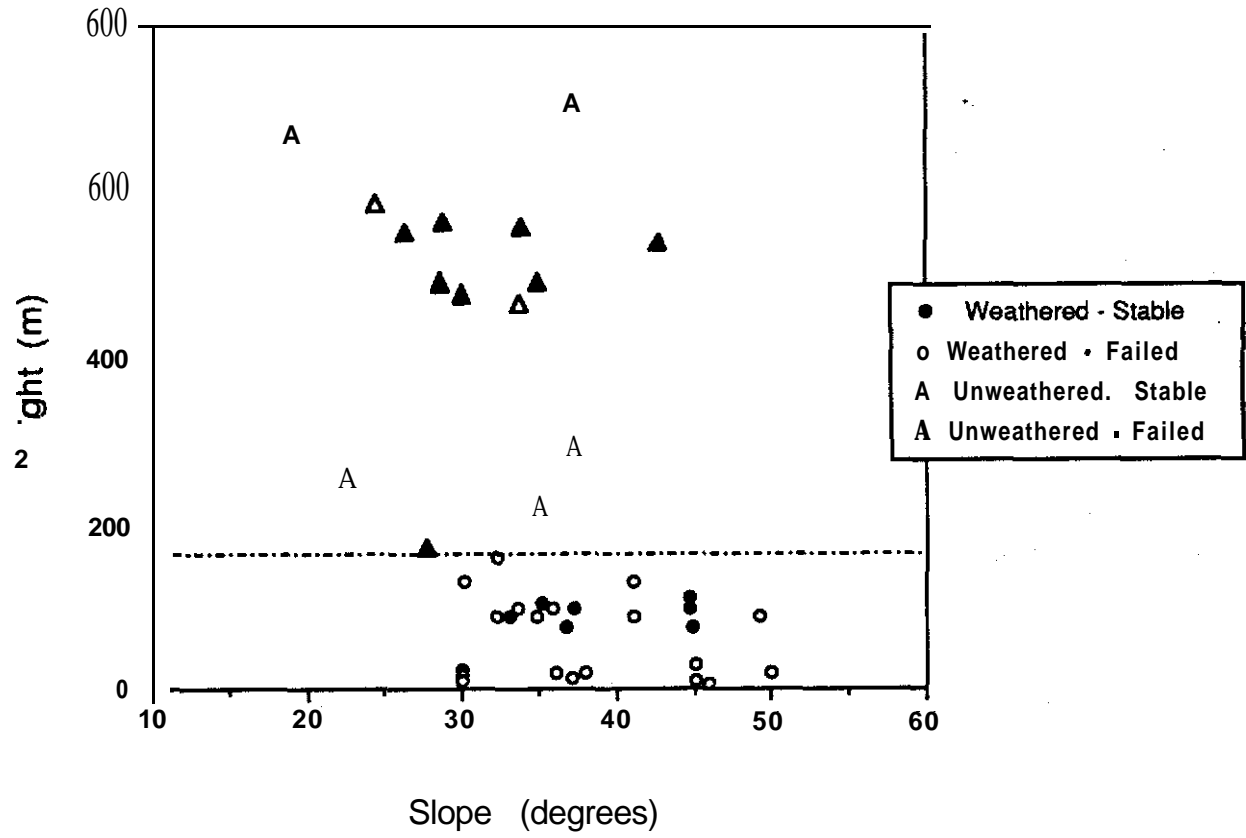


Figure 8

Darrington Phyllite
(Weathered vs. Unweathered)



Appendix 7

BigDirt: Deep-Seated Mass Wasting Project Report

Project Description

Deep-seated mass failures can mobilize huge volumes of material and often comprise the major source of sediment in a watershed (Kelsey, 1988; Eide, 1989). As a mechanism for moving material from hillslopes, deep-seated failures form an important geomorphic component of many landscapes and are the source of expensive and often unanticipated engineering and environmental problems. With this project we are developing a method for identifying **the** locations of existing and potential deep-seated mass wasting occurrences and for anticipating the response of **deep-**seated failures to changes in the basin, e.g., changes in precipitation or in **landuse**. This method involves the coupling of models describing the physical mechanisms of deep-seated mass wasting with a geographical information system (GIS). The physical models are based on a theoretical framework reflecting observations of geomorphic processes occurring in a region. The GIS serves as a data base for organizing all pertinent information about a drainage basin in a form accessible as input to physical models of geomorphic processes. The method we are developing is modular, so that it is readily upgraded as the models on which it is based are tested and improved, and as additional information about the basin becomes available.

Identification of Susceptible Sites: Calculation of Slope Stability

To date we have successfully used the GIS as a data base for two-dimensional, limit equilibrium slope stability calculations. The result of such an analysis, illustrated with Figure 4 in the accompanying example, is a map of relative slope stability based on calculations performed for multiple transects through the slopes of interest. This method works well for large failures; the resolution of topographic data presently available (digital elevation models with a 30 meter grid spacing), however, precludes detection of features spanning less than several hundred meters. Unfortunately, failures of smaller size, typically occurring in glacial sediments composing many river terraces through this region, comprise a major source of sediment to many stream channels. One can devise strategies to make the most of the information available (see the accompanying example), but ultimately, detailed analyses require topographic data at a resolution greater than that **presently** available.

The Need for Geologic Information and Ground-Water Flow Modeling

Efforts to date have dealt with only a single landscape attribute: the topography. The geology also imposes a primary control on **hillslope** processes. We are working to incorporate geologic information, e.g., lithology, stratigraphy, structure, and **geotechnical** properties, into the GIS database. The slope-stability analyses done so far also have dealt only with static conditions and identification of sites susceptible to failure. To anticipate the effect of perturbations to a basin we must characterize the relationships connecting changeable attributes of the landscape to processes of mass wasting. This connection occurs primarily through the ground-water flow field. We are working to use the GIS in models of regional ground-water flow. Results of the regional

model provide water table elevations and water flux estimates to use in slope models which couple gravitational stresses with seepage induced stresses and pore pressures. We will complete addition of these two components, the geology and the ground-water flow field, to the slope stability analysis over the **course** of the coming year. Success here will provide a method for predicting the effects of hydrologic perturbations to the basin and the **potential for** predicting the occurrence of failures enhanced by seepage erosion.

Tests of the Method

The success of our approach for anticipating deep-seated failures in any region can be evaluated only through comparison of the predictions made to field observations. Kevin Schmidt's field work east of Bellingham provides the first test; indeed Kevin's results highlight the need for geologic information. Landslide mapping done by Dave Parks (1992), by Fisdal and Brunengo (1981), and perhaps that being done in upcoming Watershed Analyses, provide additional sites with which to test and refine this method for locating sites susceptible to **deep**-seated mass wasting.

The following examples illustrate the steps involved in the method of slope stability analysis being developed with this project.

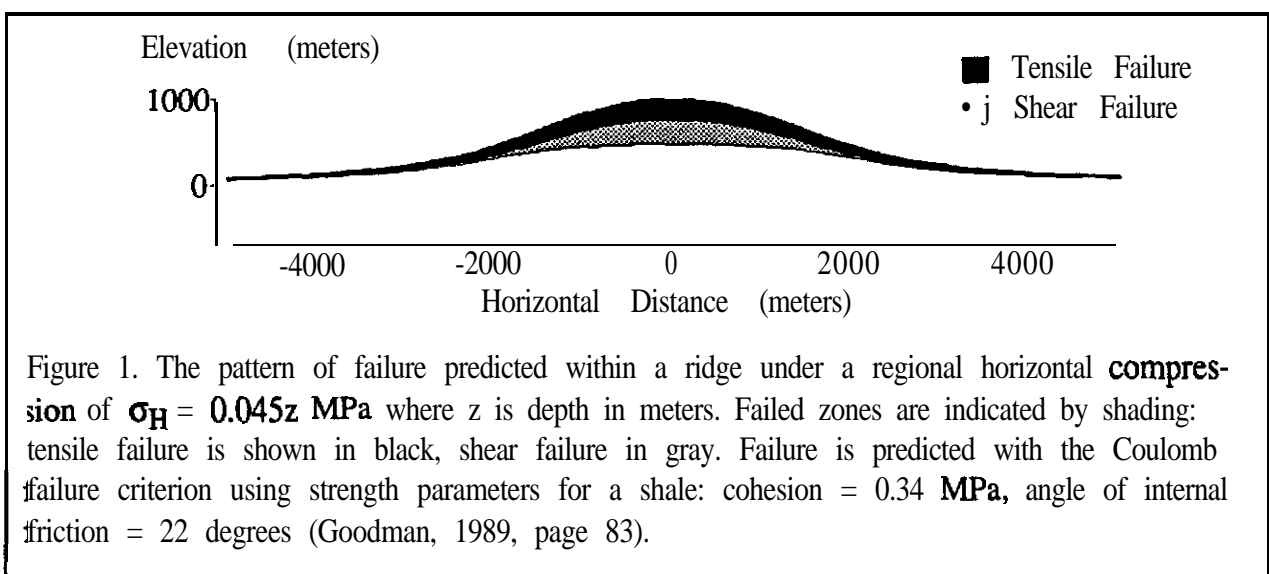
Case Study 1

The Problem

Numerous large, deep-seated landslides exist throughout portions of the North Cascades and have been mapped in detail in several basins, including the Middle Fork of the **Nooksack** River (Fiksdal and Brunengo, 1981; Schmidt, 1992). These slides present a diverse array of mass wasting types and processes (Thorsen, 1989a). To anticipate the occurrence and behavior of multiple landslide types *in a regional analysis*, we must seek similarities *in the underlying mechanisms* by which such slides are formed and by which motion on them occurs. The subsequent paragraphs and figures suggest a theoretical mechanism for the widespread occurrence of mass wasting movement spanning the length of mountain slopes, provide references to field observations in support of mat theory, and present a simple slope stability model appropriate for the physical mechanisms that may be occurring.

The Model

Regional stresses within continental zones, including the Pacific Northwest, tend to be predominantly compressional (Zoback, 1992). Interactions between compressional regionally acting stresses, the force of gravity, and the ground-surface topography cause local stresses that vary systematically through the landscape (Scheidegger, 1963; **McTigue** and **Mei**, 1981; Savage et al., 1985; Savage and Swolfs, 1986). In regions of high regional compression, local compressive stresses tend to form in valleys while local tensile stresses tend to form in ridges (Miller, 1993). This leads to a pattern of potential rock failure as shown in Figure 1 below. This figure was made by comparing the rock strength predicted with a Coulomb failure criterion (Goodman, 1989) to the stress field calculated for a symmetric ridge under a regional tectonic compression (Savage et al., 1985; Miller, 1993). These results are for shale, which is a very weak rock. Failure

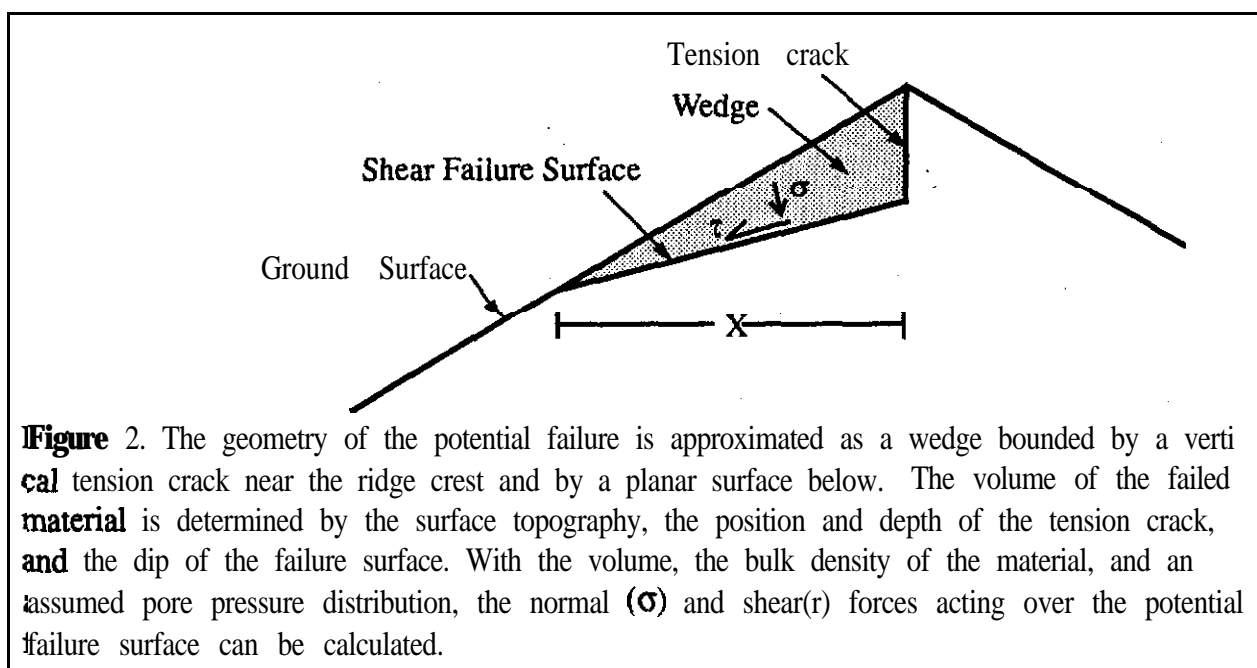


predicted for a stronger rock would be less extensive, but with a similar pattern. Likewise, the extent of failure is dependent on the magnitude of the regional horizontal stress.

The interaction of gravitational and regional tectonic forces with ground-surface topography in regions of high relief provides a potential mechanism for initiating regionally extensive mass wasting at scales spanning entire mountain slopes. The distribution of stress induced within a ridge suggests a pattern of fracturing characterized by steeply-dipping, tensional fractures along ridge crests underlain by shear fractures at depth. Such patterns have been inferred from field observations in many mountainous regions of the world, including the North Cascades (Thorsen, 1989b) and the Olympic Mountains (Tabor, 1971) in Washington state, the Coast Mountains of British Columbia (Bovis, 1982), and the Rocky Mountains of the Western U.S. (Radbruch-Hall et al., 1976; Savage and Varnes, 1987).

The pattern of fracturing induced by regional stresses sets the stage for a variety of mass wasting processes. Fractured rock is mechanically weak and fractures provide potential failure surfaces. Likewise, increased permeability accompanying fracture formation enhances chemical weathering of the rock and influences the ground-water flow field. Although these processes can lead to great complexity in the types of mass wasting that result, the pattern of fracturing illustrated in Figure 1 suggests a simple model with which to anticipate where gravity driven down slope movement is likely to occur. This model is based on an analysis presented in Hoek and Bray (1981) for wedge failures. The geometry is illustrated in Figure 2 below.

The stability of the wedge is determined by comparing the shear force acting over the potential failure surface to the shear strength of the material. The shear strength can be estimated with the Coulomb criterion. Values of cohesion and angle of internal friction appropriate for the materials involved, keeping in mind that the rock is fractured, must be chosen. Such values can be obtained from published compendia of geotechnical properties, e.g., Goodman (1989).



For a given set of material parameters (bulk density, cohesion, and friction angle), the stability of a slope is determined by the geometry of the wedge. I have written a computer program to find the geometry of the least stable wedge having a specified horizontal extent (**X**) for a slope of given surface topography. The potential for failure along the slope is then determined by calculating the minimum stability for wedges of varying size and position along the entire length of the slope. Each point **along** the slope is assigned the stability of the least stable wedge which contained it. This model thus provides an estimate of relative stability as a function of position along a slope. The next step is to use the GIS to provide the model with the topographic and **geotechnical** information required.

Coupling *of the Model and the GIS*

The topographic information is stored in the **GIS** as a digital elevation model (DEM) which consists of point values of elevation for a grid of points regularly spaced at 30 meter intervals. Elevations between the gridded points can be interpolated and contour lines constructed as shown in Figure 3 on the next page. Topographic profiles for slope transects can also be constructed from the DEM. The slope stability model uses a two-dimensional approximation of the actual slope geometry, i.e., in the model it is assumed that the slope extends a distance along strike large **compared** to its downslope length. To better approximate conditions assumed in the calculations, the topography of the slope can be averaged over a certain along-strike distance to produce an average profile for a section of the slope. This is illustrated by the rectangular box surrounding the transect line in Figure 3.

The profile is then used in the slope stability model to calculate a measure of stability, e.g., a factor of safety (**Fs**), for points along the profile. Transects are taken at regular intervals along all slopes and stability calculations are made for every transect. These calculations provide stability values for closely spaced points throughout the landscape. These stability values provide the information needed to locate those areas susceptible to mass wasting; the next step is to portray that information in an easily interpreted manner, i.e., as a map. The GIS serves this purpose as well. With the GIS, stability values can be interpolated between the points at which calculations were made and a map showing contours of slope stability, or polygons delineating areas of differing relative stability, can be made. Such a map is shown in Figure 4.

The model and the set of material parameters used with it are a description of how mass wasting processes might work in this landscape. We know it is not a complete description, because these calculations did not include many factors that might effect slope processes (e.g., the strike and dip of the bedding planes relative to the aspect of the slope). We would like to **find** out, however, just how good a description it is. To that end, the map provides a prediction to be tested. As shown in Figure 4, this method for estimating slope stability did pick out those areas mapped as landslide features. It **also** picked out many areas not mapped as landslides. It is possible that mass wasting processes are occurring on these additional areas, but have not been mapped as landslides, or that these areas are potentially unstable even though no landslides have yet occurred, or that the model is overly sensitive - which is quite likely since local geological **struc-**

ture was not taken into account. These possibilities are testable with field observations. Failure of the predictions to match what is observed provides guidance to improve the model, or the parameter values used in the model, or both. Likewise, as additional data are incorporated into the GIS, such as the geology (including the dip of the beds, which Kevin has shown to be of great importance to slope stability in this area), our description of mass wasting processes will improve.

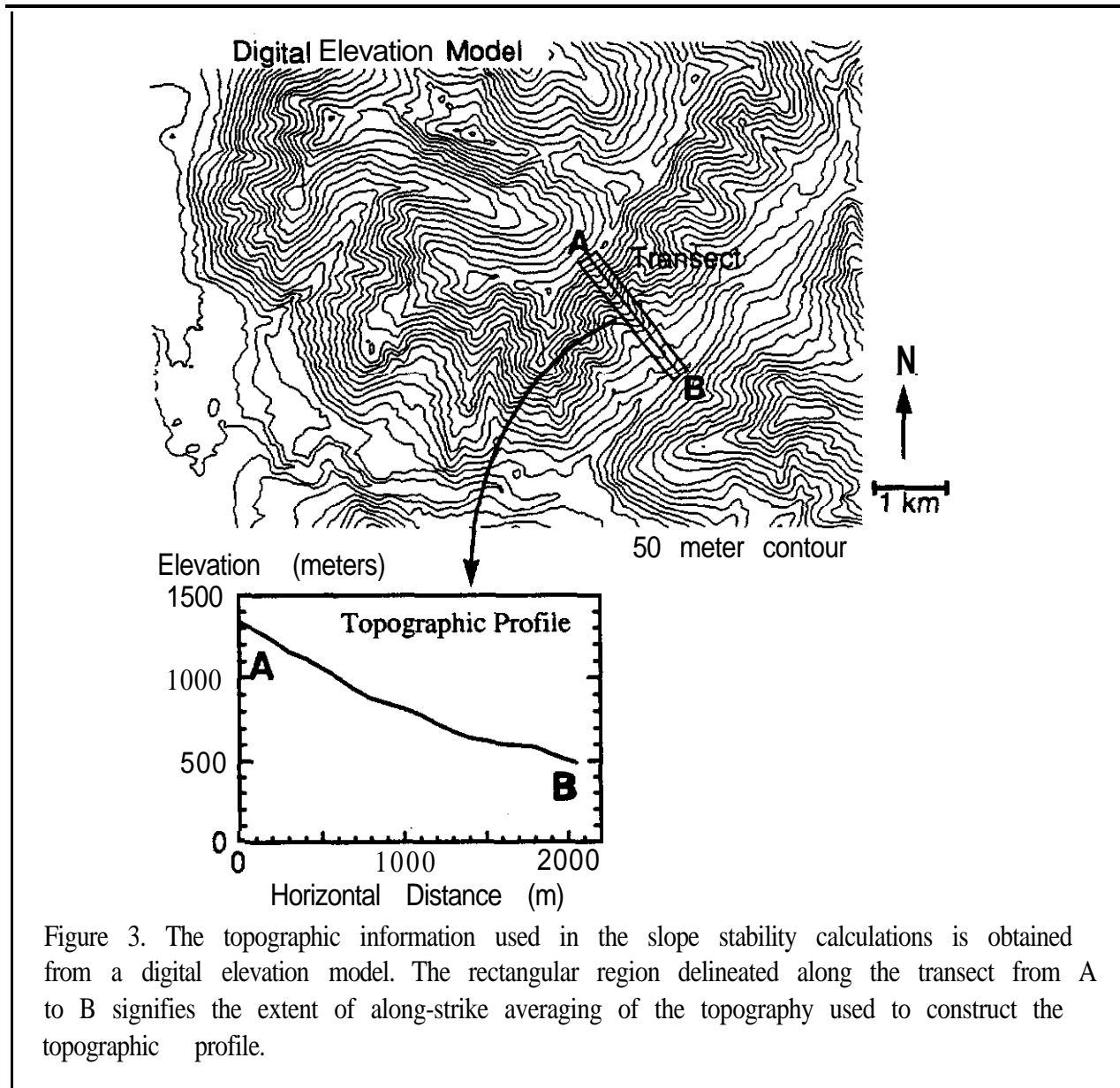
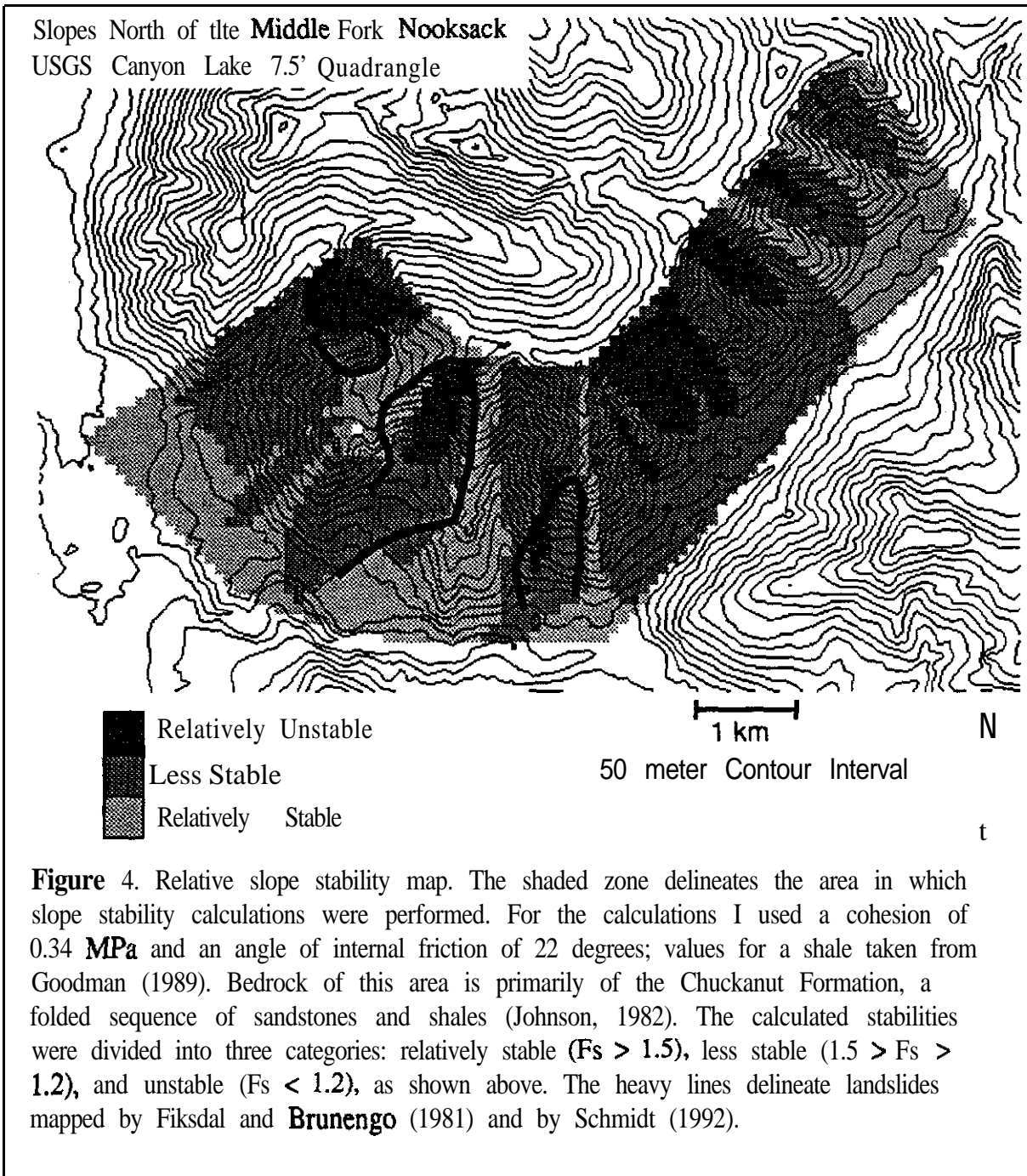


Figure 3. The topographic information used in the slope stability calculations is obtained from a digital elevation model. The rectangular region delineated along the transect from A to B signifies the extent of along-strike averaging of the topography used to construct the topographic profile.



Case Study 2

The Problem

The 30 meter grid spacing of presently available **DEMs** limits topographic resolution to features spanning hundreds of meters in horizontal extent. Such resolution **is sufficient** for delineation of large landscape features, as illustrated in the previous example. Unfortunately, slope failures of smaller **extent** comprise a significant proportion of the sediment budget in many basins (e.g., Raines, 1991; Parks, 1992). Locally, stream-side failures occurring in **terraces** composed of glacial valley-train sediments can be extensive (e.g., Schmidt, 1992). As shown in the profiles in Figure 5 below, the topographic signature of such failures is not resolved with a 30 meter DEM. This highlights the need for higher **resolution** topographic data. The work of Zhang and Montgomery (submitted, 1993) suggests that a 10 **meter** grid spacing is required to resolve the hydrologic characteristics of low-order basins; similar efforts are needed to determine the limits placed on slope stability analysis by the resolution of the DEM. Lacking higher resolution topographic data, we must devise methods to utilize the data available. Presented below is a model based on observed modes of stream-side failure in valley-bottom, glacio-fluvial sediments. As this model shows, the lack of data necessitates great generalization in our description of these mass wasting processes.

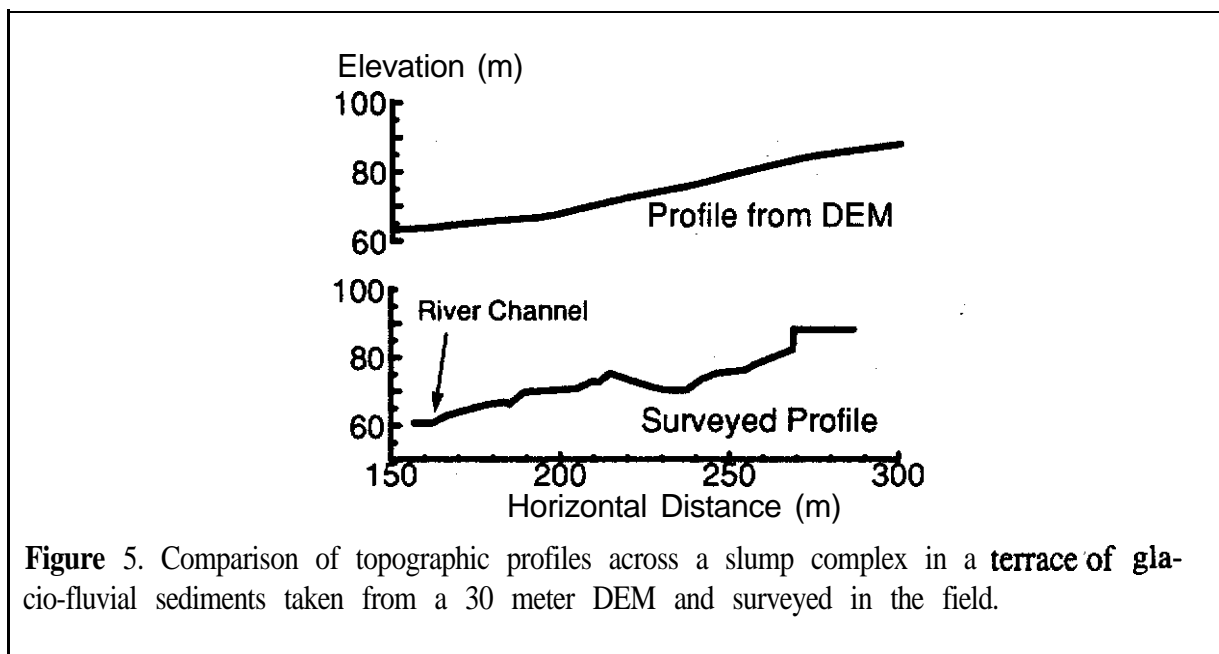


Figure 5. Comparison of topographic profiles across a slump complex in a **terrace of glacio-fluvial** sediments taken from a 30 meter DEM and surveyed in the field.

The Model

Figure 6 below shows a set of profiles for slopes in glacio-fluvial sediments adjacent to the Middle Fork **Nooksack** River surveyed by Kevin Schmidt. Vegetated slopes showing no indication of ongoing mass wasting are labeled as **stable**; exposed slopes with fresh exposures of the valley-bottom glacial sediments indicative of **recent** failure (typically, landslide blocks are still present in the channel) are labeled as **failed**. These profiles suggest that stable and recently failed

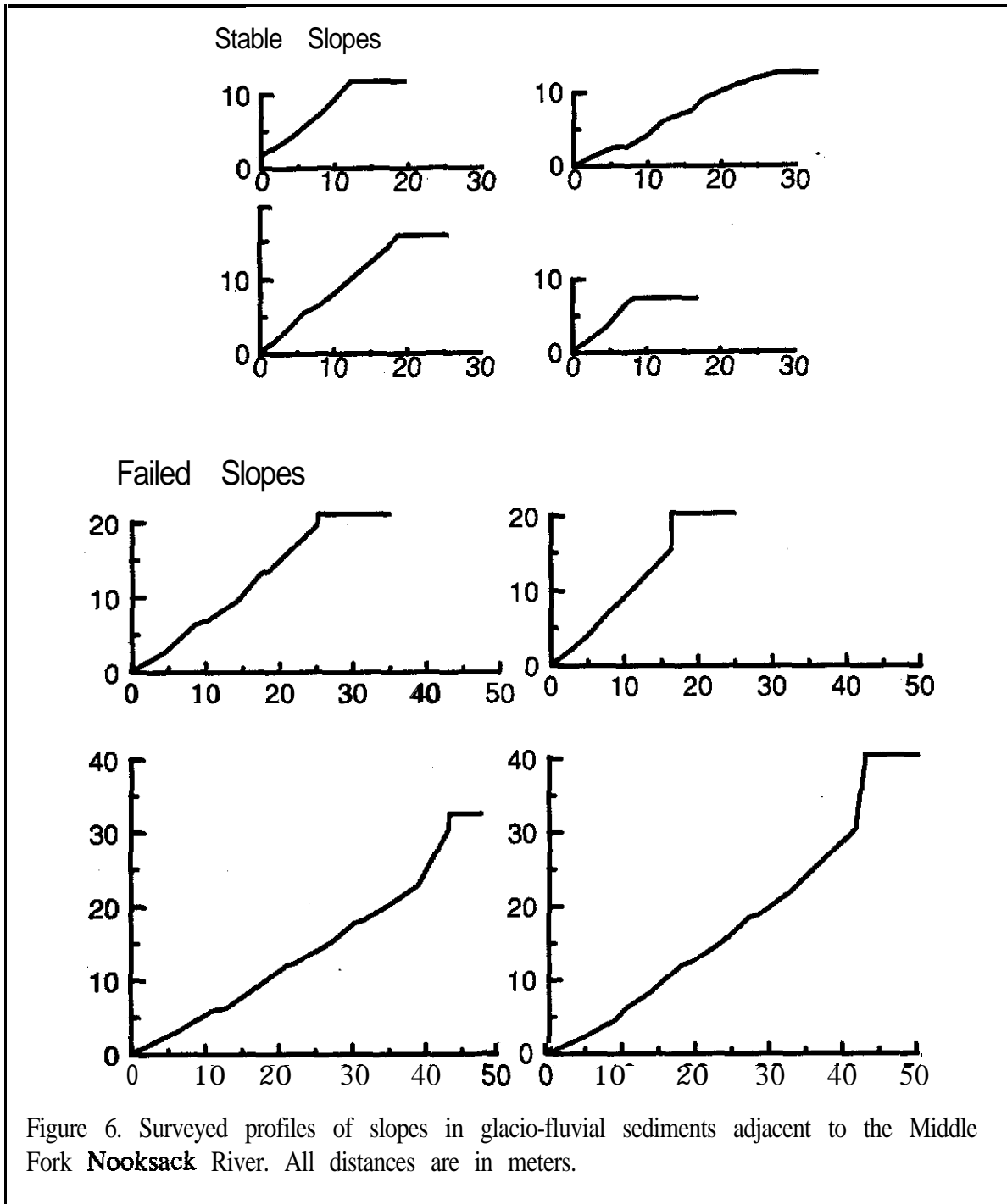


Figure 6. Surveyed profiles of slopes in glacio-fluvial sediments adjacent to the Middle Fork **Nooksack** River. All distances are in meters.

slopes within these glacial sediments may be described with characteristic geometries. Stable slopes are relatively straight with a gradient of 30 to 40 degrees extending from the channel edge to the terrace top. Some stable slopes have a portion of the toe removed, suggestive of stream erosion into the slope. Failed slopes have a straight section extending from the channel edge to the base of a steep head **scarp**.

Field observations together with air photo analysis suggest that slope instabilities within these sediments are typically initiated by stream erosion into the toe of the slope. We suggest the

following model for **describing this** process. Over time, processes of mass wasting produce relatively straight, stable slopes near the angle of repose for unconsolidated sediments. Erosion of the toe alters the geometry with a consequent redistribution of stresses within the slope. **This change** in geometry thus changes the stability of the slope. Using the profiles of failed slopes shown in Figure 6 as a guide, the potential failure is represented with the wedge geometry shown in Figure 7 below. Because the angles θ_1 and θ_2 (refer to Figure 7) vary little between slopes, the stability of the wedge depends only upon the strength properties of the material, the relief of the **terrace (H)**, and the **extent** of toe erosion (X). For given material properties (e.g., bulk density, cohesion, and angle of internal friction), the position of the headscarp and the slope of the failure surface may be varied to find both the wedge having the lowest stability and, if the slope is unstable, **the** largest volume that could fail.

In this simple model, the properties of the terrace sediments are assumed to be homogeneous. This is certainly not the case: a **look** at an exposure through a typical terrace reveals a basal layer of lacustrine sediments, overlain by glacial **outwash**, with a till cap at many sites, typically topped with a thin veneer of **fluvial** floodplain deposits. Although the stratigraphy consists of a layered sequence of differing materials, the stratigraphy itself is consistent throughout the formerly glaciated basins in this region. Kevin (Schmidt, 1992) has suggested, with supporting field evidence, that one may define a set of material parameters to represent the package of sediments as a whole. We progress with that assumption.

Model Predictions

The calculations predict three distinct modes of failure, illustrated in Figure 8 on the next page. Removal of a small portion of the toe, up to 7 meters for the material parameters used in these calculations, has no effect on the slope. Removal of between 7 to 10 meters of the toe causes failures that extend partially up the slope. Removal of greater than 10 meters of the toe initiate failures that extend to the crest of the slope. If toe erosion exceeds a certain limit, depending

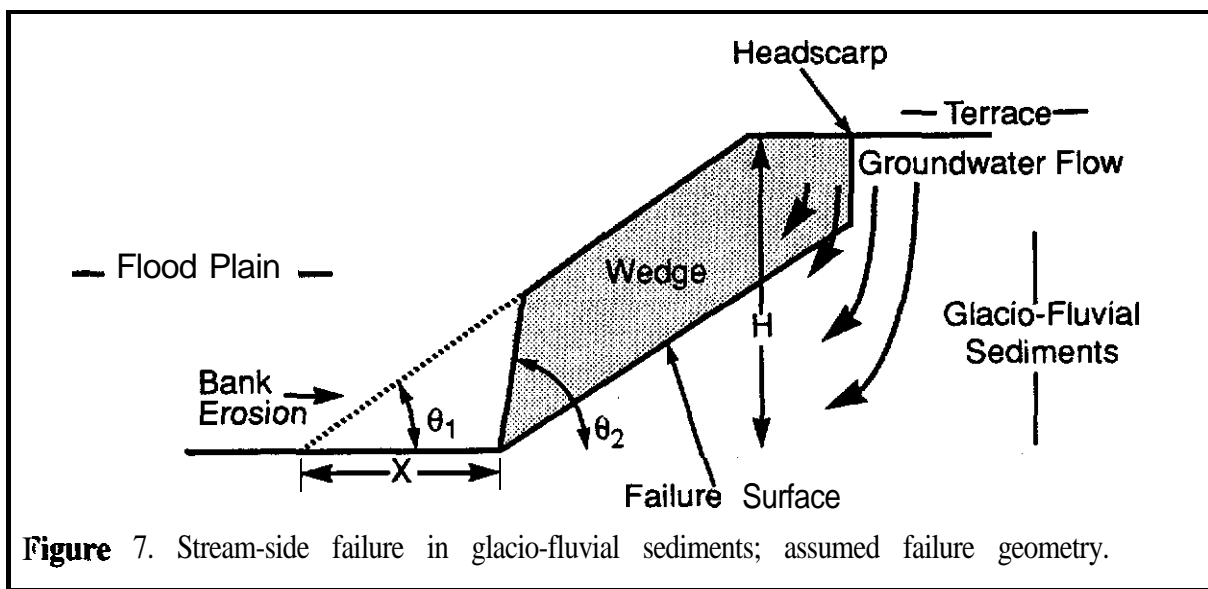


Figure 7. Stream-side failure in glacio-fluvial sediments; assumed failure geometry.

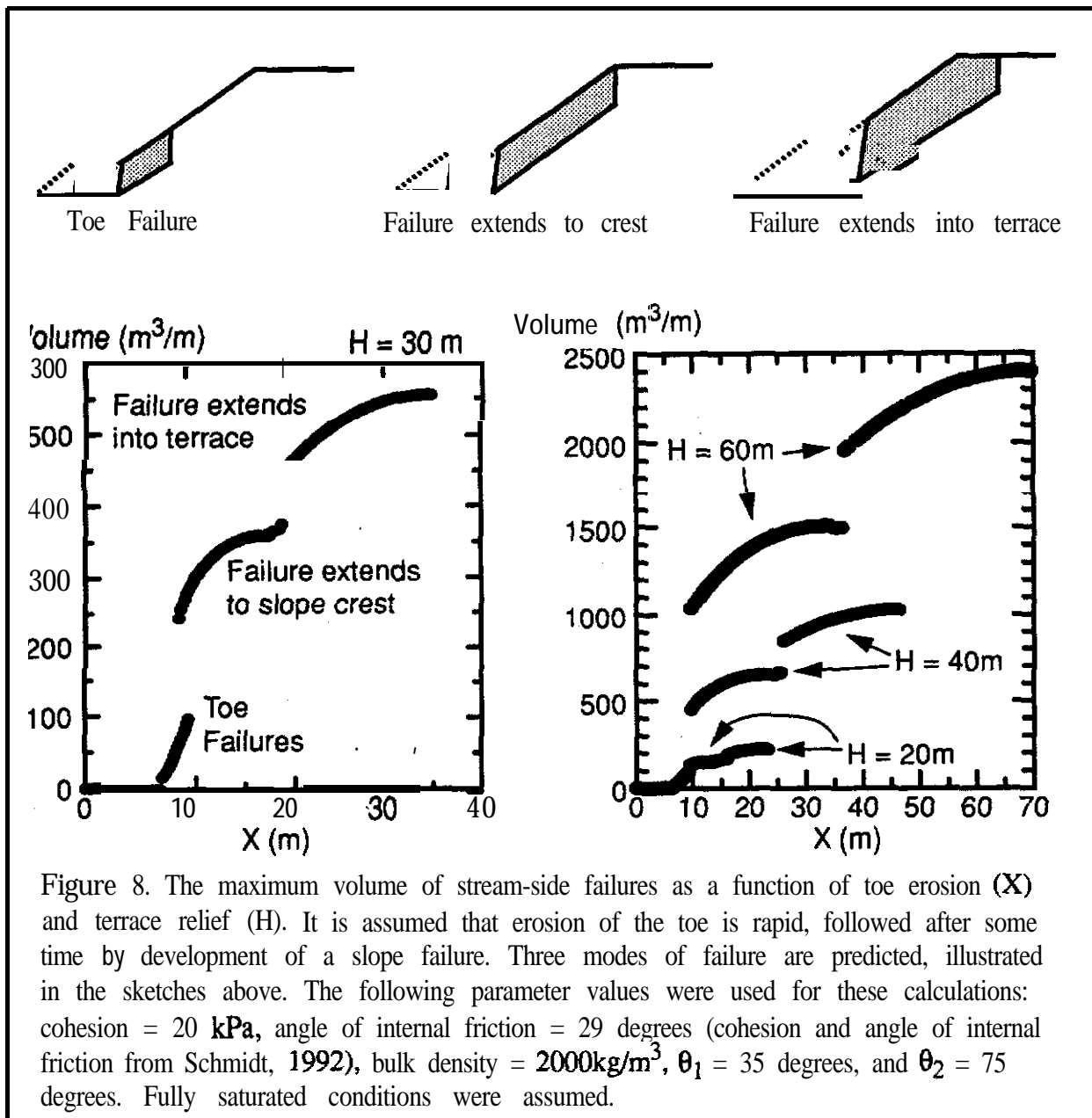


Figure 8. The maximum volume of stream-side failures as a function of toe erosion (X) and terrace relief (H). It is assumed that erosion of the toe is rapid, followed after some time by development of a slope failure. Three modes of failure are predicted, illustrated in the sketches above. The following parameter values were used for these calculations: cohesion = 20 kPa, angle of internal friction = 29 degrees (cohesion and angle of internal friction from Schmidt, 1992), bulk density = 2000kg/m³, θ_1 = 35 degrees, and θ_2 = 75 degrees. Fully saturated conditions were assumed.

on the total relief of the terrace, the failures extend into the terrace. These three modes of failure involve progressively increasing volumes of material, as shown in the graphs above. For failures extending to the top of the terrace, the volume of material mobilized by the failure is a function of the total relief of the terrace, as shown in the graph to the right above.

This model provides easily tested predictions. Moreover, it ties sediment supply from the hillslope directly to occurrences in the channel, i.e., to the extent of bank erosion. Use of the model requires only a measurement of the total **relief** of the terrace, a quantity which can in some cases be obtained with presently available topographic data.

References

- Bovis, M. J., 1982, Uphill-facing (antislope) **scarps** in the Coast Mountains, southwest British Columbia: Geological Society of America Bulletin, v. 93, pages 804-812.
- Eide, J., 1989, A **48-Year** Sediment Budget (1942-1989) for Deer Creek Basin, Washington: **M.S.** Thesis, Western Washington University, Bellingham, 122 pages.
- Goodman, R. E., 1989, Introduction to Rock Mechanics, 2nd Edition: John Wiley and Sons, 562 pages.
- Fiksdal, A. J., and **M. J. Brunengo**, 1981, Forest Slope Stability Project, Phase **II**: Washington Department of Ecology, Technical Report WDOE 81-14, 62 pages + maps.
- Hoek, E., and **J. W. Bray**, 1981, Rock Slope Engineering: Prentice-Hall, 402 pages.
- Johnson, S. Y., 1982, Stratigraphy, Sedimentology, and Tectonic Setting of the Eocene Chuckanut Formation, Northwest Washington: Ph.D. Dissertation, University of Washington, Seattle
- Kelsey, H. M., 1988, Formation of inner gorges: Catena, v. 15, pages 433-458.
- Mcligue, D. F., and C. C. **Mei**, 1987, Gravity-induced stresses near topography of small slope: Journal of Geophysical Research, v. 86 (**B10**), pages 9268-9278.
- Miller, D. J., 1993, Topographically Induced Stress Fields and Patterns of Bedrock Fracturing: Ph.D. Dissertation, University of Washington, Seattle, in preparation.
- Parks, D. S., 1992, A Landslide Inventory of the Finney Creek Watershed, Skagit County, Washington: M.S. Thesis, University of Washington, Seattle, 164 pages.
- Radbruch-Hall, D. H., **D. J. Vames**, and **W. Z. Savage**, 1976, Gravitational spreading of **steep-sided ridges ("sackung")** in Western United States: Bulletin of the International Association of Engineering Geology, **#14**, pages 23-35.
- Raines, M. A., 1991, Sediment Budget for the Grouse Creek Basin, Humboldt County, California: M.S. Thesis, Western Washington University, Bellingham, 110 pages.
- Schmidt, K. M., 1992, Mountain-scale strength properties, deep-seated landsliding, and limits to local relief: EOS Transactions, American Geophysical Union, v. 73, **#4**, page 227.
- Savage, W. Z., H. S. Swolfs, and **P. W. Powers**, 1985, Gravitational stresses in long symmetric ridges and valleys: International Journal of Rock Mechanics and Mining Sciences & Geomechanics Abstracts, v. 22 (**5**), pages 291-302.

- Savage, W. Z., and H. S. Swolfs, 1986, Tectonic and gravitational stresses in long symmetric ridges and valleys: *Journal of Geophysical Research*, v. 91 (**B3**), pages 3677-3685.
- Savage, W. Z., and Varnes, 1987, Mechanics of gravitational spreading of steep-sided ridges (“**sackung**”): *Bulletin of the International Association of Engineering Geology*, #35, pages 31-36.
- Scheidegger, A. E., 1963, On the tectonic stresses in the vicinity of a valley and a mountain range: *Proceedings of the Royal Society of Victoria*, v. 76, pages 141-145.
- Tabor**, R. W., 1971, Origin of ridge-top depressions by large-scale creep in the Olympic Mountains, Washington: *Geological Society of America Bulletin*, v. 82, pages 1811-1822.
- Thorsen, G. W., **1989a**, Landslide provinces in Washington, in **Galster**, R. W. (ed), *Engineering Geology in Washington, Volume I: Washington Division of Geology and Earth Resources, Bulletin 78,632* pages.
- Thorsen, G. W., **1989b**, Splitting and sagging mountains: *Washington Geologic Newsletter, Division of Geology and Earth Resources*, v. 17 (**4**), pages 3-13.
- Zhang**, W. and D. Montgomery, 1993, Digital elevation model grid size, landscape representation and hydrologic simulations: submitted to *Water Resources Research*
- Zoback**, M. L., 1992, First- and second- order patterns of stress in the Lithosphere: the world stress map project: *Journal of Geophysical Research*, v. 97 (**B8**), pages 11703-11728.

Appendix 8

Deep-Seated Bedrock Landslides and Rock Mass Strength Analysis

Kevin M. Schmidt
Department of Geological Sciences, AI-20
University of Washington
Seattle, WA. 98195

HIERARCHY OF LANDSLIDE HAZARD RECOGNITION

As a portion of the deep-seated mass wasting study, we are developing a multi-level approach for identifying deep-seated landslide locations and estimating their relative hazard. At the broadest level, this method entails aerial photograph, topographic map, and geologic map investigation to characterize the material properties and common modes of failure of the geologic units under study. This level of analysis also denotes the portions of the landscape with high degrees of instability that may be chronic sources of sediment to the adjacent channels. For further details see Schmidt **and** Montgomery, this report.

The second level of analysis involves the coupling of a model describing the mechanics of landslide failure with a geographic information system (**GIS**) (see Miller, this report). This level can be used not only to identify the locations of active landslides in a regional context, but also to predict the potential locations of future areas of instability. In addition, it can be used to anticipate **the** response of landslides to hydrologic changes within the basin. Current efforts include the addition of geologic parameters to the topographic base, a digital elevation model, in the GIS database. Field studies have highlighted the importance of the geologic features that lead to decreased hillslope strength (e.g. bedding planes, joints, slope aspect, and water content).

The third level involves the local characterization of rock strength at the outcrop scale. Rock strength can be quantified through an approach termed rock mass strength (Selby, 1980). The following parameters are included in the classification: intact rock strength; state of weathering of the rock; joint spacing; orientation of joints with respect to the hillslope; width of joints, lateral or vertical continuity of the joints; infilling of the joints; and *movement* of water out of the rock mass. Each parameter is assigned a rating and the sum of the ratings determines the

rock mass strength on a scale with a maximum rating of 100. Certain aspects of Selby's classification system have been tailored for use in slope stability evaluation.

APPLICATION TO STUDY AREA

Outcrops of the Chuckanut Formation were examined in areas of both stable hillslopes and recognized landslide sites. Rock mass strengths were determined at the outcrop scale using a modified version of Selby's method. Sites were chosen such that the outcrops examined were located in areas of the landscape that were used to define the limit to topographic relief development and back-calculated strength values described in the text and denoted in Figure 3 of Schmidt and Montgomery, **this** report. A similar plot was generated depicting the rock mass strength characteristic of a transect (Figure 1). Where multiple outcrop ratings were determined for one topographic transect, the values were simply averaged.

If all valleys in a landscape were incised to the full relief supportable by the bedrock strength, then Figure 1 would be stratified such that rock mass strengths increase with height for a given slope, or with slope for a given height. However, erosion does not proceed such that the relief potential of all the hillslopes is synchronously maximized. Even so, Figure 1 reveals that the rock mass strength of the landslide sites is consistently lower than the neighboring values for stable hillslopes. Furthermore, a partitioning of Figure 1 into the individual components of relief (height) and hillslope gradient demonstrates that all hillslopes with rock mass strengths greater than 69 are stable (Figures 2 & 3). It appears as if rock of the Chuckanut Formation producing strength values over 69 is strong enough to retard deep-seated landsliding under the present erosional regime. Therefore, once a material strength is **characterized**, field studies of rock strength at the outcrop scale may aid in future landslide prediction and evaluation.

This approach incorporates and quantifies the effects of geologic structure such as the orientation and aspect of the weak links of shale in the strongly-bedded Chuckanut Formation. In addition, it can account for varying percentages of lithologies with different intact rock strengths. For example, failures have been recognized in the Chuckanut Formation where the local proportion of shale dramatically increases. With respect to the Darrington Phyllite, the effects of weathering also is reflected in the intact rock strength. In general, data is easily collected by walking or driving roads and examining bedrock in roadcuts. Rock mass

strength characterization provides a simple method to refine and supplement both the data available on geologic maps and -the predictions made by GIS analyses.

REFERENCES

Selby, **M.J.**, 1980, A rock mass strength classification for **geomorphic** purposes: with tests from Antarctica and New Zealand: *Zeitschrift für Geomorphologie*, vol. 24, no. 1, p. 31-51.

FIGURE CAPTIONS

Figure 1. Plot of transects for Chuckanut Formation showing characteristic rock mass strength ratings with respect to topographic relief development. Landslide sites, enclosed by open circle, typically have lower strengths than neighboring stable hillslopes.

Figure 2. Plot of rock mass strength rating vs. topographic height of hillslope for Chuckanut Formation. Landslide sites are constrained below a rock mass strength value of 69.

Figure 3. Plot of rock mass strength rating vs. topographic gradient of hillslope for Chuckanut Formation. Landslide sites are constrained below a rock mass strength value of 69.

Figure 1
 Rock Mass Strength in Relation to
 Topographic Development

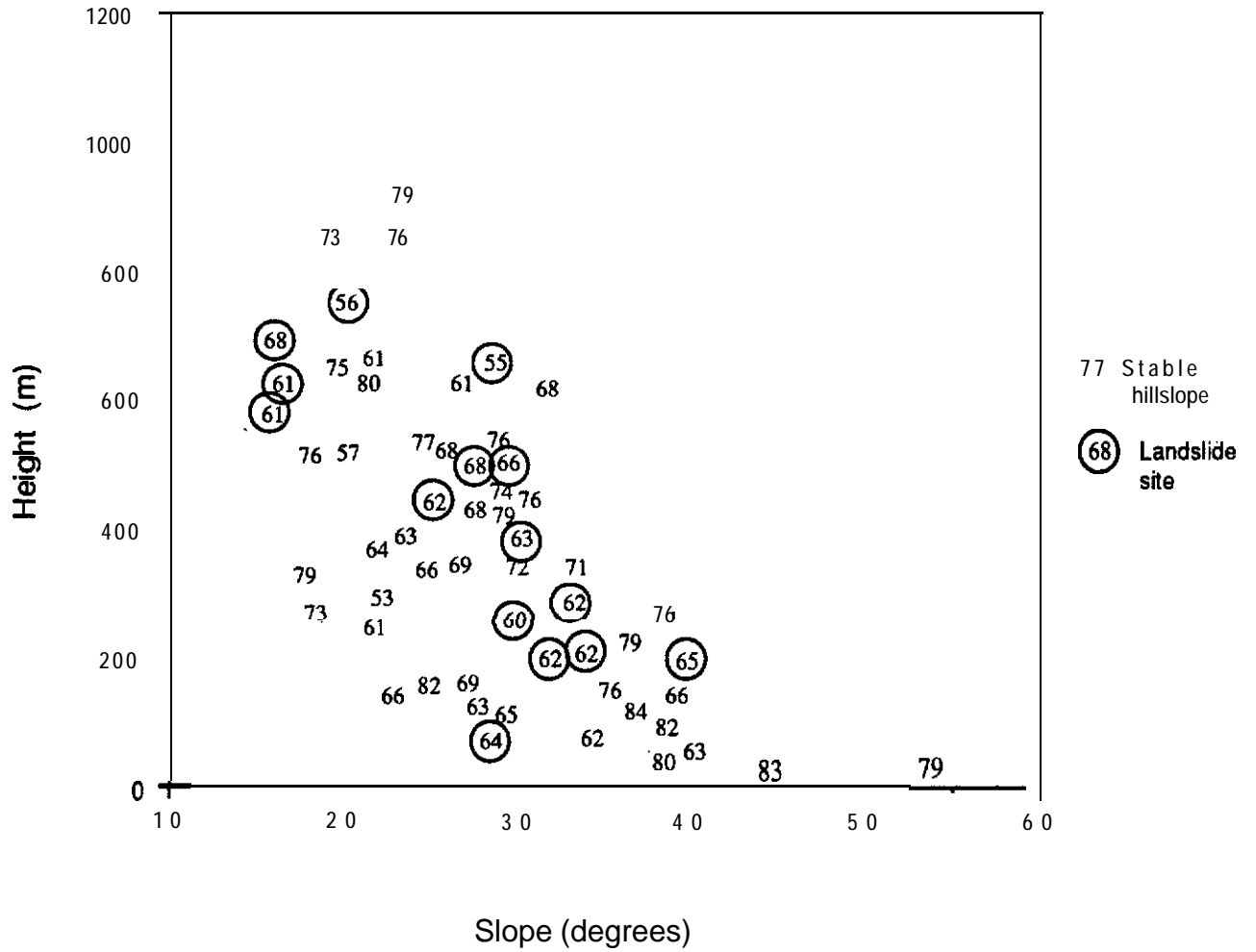


Figure 2

Rock Mass Strength vs. Height for Chuckanut

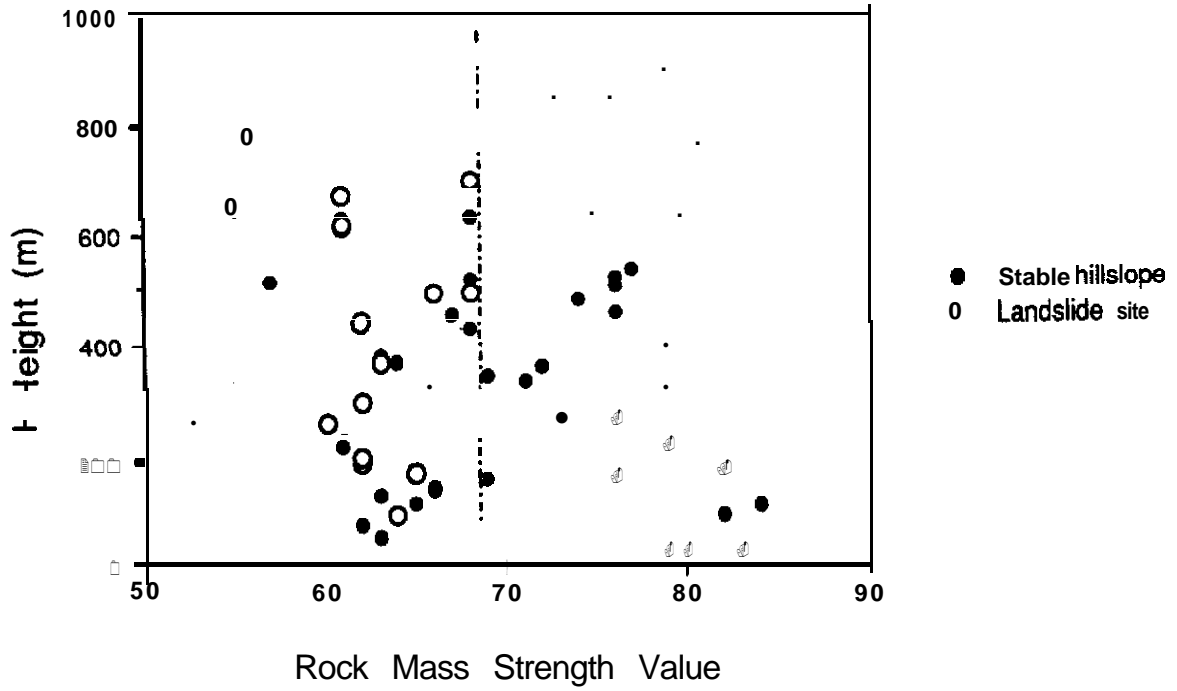
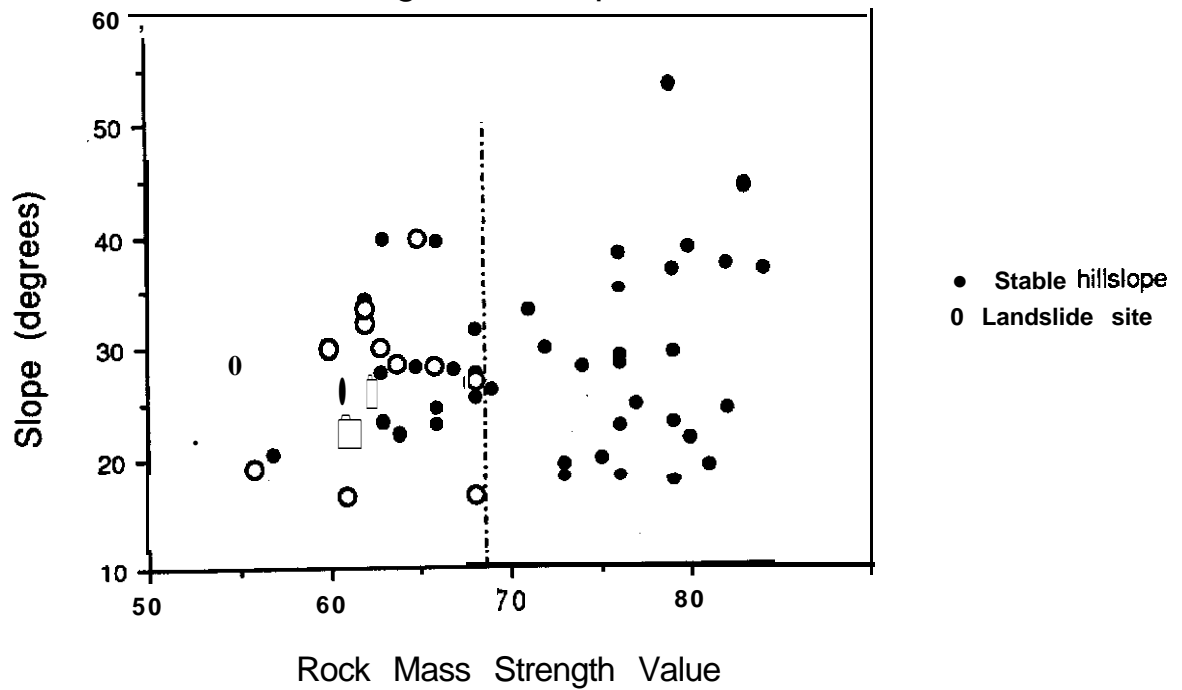


Figure 3

Rock Mass Strength vs. Slope for Chuckanut



Appendix 9

Fluvial Processes and Interpretation of Stream-bed Surface Textures

John M. Buffington

Department of Geological Sciences and **Quaternary** Research

University of Washington

Seattle, Wa. 98195

June 24, 1993

DRAFT

Do not duplicate without author's permission.

Abstract

A discussion of the controls on bed surface texture is presented in order to highlight potentially erroneous channel assessment conclusions using the method proposed by *Dietrich et al. [1989]*. It is emphasized that interpretation of surface textures should not be made in isolation from other **fluvial** processes that contribute to their formation.

Introduction

The size, sorting, and packing assemblage of bed grains determine a channel's surface texture. Analysis of bed surface **textures** can provide valuable insight into stream dynamics, because surface textures directly reflect the hydraulic processes and sediment loading conditions of a channel, which together govern sediment transport rates. As such, surface textural analysis can effectively be used as a surrogate for direct measures of hydrologic and **sedimentologic** parameters. It has recently been suggested that **surface-grain** analysis can be used to interpret channel condition in terms of sediment loading [*Dietrich et al., 1989; Kinerson, 1990; Dietrich et al., 1993*]. Channel assessment of this sort has direct application for evaluation of existing or potential stream degradation due to land management practices [*Dietrich et al. 1989; Dunne and Dietrich, 1991*]. A method for assessing channel condition in terms of sediment supply was proposed by *Dietrich et al. [1989]* and subsequently implemented for watershed analyses in the state of Washington [*WFPB, 1992*]. The purpose of this paper is to examine the controls on surface textures in terms of **fluvial** processes and discuss qualifications concerning the direct application of the method proposed by *Dietrich et al. [1989]*.

Textural Response to Sediment Supply

Many previous studies have documented surface-grain response to changes in sediment supply associated with dam construction [Leopold *et al., 1964*]. **Stream** beds respond dynamically to changes in sediment supply. Channel beds tend to coarsen (or armor) when deprived of sediment and fine when inundated with sediment. Armoring

occurs by selective transport or horizontal winnowing [Milhous, 1973] of finer exposed grains in low sediment supply environments; vertical winnowing associated with "kinematic sieving" due to dilatational bed shearing may also be an important mechanism for surface coarsening [Parker and Klingeman, 1982; Jiang and Haff, 1993]. Textural fining in high sediment supply regimes occurs mainly by particle distraintment [Drake, 1988; Buffington et al., 1992] of fines over rough bed surfaces, resulting in partial burial of larger bed grains and general smoothing of the bed surface.

Dietrich et al. [1989] proposed that surface textural adjustments associated with changes in sediment supply occur to accommodate imposed sediment loads. They developed a dimensionless transport ratio, q^* , that is the transport rate of the surface material normalized by that of the load (approximated by the subsurface [Milhous, 1973; Kuhnle, 1993]) and is in effect an efficiency equation, defined as

$$q^* = \left(\frac{\tau_b - \tau_{cs}}{\tau_b - \tau_{cl}} \right)^{1.5} \quad (1)$$

where τ_b is the basal shear stress and τ_{cs} and τ_{cl} are the critical shear stresses of the surface and load respectively. Values of q^* close to 1 represent efficient sediment-transporting channels with high sediment loads and fine surface textures; q^* values near 0 indicate inefficient sediment transport over coarse bed surfaces in low sediment supply regimes. The potential values of q^* represent a range of textural response that can occur to accommodate variations in sediment load without otherwise causing significant morphologic change. As such, q^* is a valuable indicator of channel condition with regard to sediment 'supply'. However, a valid interpretation of surface textures requires an understanding of all fluvial processes that contribute to an observed texture. The following discussion details some aspects of sediment supply not explicitly considered in the q^* hypothesis.

The flume data used to develop the q^* hypothesis document textural response to changes in the volume of a given mixture of supplied sediment, but do not provide any information on bed surface response to changes in the size distribution of the sediment input. Presumably transport of the same volume of a finer-sized supply **could** be accommodated by an even coarser surface than the existing one. Conversely, a **coarser-sized** supply of equal volume would require a **finer** bed surface in order to have a comparable transport rate. Extreme changes in supply regime may result a substantial reorganization of the channel morphology and roughness configuration [Montgomery *and Buffington, 1993*], **making** simple textural responses insignificant in comparison.

The author interprets the q^* hypothesis to assume that the bed is self-formed and that all grain sizes are transportable; as an ideal efficiency equation q^* cannot be less than 0, and at q^* equal to 0 the entire bed is at the threshold for motion. Many river-beds are not self-formed per se, but rather have large grain sizes imposed on them by confluences of steep, highly competent, tributary channels or by mass wasting events. Often the **mainstem** river is not competent enough to carry this imposed coarse load which then accumulates as lag. If the slope does not increase concurrently with the coarse sediment lag, then the rougher bed surface **will** cause a reduction in the sediment transport rate [Iseya and Ikeda, 1987]. Furthermore, if the **bedload** size distribution does not change in response to the imposition of large immobile grains, then an apparently lower q^* will result, erroneously indicating a high capacity to convey increased sediment loads. Where **coarse-grained** inputs change **the mainstem** slope, as in portions of the Colorado and Snoquahnie rivers, transport rates are likely to be increased. The **bedload** size distribution in **these** channels and in channel morphologies such as step-pool and cascade channels [see discussion in *Montgomery and Buffington, 1993*] is clearly finer than the surface distribution, indicating a low q^* and a high relative transport capacity; however, quantification of q^* using the surface grain sizes of these channels is not advised, because the bed grain sizes may be adjusted to longer-term recurrence intervals than in **lower-**

gradient channels [see discussion in *Montgomery and Buffington, 1993*], making it **difficult** to evaluate different portions of the network on similar temporal scales of process. Bat&full-equivalent evaluations of q^* using such bed grain sizes may result in negative values. Nevertheless, q^* can be confidently applied in many lower-gradient channels.

Finally, in many channels **bedload** transport may be a function of both season and antecedent discharge events [*Nanson, 1974 Griffiths, 1980; Milhous, 1973; Sidle, 1988; Reid et al., 1985*], indicating that surface textures are highly variable during any **given** year. Several investigators have noted changes in the **degree** of armoring between seasons and hydrologic events [*Milhous, 1973; Reid et al., 1985*], as well as grosser textural changes caused by seasonal pool-filling by fine material [Campbell *and* Sidle, 1985; Lisle *and* Hilton 1992]. These observations demonstrate the potential for a large degree of variability in the **evaluation** of channel condition for a particular stream or for comparisons between channels.

Textural Response to Hydraulic Processes

Variations in texture can occur **in** a reach due to differential spatial patterns of shear stress caused by **channel** curvature and topographic steering [*Dietrich and Smith, 1983; 1984a; 1984b; Dietrich and Whiting, 1989; Dietrich et al., 1979*]. For example, in a meander bend it is commonly observed that surface grains fine both downstream along the point bar and cross-stream from the pool to the bar. These textural variations reflect the shifting of the high velocity core across the bar toward the pool, causing flow convergence *in the* pool and divergence downstream along the bar [*Dietrich and Smith, 1983; 1984a; 1984b; Dietrich and Whiting, 1989; Dietrich et al., 1979*]. Other channel types also exhibit spatial variability of textures due to basic **channel** morphology and roughness configuration. For example, steep-gradient step-pool and cascade channels are composed mainly of coarse-grained bed material, but **finer** textures may exist in low energy

environments associated **with** pools formed by steps and boulder clusters and with velocity shadows created by large grains [see *Montgomery and Buffington, 1993*].

Recent investigation of gravel- and cobble-bedded channels has documented textural response to energy dissipation caused by in-channel roughness elements [*Buffington, 1992; Buffington and Montgomery, 1992; Buffington, thesis in prep.*]. A **bankfull threshold channel model** was used to predict median surface grain sizes and serve as a reference point from which to examine textural response to various roughness elements. Three different channel types showing increasing complexity of roughness were examined in order to partition the relative effects of grain, **bedform**, and large woody debris (**LWD**) roughness. Detailed textural and topographic mapping was conducted, as well as subsurface grain size analysis. Results from the study of forty **channels** in coastal Alaska and Washington show that textural response to roughness elements occurs at both local and reach scales. Spatial averaging of textures on a reach scale results **in** segregation by channel type into distinct zones of textural response (Figure 1), such that increasing roughness due to **barforms** and LWD produces progressively **finer** surface textures. Although streams with more in-channel **roughness** typically have more extensive patches of finer textures, the results of Figure 1 are not simply an effect of the averaging-in of these patches. The study sites segregate in a similar fashion when the dominant (i.e. most common) **texture** is plotted rather than the average texture, indicating that in-channel roughness elements have a reach-wide effect on surface textures.

In terms of channel condition, Figure 1 shows that channels with abundant LWD exhibit the strongest textural **fining** and are thus hypothesized to have the least capacity to convey increased sediment loads by further textural **fining**. Analysis of **field** and laboratory studies of textural response to sediment supply indicate that surface fining due to increased sediment loads can be of comparable magnitude to the response caused by in-channel roughness elements (Figure 2). The Figure 2 schematic is intended to show that surface textures are a function of channel shear stress (**proportional** to the product of depth and

slope), channel roughness features, and sediment load. It is surprising to note that the segregation of textural response by channel type shown in Figure 1 is observed without any consideration of sediment loading. This may indicate that unless changes in sediment supply are pronounced and persistent, textural response is dominated by the presence of roughness elements.

Conclusion

Surface textural analysis is a valuable tool for understanding channel dynamics and assessing channel condition. However, in order to avoid erroneous conclusions, surface textures must be interpreted in terms of a variety of **fluvial** processes that may *contribute to* textural formation. Bed surface textures may be controlled by numerous factors and processes, including: long-term and seasonal sediment supply (both volume and caliber) of material that the channel can competently carry; supply of over-huge lag material, energy dissipation caused by the presence of in-channel roughness elements, which include the stable *roughness* configuration for a given morphology (e.g. bars and **pools**), as well **as** any imposed roughnesses (**LWD**, forced curvature, etc.); antecedent discharge events; and spatial patterns of shear stress governed by channel morphology. Interpretation of channel condition **through** use of assessment methods such as q^* [**Dietrich et al., 1989**] should be qualified by the above listed factors in order to separate other effects from that of the volume of supplied *sediment*. However, partitioning of these relative **effects is not a** trivial matter and deserves further investigation; the author [**Buffington, thesis in prep.**] is currently addressing portions of this problem. Assessment of **channels** without significant **bedforms** or high woody debris loading (i.e. plane-bed channels) may provide the most unambiguous application of q^* . Furthermore, it is important to recognize that even properly interpreted q^* analyses provide only a “snap-shot” of current sediment loading conditions and must be **evaluated** in conjunction with other indicators of channel assessment.

DRAFT

Do not duplicate without author's permission.

References

- Buffington, **J.M.**, Channel assessment and relative roughness partitioning in gravel-bedded streams, in *Geomorphological Watershed Analysis Project Annual Report for the period 10/91-5/92*, app. 7, submitted to the Sediment, Hydrology and Mass Wasting Committee of the **Timber/Fish/Wildlife** Agreement, 1992.
- Buffington, J.M. and D.R. Montgomery, Effects of hydraulic roughness and sediment supply on bed surface textures in gravel-bed streams, *EOS, Trans AGU*, **73**, p. 231, 1992.
- Buffington, J.M., **W.E.** Dietrich, and J.W. Kirchner, Friction angle measurements on a naturally formed gravel streambed: Implications for critical boundary shear stress, *Water Resour. Res.*, **28**, 41 1-425, 1992.
- Campbell, A.J. and R.C. Sidle, **Bedload** transport in a pool-riffle *sequence* of a coastal Alaska stream, *Water Resour. Bull.*, **21**, **579-590**, 1985.
- Dietrich, W.E. and J.D. Smith, Influence of the point bar on flow through curved channels, *Water Resour. Res.* **19**, 1173-1192, 1983.
- Dietrich, W.E. and J.D. Smith, Bed load transport in a river meander, *Water Resour. Res.*, **20**, 1355-1380, 1984a.
- Dietrich, W.E. and J.D. Smith, Processes controlling the equilibrium bed morphology in river meanders, in *River Meandering, Proceedings of the Conference Rivers '83*, edited by C.M. Elliot, pp. 759-769, Am. Soc. Civ. Eng., New York, 1984b.
- Dietrich, W.E., and P. Whiting, Boundary shear stress and sediment transport in river meanders of sand and gravel, in *River Meandering, AGU Water Resour. Monogr. Ser.*, **12**, edited by S. Ireda and G. Parker, pp. 1-50, AGU, Washington, D.C., 1989.
- Dietrich, W.E., D. Kinerson, and L. Collins, Interpretation of relative sediment supply from bed surface texture in gravel bed rivers, *EOS, Trans. AGU*, **74**, p. 151.1993.

- Dietrich, W.E., Kirchner, J.W., **Ikeda**, H., and Iseya, F., Sediment supply and the development of coarse surface layer in gravel-bedded rivers, *Nature*, 334,215-217, 1989.
- Dietrich, W.E., J.D. Smith, and T. **Dunne**, Flow and sediment transport in a sand bedded meander, *J. Geol.*, 87,305-315, 1979.
- Drake, T.G., R.L. **Shreve**, W.E. Dietrich, P.J. Whiting, and L.B. Leopold, **Bedload** transport of fine gravel observed by motion-picture **photography**, *J. Fluid Mech.*, 192, 193-217, 1988.
- Dunne, T. and W.E. Dietrich, *Geomorphical Watershed Analysis Project*, proposal submitted to the Washington State **Timber/Fish/Wildlife** Agreement, 27 pp., 1991.
- Griffiths**, G.A., Stochastic estimation of bed load yield in pool-and-riffle mountain streams, *Water Resour. Res.*, 16, 931-937, 1980.
- Iseya, F. and H. **Ikeda**, Pulsations in **bedload** transport rates induced by a longitudinal sediment sorting: a flume study using sand and gravel mixtures, *Geogr. Annlr*, 69, 15-27, 1987.
- Jiang, Z. and P.K. Haff, Multiparticle simulation methods applied to the micromechanics of bed load transport, *Wat. Resour. Res.*, 29, 399-412, 1993.
- Kinerson, D., Bed surface response to sediment supply, unpublished M.S. thesis, University of California, Berkeley, California, 1990.
- Kuhnle**, R.A., Equal mobility on Goodwin creek, *EOS, Trans. AGU*, 74, p. 158, 1993.
- Leopold, L.B., M.G. **Wolman**, and J.P. Miller, *Fluvial Processes in Geomorphology*, W.H. Freeman and Company, 522 pp. 1964.
- Lisle, T.E. and **S. Hilton**, The volume of fine sediment in pools: an index of sediment supply in gravel-bed streams, *Water Res. Bull.*, 28, 371-383, 1992.
- Milhous, R.T., Sediment transport in a gravel-bottom stream, unpublished Ph.D. dissertation, Oregon State University, Corvallis, Oregon, 232 pp., 1973.

- Montgomery, D.R., and J.M. Buffington, *Channel Classification, Prediction of Channel Response, and Assessment* of Channel Condition, Washington State Department of Natural Resources **Timber/Fish/Wildlife** Agreement, TFW-93-002.83 pp. 1993.
- Nanson, G.C., **Bedload** and suspended-load transport in a small, steep, mountain stream, *Am. J. Sci.*, **274**, 471-486, 1974.
- Parker, G. and P.C. Klingeman, **On** why gravel bed streams are paved, *Water Resour. Res.*, **18**, 1409-1423, 1982.
- Reid, I., L.E. Frostick, and J.T. Layman, The incidence and nature of **bedload** transport during flood flows in coarse-grained alluvial channels, *Earth Surf. Proc. Landforms*, **10**, 3344, 1985.
- Sidle, R.C., Bed load *transport* regime of a small forest *stream*. *Water Resour. Res.*, **24**, 207-218, 1988.
- Washington Forest Practice Board, *Standard Methodology for Conducting Watershed Analysis*, version 1.10, 1992.

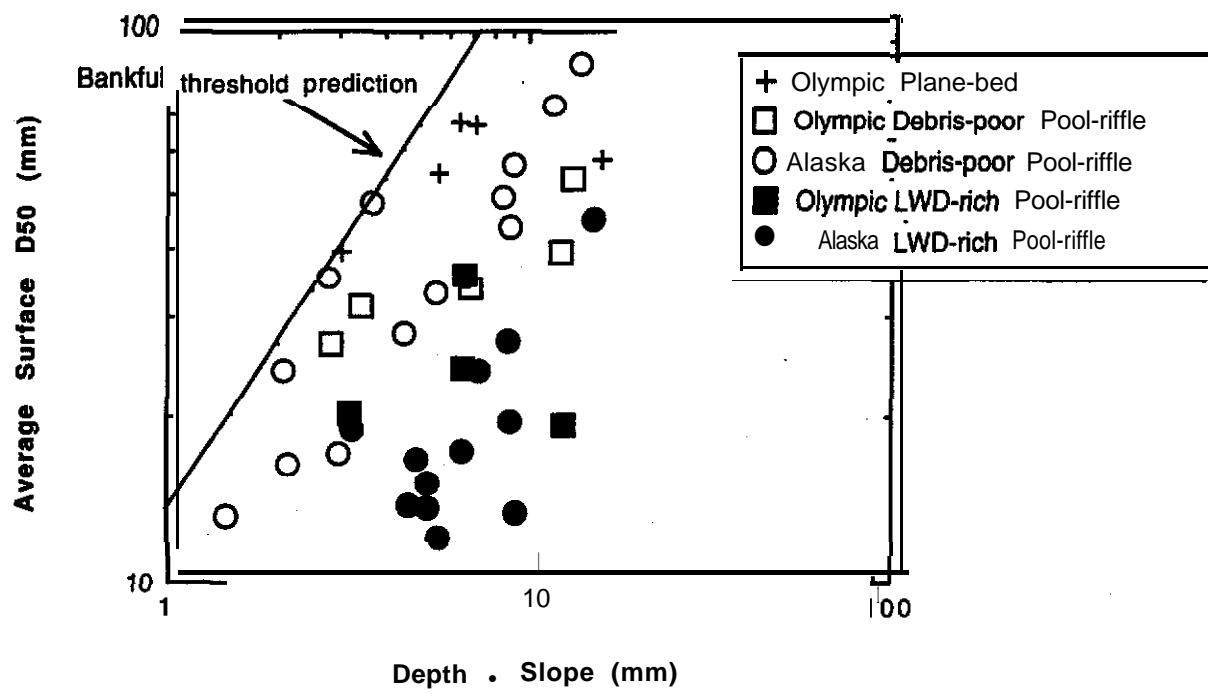


FIGURE 1

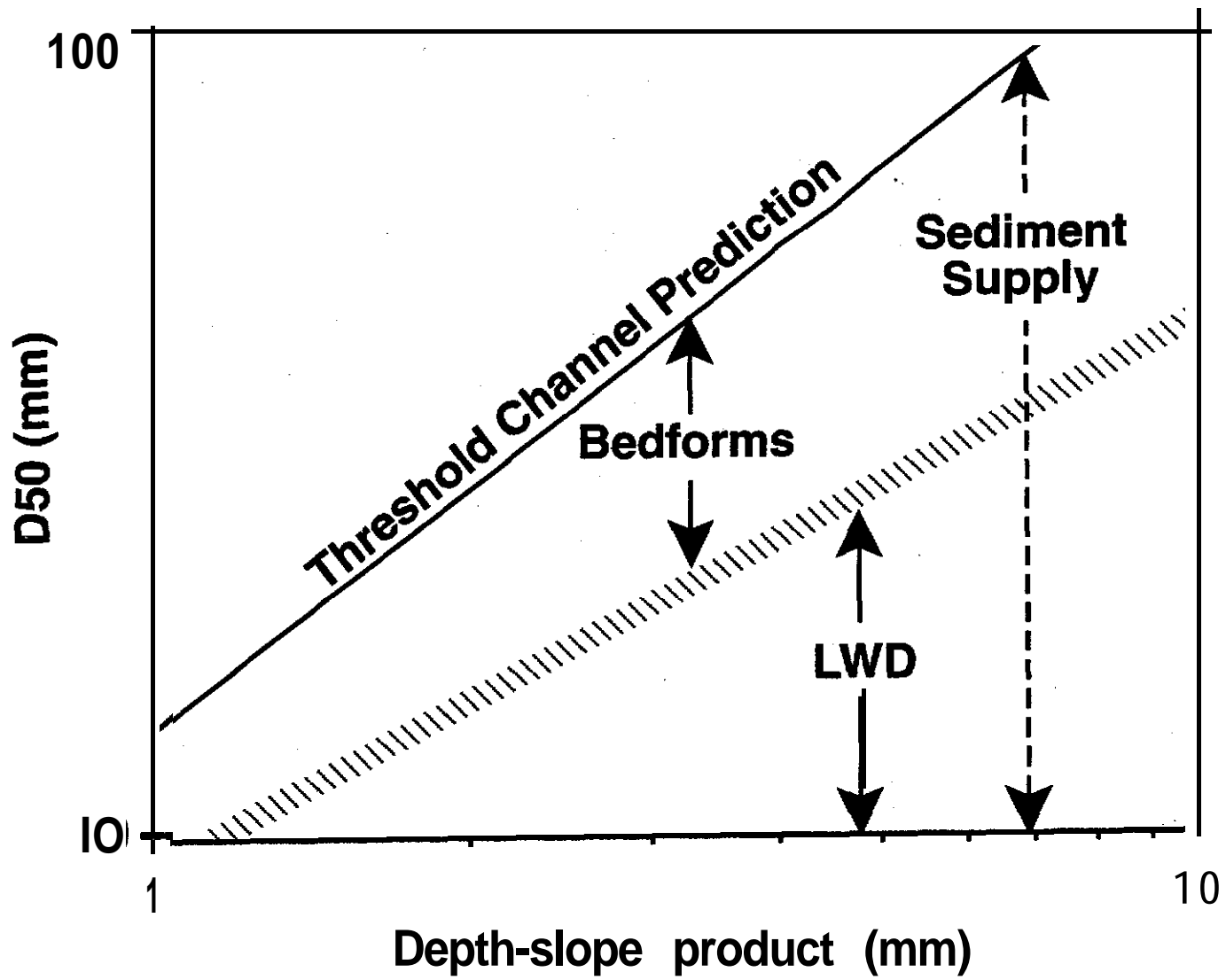


FIGURE 2